

# Engineering Immunity: Enhancing T Cell Vaccines and Combination Immunotherapies for the Treatment of Cancer

by

Kelly D. Moynihan

B.S. Biomedical Engineering  
University of Texas at Austin, 2012

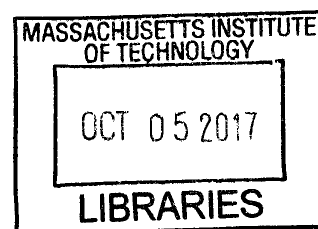
Submitted to the department of Biological Engineering in partial fulfillment of the requirements  
for the degree of

DOCTOR OF PHILOSOPHY IN BIOLOGICAL ENGINEERING  
at the  
MASSACHUSETTS INSTITUTE OF TECHNOLOGY

September 2017

© 2017 Kelly D. Moynihan. All rights reserved.

The author hereby grants to MIT permission to  
reproduce and distribute this publicly paper and electronic  
copies of this thesis document in whole or in part in any  
medium now known or hereafter created.



ARCHIVES

**Signature redacted**

Signature of Author: \_\_

\_\_\_\_\_  
Kelly D. Moynihan  
Biological Engineering  
August 10, 2017

**Signature redacted**

Certified by: \_\_

\_\_\_\_\_  
Darrell J. Irvine  
*Professor of Biological Engineering*  
*Thesis Supervisor*

**Signature redacted**

Accepted by: \_\_

\_\_\_\_\_  
Mark Bathe  
*Associate Professor of Biological Engineering*  
*Graduate Program Chair*

Signature redacted

Certified by: 




\_\_\_\_\_

Dane K. Wittrup

*Professor of Biological Engineering*

Graduate Committee Chair

Signature redacted

Certified by: 

\_\_\_\_\_

Glenn Dranoff

*Global Head of Immuno-Oncology*

*Novartis Institutes for BioMedical Research*

# Engineering Immunity: Enhancing T Cell Vaccines and Combination Immunotherapies for the Treatment of Cancer

by

Kelly D. Moynihan

Submitted to the Department of Biological Engineering  
on August 10<sup>th</sup>, 2017, in partial fulfillment of the  
requirements for the degree of Doctor of Philosophy  
in Biological Engineering

## ABSTRACT

Checkpoint blockade with antibodies against CTLA-4 or PD-1 has demonstrated that an endogenous adaptive immune response can be stimulated to elicit durable tumor regressions in metastatic cancer, but these dramatic responses are confined to a minority of patients<sup>1-3</sup>. This outcome is likely due in part to the complex network of immunosuppressive pathways present in advanced tumors, which necessitates the development of novel therapeutics and combination immunotherapies to generate a counter-directed network of pro-immunity signals<sup>4-8</sup>. In Chapters 2 and 3 of this thesis, we describe methods for enhancing T cell priming against tumor antigens via covalent modification of molecular vaccines to enhance lymphatic drainage, serum stability, or cytosolic access to improve presentation on MHC class I. In Chapter 4, we demonstrate a combination immunotherapy that recruits a diverse set of innate and adaptive effector cells, enabling robust elimination of large tumor burdens that to my knowledge have not previously been curable by treatments relying on endogenous immunity. Maximal anti-tumor efficacy required four components: a tumor antigen targeting antibody, an extended half-life IL-2<sup>9</sup>, anti-PD-1, and a powerful T-cell vaccine<sup>10</sup>. This combination elicited durable cures in a majority of animals, formed immunological memory in multiple transplanted tumor models, and induced sustained tumor regression in an autochthonous BRraf<sup>V600E</sup>/Pten<sup>-/-</sup> melanoma model. Finally, in Chapter 5, we show preliminary data on combination immunotherapies used to treat antigenically heterogeneous tumors. Taken together, these data define design criteria for enhancing the immunogenicity of molecular vaccines and elucidate essential characteristics of combination immunotherapies capable of curing a majority of tumors in experimental settings typically viewed as intractable.

Thesis Supervisor: Darrell J. Irvine

Title: Professor of Materials Science & Engineering and Biological Engineering

# ACKNOWLEDGMENTS

In my time as a graduate student, I have been extremely fortunate to have had a number of wonderful mentors, collaborators, colleagues, and friends.

First and foremost, I would like to thank my thesis advisor, Darrell, whose encouragement and guidance (both scientifically and more broadly) has supported me throughout my PhD, and whose scientific curiosity, dedication, and desire to positively impact human health has been a constant source of motivation for me. I am also immensely grateful to Dane Wittrup for his guidance and support as my thesis advisor chair, close collaborator, and mentor. I am greatly appreciative of Glenn Dranoff's scientific inquisitiveness and helpful advice during my thesis committee meetings. Thank you also to Michael Birnbaum for helpful career discussions, perspective, and advice.

To Cary Opel, my collaborator of three years, thank you for your patience, meticulousness, efficiency, and friendship. Thank you to other collaborators without whom this thesis would have been impossible, especially to Naveen Mehta, Kavya Rakhra, and Rebecca Holden. Thank you to Simon Liang for your help and perpetual optimism.

Thank you to Jennifer Montana and all of The Innovation Institute for helping me grow as an instructor and for constantly reminding me that science is exciting and something to be enthusiastically shared.

Thank you to the Hertz Foundation for providing an invaluable community of peers and mentors, and for supporting retreats and symposia to foster this network. Thank you especially to Vyas, Jim, Max Mankin, Dan, Jon, Jesse, Joshu, Ashvin, Max Kleinmen-Weiner, Thomas, DJ, Cooper, and Katie for beach bonfires, beer festivals, and marshmallows.

Thank you to BE 2012, my soccer teams, my lab mates, and especially to Ryan, Griffin, Santiago, Shawn, Frances, Claire, Adrienne, Kunal, and Khoi and for providing sanity, support, and friendship. And last but not least, thanks to Mini, Atlas, Oakley, 7, Brisbane, and Gus.



# TABLE OF CONTENTS

<b>CHAPTER 1: INTRODUCTION</b> .....	<b>9</b>
1.1 CANCER IMMUNOTHERAPY ENTERS MAINSTREAM ONCOLOGY.....	9
<i>A renaissance of immuno-oncology</i> .....	9
<i>A brief overview of immunotherapy strategies</i> .....	10
1.2 ENGINEERING NEW APPROACHES TO CANCER VACCINES .....	14
<i>Motivation for cancer vaccine engineering</i> .....	14
<i>Targeting vaccines to lymph nodes</i> .....	15
<i>Vaccine-Mediated programming of T-cell homing to tumor sites</i> .....	18
<i>Exploiting the tumor site as an antigen source</i> .....	20
<i>Active depots with implantable vaccine scaffolds</i> .....	22
<i>Outlook</i> .....	24
1.3 COMBINATION IMMUNOTHERAPIES: ROLES FOR INNATE IMMUNITY .....	25
<i>Introduction</i> .....	25
<i>Roles of innate immune effectors in immunotherapy</i> .....	25
<i>Combination treatments recruiting innate and adaptive immunity</i> .....	28
<i>Conclusions</i> .....	34
<b>CHAPTER 2: ENHANCING T CELL VACCINES VIA ALBUMIN HITCHHIKING</b> .....	<b>36</b>
2.1 INTRODUCTION .....	36
2.2 RESULTS: CHARACTERIZATION OF THE AMPHIPHILE VACCINE SYSTEM.....	37
<i>Amph-peptides achieve broad lymphatic distribution and extended in vivo presentation</i> .....	37
<i>Amph-vaccine does not rely on FcRn, short amph-peptides require Batf3 dendritic cells for optimal responses</i> .....	39
<i>DSPE-PEG<sub>2000</sub> conjugation protects peptide integrity in serum; the impact of chemistries and terminus of linkage to peptide on priming</i> .....	41
<i>Amph-peptides prime with various adjuvants; trafficking and priming is diminished by IFA</i> .....	43
<i>The amph-vaccine traffics efficiently in non-human primates</i> .....	43
2.3 RESULTS: EXPANDING BEYOND THE ALBUMIN-BINDING DIACYL LIPID .....	47
<i>Albumin binding peptides to enhance peptide trafficking and immunogenicity</i> .....	47
<i>Vitamin E modification of CpG and peptides enhance trafficking and immunogenicity</i> .....	48

<i>Vitamin E ssRNA TLR7 agonist does not effectively adjuvant T cell responses</i> .....	50
<i>Y-form DNA STING agonist does not activate STING in the absence of transfection</i> .....	51
<i>Maleimide-peptide constructs to bind Cys34 on albumin in vivo</i> .....	53
2.4 DISCUSSION AND FUTURE WORK .....	55
2.5 METHODS .....	58
<i>Peptide and oligo conjugate synthesis</i> .....	58
<i>Mice and immunizations</i> .....	59
<i>Adoptive transfer proliferation studies</i> .....	59
<i>In vitro peptide stability assay</i> .....	60
<i>TLR and STING reporter assays</i> .....	60
<i>Evaluation of immune responses and flow cytometry</i> .....	61
<i>Trafficking studies in rhesus macaques</i> .....	61
<i>Statistical analysis</i> .....	62

### **CHAPTER 3: CELL PENETRATING PEPTIDE ANTIGEN CONJUGATES TO ENHANCE ANTIGEN**

<b>PRESENTATION</b> .....	<b>63</b>
3.1 INTRODUCTION .....	63
3.2 RESULTS .....	64
<i>In vitro survey of CPP-antigens</i> .....	64
<i>In vivo priming of transferred pmel-1 T cells with EGP-penetratin</i> .....	67
<i>Endogenous priming with CPP-antigen constructs</i> .....	68
<i>Trafficking of CPP constructs</i> .....	70
<i>Double modification of peptide to enhance both trafficking and cytosolic access</i> .....	70
<i>Are CPP-antigens presented by non-professional APCs in vivo?</i> .....	72
3.3 DISCUSSION AND FUTURE WORK .....	74
3.4 METHODS .....	76
<i>Peptide synthesis</i> .....	76
<i>Evaluation of immune responses and flow cytometry</i> .....	77
<i>In vitro presentation assay</i> .....	77
<i>Adoptive transfer proliferation studies</i> .....	78
<i>Lymph node antigen presenting cell sort and in vitro co-culture</i> .....	78
<i>Cells and tumor challenge</i> .....	78
<i>Lymph node uptake of fluorescent constructs</i> .....	79

<i>Statistical analysis</i> .....	79
<b>CHAPTER 4: COMBINATION IMMUNOTHERAPY ENGAGING INNATE AND ADAPTIVE IMMUNITY .....</b>	<b>80</b>
4.1 INTRODUCTION .....	80
4.2 RESULTS.....	81
<i>Combining a potent vaccine with anti-tumor antibody, extended-PK IL-2, and checkpoint blockade eradicates large established tumors.....</i>	<i>81</i>
<i>AIPV therapy remodels the tumor microenvironment and promotes a combined innate and adaptive immune attack on tumors. ....</i>	<i>84</i>
<i>Combination therapy elicits a polyclonal antibody response targeting diverse tumor cell antigens, which can protect against tumor challenge. ....</i>	<i>95</i>
<i>AIPV therapy regresses tumors in the inducible Braf/Pten melanoma model.....</i>	<i>98</i>
4.3 DISCUSSION AND FUTURE WORK.....	100
4.4 METHODS .....	103
<i>Mice</i> .....	<i>103</i>
<i>Cells</i> .....	<i>104</i>
<i>Vaccine and protein production</i> .....	<i>104</i>
<i>Tumor inoculation and subcutaneous tumor therapy</i> .....	<i>105</i>
<i>Flow cytometry</i> .....	<i>106</i>
<i>Depletions</i> .....	<i>106</i>
<i>Autochthonous tumor model induction and therapy</i> .....	<i>107</i>
<i>Liver enzyme measurements</i> .....	<i>107</i>
<i>Endogenous antibody detection and serum transfer</i> .....	<i>107</i>
<i>Generation of Trp2 KO cell line</i> .....	<i>108</i>
<i>ELISPOT assay</i> .....	<i>110</i>
<i>Immunoblot</i> .....	<i>110</i>
<i>Tumor cytokine Luminex assay</i> .....	<i>110</i>
<i>Histology</i> .....	<i>111</i>
<i>Multivariate Analysis of Cytokine Data</i> .....	<i>111</i>
<i>Statistical Analysis</i> .....	<i>111</i>
<b>CHAPTER 5: ANTIGEN HETEROGENEITY IN SOLID TUMORS .....</b>	<b>113</b>
5.1 INTRODUCTION .....	113

5.2 RESULTS.....	114
<i>Generation and characterization of antigen knockout lines.....</i>	<i>114</i>
<i>Antigenically heterogeneous tumors: mosaics with cells lacking Trp1 expression.....</i>	<i>116</i>
5.3 DISCUSSION AND FUTURE WORK.....	120
5.4 METHODS .....	122
<i>Reagents and flow cytometry.....</i>	<i>122</i>
<i>ELISPOT.....</i>	<i>122</i>
<i>Tumor studies .....</i>	<i>123</i>
<b>CHAPTER 6: CONCLUSIONS AND OUTLOOK.....</b>	<b>124</b>
<b>FUNDING.....</b>	<b>141</b>
<b>APPENDICES .....</b>	<b>142</b>
I.    SUBCUTANEOUS INJECTIONS AT THE TAIL BASE .....	142
II.   TETRAMER STAIN PROTOCOL.....	143
III.  ICS PROTOCOL .....	146
IV.  LIST OF SELECTED MURINE CD8 <sup>+</sup> T CELL EPITOPES FOR AMPH-VACCINATION .....	149
V.   DNA SYNTHESIS CHECKLIST.....	151

# CHAPTER 1: INTRODUCTION

## ***1.1 Cancer immunotherapy enters mainstream oncology***

### **A renaissance of immuno-oncology**

Cancer immunotherapy, also called immuno-oncology, has exploded in popularity in recent years and is transforming the way oncology is practiced clinically. Cancer immunotherapy refers to therapeutic strategies aimed at recruiting the immune system to recognize and eliminate tumors, and it has garnered considerable enthusiasm because of its potential to induce durable responses against cancers. Examples of this excitement are readily found in mainstream media. In April 2016, Time Magazine's front cover showed a picture of an i.v. drip with the provocative question, "What if your immune system could be taught to kill cancer?"<sup>11</sup> In July 2016, the New York Times ran a front-page story on cancer immunotherapy, with the subtitle "Harnessing the Power of the Immune System"<sup>12</sup>, and there are even examples of celebrities receiving immunotherapy treatment<sup>13</sup>.

Although immunotherapy has come to the forefront of cancer treatment in recent years, it is not a new technique. William Coley is often credited as the father of cancer immunotherapy because he treated tumors with "Coley's toxins," a mixture of killed bacteria administered intratumorally, during the late 1800s<sup>14</sup>. It was approximately 100 years later, in 1992, that IL-2 was approved for the treatment of renal carcinomas, arguably the first effective modern immunotherapy treatment for human cancer<sup>15</sup>. In 2011, the first checkpoint inhibitor, ipilimumab, received approval by the FDA and initiated the current flood of checkpoint blockade immunotherapy. This occurred about 15 years after the initial proof of concept studies were performed in mice by Jim Allison and colleagues<sup>16</sup>. The next wave of checkpoint antibodies began with the approval of Merck's antibody targeting programmed cell death protein 1 (PD-1), pembrolizumab, in 2014, followed shortly by many others; to date there are three approved anti-PD-L1 and two approved anti-PD-1 antibodies<sup>17</sup>. In July 2017, Novartis received a unanimous vote recommending approval by the FDA for their chimeric antigen receptor T cell (CAR-T) therapy CTL019, the first CAR-T therapy to reach this milestone<sup>18</sup>. There are countless preclinical investigations exploring novel immunotherapy targets and strategies and more than

600 ongoing clinical trials using antibodies against immune checkpoints as monotherapy or in combination in the US alone<sup>\*</sup>.

What is it about immuno-oncology therapy that is creating so much excitement? To start with, immunotherapy is a fundamentally different approach to cancer treatment. Unlike preceding techniques, immunotherapies treat the immune system, not the tumor itself, per se; it is the immune system that imparts anti-tumor activity. One important aspect of immunotherapies is the “tail of the curve” phenomenon, which refers to the observation that the survival curves for immunotherapies and targeted therapies are fundamentally different in shape<sup>19</sup>. With targeted therapies (ex. Braf inhibitors), patients harboring the relevant mutation nearly universally respond initially, but the effect of intervention is a limited extension of survival for patients (shifting the curve to the right in time), and overall survival looking at long time points is unchanged from standard-of-care chemotherapy<sup>19</sup>. In contrast, with immunotherapy, not all patients receive benefit but those that do often receive durable benefit, leading to an overall difference in survival for immunotherapy-treated patients (shifting the curve up in percent survival)<sup>19</sup>. This observation has given hope to many, because one could envision a future in which better immunotherapies lead to a shifting of this survival curve farther up, with more patients receiving durable clinical benefit.

## **A brief overview of immunotherapy strategies**

A brief introduction to immunotherapy approaches under development for the treatment of cancer is presented here. Approaches are described here as individual therapeutics, although many of these are being explored in combination. (Combination immunotherapy approaches are discussed separately in depth in the last section of this introductory chapter and in Chapter 4.) This section is not meant to be exhaustive and the descriptions given are succinct; the objective is to introduce some of the major approaches being investigated clinically for the treatment of cancer in order to frame this thesis.

### ***Checkpoint blockade***

Checkpoint blockade refers to a strategy that seeks to block ligand-receptor interactions that would normally suppress T cell function. The first FDA approved checkpoint antibody, ipilimumab, engages cytotoxic T lymphocyte-associated antigen 4 (CTLA-4)<sup>20</sup>. Although it is the

---

<sup>\*</sup>According to a search performed on [clinicaltrials.gov](http://clinicaltrials.gov) on 7/24/2017.

removal of suppressive signals to T cells that formed the basis of anti-CTLA-4 as a therapeutic, evidence has since emerged in preclinical models that depletion of CTLA-4-expressing T regulatory cells ( $T_{reg}$ s) may play a large role in therapy<sup>21-23</sup>. Clinical data on blockade at this immunological checkpoint is the oldest; a recent pooled analysis suggests that for advanced melanoma, the survival curve plateaus just above 20% after 3 years<sup>24</sup>. The first PD-1 blocking antibody, Merck's pembrolizumab, was approved in 2014<sup>17</sup>, followed by numerous others targeting either PD-1 or its ligand, PD-L1. There have been studies showing that patients whose tumors express PD-L1 are more likely to benefit from blockade of this immunological axis<sup>2</sup>, however it is not entirely predictive, and there are also patients who are classified as PD-L1<sup>-</sup> that still show clinical benefit to anti-PD-1<sup>25</sup> (though this may be related to issues dealing with histological techniques used for determining PD-L1 status). Other, next-generation T cell checkpoints currently under investigation are numerous, and include TIM-3, LAG-3, and TIGIT<sup>26</sup>.

### ***Agonistic co-stimulatory antibodies***

If checkpoint blockade can be described as taking the brakes off of an immune response, agonistic antibodies against T cell co-stimulatory molecules can be described as putting the foot on the gas pedal. Engagement of this class of antibody with co-stimulatory receptors on T cells can promote activation, proliferation, survival, and effector function of T cells<sup>27</sup>, but can also result in severe systemic inflammatory toxicities, as was seen in a phase I trial in 2006 with an agonistic antibody against CD28, which induced cytokine storm in all of the 6 patients dosed<sup>28</sup>. The most advanced clinical studies using this class of antibody have been performed with therapies targeting 4-1BB, which is also expressed by NK cells<sup>29</sup>. Initial studies in melanoma patients have shown therapeutic activity<sup>30</sup>, but a subsequent study had to be suspended because of toxicities seen in patients<sup>31</sup>, indicating a need for careful consideration of dosing regimens for these agonistic antibodies. Other notable examples of targets for this class of therapeutic include OX40, ICOS, and GITR<sup>27</sup>.

### ***Adoptive transfer of T cells***

Adoptive transfer approaches involve the transfer of large numbers of *ex vivo* expanded tumor-reactive T cells into patients. These T cells can be expanded from tumor infiltrating lymphocytes (TILs), or can be artificially engineered to express T cell receptors (TCRs) or chimeric antigen receptors (CARs) of interest<sup>32</sup>. Currently, the approaches being tested late-stage clinically rely on autologous cells, meaning that the cells are removed from the patient,

manipulated *ex vivo* and expanded, then re-infused, although there is a possibility that allogeneic T cells may be used<sup>33</sup>, which would significantly ease translation of these therapies at scale. In July 2017, Novartis received a unanimous vote recommending FDA approval for their CAR-T therapy CTL019 (Tisagenlecleucel-t), which targets the B-cell associated receptor CD19, for B-cell acute lymphoblastic leukemia (ALL)<sup>18</sup>. This is the first CAR-T therapy to reach this milestone. Kite Pharma is following closely behind with their CD-19 targeted CAR-T therapy, Axicabtagene ciloleucel, and early studies are beginning on the next wave of CAR-T therapies targeting different antigens, including mesothelin, MUC16, and prostate stem cell antigen (PSCA)<sup>34</sup>.

### **Vaccines**

Cancer vaccines aim to prime T cells against tumor antigens to impart anti-tumor activity. Vaccination has been one of the most effective interventions in public health for the prevention of infectious disease, but application to the treatment of cancer has thus far been largely ineffective, with only one example of a therapeutic cancer vaccine receiving FDA approval to date<sup>35,36</sup>. Recently, however, clinical studies in small numbers of patients who received immunization against mutant tumor epitopes (called neoantigens) have garnered considerable excitement in the field<sup>37,38</sup>. Vaccination against tumor epitopes and novel approaches for immunization are discussed in depth in the second section of this chapter, entitled “Engineering new approaches to cancer vaccines.”

### **Cytokine therapies**

Cytokines are small immunomodulatory proteins that regulate immune responses in either autocrine or paracrine fashion<sup>39</sup>. IL-2, which can promote activation and survival of both T cells and NK cells (and is discussed further in the third section of this chapter) was approved for clinical use based on its demonstration of anti-tumor activity in 1992, although treatment was associated with considerable toxicities, including fever, chills, joint pain, and capillary leak syndrome<sup>15,40</sup>. Interferon- $\alpha$  (IFN- $\alpha$ ) has been used to treat chronic myeloid leukemia (CML) and showed superior survival compared to standard of care as early as the mid-90's, but there were serious treatment associated toxicities, including two treatment-attributable deaths in one study with 218 IFN- $\alpha$  treated patients<sup>41</sup>. In general, the short half-life of these small proteins and the associated inflammatory toxicities make translation challenging, but the therapeutic benefits are undeniable; thus, the design of improved dosing regimens or novel cytokine constructs has the potential to provide transformative therapeutics. Many engineered cytokine variants are



currently under preclinical or clinical investigation, including IL-15 superagonist<sup>42,43</sup>, engineered IL-2 variants<sup>9,44,45</sup>, and synthetic constructs<sup>46</sup>.

### ***Anti-tumor monoclonal antibodies***

Monoclonal antibodies (mAbs) against targets expressed by tumor cells have been approved for almost 20 years<sup>47</sup>. Many of these were designed originally to block oncogenic signaling pathways, but it has come to light in recent years that innate effectors that express receptors to bind the Fc region (FcγRs) can play a significant role in mediating anti-tumor effects in treatment with anti-tumor mAbs<sup>47</sup>. Tumor cells coated in antibody can be eliminated via complement-mediated lysis or antibody-dependent cellular cytotoxicity (ADCC), a process by which crosslinking of FcγRs results in the release of cytotoxic granules that contain perforin and granzyme by effectors like NK cells<sup>47</sup>. Antibodies also form an effective bridge to adaptive immunity, as antibody-opsionized antigen is effectively cross presented to prime *de novo* CD8<sup>+</sup> T cell responses<sup>48,49</sup>. Anti-tumor mAbs are discussed in further details in the last section of this chapter, entitled “Combination immunotherapies: roles for innate immunity.”

### ***Intratumoral innate immunity immunomodulators***

Tumors are immunosuppressed, and the goal of this class of therapeutic is to re-polarize the microenvironment to promote immunity for clinical benefit. This class of therapeutic is very heterogeneous, and includes stimulator of interferon genes (STING) pathway agonists, toll-like receptor (TLR) agonists, oncolytic viruses, and others (including Coley’s toxins), and effective tumor rejection often generates systemic adaptive anti-tumor immunity.<sup>50</sup> One challenge associated with this class of therapy is that the tumor must be accessible for injection, but local administration may allow for the minimization of systemic inflammatory side effects. A recent review<sup>51</sup> presented an extensive list of ongoing clinical trials for this class of therapy.

In this introductory chapter, we seek to motivate the application of engineering to enhance vaccination in the section entitled “Engineering new approaches to cancer vaccines,” which directly relates to Chapters 2 and 3 of this thesis. Then we give an overview of combination immunotherapy approaches with a focus on recruiting both innate and adaptive immunity to set the stage for Chapters 4 and 5 in the section entitled “Combination immunotherapies: roles for innate immunity.” Note that there are also chapter-specific introductions with a more focused overview of relevant literature; these are meant to provide a general overview to motivate the thesis.

## 1.2 Engineering new approaches to cancer vaccines

Adapted from: Mehta NK\*, Moynihan KD\*, and Irvine DJ. Engineering new approaches to cancer vaccines. *Cancer Immunol Res.* 2015 Aug; 3(8): 836–843. DOI:10.1158/2326-6066.CIR-15-0112.

### Motivation for cancer vaccine engineering

Therapeutic vaccination is one of the oldest and most studied concepts in cancer immunotherapy. Yet, in contrast to prophylactic vaccines against infectious disease, which have had a major impact on public health, therapeutic vaccines against cancer have generally been much less successful, and only a single cancer vaccine has been FDA approved to date<sup>35,36</sup>. This is likely due to a variety of factors, including a relative paucity of truly foreign antigens expressed by tumor cells, lack of infection-associated inflammatory cues that drive productive immunity, chronic antigen exposure, the presence of a highly immunosuppressive microenvironment in solid tumors, and our as yet still poor understanding of how to induce strong and sustained T-cell-mediated immune responses in humans. However, there are at least three reasons why cancer vaccines should see renewed interest as part of the cancer immunotherapy armamentarium, based on recent rapid advances in the field: First, the advent of clinical-stage therapeutics that can directly influence the immunological status of the tumor microenvironment, such as checkpoint blockade antibodies<sup>7</sup>, regulatory T-cell-modulating chemotherapy<sup>52</sup>, and IDO inhibitors<sup>53</sup> (to name a few), now provide a number of ways to overcome immunosuppressive pathways in patients. Secondly, the availability of an ever-growing array of targeted drugs that can dramatically (but transiently) lower tumor burden provides a window of opportunity for vaccines to act in a setting of minimal disease, and some of these drugs may act synergistically with the immune response<sup>54</sup>. Lastly, powerful genomic sequencing capabilities are enabling the possibility of patient-specific vaccines targeting defined neoantigens, which have the potential for alleviating the safety and efficacy challenges of targeting unmutated self antigens<sup>55-57</sup>. Indeed, numerous clinical trials are currently underway with vaccines targeting these neoantigens in melanoma<sup>37,38</sup>, and improving the magnitude of T cell response that can be primed against tumor neoantigens will likely increase the impact seen clinically with such approaches. Altogether, these recent developments in cancer therapy strongly motivate renewed efforts to develop effective therapeutic cancer vaccine approaches.

How might we enhance the vaccines themselves to enable therapeutic immunization to reach its full potential in this new era of cancer immunotherapy? First is the issue of vaccine

potency, as measured by the number, functionality, and avidity of antigen-specific T-cells induced by cancer vaccines. A number of experimental and licensed infectious disease vaccines induce robust multifunctional CD4<sup>+</sup> and CD8<sup>+</sup> T-cell responses in humans that can be detected directly *ex vivo* and measured even by relatively low-sensitivity methods like peptide-MHC tetramer staining<sup>58,59</sup>. By contrast, with a few exceptions<sup>60,61</sup>, the response to cancer vaccines is often only robustly detected by expanding/stimulating patient T-cells over 1-2 weeks *ex vivo*<sup>62-64</sup> – a direct indicator of the low frequency of responding cells. These results may be partly due to issues of tolerance to self-antigens and systemic immunosuppression in cancer patients, but also may reflect the common use of minimal-epitope peptide vaccines and weak adjuvants which have known immunological shortcomings<sup>65</sup>. Equally important is for vaccines to be capable of promoting T-cell responses enriched in high-avidity, polyfunctional T-cells with high proliferative capacity that avoid induction of an exhausted/terminally-differentiated phenotype. Finally, devising vaccine strategies that prime effective trafficking of effector cells to tumor sites is critical, which in cases such as mucosal tumors, could be directly influenced by vaccines that program expression of appropriate tissue homing receptors<sup>66</sup>. Thus, a number of strategies exist to enhance current vaccine approaches to increase the efficacy of therapeutic anti-tumor immune responses.

There are many ways to improve therapeutic vaccines rooted in traditional vaccinology principles such as microbial vector development, molecular biology, and adjuvant design, but in this section, we will review promising recent preclinical and early clinical developments derived from approaches based in immune engineering—bringing methods from chemistry, chemical engineering, materials science, and biological engineering to bear on the problem of therapeutic vaccine design. Such approaches are particularly well suited to augmenting vaccines based on subunit antigen (defined protein, peptide, or polysaccharide epitopes) and tumor cell lysate-based vaccines, and we focus on these two ubiquitous classes of cancer vaccine antigens.

## **Targeting vaccines to lymph nodes**

A very basic issue in generating robust immunity with cancer vaccines is efficient delivery of vaccine components to lymphoid tissues, the sites of immune response orchestration. Nearly all vaccines are administered parenterally, either intramuscularly or subcutaneously. Following injection of soluble protein/peptide vaccines, antigen arrives in draining lymph nodes in two phases: first, lymph node-resident dendritic cells (DCs) directly access antigen as it drains through afferent ducts, and present antigen to T cells to initiate an

immune response. This response is sustained during the second phase, when migratory DCs or monocytes that have phagocytosed additional antigen at the site of injection arrive in the lymph node<sup>67</sup>. In some settings, however, only the first phase may be necessary: In mice vaccinated with protein antigens fused to an anti-CD205 antibody to target cross-presenting lymph node-resident DCs, migratory DC depletion actually enhanced T cell priming<sup>68</sup>. Migratory DCs were shown to contain expression signatures enriched in genes associated with immune suppression, compared to cross-presenting lymph node-resident DCs. That lymph node delivery is key to vaccine potency is shown by studies of intra-lymph node injections, which demonstrated that peptide or DNA vaccines injected directly into LNs are 100-fold more potent than the same vaccine administered subcutaneously<sup>69,70</sup>.

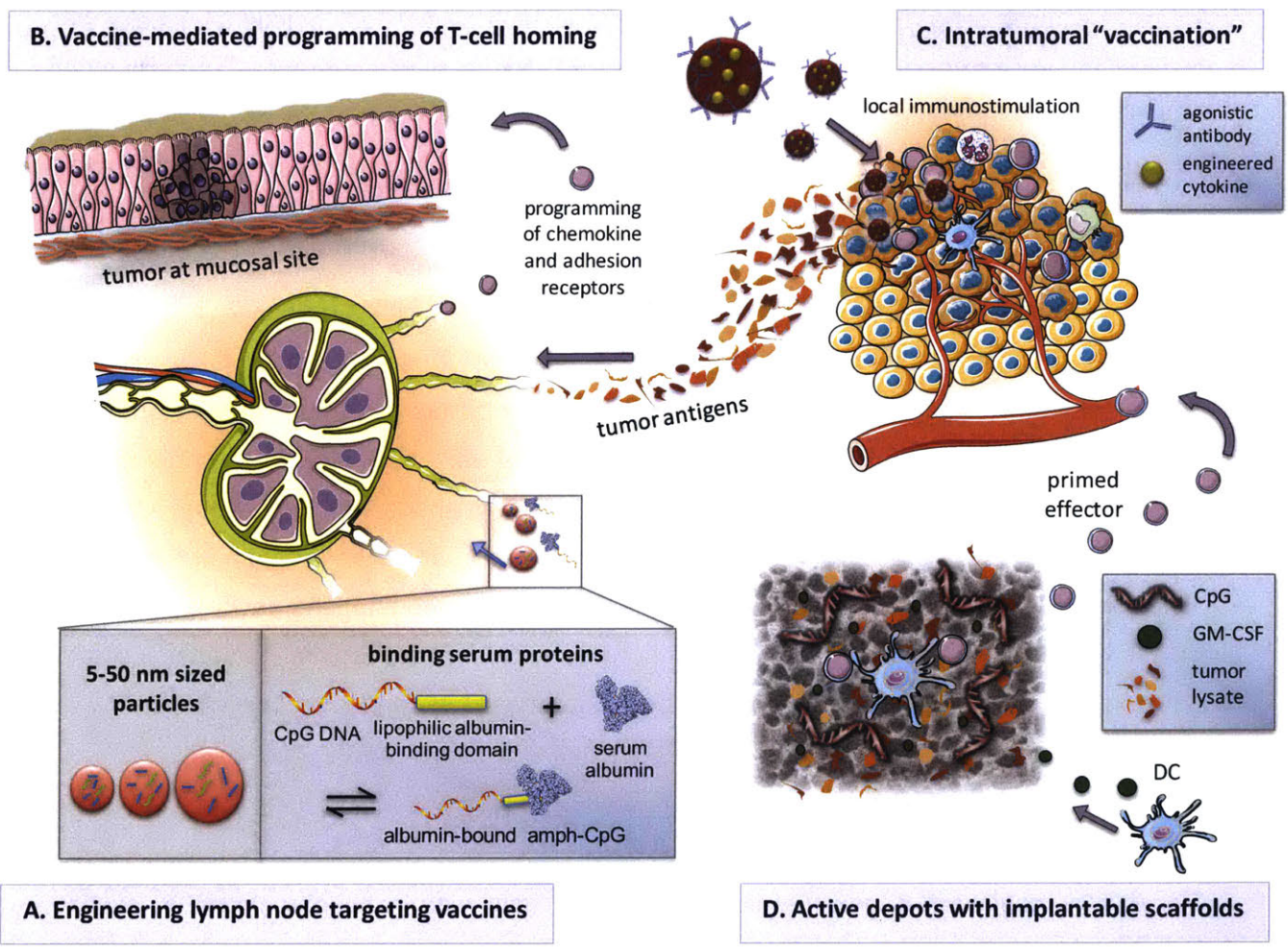


Figure 1 **A schematic showing four strategies for engineering more effective cancer vaccines.** In (A), vaccines are engineered to drain efficiently to lymph nodes. Particles between 5-50nm drain more effectively than particles of other sizes, and molecular vaccines can be engineered to bind serum proteins to meet this size criteria for effective lymphatic drainage. In (B), T-cell homing to specific sites can be directed by the route of administration. For sites like the lung and the gut, engineering of biomaterial carriers may facilitate delivery. Immunomodulatory therapies can be introduced directly into the tumor to generate anti-tumor responses, shown in (C). Implantable biomaterial scaffolds can be loaded with tumor antigens and inflammatory signals to create and in-situ dendritic cell vaccine, shown in (D).

Although the fate of injected vaccines is a complex interplay of numerous parameters, the physical size of vaccine components— whether they be particulates or individual molecules— plays a significant role in determining the outcome, as shown in Figure 1A<sup>71</sup>. Molecules or particles injected in tissue can be cleared by either entering the blood or the lymph. In classic studies in sheep comparing the biodistribution of a series of molecules of varying molecular weight from tissues following injection, Supersaxo and colleagues showed that large proteins preferentially convected to the lymph node rather than being lost to systemic circulation<sup>72</sup>. This is because the lymphatic endothelium has valve-like openings enabling the entry of large particles, while the capillary endothelium is lined by an uninterrupted basement membrane that blocks the transit of large macromolecules. A linear correlation is observed between molecular weight and the fraction of lymph node (LN) uptake up to a threshold of 45 kDa (corresponding to a size of approximately 4-5 nm in diameter for a globular protein), at which point nearly 100% of protein is delivered to the lymph and downstream draining lymph node<sup>73</sup>. Consistent with this finding, unformulated peptides<sup>10</sup>, molecular adjuvants<sup>10,74,75</sup>, and small protein antigens show very poor uptake in lymph nodes, and soluble small-molecule adjuvants often show significant systemic inflammatory toxicity<sup>10,74,75</sup>. While both preclinical and clinical studies have often sought to solve this problem by administering vaccines in “depot”-based adjuvants such as incomplete Freund’s adjuvant, it has been shown that passive, non-inflammatory depots of antigen at the injection site become a decoy for effector cells that leads to deletion of the very T-cells that are meant to be primed by the vaccine<sup>76</sup>.

The size-dependent physiology of lymphatic trafficking has motivated studies of synthetic nanoparticles larger than individual proteins as carriers to efficiently deliver small antigens/molecular adjuvants to the lymph node. Maximal lymph node targeting is a size optimization problem as particles that are larger than the average pore size in the extracellular matrix may become entrapped in the tissue rather than convecting to lymphatics. A series of studies by three different groups demonstrated that nanoparticles with diameters under ~50 nm target lymph nodes much more efficiently than larger particles. Reddy et al. injected labeled 20 nm, 45 nm, and 100 nm poly(propylene sulfide) nanoparticles intradermally and sampled the draining lymph nodes up to 120 hours later; while the 20 nm and 45 nm ultra-small nanoparticles were present in the lymph node throughout the time points sampled, 100 nm particles could not be detected<sup>77</sup>. Manolova, et al.<sup>78</sup> and Fifis et al.<sup>79</sup> reached similar conclusions using virus-like particles or synthetic polystyrene nanoparticles of different sizes as carriers for vaccines, demonstrating that particles in the 20-40 nm size range were much more effective for lymph node delivery and subsequent vaccine responses than larger particles. Nanoparticles can



also be used to deliver potent molecular adjuvants to lymph nodes, and promising data in both mice<sup>75,80-85</sup> and non-human primates<sup>81,86</sup> suggests this is an approach that should be moved toward clinical testing, especially for small molecule adjuvants where such approaches can increase both the safety and potency. Finally, on arrival in lymph nodes, nanoparticles have the potential to impact multiple aspects of antigen processing and presentation by enabling antigen and adjuvant to be co-delivered into recipient antigen presenting cells<sup>87</sup>, promoting cross-presentation of antigen<sup>80,88</sup>, and acting as intracellular/extracellular vaccine depots<sup>88,89</sup>. An exciting recent study demonstrated a method to coat polymer nanoparticles with native tumor cell-derived plasma membranes, leading to cross-presentation of tumor membrane-associated antigens, providing a means to combine complex tumor-derived antigen mixtures with particle-based lymph node targeting<sup>90</sup>.

A second strategy to target vaccines to lymph nodes is to exploit reversible binding to proteins naturally meeting the size-dependent criteria for effective lymphatic uptake. For example, albumin, the most prevalent protein in blood and interstitial fluid, is a 66 KDa globular protein with a hydrodynamic diameter of approximately 5 nm– and thus traffics one way from the blood to the lymph in the interstitial space. Liu et al. conjugated peptide antigens and CpG adjuvant to saturated hydrocarbon lipid tails chosen to promote binding to fatty acid-binding pockets of albumin<sup>10</sup>. Importantly, these conjugates were comprised of an albumin-binding tail linked to the antigen via a highly water soluble poly(ethylene glycol) (PEG) chain. This PEG spacer solubilized the conjugates and prevented the conjugate from stably inserting in cell membranes, an important distinction from traditional lipopeptide vaccines. Upon injection, these vaccine amphiphiles bound to albumin, leading to >10-fold increases in lymph node accumulation relative to the parent vaccine molecules. In therapeutic melanoma and cervical cancer tumor models, lipid-conjugated vaccines were able to significantly delay growth of established tumors at doses where traditional peptide/adjuvant vaccines were completely ineffective.

### **Vaccine-Mediated programming of T-cell homing to tumor sites**

It has been observed in many clinical studies that the presence of circulating tumor antigen-specific T-cells does not correlate with clinical outcome, and this is consistent with the expectation that activated T-cells must home to tumor sites to impact disseminated disease. Cancer vaccines can impact this phase of the immune response by ensuring induction of appropriate tissue-homing receptor profiles on newly primed tumor-specific lymphocytes, as

seen in Figure 1B. A key strategy to control tissue-specific effector cell trafficking is via choice of vaccination site, because dendritic cells in lymph nodes draining different tissue sites express factors regulating the expression of tissue homing receptors on T-cells primed in these sites. Thus, T-cells primed in mediastinal lymph nodes express  $\alpha_4\beta_1$  integrins and home to the lungs; DCs in skin-draining lymph nodes induce T-cells to express cutaneous lymphocyte antigen (CLA) and CCR4 to home to the skin; and DCs of the gut-associated lymphoid tissues secrete retinoic acid, programming expression of  $\alpha_4\beta_7$  and CCR9 on T-cells for homing to the gut lamina propria<sup>91</sup>. While these tissue-specific homing patterns have all been defined in the setting of T-cell trafficking to normal tissues, they are also critical in the therapeutic setting of effector T-cells homing to tumor sites. For example, in orthotopic tumor models of head and neck and lung cancer, Sandoval, et al. demonstrated that mucosal, but not intramuscular, delivery of vaccines can promote CD8<sup>+</sup> T cell-mediated rejection of mucosal tumors<sup>92</sup>. Human papillomavirus 16 E7-expressing TC-1 cells were engrafted in the submucosal lining of the tongue or in the lung as model mucosal tumors. Shiga toxin 1 subunit B (STxB) E7 fusions in combination with  $\alpha$ GalCer adjuvant were administered intranasally or intramuscularly, and while both vaccines generated systemic CD8<sup>+</sup> T-cell responses, intranasal delivery resulted in more efficient tumor clearance in both models. Mechanistically, this was traced to mucosal imprinting of activated antigen-specific T cells, as measured by CD49a and CD103 expression, which allowed for effective homing and infiltration at the tumor site. Thus, strategies to enhance local tissue immunization may have a significant impact on the efficacy of cancer vaccines.

To this end, nanoparticle formulations discussed above for parenteral immunization have also been shown to enhance vaccine antigen/adjuvant uptake across pulmonary and nasal mucosa, which could promote tumor-homing T-cell responses in the setting of lung carcinoma, head and neck cancer, and treatment of lung metastases in a variety of other cancers. Nanoparticles can co-deliver antigen and molecular adjuvants to dendritic cells in the airway mucosa and promote uptake by DCs prior to mucociliary clearance<sup>83,93,94</sup>. For example, exploiting the high density of dendritic cells lining alveoli in the lungs, pulmonary vaccination with lipid nanocapsules carrying a protein antigen and Toll-like receptor agonists led to increased persistence of antigen in the lungs 24 hours after administration, and subsequently greatly increased trafficking of antigen to lung-draining lymph nodes several days later. This enhanced antigen delivery translated to >10-fold increases in T-cell priming compared to soluble forms of the same antigen and adjuvant, and enabled pulmonary nanocapsule vaccination to be 100% protective in a lung metastasis model, compared to only 20% protection in the equivalent soluble vaccine<sup>95</sup>. In a similar vein, intranasal vaccination with antigen-carrying

poly( $\gamma$ -glutamic acid) nanoparticles enhanced therapeutic protection against melanoma lung metastases<sup>96</sup>. Pulmonary vaccination with PEGylated poly(propylene sulfide) nanoparticles conjugated to antigens using a reduction-sensitive linker combined with soluble CpG has been shown to enhance antigen uptake in lung-draining lymph nodes and subsequent lung-homing antigen specific T-cell populations<sup>97,98</sup>. Thus, several types of nanoparticle formulations have shown efficacy in enhancing mucosa-homing T-cell responses and mucosal anti-tumor immunity.

Analogous to pulmonary vaccination for protection of airway mucosal tissues, oral vaccination may facilitate anti-tumor immunity in the gastrointestinal tract, and could thus help protect against cancers of the throat, stomach, intestine, and colon. A non-obvious benefit of vaccinating the gastrointestinal tract is that T cell priming in the lymphoid organs of the large intestine can induce protection of rectal and vaginal mucosa, which are difficult to vaccinate directly<sup>99</sup>. The design of effective oral vaccines that reach the large intestine has been challenging largely because of the low pH and destructive enzymatic activity characteristic of the gut. To solve this problem, Zhu et al. developed PLGA nanoparticles that encapsulated peptide antigen and three TLR agonists: MALP-2, poly(I:C), and CpG<sup>99</sup>. These nanoparticles were subsequently encapsulated within anionic pH-responsive polymer capsules. The capsules were designed to have mean diameters  $> 10 \mu\text{m}$  to prevent non-specific phagocytosis and uptake by Peyer's patches in the small intestine, and to dissolve at pH values greater than 7, characteristic of the terminal ileum of the large intestine, to allow for vaccine release only in this localized region of interest. Significantly stronger T cell responses in the large intestine were generated when capsules of appropriate pH responsiveness were used as a coating rather than an alternative polymer that dissolved at more acidic pH. This general delivery strategy may thus hold potential in the treatment of colorectal tumors and establishes a paradigm for targeting other regions of the GI tract. Together, these studies demonstrate that physically programmable properties of particulate vaccine carriers can be used to specifically target different organs to target the immune response to the required site of protection.

### **Exploiting the tumor site as an antigen source**

A seminal observation in cancer immunology was Dr. William Coley's discovery in 1893 that repeated intratumoral injection of bacteria could induce tumor rejection. Nearly one hundred years later, trials in humans found that intratumoral administration of BCG in metastatic melanoma lesions resulted not only in the regression of 90% of the injected lesions, but also



17% of distal tumors<sup>100</sup>. Although intratumoral injections of immunomodulators are intended to be local treatments, in many cases they can generate a systemic immune response capable of targeting distal tumors in a vaccine-like manner, turning the tumor itself into an *in situ* vaccine, as depicted in Figure 1C. Importantly, this strategy does not depend on the discovery of tumor-specific antigens, and instead exploits the tumor itself as a source of antigen.

Local administration of diverse immunostimulatory agents to an accessible lesion has been effective at promoting systemic tumor rejection in animal models and humans. For example, intratumoral injection of CpG, anti-OX40, and anti-CTLA4 in mouse lymphoma models can eradicate regulatory T-cells from tumors<sup>101</sup>. In humans, topical application of a cream prepared with 5% imiquimod, a TLR7 agonist, has been shown to induce 80% histological clearance in human patients with superficial basal cell carcinoma<sup>102</sup>. In some cases, local administration of immunomodulators increases susceptibility to subsequent systemic therapy. In mouse melanoma models with tumors on both the right and left flank, Zamarin et al. showed that oncolytic virus injections into one tumor increased lymphocytic infiltration even in the contralateral tumor, improving the efficacy of systemically administered anti-CTLA4 therapy<sup>103</sup>. Analogously in humans, early clinical trials suggest that stereotactic body radiotherapy, where radiation is precisely delivered to tumor sites to enhance local inflammation, can improve responses to IL-2 therapy in patients with metastatic lesions<sup>104</sup>. Despite the promise of intratumoral injections in promoting anti-tumor immunity, one deficiency in intratumoral administration of soluble therapeutics is that locally-applied drugs can still rapidly leak into the systemic circulation. This has been observed in many studies in small animals<sup>105-107</sup> and with immunotherapy in humans, where intratumorally-injected cytokines have been measured in the systemic circulation within minutes<sup>108</sup>. Such systemic dissemination both weakens the potency of the therapy by clearing the drug from the tumor and gives rise to systemic inflammatory toxicity.

To promote such "*in situ* vaccination", biomaterials have been designed to trap immunomodulatory molecules in the tumor environment. For example, slow-release particles or hydrogels have been injected peritumorally or intratumorally, to allow local permeation of tumors with immunostimulatory drugs released from localized depots. This has been demonstrated with biodegradable microspheres releasing IL-12<sup>107</sup> and hydrogel matrices releasing an IL-15 superagonist<sup>109</sup>, both of which led to non-toxic but potent induction of CD8<sup>+</sup> T-cell responses against treated tumors. Such approaches can enable otherwise toxic treatments to be safely administered while eliciting systemic anti-tumor immunity. For example, anti-CD137 and IL-2 administered directly into solid melanoma tumors disseminated into the systemic circulation,

inducing systemic inflammation, including IL-6 and TNF- $\alpha$  in serum and major weight loss in mice<sup>105</sup>. However, intratumoral injection of these same immunomodulators covalently anchored to liposomes prevented their dissemination outside of the local microenvironment<sup>105,106</sup>, eliminating their toxicity and enabling the drugs to remain concentrated at the tumor site for 96 hours post injection. These intratumoral immunoliposomes acted as vaccines and elicited systemic T-cell responses; mice that rejected treated tumors on one flank could also substantially delay the growth of an untreated tumor on the contralateral flank, in the complete absence of supporting systemic therapy. Thus, even relatively simple strategies can be employed to significantly alter the efficacy and safety of immunotherapeutic drugs in this setting.

### **Active depots with implantable vaccine scaffolds**

The only FDA-approved cancer vaccine to date is Provenge, an autologous cell-based therapeutic vaccine against castration-resistant metastatic prostate cancer<sup>110</sup>. Although this vaccine was shown to extend survival in prostate cancer patients by 4 months, its implementation is clinically complex, since peripheral blood is first collected from patients, shipped to a cell preparation facility, treated with antigen *ex vivo*, shipped back to the clinical site, and subsequently re-infused into the patient. Clinical trials of related processes based on the isolation of precursor cells, differentiation of these cells into dendritic cells *in vitro*, activation and antigen loading of the resulting DCs, and injection as cellular vaccines have also shown promise<sup>111,112</sup> but with the same logistical concerns. In an attempt to harness the power of DC vaccines without the practical limitations of cell therapy, several strategies have been developed to create implantable or injectable implants that would mimic this series of *ex vivo* treatment steps directly in patients. The common premise of these approaches is to employ a synthetic matrix or scaffold that when placed *in vivo* (e.g., following a minor subcutaneous implantation procedure) would release/present cues in the local tissue that enable the processes of attracting, differentiating, activating, and antigen loading dendritic cells, which would subsequently traffic to local draining lymph nodes to initiate an anti-tumor immune response. This concept leverages a large body of experience from the tissue engineering and regenerative medicine field, where biomaterial scaffolds designed to attract and program cell fate have been studied for more than 20 years<sup>113</sup>. These biodegradable scaffolds may release immunomodulatory agents with defined spatial and temporal profiles that can be engineered by manipulating the material properties of the implant. Multiple agents can be loaded into a single

immunomodulatory scaffold, including antigen, adjuvant, and cytokine support, and they can be designed to promote cell recruitment and modulation within the scaffold itself.

One of the first reports of a DC-programming vaccine system utilized millimeter scale polymer rods that released the chemoattractant CCL19 along with tumor lysate as an antigen preparation<sup>114</sup>. These attractant-releasing implants recruited antigen presenting cells to the vaccine site, which correlated with enhanced tumor regression in a therapeutic lung carcinoma model. More recently, Ali et al. designed centimeter-scale porous polymer disks composed of the same polymer used in resorbable sutures (poly(lactide-co-glycolide) or PLGA); these disks were loaded with 3 components: GM-CSF, CpG DNA, and tumor lysate, as shown in Figure 1D<sup>115</sup>. These scaffolds released GM-CSF to recruit and differentiate dendritic cells into the structure and CpG as a danger signal to activate DCs internalizing antigens in the tumor lysate. These scaffolds were capable of protecting mice from B16F10 melanoma challenge in a prophylactic setting. In a follow up study, this scaffold vaccine, in combination with vaccination using irradiated tumor cells transduced to express GM-CSF, was shown to also greatly enhance protection relative to non-scaffolded vaccines or GM-CSF-producing tumor cell-based vaccination alone in the therapeutic setting, results which correlated with enhanced recruitment of plasmacytoid DCs, cross-presenting CD8<sup>+</sup> DCs, and elevated IL-12 production in the scaffold implants<sup>116</sup>. In a rat glioma model, PLGA scaffold vaccines implanted after partial tumor resection resulted in significantly enhanced survival over control blank PLGA matrices<sup>117</sup>. Efficacy in this model was only seen when scaffolds were placed next to the resection site but not within the resection site, highlighting the importance of implantation site for these implantable scaffold-based vaccines. Based on these encouraging preclinical results, this promising PLGA scaffold vaccine system was recently moved into a first-in-human phase I trial in patients with melanoma<sup>118</sup>.

A number of strategies have sought to generate an *in situ*-forming immunomodulatory depot that does not require surgical implantation like the PLGA-based scaffolds described above. In a recent report, antigen and adjuvant were mixed with chitosan and hydroxyapatite and co-injected with crosslinking agent tripolyphosphate and chondroitin sulphate via a two needle aligned injection<sup>119</sup>. These two aqueous solutions crosslinked *in vivo* to form a biodegradable hydrogel vaccine that was capable of inducing humoral responses durable for more than a year after implantation following a single injection; this type of sustained release implant may also be of interest for driving anti-tumor T-cell responses. In a second example, Kim et al. demonstrated that biodegradable mesoporous silica rods could nonspecifically coalesce to form a scaffold-like structure following subcutaneous injection<sup>120</sup>. When formulated

with GM-CSF, CpG, and antigen, these injectable scaffolds were capable of recruiting DCs and priming T-cell responses that were capable of delaying the outgrowth of OVA-expressing tumors in a prophylactic setting. While still in early stages of preclinical development, these “injectable scaffold” approaches may provide a facile strategy to repeatedly prime and boost anti-tumor immunity. Importantly, both implanted and injectable matrix-based vaccines are powerful technological platforms for examining the importance of timing, dosing, and physical localization of immunostimulatory cues on the output immune response, making these systems both potential therapeutics and valuable tools for determining how these factors quantitatively influence the immune response.

## **Outlook**

Although traditional techniques inspired by prophylactic vaccines activate immune responses, new vaccine concepts are of interest to overcome tumor antigen tolerance and tumor-induced immunosuppression in the setting of advanced cancer and to drive immune responses of the appropriate magnitude and quality to treat large metastatic tumor burdens. Approaches grounded in engineering methods for creating synthetic materials and synthesizing new molecules offer a number of strategies to enhance cancer immunotherapy and cancer vaccines in particular, including improving the delivery of vaccine components to lymphoid organs, optimally programming activated T-cells to home to tumor sites, prolonging immunomodulation of lesions following intratumoral injection, and programming sequential events in immunization from a single injectable or implantable device. Overall, such engineering-based approaches have shown great promise in pre-clinical models, and the next few years should see a number of these approaches moved into clinical testing in patients.

## **1.3 Combination immunotherapies: roles for innate immunity**

### **Introduction**

The heterogeneity of human cancers combined with the diversity of mechanisms acting in concert within established tumors to suppress the immune response make it unlikely that any single-agent immunotherapy will elicit meaningful tumor regression in a majority of patients— an expectation that has prompted the search for safe and efficacious combination therapies. The countless number of potential combination therapy permutations possible even within the existing pool of immunotherapy drugs in early clinical testing motivates the need for rational approaches to identify promising combination therapies. Progress in understanding the tumor microenvironment and anti-tumor immunity has led to the proposal that several functional steps are required for the immune response to eliminate established tumors, including blockade of immunosuppression, promotion of immune infiltration, induction of immunogenic tumor cell death, activation of antigen presenting cells, and enhancement of effector cell activity<sup>6,8,121</sup>. Identification of these target functional requirements sets the stage for designing combination treatments that address distinct barriers to tumor rejection.

Many studies have focused on combination therapies that promote complementary features of T cell activity (e.g., treatment with vaccines, antibodies blocking inhibitory receptors, and antibodies agonizing co-stimulatory receptors) or which synthetically substitute for B cells (anti-tumor monoclonal antibodies). However, natural immune responses are never based solely in adaptive immunity; innate immune cells play an important role in complementing the effector activities of CD4<sup>+</sup> and CD8<sup>+</sup> T cells, and provide unique pathways to bolster an ongoing adaptive response. In this section, we discuss pertinent features of innate responses to tumors, and examine findings from recent combination immunotherapy studies that have revealed unexpected important roles for innate immunity in successful anti-tumor therapies.

### **Roles of innate immune effectors in immunotherapy**

Cells of the innate immune system are often described as having a dichotomous role in cancer, capable of both promoting and inhibiting tumor growth, depending on the context. There is mounting evidence that innate immune effectors can be driven to impart anti-tumor immunity both directly and indirectly, given the proper cues (Figure 2). Dendritic cells (DCs) play a critical

role in immunotherapy by processing and presenting tumor antigens to T cells, and their role in anti-tumor immune responses has been discussed in recent reviews<sup>48,49,122,123</sup>. Here we focus our discussion here on four key functions of other innate immune cells that can have their own direct anti-tumor activity.

### ***Direct tumoricidal activities of innate cells***

Several innate immune cell populations, appropriately activated, can directly kill tumor cells. Natural killer (NK) cells and NK T cells can recognize cell surface stress ligands and tumor-derived glycolipids expressed by tumor cells, respectively, leading to innate cell activation and tumor cell lysis<sup>122</sup>. Macrophages can kill tumor cells through secretion of nitric oxide species<sup>124</sup>. Activated eosinophils also exhibit tumoricidal activity through the release of secretory granules containing multiple cytotoxic molecules including membrane-disrupting major basic protein and granzyme A, though mechanisms of tumor cell recognition by eosinophils remain undefined<sup>125</sup>. Thus, immunotherapies stimulating these innate immune cell populations have the potential to augment the cytotoxic activities of T cells.

### ***Antibody-mediated killing of tumor cells***

Therapeutic monoclonal antibodies have been approved for use in humans against cancer for nearly two decades<sup>47</sup>. Although many of these were originally designed to antagonize oncogenic signaling pathways, it has subsequently been shown that antibodies directed against tumor surface antigens can recruit effector functions of innate immune cells via interaction of the Fc region with FcγR-expressing cells, which can result in direct killing by multiple mechanisms. NK cells, neutrophils, and other myeloid cells can kill through antibody-dependent cellular cytotoxicity (ADCC), a process by which crosslinking of FcγRs by antibody-opsonized tumor cells results in the release of cytotoxic granules that contain perforin and granzyme<sup>47</sup>. Both neutrophils and NK cells were shown to be critical for ADCC-mediated elimination of CD52-expressing tumor cells treated with the anti-CD52 antibody alemtuzumab<sup>126</sup>, and in separate studies, FcγR-competent neutrophils were shown to be crucial effectors for antibody therapy against syngeneic melanomas in mice<sup>127</sup>. In addition to mediating ADCC, macrophages can engulf and destroy tumor cells through antibody-dependent cellular phagocytosis (ADCP)<sup>128</sup>. Further, opsonization of tumor cells with anti-tumor antibodies can also lead to complement-mediated lysis, which has been shown to be important for the mechanism of B cell depletion with the anti-CD20 mAb rituximab<sup>129</sup>. In addition to promoting direct killing, antibodies can form

a crucial bridge between these innate responses and adaptive immunity through DCs, which efficiently cross-present antibody-opsonized tumor antigens<sup>48,49</sup>.

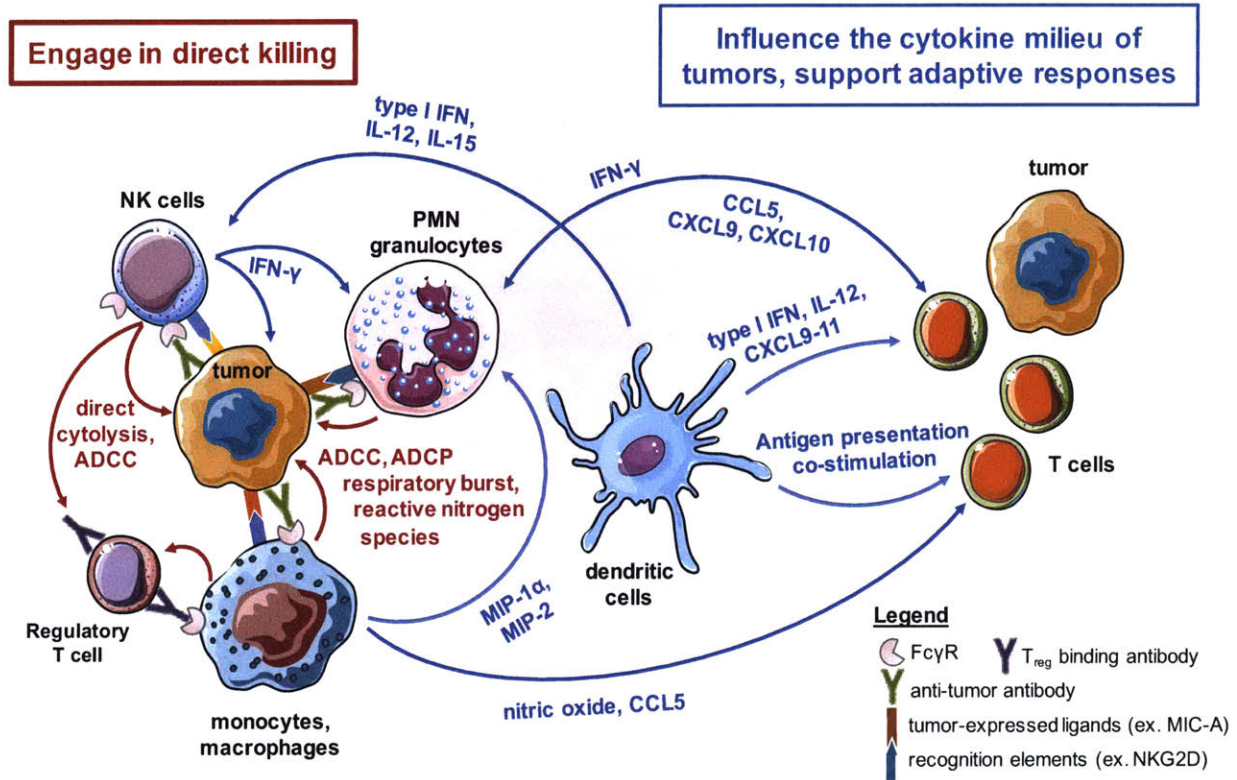


Figure 2: **Roles for innate immune effectors in anti-tumor immunity.** Innate immune effectors including NK cells, polymorphonuclear granulocytes like neutrophils and eosinophils, macrophages, and monocytes can engage in direct tumoricidal activity or exert Fc-mediated effector functions against antibody-opsonized tumor cells utilizing multiple mechanisms (red). In therapies with antibodies against targets overexpressed by T<sub>reg</sub>s, like anti-CTLA-4, these Fc $\gamma$ R-expressing effectors may also deplete intratumoral T<sub>reg</sub>s. Tumor-infiltrating innate immune cells may also secrete factors that modulate the cytokine and chemokine milieu of the tumor (blue).

### Shaping the microenvironment of tumors

Innate immune cells can also play an important role in shaping the cytokine and chemokine milieu of the tumor microenvironment, thus influencing DC activation and differentiation of effector T cells<sup>122</sup>. Tumor-infiltrating neutrophils have been shown to engage in pro-immunity cross-talk with T cells, secreting inflammatory factors and expressing co-stimulatory molecules that bolster T cell function and proliferation in a feed-forward loop<sup>130</sup>. Intratumoral innate leukocytes can also undergo productive cross-talk with other innate cells. For example, activated eosinophils promote polarization of intratumoral macrophages toward an

M1 phenotype<sup>131</sup>. In cetuximab-treated head and neck cancer (HNC) patients, NK cells were shown to enhance therapy through interactions with DCs resulting in maturation and priming of anti-tumor CD8<sup>+</sup> T cells<sup>132</sup>. This NK-DC cross-talk relied on the interaction of FcγRIIIa on NK cells with antibody-opsonized EGFR<sup>+</sup> tumor cells, cytokines released by the cetuximab-activated NK cells, and NKG2D-MICA engagement, which in concert resulted in enhanced DC maturation and cross-presentation to prime EGFR-specific T cells.

Additionally, there is mounting preclinical evidence that checkpoint inhibitors targeting molecules expressed at high levels by regulatory T cells (T<sub>reg</sub>S), such as cytotoxic T-lymphocyte-associated protein 4 (CTLA-4), glucocorticoid-induced TNFR-related protein (GITR), and OX40, may exert their antitumor activity in part by depleting intratumoral T<sub>reg</sub>S, relieving immunosuppression within the tumor and allowing for immune-mediated tumor destruction. This selective T<sub>reg</sub> depletion is enacted via ADCC and/or ADCP by innate immune effectors, and requires an activating antibody isotype. This first demonstrated for anti-CTLA-4: effective treatment markedly reduced intratumoral T<sub>reg</sub>S, and depletion was mediated by FcγR-expressing macrophages<sup>21-23</sup>. This phenomenon was also expanded to include anti-GITR and anti-OX40 antibodies as well<sup>23,133</sup>.

### ***Recruitment of immune cells to tumors***

A final important role of innate cells in the immune response to tumors lies in their capacity to promote additional leukocyte migration to tumors, mediated by several complementary activities. Macrophages polarized toward an M1 phenotype secrete nitric oxide species that activate endothelial cells and chemokines that together promote the recruitment of T cells to tumors<sup>134</sup>. Activated eosinophils secrete inflammatory chemokines and also promote normalization of tumor vasculature, which further augments T cell recruitment to tumors<sup>131</sup>.

### **Combination treatments recruiting innate and adaptive immunity**

The multiple functions of innate immune effectors in the setting of cancer described above motivate the design of combination immunotherapies that leverage their activities to enhance tumor immunity. A number of combination treatments have now been found to have important innate immune stimulatory features that contribute in important ways alongside adaptive immune effectors to control tumor progression.



### ***Combinations employing anti-tumor antibodies***

Due to their ability to recruit multiple innate immune cell types and enhance cross-presentation, anti-tumor monoclonal antibodies (mAbs) have been incorporated into a number of combination immunotherapies. Phagocytosis of antibody-opsinized cells is restrained by tumor cell expression of the self-recognition signal CD47, but immunotherapies combining anti-tumor mAbs with an engineered high affinity form of the natural ligand for CD47 (SIRP- $\alpha$ ) were shown to elicit synergistic increases in tumor cell phagocytosis *in vitro* and *in vivo*<sup>135</sup>. Carmi et al. demonstrated that passively transferred allogeneic Ig antibodies could opsonize tumors and lead to their eradication, if tumors were also treated by intratumoral administration of a TLR3 agonist or CD40L combined with TNF- $\alpha$  to activate tumor-associated DCs<sup>136</sup>. Though this study focused on the role of antibodies in promoting cross-presentation of antigen by DCs, the initial step of tumor killing/antigen release following opsonization was likely dependent on innate immune-mediated tumor killing. Antibody-drug conjugates (ADCs) introduce additional pathways for synergy with immunotherapy agents. Treatment with trastuzumab-DM1, an anti-Her2/maytansine derivative ADC, elicited T cell infiltration in orthotopic murine Her2-expressing breast tumors as well as patient breast tumors. Motivated by these observations and the DC-activating properties of a drug related to DM1, this ADC was combined with checkpoint blockade (anti-CTLA-4 + anti-PD-1), leading to a dramatic reshaping of the composition and phenotypic status of TILs in the murine model<sup>137</sup>: Conventional T cells increased in frequency in treated tumors, but also  $\gamma/\delta$  T cells, NK cells, and NK T cells; tumor-associated macrophages increased PD-L1 expression but substantially decreased arginase expression. Despite these significant alterations in the innate immune composition of treated tumors, the mechanistic role of innate cells in this therapy were not explored.

### ***Combination therapies reprogramming the tumor microenvironment via innate immune cells***

Immunotherapy regimens aiming to drive T cell responses against tumors are often limited by the lack of activated antigen presenting cells in tumors and tumor-draining lymph nodes<sup>136</sup>. To this end, intratumoral treatment with agonists of pattern recognition receptors and other innate danger sensors expressed by DCs and macrophages has been successfully used to substantially reshape the number and phenotype of tumor infiltrating leukocytes. For example, intratumoral injection of a lipid-conjugated TLR7 agonist designed for retention at a local injection site led to anti-tumor efficacy in several tumor models, dependent in part on IFN- $\gamma$ , CD8<sup>+</sup> T cells, B cells, and tumor-associated macrophages<sup>124</sup>. TLR7 agonist therapy activated

DCs in tumor-draining lymph nodes and enhanced the recruitment of macrophages with an M1 phenotype to tumors, which were capable of direct nitric oxide-mediated tumor cell killing. Combined treatment with checkpoint blockade (anti-CTLA-4) was highly synergistic, increasing anti-tumor efficacy and eliciting systemic immunity. In a murine head and neck cancer model, treatment with anti-PD-L1 alone was ineffective, but when combined with intratumoral administration of the STING agonist  $R_p,R_p$  dithio-c-di-GMP, the combination elicited significantly more complete tumor rejections than either therapy individually<sup>138</sup>. Administration of the STING agonist increased the type I IFN signature of the tumor and draining lymph node, which was concurrent with an increase in dendritic cell transcripts for antigen processing machinery and surface expression of co-stimulatory molecules for superior T cell priming and tumor control. In a murine model of HER2<sup>+</sup> breast tumors, when the STING agonist ADU-S100 was given as an intratumoral monotherapy in a HER2-tolerant setting with transgenic neu/N mice, little efficacy was observed<sup>139</sup>. Analysis of the anti-tumor CD8<sup>+</sup> T cell responses showed defective expansion and high expression of exhaustion markers. Combination of intratumoral STING agonism with anti-PD-1 and OX-40 stimulation, however, resulted in enhanced T cell expansion and activity, resulting in complete clearance in 40% of the treated mice, demonstrating that the combination of STING agonism, checkpoint blockade, and ligation of co-stimulatory receptors can overcome tumors even in an antigen-tolerant setting.

Radiation therapy (RT) also acts to promote a pro-immune inflammatory microenvironment in tumors. Local RT activates DCs and myeloid cells via complement<sup>140</sup>, and triggers tumor-associated macrophages to secrete factors normalizing the tumor vasculature and promoting T cell recruitment to tumors<sup>134</sup>. Thus, RT combined with adoptive cell therapy showed strong synergy and enhanced survival in mouse models of pancreatic cancer<sup>134</sup>. Tumor-associated macrophages have also been targeted by immunotherapy: antibody-mediated blockade of CSF1/CSF1R was shown to repolarize tumor-associated macrophages toward a productive anti-tumor phenotype in pancreatic tumors, and this treatment was highly synergistic with anti-CTLA-4, anti-PD-1, or the combination of these two checkpoint blockade agents<sup>141</sup>.

CD39, CD73, and adenosine receptors form an interacting triangle in tumors, with the CD39 and CD73 ecto-enzymes decomposing extracellular ATP to adenosine, which acts to suppress immune reactions on binding to adenosine receptors on T cells. Despite this interrelationship, co-inhibition of CD73 via a mAb and adenosine receptor through a small molecule adenosine inhibitor was recently shown to exhibit significant synergy in blocking lung metastasis in several tumor models<sup>142</sup>. Intriguingly, this response involved expansion of

neutrophils and was strongly dependent on NK cells, neutrophils, and activating FcRs in the host.

### ***Immunotherapy agents acting on innate and adaptive immune cells in tandem***

A number of immunotherapy agents, particularly immunoregulatory cytokines, act on both adaptive and innate immune cells with anti-tumor effects. For example, agonistic antibodies against the co-stimulatory receptor CD137 stimulate both T cells and NK cells. Leveraging the observation that activated NK cells upregulate CD137 expression, Kohrt et al. demonstrated in mouse models potent synergy of anti-CD137 and the anti-HER2/neu mAb trastuzumab<sup>143</sup>, and later studies showed this observation translated to the EGFR-targeting mAb cetuximab as well<sup>144</sup>. A second prominent immunotherapy agent acting on both innate and adaptive immune cells is IL-2: IL-2 expands T cells and promotes their effector functions but also enhances NK cell sensitivity to targets, expands NK cells and indirectly expands eosinophils<sup>145</sup>. Recently, Zhu et al. demonstrated a remarkable synergy of co-therapy employing an anti-tumor antibody and a long half-life IL-2 molecule<sup>9</sup>. A coordinated network of anti-tumor immunity resulting from this therapy was established: macrophages were induced to release the chemoattractant MIP-2, which recruited FcγR-expressing neutrophils, which (along with other polymorphonuclear (PMN) cells) destroyed tumor cells via ADCC. In addition to mediating direct killing themselves, the IL-2-activated T-cells and NK cells released IFN-γ, which bolstered PMN effector function. Interrupting this coordinated network of innate-adaptive interactions, for example with cellular depletions or blocking antibodies, significantly hindered therapy. Expanding on these findings, antibody/IL-2 therapy with a potent lymph node targeting vaccine and checkpoint blockade was shown to enable complete elimination of large established tumors in several transplanted tumor models as well as regressions in a genetically-engineered melanoma model<sup>146</sup>. This four-component immunotherapy relied not only on CD8<sup>+</sup> T cells, but also on FcγR-expressing innate effectors, including neutrophils, macrophages, and NK cells. In addition to mediating destruction through ADCC and/or ADCP, an antibody-dependent vaccinal effect was observed in this combination therapy, whereby antigen spreading to T cell epitopes not included in the vaccine was detected. Thus, therapies effectively recruiting both innate and adaptive immune effectors against tumors show substantial curative potential even against established tumors.

### ***Adoptive cell transfer of innate effectors***

Adoptive transfer of T cells is showing remarkable efficacy for the treatment of some hematologic cancers, and there are many efforts underway to expand their activity for other tumor types<sup>147</sup>. The refinement of clinical pipelines for implementation of these T cell based therapies at scale may result in lower barriers to entry for cell-based therapies utilizing other immune cell types. In particular, NK cells are attractive to consider for combination immunotherapy because they can kill in a non-MHC restricted manner and their cytotoxicity can be directed using anti-tumor antibodies<sup>47</sup>. NK cells integrate inhibitory and activating signals when deciding whether or not to kill a target, and MHC class I is inhibitory to NK cells<sup>148</sup>. Because of this feature, NK cells may be particularly well suited to tackle tumors that have downregulated or lost MHC class I expression due to T cell pressure, a known mechanism of resistance to checkpoint blockade<sup>149</sup>, and should thus be considered in combination for augmenting immunotherapies that drive T cell activity.

Adoptive transfer of autologous or allogeneic activated NK cells thus far has shown somewhat disappointing outcomes clinically. In one study, melanoma and renal cell patients received autologous activated NK cells were transferred and no detectable therapeutic benefit was seen<sup>150</sup>. Although the NK cells could be detected in circulation for at least one week post transfer, analysis of the transferred NK cells showed defective *ex vivo* killing and loss of expression of the key activating receptor NKG2D. In another study, non-Hodgkin's lymphoma patients received adoptive transfer of allogeneic NK cells in combination with IL-2 and rituximab<sup>151</sup>. Successful engraftment of NK cells was only detected in 1/3 of patients treated one week following transfer, and all patients showed substantial increases in T<sub>reg</sub> numbers in response to the IL-2 treatment<sup>151</sup>. Taken together, these studies suggest that further optimization of the expansion and activation protocol, genetic manipulation, and/or the delivery of improved immunomodulators (for example, engineered IL-2 to decrease T<sub>reg</sub> expansion<sup>45</sup>) may be necessary to achieve therapeutic benefit with NK cell based adoptive transfer studies. To this end, blocking NK cell checkpoints by targeting inhibitory receptors in the KIR- or LIR/ILT-family members with blocking antibodies may prove fruitful<sup>152</sup>. Genetic manipulation may also be beneficial; NK cells have been engineered to express chimeric antigen receptors<sup>153</sup>, or separately, higher levels of CD16 and the chemokine receptor CCR7 to improve migration towards CCL19 and ADCC in combination with rituximab, demonstrating NK cells can be genetically engineered to augment trafficking and functional capacity *in vitro*<sup>154</sup>.

Another cell type to consider employing in combination immunotherapies utilizing adoptive transfer of effectors is  $\gamma\delta$  T cells. This population is often considered to fall somewhere

between innate and adaptive immunity, and they share important features with innate effectors including germline-encoded recognition elements and the ability to exert cytotoxic function in an MHC-independent manner, making them attractive for immunotherapy applications. We refer the reader to a recent review (ref <sup>155</sup>) for an overview of the use of  $\gamma\delta$  T cells in adoptive transfer strategies for the treatment of cancer.

### ***Temporal aspects of combination immunotherapy regimens***

Timing of the relative administration for each agent in combination immunotherapies can be crucial, and treatment regimens must be designed with a clear picture of the sequence of events expected in response to the combination. For example, in their studies of anti-CD137 co-therapy with the anti-HER2/neu antibody trastuzumab, Kohrt et al. demonstrated that optimal therapeutic responses occurred when the CD137 agonist was administered one day after the anti-tumor antibody (and not before or coincident with the HER2/neu mAb), due to the sequential steps of trastuzumab first binding to Fc receptors on NK cells followed by upregulation of CD137 on the responding cells<sup>143</sup>. In a three-component immunotherapy employing long half-life IL-2, an anti-tumor mAb, and interferon- $\alpha$  (IFN- $\alpha$ ), Tzeng et al. demonstrated that the timing of administration of IFN- $\alpha$ , acting as a DC maturation stimulus, was critically important for treatment efficacy<sup>156</sup>. Optimal responses were only seen when IFN- $\alpha$  was delayed following the anti-tumor mAb/IL-2 treatment; this sequential treatment allowed for a bolus of immunogenic tumor debris to be taken up by DCs, which were then matured with IFN- $\alpha$  for optimal cross-priming of tumor reactive T cells. If DCs were matured prematurely by administering IFN- $\alpha$  prior to this tumor antigen uptake, therapy failed.

### ***Combination therapies recruiting innate and adaptive immunity in the clinic***

Importantly, a number of combination immunotherapies that stimulate both innate and adaptive immunity are currently in clinical trials or have an open path to clinical testing. Innate immune-stimulatory local radiotherapy has been combined with GM-CSF, local intratumoral CpG, or anti-CTLA-4 administration in small clinical studies to increase abscopal responses in patients<sup>157</sup>. Rituximab has been combined with PD-1 blockade in a phase II trial in relapsed follicular lymphoma patients; although it was a single-arm trial, the combination was well tolerated and response rates compared favorably to previous trials with rituximab alone in similar patient cohorts.<sup>158</sup> Trastuzumab has been combined with an allogeneic cell-based vaccine and cyclophosphamide in Her2<sup>+</sup> breast cancer patients<sup>159</sup>, and the anti-CTLA-4 antibody tremilumumab has been combined with IFN- $\alpha$ 2b in stage IV melanoma patients<sup>160</sup>.

Trastuzumab-DM1 discussed above has successfully completed clinical trials in breast cancer, as have combinations of anti-CTLA-4 and anti-PD-1 in several cancers, paving the way for the promising preclinical data generated with these 3 drugs in preclinical models to be tested in patients<sup>137</sup>. Similarly, studies of combination therapy with long half-life IL-2, anti-tumor antibodies, and checkpoint blockade which elicited striking responses in melanoma models in mice could potentially be translated immediately, using low dose continuous infusion of IL-2, approved anti-PD-1 antibodies, and a melanoma-recognizing anti-TYRP1 mAb that recently completed phase I clinical evaluation<sup>161</sup>. Thus, a number of combination therapies with likely synergistic innate and adaptive immune stimulatory activity are either actively being investigated in the clinic or positioned for testing in the near future.

## **Conclusions**

Many preclinical studies and some early clinical trial data support the notion that combination immunotherapies eliciting convergent innate and adaptive immune responses may be capable of enhanced anti-tumor activity relative to therapeutic strategies focused on single effector cells or arms of immunity. Although the T cell (and possibly B cell) response to tumors provides an amplifying immune response capable of responding to changes in antigen profiles and the establishment of protective memory, in patients with existing tumors adaptive immunity will often start from a state of poorly-expanded tumor-specific populations that are actively immunosuppressed. Therapies recruiting innate immunity in concert provide an important means to rapidly alter the tumor microenvironment via immediately-responsive innate leukocytes that can be recruited in large numbers from the circulation, or through repolarization of innate cells already present in tumors. Innate immune stimulation can thus provide a supportive window for an adaptive response to be successfully initiated and subsequently supported, just as innate immunity holds infectious pathogens in check and regulates the microenvironment at sites of infection to promote successful adaptive immune-mediated clearance.

An ongoing challenge with moving these concepts into clinical testing is the potential for synergistic increases in toxicity in parallel to increases in anti-tumor efficacy, and toxicities elicited from combination immunotherapies remain difficult to predict based on single-agent trials or preclinical models. However, progress in managing patients and designing trials to safely identify functional and non-toxic doses of immunotherapy agents are rapidly improving. Compelling data on synergistic innate/adaptive-stimulatory therapies from preclinical models

motivates a continued exploration of these approaches and translation to determine which of these strategies are capable of translating to enhanced survival in patients.

## ***1.4 Scope of thesis***

Section 1.2, entitled “Engineering new approaches to cancer vaccines,” motivates Chapters 2 and 3 of this thesis. In Chapter 2, molecular vaccines are engineered to have improved lymphatic delivery by adding covalent modifications that include albumin binding domains. We demonstrate that many albumin binders enhance lymphatic drainage and the resulting immunogenicity for both antigens and adjuvants, as well as explore aspects contributing to their mechanism of action. In Chapter 3, antigens are covalently linked to cell penetrating peptides in order to enhance display on MHC class I. We survey a number of cell penetrating peptides and demonstrate priming enhancements of 10-fold for some cell penetrating peptide sequences. Section 1.3 entitled “Combination immunotherapies: roles for innate immunity” motivates chapters 4 and 5. In Chapter 4, we demonstrate a combination immunotherapy composed of four components: an extended PK IL-2, an anti-tumor antibody, a checkpoint blockade antibody, and the vaccine platform detailed in Chapter 2. We show remarkable efficacy in multiple models and explore mechanistically the properties of the resulting anti-tumor immune response. In Chapter 5, we utilize a combination immunotherapy in antigenically heterogeneous tumors and demonstrate killing of minority populations of antigen-deleted tumor cells. Finally, Chapter 6 offers a short summary of the major findings of this thesis and a brief perspective on the future of immunotherapy.

# CHAPTER 2: Enhancing T cell vaccines via albumin hitchhiking

## 2.1 Introduction

Anti-tumor T cell responses have the potential to be curative in cancer patients, but the induction of potent anti-tumor T cell responses through vaccination remains a largely unmet goal of immuno-oncologists<sup>162,163</sup>. Recent studies in which a handful of patients received vaccines against predicted neoantigens have generated significant enthusiasm in the field because they demonstrate the feasibility of identifying and immunizing against neoantigens in a patient-specific manner<sup>164,165</sup>. This exciting neoantigen vaccine movement may be even further bolstered with the introduction of next-generation vaccine platforms that enhance the magnitude of T cell responses generated. For example, the vaccine regimen implemented by Ott et al. used peptides, which are attractive due to their defined nature, relatively easy manufacturability, and favorable safety profile, but there are a number of known drawbacks, including poor lymphatic drainage and short *in vivo* half-life of linear peptides<sup>10,166-168</sup>. We have previously demonstrated that enhanced lymph node targeting of peptides can be achieved by covalently modifying peptides and molecular adjuvants with diacyl lipids (with the peptides linked through a PEG spacer, “amph-vaccines”), and this trafficking enhancement results in a corresponding increase in T cell priming<sup>10</sup>. The mechanism of action is thought to involve diacyl lipid-mediated binding of serum albumin, allowing peptides and molecular adjuvants to “hitchhike” to the draining lymph node, similar to the mechanism of action of sentinel lymph node mapping dyes used clinically<sup>169,170</sup>.

Here we expand upon the amph-vaccine, demonstrating that diverse albumin binders are capable of enhancing lymphatic drainage and resultant T cell priming when covalently linked to peptide antigens or molecular adjuvants. We show that amph-vaccines are not reliant upon the albumin-binding neonatal Fc receptor (FcRn), but amph-peptides do require processing by Batf3-expressing DCs for optimal priming. We reveal that amph-peptides are protected from degradation by serum proteases, and that conjugation with PEG is sufficient for protection. Amph-peptides are transported to many lymph nodes throughout the lymphatic chain, are presented *in vivo* for at least one week following immunization, and induce exceptional priming with a variety of adjuvants, but are incompatible with Incomplete Freund’s Adjuvant (IFA), likely



due to hampered lymphatic drainage when formulated as a water-in-oil emulsion. Trafficking studies performed in rhesus macaques demonstrate that the enhancement in lymph node uptake with amph-vaccines observed in mice is recapitulated in non-human primates. Finally, constructs designed as albumin-binding molecular antigens or adjuvants that failed to prime effective T cell responses *in vivo* are presented, along with discussion of likely modes of failure.

Taken together, these data support the use of albumin-binding as a general design criterion for improving molecular vaccines by improving stability and lymphatic distribution, resulting in enhanced and prolonged antigen presentation in the lymph node for superior T cell priming.

## **2.2 Results: Characterization of the amphiphile vaccine system**

### **Amph-peptides achieve broad lymphatic distribution and extended *in vivo* presentation**

Enhancement of presentation of an antigen *in vivo* may result from a number of distinct processes. For example, quantitatively more peptide can be taken up in a given node, presentation can occur in more lymph nodes throughout the lymphatic chain, or presentation can occur for an extended duration of time. We have previously shown using fluorescence that amph-peptides show quantitative enhancements in the direct draining inguinal and axillary nodes<sup>10</sup>, so we sought to explore if presentation of amph-peptide occurs in distal nodes or for extended durations of time. To probe for the presence of antigen, we utilized adoptive transfer of naïve pmel-1 CD8<sup>+</sup> T cells, which recognize the optimal EGP 9mer, a peptide derived from the gp100 melanoma-associated antigen in the context of H-2D<sup>b</sup>. Mice were immunized with amph-EGP, EGP peptide, or adjuvant alone. CFSE-labeled pmel-1 CD8<sup>+</sup> T cells were transferred intravenously 24h later, followed by transfer of violet-labeled pmel-1 CD8<sup>+</sup> T cells an additional 24h after that (Figure 3a). Under these conditions, the CFSE-labeled pmel-1 T cells that encounter antigen will proliferate in the node in which they first encounter antigen and serve as an effective proxy for antigen presence at 24h after immunization; the violet labeled pmel-1 T cells (which do not have sufficient time to divide) upregulate CD69 in response to antigen

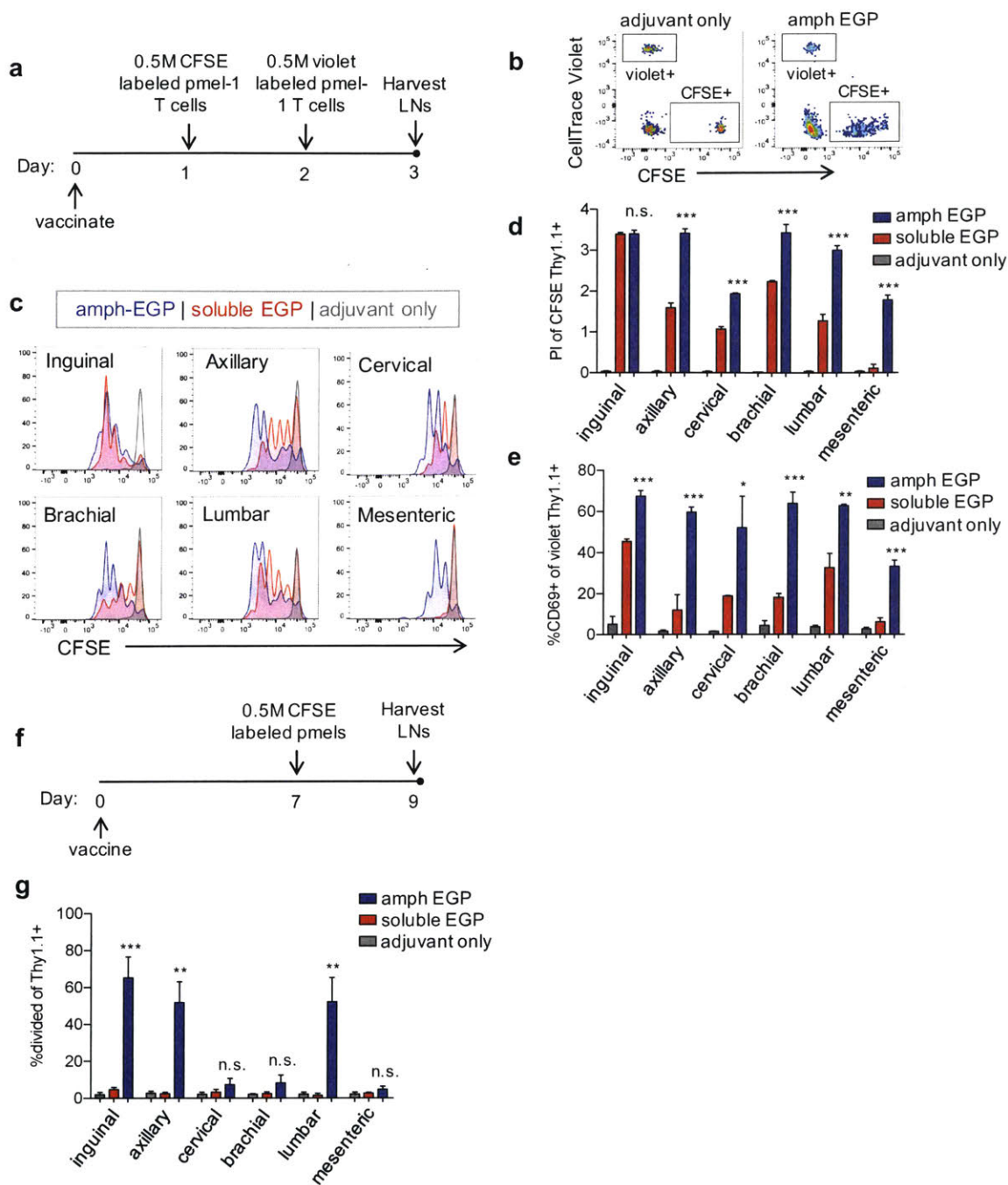


**Figure 3 Amph-peptides achieve broad lymphatic distribution and extended presentation.** **a-e**, 8-week old C57BL6/J female mice were immunized with 25 $\mu$ g c-di-GMP and either 5nmol EGP peptide, amph-EGP peptide, or no antigen. Twenty-four hours later, 0.5 million CFSE-labeled pmel-1 CD8<sup>+</sup> T cells were transferred intravenously, and 48h after immunization an additional 0.5 million CellTrace Violet labeled pmel-1 CD8<sup>+</sup> T cells were transferred intravenously. Recipient mice were euthanized and lymph nodes were isolated and processed for flow cytometry analysis 72h after immunization. Shown are the experimental timeline, **a**, and gating strategy to identify the two pmel-1 CD8<sup>+</sup> T cell transferred populations, **b**, gated on live CD8<sup>+</sup> T cells. Representative plots showing CFSE dilution among cells transferred in 24h after immunization in the indicated lymph nodes (**c**, **d**, Mean proliferation index of pmel-1 T cells transferred 24h after immunization in the indicated lymph nodes ( $n = 3$ , student's t-test between EGP and amph-EGP, representative of 3 independent experiments). **e**, Mean %CD69<sup>+</sup> of violet pmel-1 T cells transferred in at 48h in the indicated lymph nodes ( $n = 3$ , student's t-test between EGP and amph-EGP, representative of 3 independent experiments). **f-g** 8-week old C57BL6/J female mice were immunized with 25 $\mu$ g c-di-GMP and either 5nmol EGP peptide, amph-EGP peptide, or no antigen. Seven days later, 0.5 million CFSE-labeled pmel-1 CD8<sup>+</sup> T cells were transferred intravenously. Recipient mice were euthanized and lymph nodes were isolated and processed for flow cytometry analysis 48h after transfer of pmel-1 CD8<sup>+</sup> T cells. Shown are the experimental timeline, **f**, and % divided of CD8<sup>+</sup> Thy1.1<sup>+</sup> in the indicated lymph nodes, **g** ( $n = 3$ , student's t-test between EGP and amph-EGP, representative of 2 independent experiments). \* $P < 0.05$ , \*\* $P < 0.01$ , \*\*\* $P < 0.001$ .

encounter and serve to inform about antigen levels 48h after immunization (Figure 3b). Substantially higher proliferation was seen with amph-EGP compared to EGP peptide in all nodes examined except the direct draining inguinal node, where responses may have been saturated (Figure 3c-d). Consistent with this, CD69 was upregulated among pmel-1 T cells transferred in 48 hours after immunization to a much higher extent in all nodes examined with amph-EGP compared to unconjugated peptide (Figure 3e). Presentation of amph-EGP was seen even in the distal mesenteric nodes, indicating that amph-peptides achieve broad lymphatic distribution and are presented in many lymph nodes *in vivo*.

To explore the duration of antigen presentation, mice were immunized and CFSE-labeled pmel-1 T cells were transferred in 7 days later. In lymph nodes that were resected 48 hours after transfer, no proliferation in any node was seen with unmodified EGP peptide, but amph-EGP resulted in proliferation in the inguinal, axillary, and lumbar nodes, indicating that amph-peptide is presented for at least one week *in vivo* (Figure 3f-g). Thus, amph-peptides achieve broad lymphatic distribution and extended *in vivo* presentation.

### **Amph-vaccine does not rely on FcRn, short amph-peptides require Batf3 dendritic cells for optimal responses**

We wondered if there may be receptor-specific interactions that albumin-binding molecular vaccines utilize. The neonatal Fc receptor (FcRn) is the best characterized receptor for albumin, and some studies have indicated a role for FcRn in cross presentation of immune complexes<sup>171,172</sup>. The amph-vaccine showed no reliance upon FcRn, however, as FcRn<sup>-/-</sup> mice generated indistinguishable T cell responses to amph-vaccines compared to wild type mice (Figure 4a-b).

Conjugation of optimal MHC I epitopes with DSPE-PEG<sub>2000</sub> has enhanced activity for a number of antigens<sup>10</sup>, but it is unclear if this linkage changes the antigen presentation requirements of short peptides. Namely, short soluble peptides may peptide exchange and load directly onto MHC of non-professional antigen presenting cells (APCs), which may actually promote tolerance in some circumstances<sup>173-175</sup>, but amph-peptides may avoid this if their presentation requires processing by professional antigen presenting cells. Batf3<sup>-/-</sup> mice lack the transcription factor necessary to develop cross-presenting dendritic cells<sup>176</sup>, and vaccination with optimal 9-mer amph-peptide was severely compromised in Batf3<sup>-/-</sup> mice, indicating that short amph-peptides may be reliant upon cross presenting dendritic cells for effective priming (Figure 4c-d).

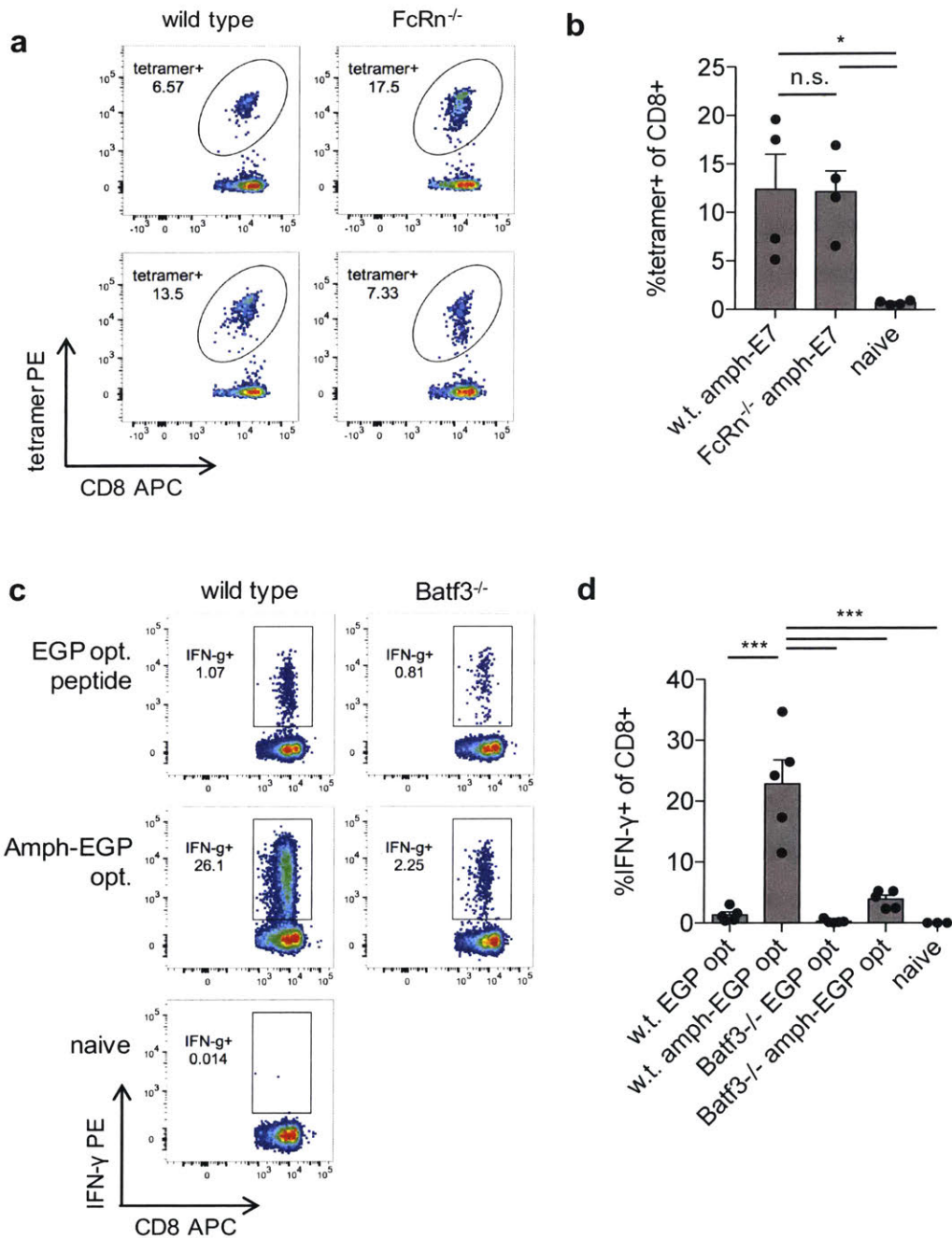


**Figure 4 Amph-vaccine does not rely on FcRn; short amph-peptides require Batf3 dendritic cells for optimal responses.** **a-b** 8- to 10-week old C57BL6/J or FcRn<sup>-/-</sup> female mice were primed on day 0 and boosted on day 14 with 10μg amph E7 peptide and 1.24nmol lipoCpG, and tetramer staining was performed on day 21. Shown are representative tetramer plots, gated on live CD8<sup>+</sup> T cells, **a**, and mean tetramer responses quantified as % tetramer<sup>+</sup> of CD8<sup>+</sup>, **b** ( $n = 4$ , ANOVA with Tukey post-test). **c-d**, 8- to 12-week old C57BL6/J or Batf3<sup>-/-</sup> female mice were primed on day 0 and boosted on day 14 with 5nmol EGP peptide or amph-EGP and 1.24nmol lipoCpG, and ICS was performed on day 22. Shown are representative IFN-γ plots, gated on live CD8<sup>+</sup> T cells, **c**, and mean T cell responses quantified as % IFN-γ<sup>+</sup> of CD8<sup>+</sup>, **d** ( $n = 5$ , ANOVA with Tukey post-test, representative of 2 independent experiments). \* $P < 0.05$ , \*\* $P < 0.01$ , \*\*\* $P < 0.001$ .

## **DSPE-PEG<sub>2000</sub> conjugation protects peptide integrity in serum; the impact of chemistries and terminus of linkage to peptide on priming**

Conjugation of molecules with PEG has been shown to enhance serum stability of peptides by protecting from serum proteases<sup>167,177</sup>. We wondered if some of the performance enhancement of amph-peptides over free peptides may be due to increased protection from serum proteases due to PEG conjugation, independent of the albumin-binding moiety. To test susceptibility to degradation in serum, fresh mouse serum was incubated with unmodified peptide, amph-EGP linked either through an N-terminal or C-terminal cysteine, or PEG<sub>2000</sub>-EGP without the diacyl lipid (linked N-terminally). CD8<sup>+</sup> T cell effectors specific for gp100 were incubated with dilutions of either serum-treated or fresh constructs, and loss in immunogenicity between fresh and serum-treated peptide constructs was quantified (Figure 5a-d). Unmodified EGP peptide showed substantial loss of activity after incubation overnight with serum (Figure 5a), but all DSPE-PEG<sub>2000</sub> and PEG<sub>2000</sub> conjugates tested showed similar activity after incubation with serum (Figure 5b-d), indicating that consistent with previous reports, conjugation with PEG<sub>2000</sub> protects from serum degradation.

To test if this translated to an enhancement in priming, mice were immunized with amph-EGP or the identical construct lacking the diacyl lipid, PEG<sub>2000</sub>-EGP. Impressively, the PEG<sub>2000</sub>-EGP retained approximately 1/3 to 1/2 of the activity of the albumin-binding amph-EGP (Figure 5e), indicating that protection from serum proteases is likely an important mechanism of improvement in activity for amph-peptides compared to free peptides. Interestingly, when mice were immunized with either N- or C-terminal DSPE-PEG<sub>2000</sub> or ABP-PEG<sub>2000</sub> constructs, both showed a trend towards N-terminal conjugation being superior to C-terminal conjugation (Figure 5f).

It may be advantageous to utilize different chemistries to link the DSPE-PEG<sub>2000</sub> to the peptide, for example, if the sequence of interest has an internal cysteine, then cysteine-maleimide chemistry may be undesirable because it could link to this internal cysteine in addition to the terminal one. To explore which chemistries can be used, constructs were synthesized where DSPE-PEG<sub>2000</sub> was either linked using cysteine-maleimide chemistry, copper-free click chemistry, or via an amide bond. When mice were immunized with these constructs, all demonstrated superior priming over unmodified peptide, and the chemistries used to link the DSPE-PEG<sub>2000</sub> were not statistically different from another (Figure 5g), indicating that multiple types of linkages can be used to synthesize amph-peptides.



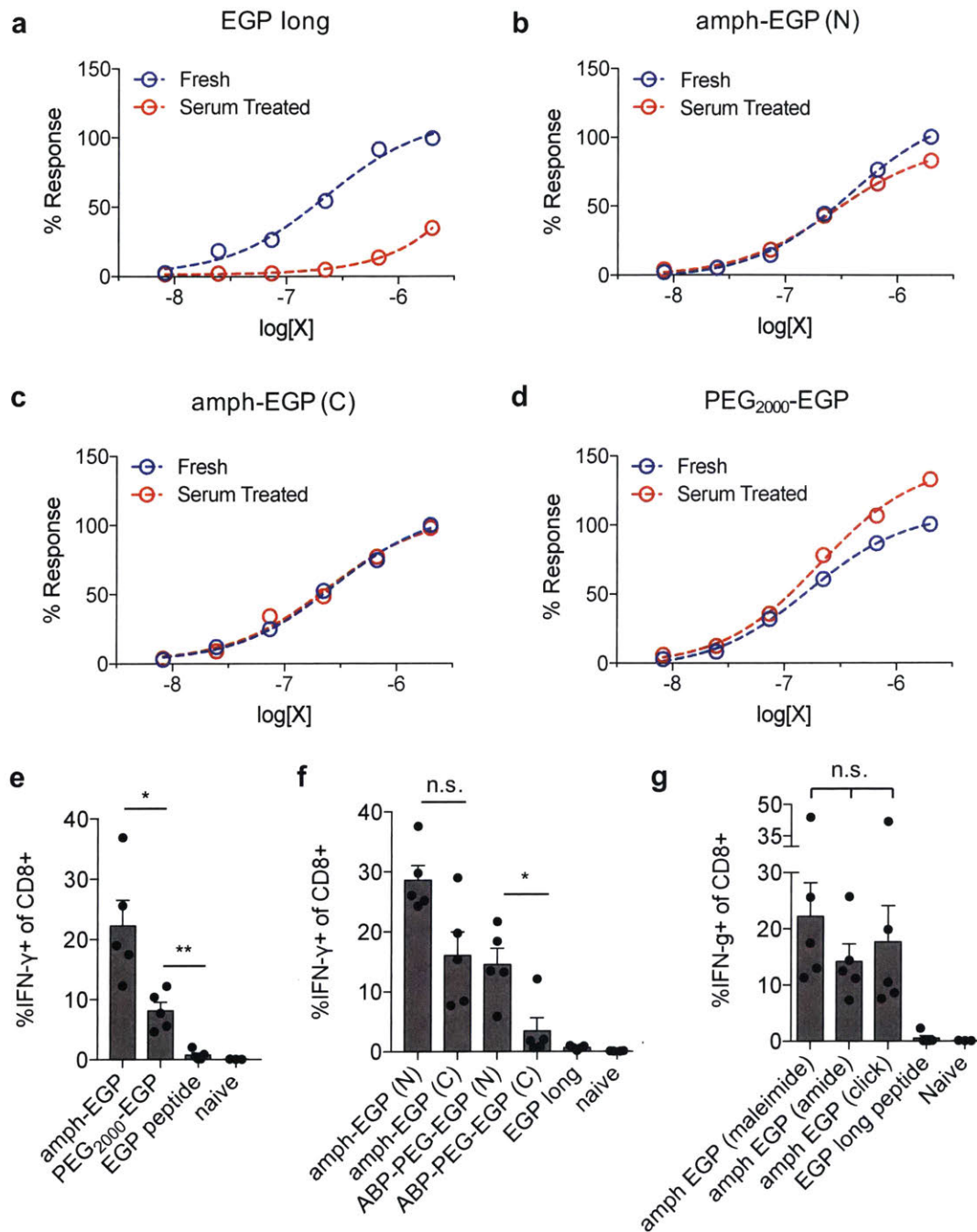


**Figure 5 DSPE-PEG<sub>2000</sub> conjugation protects peptide integrity in serum; the impact of chemistries and terminus of linkage to peptide on priming.** **a-d**, EGP peptide constructs were subjected to overnight incubation at 37°C in RPMI with 10% fresh mouse serum. Serum-treated or fresh constructs were incubated with pooled splenocytes from previously amph-EGP immunized mice for 24 hours at 37°C, with brefeldin A added at 18 hours and ICS was performed. Shown are normalized responses for EGP peptide, **a**, amph-EGP with N-terminal conjugation of DSPE-PEG<sub>2000</sub>, **b**, amph-EGP with C-terminal conjugation of DSPE-PEG<sub>2000</sub>, **c**, and PEG-EGP with N-terminal conjugation of PEG<sub>2000</sub>, **d** (representative of 2 independent experiments). **e-g**, 8- to 10-week old C57BL6/J female mice were primed on day 0 and boosted on day 14 with 25 $\mu$ g c-di-GMP and 5nmol EGP peptide or peptide construct as indicated, and ICS was performed on day 20-21. Shown are mean T cell responses quantified as % IFN- $\gamma$ <sup>+</sup> of CD8<sup>+</sup> ( $n = 5$ , student's t-test for indicated comparisons of interest, plots are independent experiments). \* $P < 0.05$ , \*\* $P < 0.01$ , \*\*\* $P < 0.001$ . Data in **a-d** were kindly contributed by Naveen Mehta.

## **Amph-peptides prime with various adjuvants; trafficking and priming is diminished by IFA**

Incomplete Freund's Adjuvant is a water-in-oil emulsion that induces local inflammation and forms a depot, protecting antigens from degradation and releasing them over time<sup>178</sup>. While this mechanism of action would be expected to improve priming against unmodified peptide antigens, for antigens modified for serum stability and enhanced lymphatic drainage, it is unclear if there would be additional benefit with formulation in IFA. Mice were primed and boosted with soluble or amph-antigen adjuvanted with c-di-GMP or polyI:C, either injected in saline or formulated in IFA. T cell responses were quantified with ICS six days after boosting. (Figure 6a). The weak responses to free peptide adjuvanted with either polyI:C or CDN were improved with formulation IFA, but responses to amph-peptide were hindered by formulation in IFA, decreasing approximately 50% in magnitude compared to formulation in saline. To see how formulation in IFA impacted lymphatic drainage of amph-peptides, FAM-labeled amph-EGP was formulated with lipoCpG, c-di-GMP, polyI:C, or IFA, and injected subcutaneously at the tail base. Drainage to the inguinal and axillary nodes was quantified by IVIS (Figure 6b-d). Formulation of amph-antigen with lipoCpG, c-di-GMP, or polyI:C did not substantially hinder drainage, but formulation in IFA clearly prevented efficient lymphatic drainage of the lipid tail-conjugated antigen at 24h. Thus, in contrast to free peptides, which show an enhancement in priming when formulated in IFA, amph-peptides show decreased activity when formulated in IFA, likely due to hampered lymphatic drainage.

## **Amph-vaccines traffic efficiently in non-human primates**

It is important to test potential drugs in higher mammals that better mimic human biology when translating a therapy. Because lymphatic drainage is a physical process, and humans and mice exist in significantly different length scales, we wanted to verify that the enhancement in trafficking observed in mice can be recapitulated in non-human primates. To assess this, we used fluorescently labeled versions of amph-CpG and amph-peptides compared to unlipidated CpG and peptides and analyzed uptake 24h after injection (Figure 7a). TAMRA-labeled CpG and TAMRA-labeled amph-CpG (sequence 7909) were synthesized; FAM-labeled peptide and amph-peptide ('gag2', a 32-mer chosen from HIV gag) were synthesized. Fluorescent vaccine (100µg peptide and 200µg CpG) were formulated into 1mL in sterile saline and injected in one of three sites: 1) subcutaneously at the axillary node site (close to the node, but not an

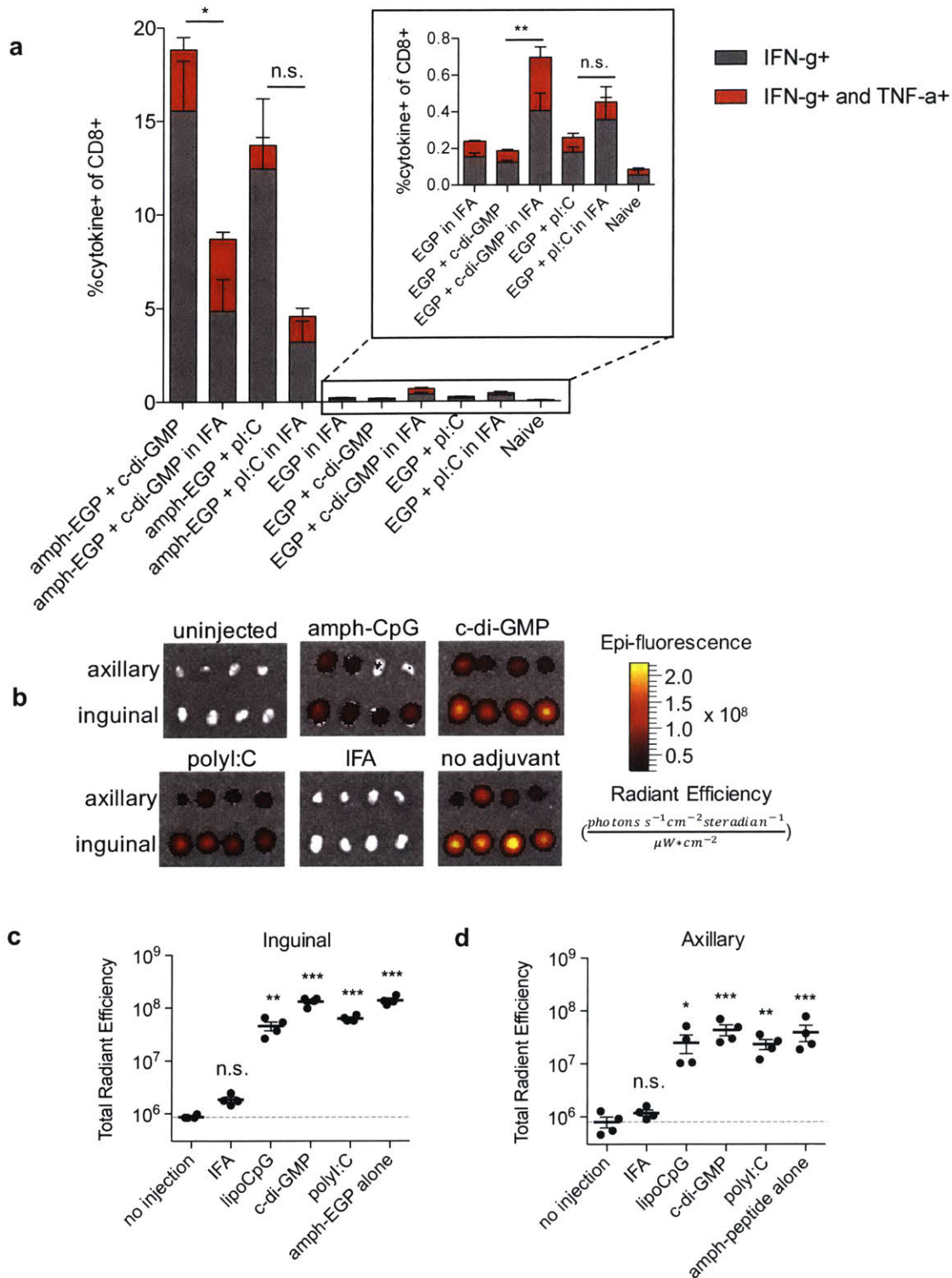


**Figure 6 Amph-peptides prime with various adjuvants; trafficking and priming is diminished by IFA.** **a**, 8-week old C57BL6/J female mice were primed on day 0, boosted on day 14, and boosted again on day 28 with 25 $\mu$ g c-di-GMP and 5nmol EGP peptide or peptide construct as indicated, and ICS was performed on day 35. Shown are mean cytokine responses quantified as % cytokine<sup>+</sup> of CD8<sup>+</sup> ( $n = 5$ , student's t-test for indicated comparisons of interest). **b-d**, mice were immunized 15nmol FAM-labeled amph-EGP alone, formulated in IFA, or with the indicated adjuvant. Lymph nodes were resected 24h later and uptake was quantified using IVIS. Shown are images of resected nodes, **b**, and quantification of background-subtracted radiant efficiency, ((photons\*s<sup>-1</sup>\*cm<sup>-2</sup>\*steradian<sup>-1</sup>)/( $\mu$ W\*cm<sup>2</sup>)) in inguinal and axillary nodes, **c-d** ( $n = 4$ , ANOVA with Dunnett's post-test comparing each group to no injection, representative of 2 independent experiments). \* $P < 0.05$ , \*\* $P < 0.01$ , \*\*\* $P < 0.001$ .



intranodal injection), 2) intramuscularly into the quadricep, or 3) subcutaneously 5cm below the knee (Figure 7b). Twenty-four hours later, lymph nodes were surgically resected for each of these three sites: 1) the axillary node, 2) the inguinal node, or 3) the popliteal node. Lymph nodes were imaged using IVIS to quantify total lymph node fluorescence for each channel, then dissociated and a single cell suspension was created. Cells were stained for flow cytometry and uptake was analyzed in lymph node resident antigen presenting cells.

Injection with amph-vaccine at either the axillary or popliteal site showed clear signal for both amph-CpG and amph-peptides in all nodes with the exception of one monkey at the axillary site (Figure 7c-e). In contrast, while some unmodified CpG signal could be detected, no free peptide could be detected via any injection route (Figure 7c-e). Consistent with previous mouse data, injection intramuscularly did not show detectable signal for either amph-CpG or amph-peptide in the inguinal lymph node (data not shown). Uptake in the popliteal node was substantially higher than at the axillary site for both amph-CpG and amph-peptide (Figure 7c-e).

The population of dendritic cells analogous to mouse  $CD8\alpha^+$  DCs or human  $XCR1^+CD141(BDCA-3)^+$ , which are most potently capable of cross-presentation, was identified in rhesus macaques for the first time in 2014<sup>179</sup>. Using a panel informed by Dutertre et al., uptake of both CpG and TAMRA was examined specifically within  $CADM1^+$  cross-presenting DCs (Figure 7f). Only with amph-vaccine at the popliteal node was there a clear population of  $CADM1^+$  DCs that showed signal for both TAMRA and FAM, indicating that they had taken up both antigen and adjuvant (Figure 7f). Thus, injection with amph-CpG and amph-peptides 5cm below the knee site shows a clear benefit for trafficking over unmodified CpG and peptides, and both molecules were taken up by the most relevant dendritic cell population for cross-presentation to prime  $CD8^+$  T cell responses.

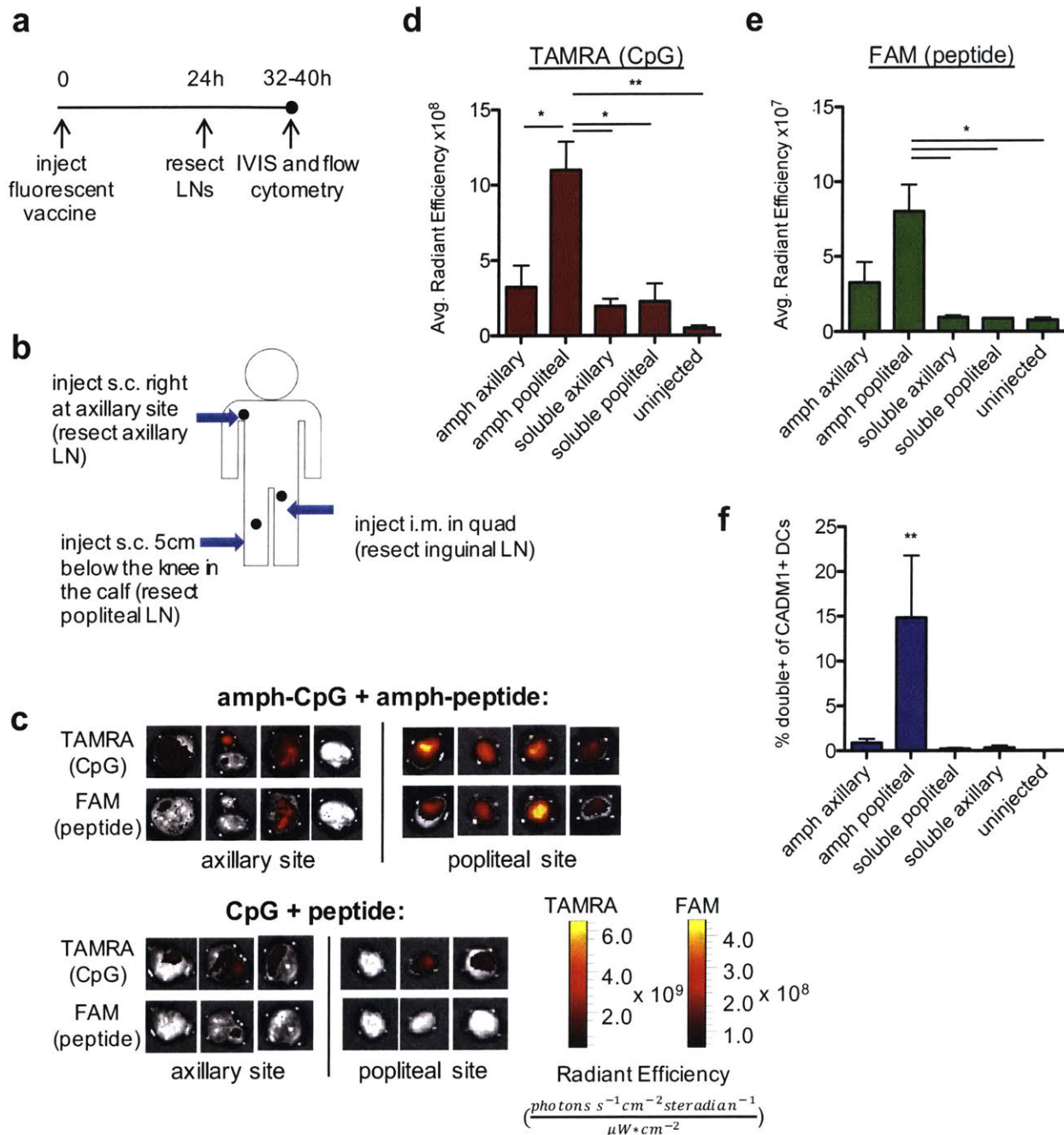


**Figure 7 Trafficking of fluorescently labeled vaccine in rhesus macaques.** **a-f**, rhesus macaques were injected with 100μg FAM-labeled peptide and 200μg TAMRA-labeled CpG via three routes, shown in **b**, and 24h later lymph nodes were surgically resected and analyzed for uptake via IVIS and flow cytometry. Shown are raw IVIS images of lymph nodes, **c**, quantification of fluorescence for CpG, **d**, and peptide, **e**. Uptake was quantified using flow cytometry, **f**, quantified as % of CADM1<sup>+</sup> cross presenting dendritic cells that were positive for both TAMRA and FAM signal. \**P* < 0.05, \*\**P* < 0.01, \*\*\**P* < 0.001 by student's t-test between conditions of interest.

## 2.3 Results: expanding beyond the albumin-binding diacyl lipid

### Albumin binding peptides to enhance peptide trafficking and immunogenicity

Albumin-binding peptides (ABPs) have remained largely unexplored in the context of vaccinology, but modification of peptide antigens with albumin binding peptides may be expected to offer enhancements in lymph node targeting and immunogenicity via a similar mechanism as the diacyl lipid modification that we previously described (DSPE-PEG<sub>2000</sub>-EGP, amph-EGP)<sup>10</sup>. Cyclized albumin-binding peptides were linked via PEG<sub>2000</sub> spacer to the gp100 antigen EGP (ABP-PEG<sub>2000</sub>-EGP, Figure 8a). When mice were injected subcutaneously with TAMRA labeled ABP-EGP or EGP peptide and lymph nodes were resected, the ABP-PEG<sub>2000</sub>-EGP accumulated at substantially higher levels than unmodified EGP peptide (Figure 8b-c), and immunization with ABP-PEG<sub>2000</sub>-EGP showed a more than 5-fold increase in T cell priming over unmodified

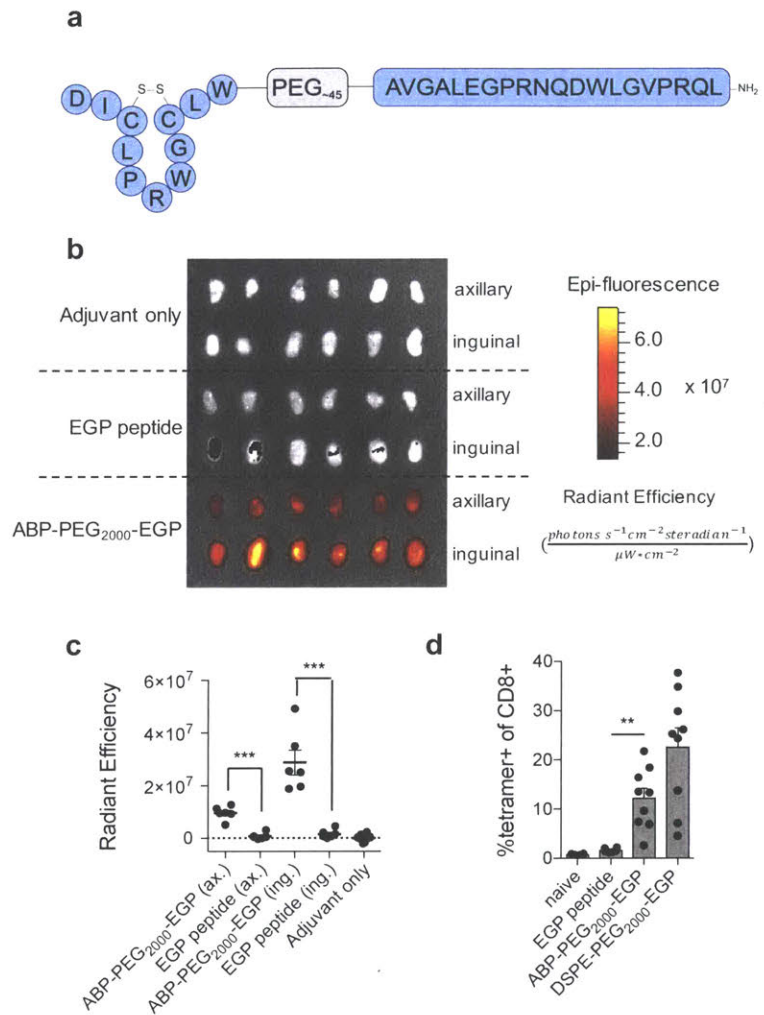


**Figure 8 Albumin-binding peptide conjugation enhances lymph node targeting and immunogenicity of peptide antigens.**

**a**, A cyclized albumin-binding peptide conjugated to EGP peptide via PEG<sub>2000</sub> spacer. **b-c**, 8-week old C57BL6/J female mice were injected subcutaneously at the tail base with 15nmol TAMRA labeled EGP peptide or albumin-binding peptide and 25µg c-di-GMP adjuvant and lymph nodes were resected 24h later and imaged using IVIS. Shown are images of resected nodes, **b**, and quantification of background-subtracted radiant efficiency,  $((\text{photons} \cdot \text{s}^{-1} \cdot \text{cm}^{-2} \cdot \text{steradian}^{-1}) / (\mu\text{W} \cdot \text{cm}^2))$ , **c** ( $n = 6$ , student's t-test, representative of 2 experiments). **d**, 8-week old C57BL6/J female mice were primed on day 0 and boosted on day 14 with 5nmol EGP peptide or EGP-conjugate as indicated and 25µg c-di-GMP, and tetramer staining was performed on day 21. Shown are mean tetramer responses quantified as % tetramer<sup>+</sup> of CD8<sup>+</sup> ( $n = 6-9$ , student's t-test, representative of 2 independent experiments). \* $P < 0.05$ , \*\* $P < 0.01$ , \*\*\* $P < 0.001$ .

peptide. Thus, modification with ABPs can enhance trafficking and immunogenicity of peptide antigens.

### **Vitamin E modification of CpG and peptides enhance trafficking and immunogenicity**

Although conjugation with albumin-binding peptides enhanced the activity of peptide antigens, the magnitude of increase is less impressive than constructs using a diacyl lipid. It would be advantageous to expand the repertoire of lipidic albumin-binders and to explore if others can substitute to provide similar enhancements in trafficking and immunogenicity. The most biologically active form of vitamin E,  $\alpha$ -tocopherol, has been shown to bind to serum albumin<sup>180</sup>, so we made constructs utilizing vitamin E as the albumin-binding domain for molecular antigens and adjuvants (Figure 9a-b). To see if lymphatic trafficking was enhanced with vitamin E conjugation, the TLR9 agonist CpG ODN 1826 was synthesized with 3' TAMRA fluorophore and 5'  $\alpha$ -tocopherol, and this  $\alpha$ -tocopherol-CpG (Vit. E-CpG) or free CpG were injected into mice subcutaneously at the tail base. Lymph nodes were resected and fluorescence was quantified using IVIS; Vit. E-CpG accumulated at substantially higher levels in the draining inguinal and axillary nodes compared to unmodified CpG (Figure 9c).

Consistent with this, mice immunized with whole protein ovalbumin (OVA) adjuvanted with Vit. E-CpG showed priming enhancements of 10-fold over unmodified CpG or CpG modified with Vitamin B3, which is not known to bind to serum albumin (Figure 9d-e). To see if  $\alpha$ -tocopherol offered similar enhancements to the peptide antigen,  $\alpha$ -tocopherol-PEG<sub>2000</sub>-maleimide was used to conjugate vitamin E-PEG<sub>2000</sub> to the gp100 antigen EGP long via an N-terminal cysteine (Vit. E-PEG<sub>2000</sub>-EGP) (Figure 9b), and mice immunized with Vit. E-PEG<sub>2000</sub>-EGP showed responses approximately 10-fold higher than unmodified peptide (Figure 9f-g). Thus, Vitamin E conjugation improves immunogenicity of both CpG and peptide antigens, and thus the design principle of binding serum albumin to enhance activity of antigens and adjuvants holds true for a number of different albumin binders (Figure 8, Figure 9, and ref<sup>10</sup>).



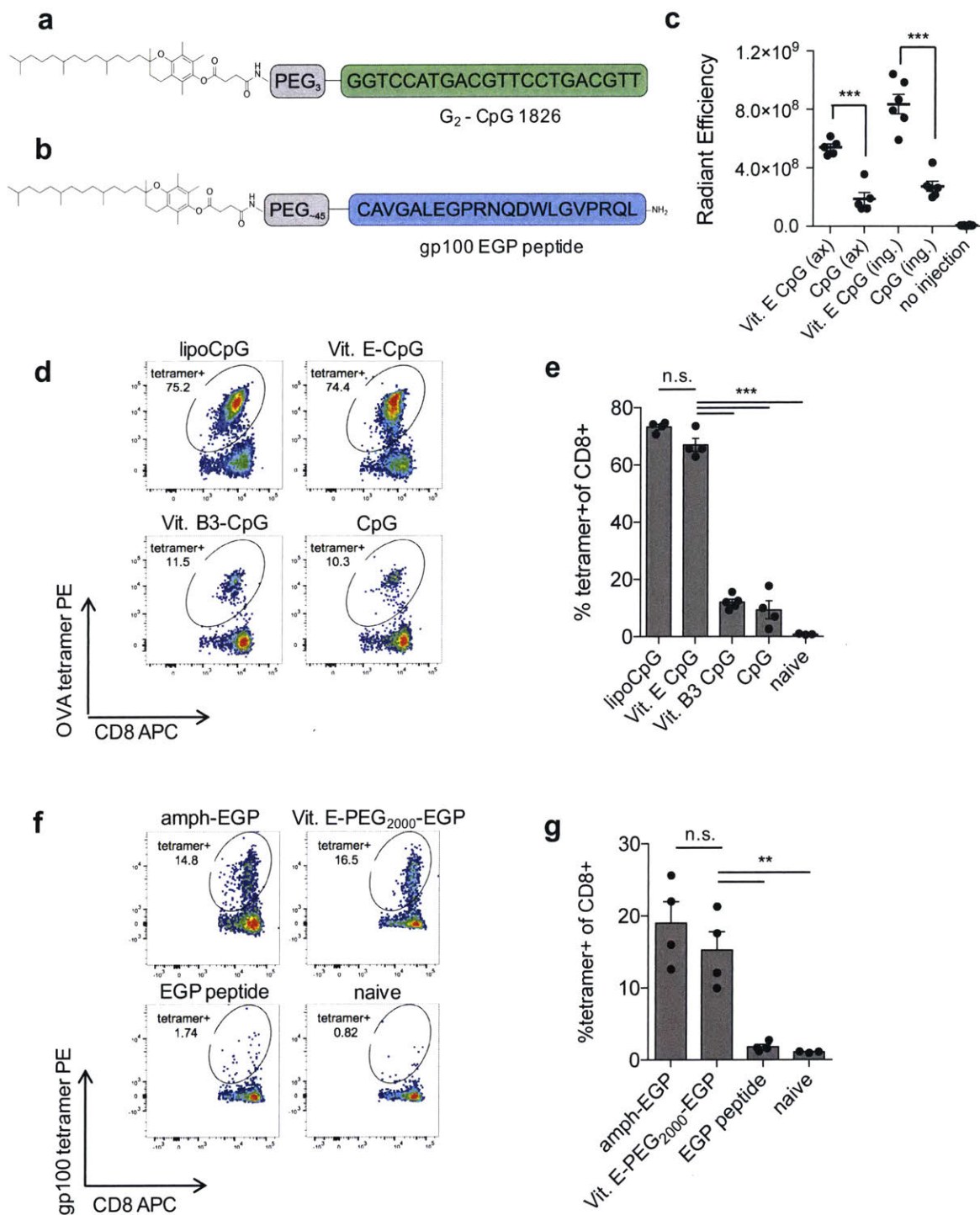


**Figure 9 Vitamin E conjugation enhances lymphatic drainage and immunogenicity of molecular vaccines.** **a**, Vitamin E linked to CpG 1826 adjuvant via a triethylene glycol spacer. **b**, gp100 EGP peptide linked to vitamin E via PEG<sub>2000</sub> spacer. **c**, Mice were injected subcutaneously with 3.3nmol TAMRA labeled CpG or lipoCpG. Axillary and inguinal nodes were resected 24h later and uptake was quantified by reading TAMRA fluorescence using IVIS. Shown is background-subtracted total radiant efficiency for each node ( $n = 5$  or 6, Student's t-test). **d-e**, 8-week old C57BL6/J female mice were primed on day 0 and boosted on day 14 with 10 $\mu$ g OVA and 1.24nmol of CpG or CpG conjugate as indicated, and tetramer staining was performed on day 21. Shown are representative plots (gated on live single CD8<sup>+</sup> T cells), **d**, and mean tetramer responses quantified as % tetramer<sup>+</sup> of CD8<sup>+</sup>, **e** ( $n = 4$ , ANOVA with Tukey post-test, representative of 2 independent experiments). **f-g**, 8-week old C57BL6/J female mice were primed on day 0 and boosted on day 14 with 5nmol EGP peptide or EGP-conjugate as indicated and 25 $\mu$ g c-di-GMP, and tetramer staining was performed on day 21. Shown are representative plots (gated on live single CD8<sup>+</sup> T cells), **f**, and mean tetramer responses quantified as % tetramer<sup>+</sup> of CD8<sup>+</sup>, **g** ( $n = 4$ , ANOVA with Tukey post-test, representative of 3 independent experiments).

## **2.4 Albumin-binding constructs that did not result in enhanced T cell priming**

A number of strategies to enhance antigen or adjuvant activity by binding to serum albumin to enhance lymphatic trafficking and serum stability proved fruitful, as described above. However, it is important to document strategies that did not yield potent antigens and adjuvants so that future scientists can make the best use of their time and not retread the same path on molecules that do not work well. Here, we describe three constructs, their rationale, immunogenicity, and potential hypotheses as to why they did not work as anticipated.

### **Vitamin E ssRNA TLR7 agonist does not effectively adjuvant T cell responses**

Adding diacyl lipids to CpG DNA results in dramatically enhanced lymphatic trafficking and *in vivo* priming, but TLR9 expression is not well conserved between mouse and human. For example, in humans, TLR9 is expressed by B cells and plasmacytoid DCs, but in mice, it is expressed by B cells, macrophages and myeloid DCs<sup>181</sup>. Therefore, it would be attractive to have albumin-binding adjuvants that activate other TLRs or other sensors (for example, STING pathway agonists) that could result in inflammatory signals. Along with small molecules like imiquimod, single stranded RNAs can be recognized by TLR7, which bind at a distinct site from small molecule agonists<sup>182</sup>, and there are examples of single stranded RNAs used as adjuvants to augment T cell responses in mice<sup>183</sup>. RNAs given as therapeutics (albeit primarily in the context of siRNA) are often packaged with stabilizing polymers, cationic lipids, or other vehicles to aid in stability, because naked RNA is degraded in seconds in serum<sup>182</sup>. Rajagopal et al. showed that immunization with a phosphorothioate-backbone polyU RNA oligo of length 21 bases activates TLR7 and can be used to adjuvant responses in mice to OVA, although extremely high immunization doses and *ex vivo* stimulation and expansion for three days were required to detect the primed T cells<sup>183</sup>. Additionally, the polyU was administered with DOTAP cationic lipid as a complex. Inspired by data demonstrating that  $\alpha$ -tocopherol (vitamin E) could effectively substitute for the diacyl lipid in amph-CpG,  $\alpha$ -tocopherol-polyU was synthesized (Figure 10a). Mice were primed and boosted with 10 $\mu$ g OVA and 50 $\mu$ g  $\alpha$ -tocopherol-polyU (or polyI:C as a positive control) and T cell responses were measured by tetramer staining. As shown in Figure 10b-c,  $\alpha$ -tocopherol-polyU did not effectively prime impressive responses to

OVA, and an *in vitro* study using the InvivoGen mTLR7 reporter (performed in media containing serum) showed no activation (Figure 10d).

There are a number of reasons why this adjuvant may have failed. One distinct possibility appears to be serum stability: phosphorothioate-backbone RNA has a poor half-life of less than 2 hours in serum<sup>184</sup>. Binding to serum albumin and/or 5' modification with  $\alpha$ -tocopherol may enhance stability, but it would likely need to be a substantial enhancement to survive long enough to adjuvant T cell responses in the lymph node. Another possibility that we did not rule out is that conjugation with  $\alpha$ -tocopherol interferes with recognition by TLR7. Future studies looking at other TLR7 agonists with superior serum stability may be more fruitful for investigation.

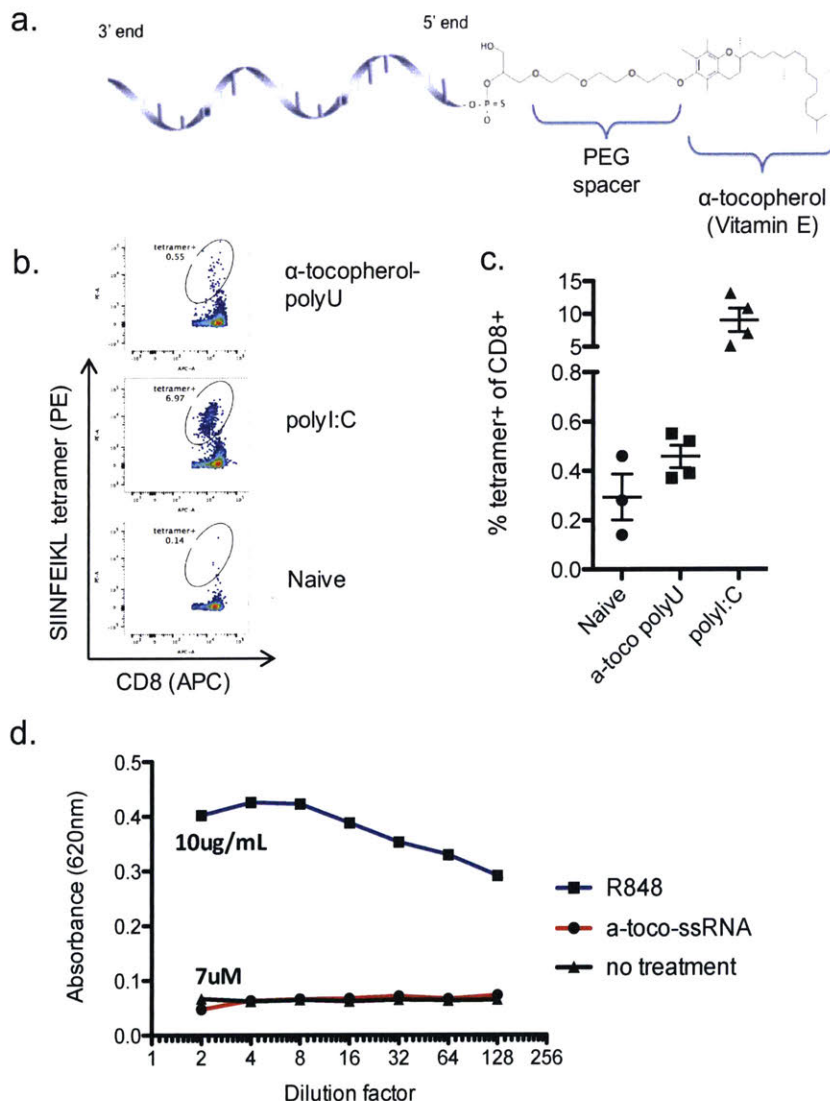


**Figure 10 Single stranded RNA TLR-7 agonist conjugated to  $\alpha$ -tocopherol does not prime T cell responses or activate TLR7 *in vitro*.** **a.** Schematic showing the construct:  $\alpha$ -tocopherol was linked via triethylene glycol spacer to the 5' end of polyU (21 bases in length) with phosphorothioate backbone. **b-c.** 8-week old C57BL/6/J female mice were primed on day 0 and boosted on day 14 with 10 $\mu$ g OVA and 50 $\mu$ g  $\alpha$ -tocopherol-polyU or polyI:C and a tetramer stain was carried out on day 21. Shown are representative tetramer plots, **b**, and quantification of the % tetramer+ of total live CD8+ T cells, **c**. (n = 4 per group). **d.** Titrations of TLR7-agonist R848 or  $\alpha$ -tocopherol-polyU were incubated with InvivoGen's HEK-Blue™ mTLR7 SEAP reporter line in complete DMEM with 10% FBS overnight in the incubator at 37°C. Initial concentrations are shown on the graph: 10 $\mu$ g/mL for R848 and 7 $\mu$ M for  $\alpha$ -tocopherol-polyU. The TLR7 activation was quantified using the QuantiBlue reagent according to the manufacturer's protocol.



## Y-form DNA STING agonist does not activate STING in the absence of transfection

STING agonists can act as potent adjuvants when either given at high doses (as shown earlier in this chapter) or at lower doses when formulated to traffic more effectively to lymph nodes<sup>185</sup>. Most currently used STING agonists used are small dinucleotides, like c-di-GMP, but

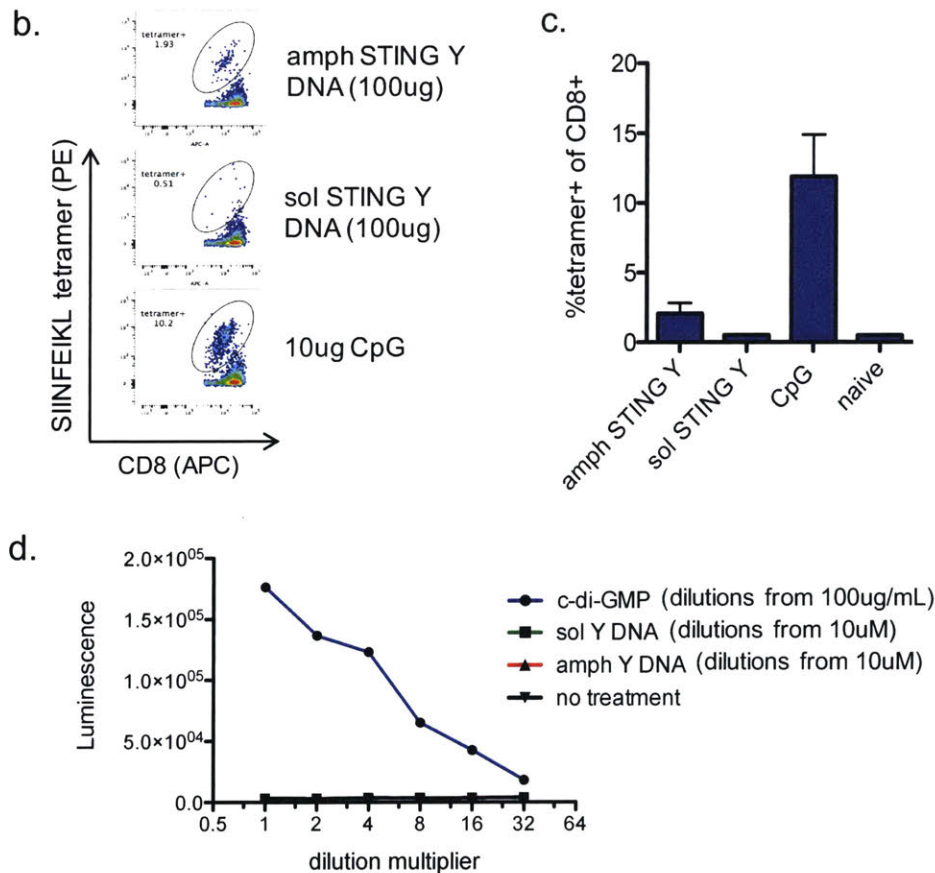


Figure 11 **Y-form DNA STING agonists do not adjuvant T cell responses to OVA *in vivo* or activate STING pathway *in vitro*.** a, schematics of the constructs used, where paired bases are shown in blue and unpaired guanine overhangs are shown in black. b-c, 8-week old female C57BL6/J mice were primed on day 0 and boosted on day 14 with 10µg OVA and 100µg of STING Y-form DNA either with or without a diacyl tail, or 10µg CpG as a positive control. Tetramer staining was performed on day 21. Shown are representative plots b, and mean tetramer responses, c. Plots in b are gated on live, single, CD8<sup>+</sup> T cells. (n = 4/group). d, RAW-Lucia™ ISG Cells from InvivoGen were incubated with dilutions of Y-form DNA constructs or c-di-GMP positive control overnight and luminescence was read out using a Tecan plate reader.



Herzner et al. recently showed a different motif of STING-pathway agonist: Y-form DNA with unpaired guanines following a double-stranded section of DNA<sup>186</sup>. These Y-form DNA constructs mimic cytosolic DNA that is found during retroviral infections and activate the STING pathway via recognition by the cytosolic protein cGAS. A number of motifs were required for activation: a double-stranded section 'stem' section that must be at least 18 base pairs in length for optimal activation, as well as unpaired overhangs (which can either be free ends or a stem-loop structure) containing at least three guanines. In this paper, all experiments were conducted *in vitro* in primary human cells and the constructs of interest were transfected to allow cytosolic access.

To explore whether these Y-form DNA STING agonists may serve as effective adjuvants, constructs were chosen to fulfill the above criteria (Figure 11a) and synthesized in-house. (Note that the backbone here is phosphodiester to match those used by Herzner et al., not phosphorothioate.) Mice were primed and boosted with OVA adjuvanted with either unmodified Y-form DNA or Y-form DNA in which an albumin-binding diacyl lipid was conjugated to one of the strands to enhance lymphatic drainage. Unfortunately, these constructs did not effectively adjuvant responses to OVA (Figure 11b-c). To explore if these constructs were capable of activating the STING pathway *in vitro*, a luciferase-based STING reporter line was used. Both constructs failed to appreciably activate the STING pathway, even at high concentrations (Figure 11d).

The most likely reason that these Y-form DNA constructs failed to effectively adjuvant T cell responses or activate STING *in vitro* is failure to gain cytosolic access. The sensor cGAS targeted by these constructs is located in the cytosol<sup>187</sup>, and there is no engineered mechanism for these constructs to escape the endosome following uptake. Indeed, all of the studies looking at STING-pathway activation in the Herzner et al. paper utilized transfection to deliver the Y-form DNA constructs of interest<sup>186</sup>. In future studies utilizing this Y-form DNA as an adjuvant, addition of a cell penetrating peptide (see Chapter 3) to enhance access to the cytosol may prove fruitful.

### **Maleimide-peptide constructs to bind Cys34 on albumin *in vivo***

Albumin has a free cysteine (Cys34), and binding to Cys34 has been used to extend blood half-life and reduce renal clearance of both imaging probes and therapeutic drugs; this can be achieved by engineering maleimide prodrugs, which have been shown to complex with albumin within minutes *in vivo* via Cys34<sup>188</sup>. Albumin is unique among proteins in circulation in

that it has an accessible free thiol group capable of reacting at physiological conditions, so maleimide prodrugs would be expected to very selectively bind to albumin upon injection<sup>188</sup>. So far, maleimide prodrugs have primarily been small molecules linked via a spacer to maleimide, but making use of this *in vivo* binding to Cys34 on albumin could prove beneficial for peptide or adjuvant molecules to enhance lymphatic trafficking like the non-covalent binders explored earlier in this chapter. There is evidence that covalent linkages via peptide bond between albumin and antigens can result in enhanced priming over unmodified peptide (Naveen Mehta, unpublished), so it is reasonable to hypothesize that reversible albumin binding is not required for activity of constructs that target lymph nodes via albumin.

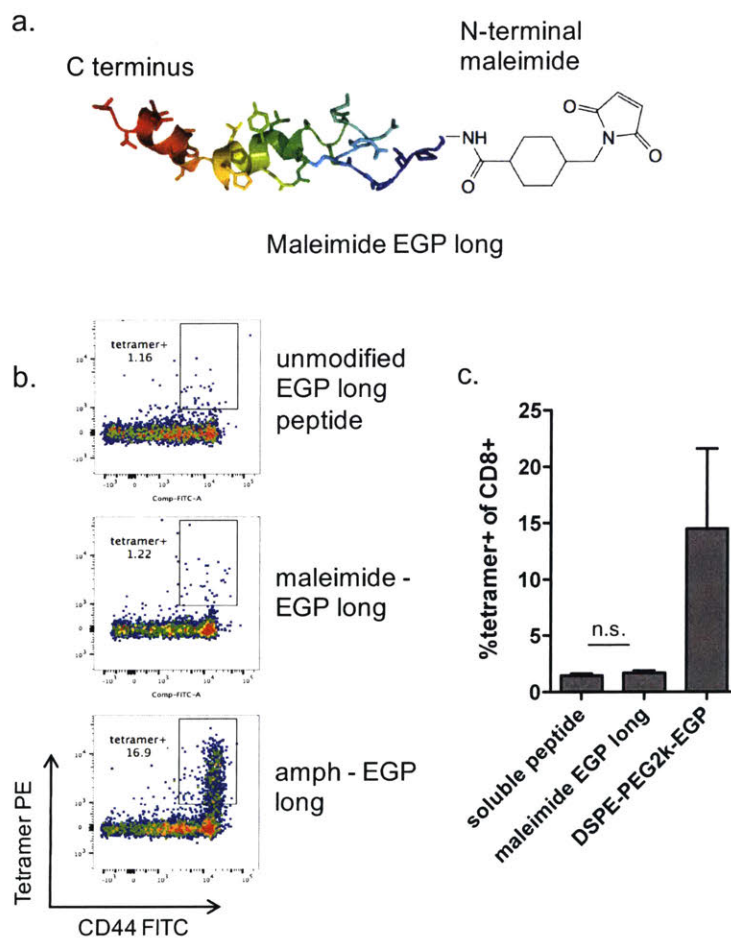


**Figure 12 Maleimide EGP long does not enhance priming over unmodified EGP peptide.** **a**, the peptide construct showing N-terminal conjugation to maleimide. **b-c**, female 8-week old C57BL6/J mice were primed on day 0 and boosted on day 14 with 25µg c-di-GMP and 10µg equivalent of EGP long peptide, maleimide-modified EGP long peptide, or amph-EGP long. T cell responses were quantified on day 20 with a tetramer stain. Shown are representative plots gated on live, single, CD8<sup>+</sup> T cells, **b**, and mean tetramer responses as a fraction of total live CD8<sup>+</sup> T cells.

To assess if adding a maleimide to allow for covalent binding to albumin *in vivo* would allow for better lymphatic drainage and enhanced T cell priming, EGP long peptide was synthesized with an N-terminal maleimide (Figure 12a). Mice were primed and boosted with this construct, and T cell responses were measured via tetramer stain. As expected, amph-EGP long demonstrated clear priming benefit over unmodified peptide, but maleimide-EGP long did not show any enhancement over free peptide (Figure 12b-c).

There are a few reasons why this construct may not have worked. First, many of the prodrugs have long flexible linkers between the active part of the small molecule and the albumin-binding maleimide<sup>188</sup>. The peptide construct here did not have this

linker, which may be required to allow for effective binding of albumin *in vivo*. Alternatively, if *in vivo* binding to albumin did occur effectively, peptide processing in DCs may have been hampered. There is evidence that having a cysteine-maleimide linkage at the N-terminus of a peptide can result in effective processing (as is the case in amph-EGP long) in the orientation where the cysteine is N-terminal to the peptide and the maleimide links via a spacer to the albumin-binder. The chemistry of this bond is different in this construct, however (the orientation of the cysteine-maleimide bond is flipped relative to the peptide), which may have impacted antigen processing. Future work in this area should verify that this construct binds to albumin and that it can be efficiently presented (for example using *in vitro* assays with the pmel-1 transgenic T cell system) and/or making constructs that include a long flexible linker like PEG<sub>2000</sub>, which would also better match the way that the amph-peptides are designed.

## **2.4 Discussion and Future Work**

We have previously shown that modification of CpG or peptides with diacyl lipids (through a PEG spacer in the peptide case) enhances lymph node uptake and T cell priming<sup>10</sup>. Here we extend those results to show that substitution of the diacyl lipid with  $\alpha$ -tocopherol as the albumin-binding moiety similarly enhances both antigen and adjuvant activity. Further, we show that non-lipidic modifications, namely albumin-binding peptides, also allow for enhancement of lymph node draining and T cell priming. This may offer an outlet for future studies to explore the effect of albumin affinity on the corresponding lymphatic drainage and T cell priming, because albumin-binding peptide libraries have been developed with peptides varying in affinity for mouse serum albumin over a wide range<sup>189</sup>.

It has previously been shown that short peptides that can peptide exchange onto MHC I can be presented by non-professional antigen presenting cells, including T cells and B cells, which may lead to suboptimal T cell priming<sup>173</sup>. Amph-peptides appear to rely on cross-presenting dendritic cells, even with short amph-peptides, which may allow them to avoid this non-optimal presentation by non-professional APCs. However, our results do not exclude the possibility that *Batf3*<sup>-/-</sup> mice show general immunological defects for T cell priming even with antigens that do not require cross presentation, and that this caused the decrease in priming seen in *Batf3*<sup>-/-</sup> mice with amph-EGP short. Unconjugated EGP short peptide would be expected to prime similar responses in wild type and *Batf3*<sup>-/-</sup> mice because EGP short peptide does not

require cross presentation for display on MHC I, but unfortunately EGP short was an extremely poor immunogen in both *Batf3*<sup>-/-</sup> and wild type mice, so responses did not exceed background to compare. However, one study has shown that *Batf3*<sup>-/-</sup> mice can prime normal responses to optimal-length SIINFEKL peptide compared to wild type<sup>190</sup>, which supports that the loss in activity with amph-EGP short in *Batf3*<sup>-/-</sup> may be due to a requirement for processing by cross presenting DCs.

The best characterized receptor for albumin, FcRn, does not play a role in the mechanism of the amph-vaccine, as *FcRn*<sup>-/-</sup> mice respond indistinguishably to amph-vaccine from wild type mice (Figure 4a-b). Although other receptors for albumin have been described, including albondin (gp60) and several scavenger receptors that bind conformationally altered albumin to redirect it for degradation, these other albumin receptors are not known to be expressed on antigen presenting cells<sup>191</sup>.

The duration of antigen presentation has been shown to impact magnitude of T cell effector and memory responses, with longer antigen exposure resulting in more effective CD8<sup>+</sup> T cell memory formation compared to brief exposure<sup>192,193</sup>, and priming in distal nodes was identified as one of the characteristics of DEC-205 targeted antigens, which promote potent CD8<sup>+</sup> T cell immunity<sup>194</sup>. We show here that amph-peptides embody both of those principles, as they are presented in multiple nodes systemically (Figure 3a-e) and for at least one week *in vivo* (Figure 3f-g). It is suggestive that immunization with amph-peptides recapitulates some traits of systemic viral infection: presentation of antigen in lymphoid organs throughout the body for a prolonged duration.

Peptide antigen modification with PEG significantly enhanced T cell priming to a surprising extent, even without including a lymphatic-targeting albumin-binding domain (Figure 5e). This was likely mediated through an increase in serum stability and *in vivo* half-life, as has been demonstrated for PEG modification of erythropoiesis stimulating peptides and anti-viral peptides previously<sup>167,177</sup>. This indicates that a substantial part of the activity of amph-peptides may simply be due to protection from serum proteases, although further significant improvements are seen with the addition of an albumin-binding domain. It is interesting to note that for both amph-peptides and ABP-peptides, *in vivo* priming was substantially lower for C-terminal conjugates compared to N-terminal conjugates (Figure 5f), in spite of similar serum stability was (Figure 5b-c); this may be reflective of differences in proteasomal processing for N- versus C-terminal adducts, or there may be other yet-unknown benefits for N- versus C-terminal attachment.

IFA is widely used to enhance immunogenicity of unmodified peptides, but our data suggests that subunit (and possibly particulate) vaccines that rely on efficient lymphatic drainage for their mechanism of action may actually be hindered in activity with formulation in IFA. The mechanism of action of IFA is thought to involve extending *in vivo* presentation of antigen by forming an antigen depot<sup>178</sup>; this may be unnecessary in the case of amph-peptides, which show an extended *in vivo* half-life (Figure 3f-g). While IFA increased priming to free peptides, IFA decreased the T cell response approximately two-fold for amph-peptides, indicating that IFA should be avoided for translation of amph-peptides clinically. This would have the dual benefit of avoiding T cell sequestration and induction of apoptosis in IFA depots, as has been observed in mice<sup>195</sup>.

The trafficking studies performed in rhesus macaques are very encouraging for translating the amph-vaccine because the enhancement in trafficking observed in mice was recapitulated in monkeys for injection at the popliteal site (Figure 7c-e). Amph-peptides showed clear uptake via both subcutaneous routes, and free peptide showed no signal above background in any monkey. The drainage of amph-vaccine to the axillary node was not impressive, and it may be related to the proximity of the injection site to the node: it was a subcutaneous injection essentially on top of the axillary node. The collecting vessels that feed the axillary nodes may not be very accessible from that location, and injection further 'upstream' may work better. Injection 5cm below the knee led to clear accumulation of amph-vaccine in the draining popliteal node, so performing an analogous injection technique for the axillary node 5cm farther down the underside of the arm may yield to better trafficking. While this trafficking data is encouraging, an important next step is to immunize with amph-vaccine in macaques to evaluate immunogenicity. It is recommended for future studies to inject subcutaneously below the knee or at analogous locations for other nodes, for example, subcutaneously on the inner thigh to reach the inguinal node. Because these experiments are very demanding and expensive to perform, we could not do a thorough survey of all injection routes and techniques, and it is likely that other sites may yield similarly impressive uptake as compared to injection 5cm below the knee for the popliteal node.

Although not all albumin-binding constructs attempted worked to enhance immunogenicity of constructs, the most likely failure modes of each of the constructs explored was not necessarily related to its ability to bind to serum albumin. Stability *in vivo* and ability to access target molecule are critically important features for activity. For future exploration of albumin binding to enhance immunogenicity of antigens and adjuvants, it is recommended that

one work on constructs that already show some weak activity on their own to improve their lymphatic targeting and stability *in vivo*.

In summary, simple covalent modification of molecular vaccines with albumin binding domains is capable of ferrying these molecules throughout the lymphatics, enhancing serum stability and duration of presentation *in vivo*, and increasing T cell responses by an order of magnitude over unmodified vaccine, and may be of interest for promoting potent anti-tumor CD8<sup>+</sup> T cells clinically.

## **2.5 Methods**

### **Peptide and oligo conjugate synthesis**

Amph-peptide synthesis was carried out as previously described<sup>10</sup>, and vitamin E-peptide conjugates were synthesized using the same reaction and purification conditions with Vitamin E-PEG<sub>2000</sub>-maleimide (Nanocs). Solid phase DNA synthesis and 5' conjugation of the amph-CpG were carried out as previously described<sup>10</sup>, with some modifications. Synthesis of the Vitamin E-CpG conjugate required the following changes from amph-CpG syntheses (as described in ref<sup>10</sup>): after conjugation in solid phage, cleavage and deprotection was performed using 3:1 tertbutylamine in water for 6 hours at 65°C and the 5' dimethoxytrityl (DMT) group was removed using 80% acetic acid at room temperature for 2 hours, followed by an ethanol precipitation. Both oligonucleotide conjugates used an ODN class B sequence 1826 with two guanine spacers for mouse experiments. For rhesus macaque experiments, ODN 7909 was utilized. Following cleavage and deprotection, oligos were purified via RP-HPLC and quantified using UV-VIS. For the Y-form DNA (note that phosphodiester linkages were used in these constructs), each strand was synthesized and purified as described previously, then strands were heated to 94°C in annealing buffer (10 mM Tris, pH 7.5, 50 mM NaCl, 1 mM EDTA) for 2 minutes then cooled to room temperature over a period of 2 hours to allow for annealing.

ABP-antigen constructs were synthesized as a single unit via automated solid phase peptide synthesis as previously described<sup>196</sup>, with manual addition of the PEG<sub>2000</sub> linker. The ABP domain was cyclized, constructs were desalted, and conjugates were analyzed via LC-MS to verify identity and purity. In more detail: following synthesis of the antigen component, the PEG<sub>2k</sub> linker (Creative PEGworks) was coupled manually onto peptidoresin containing antigen;

the resin was then transferred back to the synthesizer to complete the construct. The crude peptides were cleaved overnight at room temperature (by volume, 82.5% trifluoroacetic acid, 5% water, 5% thioanisole, 5% phenol, and 2.5% ethane dithiol), triturated, and purified via RP-HPLC. The ABP moieties were cyclized by incubating the purified constructs (0.1 mg/mL) in 0.1 M NaHCO<sub>3</sub> (Sigma), pH 8.0 for 24h to facilitate disulfide formation. The cyclized constructs were desalted via solid phase extraction and analyzed via LC-MS to verify identity and purity.

Peptide antigen sequences used are as follows: gp100 EGP long: AVGALEGPRNQDWLGVPRQL<sup>197</sup>, gag2 from HIV gag: LQPSLQTGSEELRSLYNTVATLYAVHQRIE with C-terminal FAM where the underlined A is a cysteine in the native sequence, and the ABP sequence chosen was the minimal core sequence identified in a library of albumin binders: DICLPRWGCLW.<sup>189</sup> The amph-EGP constructs with an amide bond or linked via click chemistry were synthesized by SQI (Northwestern). Maleimide-EGP long was synthesized by Life Technologies and Vitamin E-polyU was synthesized by the Yale Keck Oligo core.

## Mice and immunizations

Six- to 8-week old female C57BL/6J mice from Jackson Laboratory were used for all studies unless otherwise specified. Neonatal Fc receptor knockout mice (FcRn<sup>-/-</sup>, B6.129X1-*Fcgrt*<sup>tm1Dcr</sup>/DcrJ), Batf3<sup>-/-</sup> mice (B6.129S(C)-*Batf3*<sup>tm1Kmm</sup>/J), and pmel-1 mice (B6.Cg-*Thy1*<sup>a</sup>/Cy Tg(TcraTcrb)8Rest/J) were obtained from Jackson Laboratory and bred in-house; 6- to 12-week old female mice were used for these studies.

Immunizations were administered subcutaneously at the base of the tail in 100μL, 50μL on each side, with sterile saline diluent. Whole protein OVA (LowEndo<sup>TM</sup>, Worthington Biochemical) was dosed at 10μg. Peptides were dosed at 10μg and peptide conjugates were dosed the molar equivalent. The c-di-GMP (InvivoGen) and polyI:C (HMW, InvivoGen) were dosed at 25μg where indicated, and amph-CpG and vitamin E-CpG were dosed at 1.24nmol. For lymph node trafficking studies using the In Vivo Imaging System (IVIS), the CpG dose was 3.3nmol and the peptide dose was 15nmol.

## Adoptive transfer proliferation studies

Pmel-1 T cells were isolated from spleens magnetically with EasySep CD8<sup>+</sup> T cell Isolation Kit (Miltenyi) according to the manufacturer's protocol. Purified pmel-1 T cells were

labeled by incubating for 20 minutes at 37°C in 5µM CFSE or CellTrace Violet in PBS 0.1%BSA, quenched with FBS, and washed. T cells were resuspended in sterile saline, and 500,000 pmel-1 T cells were transferred retro-orbitally into recipient mice. Lymph nodes were collected, mechanically dissociated, stained, and run on flow cytometry. Proliferation index was quantified using  $PI = \log(FI_{nd}/MFI_{all})/\log(2)$  where  $MFI_{all}$  = median fluorescence intensity of live Thy1.1<sup>+</sup> pmel-1 T cells, and  $FI_{nd}$ =peak fluorescence intensity of viable non-divided pmel-1 T cells.

### ***In vitro* peptide stability assay**

To serum-treat the peptides, EGP constructs were subjected to overnight incubation at 37°C in RPMI with 10% fresh mouse serum. Serum-treated or fresh constructs were incubated with pooled splenocytes from previously amph-EGP immunized mice for 24 hours at 37°C (in RPMI with 10% heat inactivated FBS), with brefeldin A added at 18 hours. Cells were stained for viability with LIVE/DEAD Fixable Aqua (Life Technologies), surface stained with CD8α (53-6.7, BioLegend), fixed and permeabilized with BD Cytfix/Cytoperm, stained intracellularly with IFN-γ (XMG1.2, BioLegend), and run on the BD Canto flow cytometer.

### **TLR and STING reporter assays**

Titration of TLR7-agonist R848 or α-tocopherol-polyU were incubated with InvivoGen's HEK-Blue™ mTLR7 SEAP reporter line in complete DMEM with 10% FBS and pen/strep overnight in the incubator at 37°C. Experiments were carried out in flat bottom tissue culture 96-well plates with approximately 40,000 cells per condition. Initial concentrations are shown in Figure 10: 10µg/mL for R848 and 7µM for α-tocopherol-polyU, and two-fold dilutions were carried out as indicated. The TLR7 activation was quantified using the QuantiBlue reagent according to the manufacturer's protocol.

RAW-Lucia™ ISG Cells from InvivoGen were incubated with dilutions of Y-form DNA constructs or c-di-GMP positive control complete DMEM with 10% FBS and pen/strep overnight in the incubator at 37°C. Experiments were carried out in flat bottom tissue culture 96-well plates with approximately 100,000 cells per condition. Luminescence was read out using QUANTI-Luc™ according to the manufacturer's protocol with luminescence values read using the Tecan plate reader.



## Evaluation of immune responses and flow cytometry

Antibodies to IFN- $\gamma$  (XMG1.2), TNF- $\alpha$  (MP6-XT22), and CD8 $\alpha$  (53-6.7) were purchased from BioLegend, and CD4 (RM4-5) was purchased from eBioscience. Gp100 tetramer (iTAg Tetramer/PE H-2D<sup>b</sup> gp100) and OVA tetramer (iTAg Tetramer/PE H-2K<sup>b</sup> OVA) were purchased from MBL. Tetramer staining was performed in buffer containing 50 nM dasatinib at room temperature, followed by surface staining at 4°C for 15 minutes. Viability was assessed by LIVE/DEAD Fixable Aqua purchased from Life Technologies or DAPI. Cells were analyzed using BD FACS LSR Fortessa and BD FACSCanto flow cytometers. Data was analyzed using FlowJo. Intracellular Cytokine Staining (ICS) was performed as previously described<sup>10</sup>. Peptides used for restimulation were 10  $\mu$ g/mL of the relevant antigen: gp100<sub>25-33</sub> native (EGSRNQDWL).

For the rhesus macaque analysis of lymph nodes by flow cytometry, the following markers and clones were used: CD11c (3.9), MHC II (TU36), CD123 (7G3), CD1c (AD5-8E7), CADM1 (3E1 with anti-chicken IgY secondary), and lineage<sup>-</sup>: CD3 (SP34-2), CD8 (SK-1), CD20 (L27), CD14 (M5E2), CD16 (3G8). LIVE/DEAD Fixable Aqua (Life Technologies) was used to identify viable cells.

## Trafficking studies in rhesus macaques

Fluorescent peptide (100 $\mu$ g gag2-FAM or molar equivalent of amph-gag2-FAM) and fluorescent CpG 7909-TAMRA (200 $\mu$ g or molar equivalent of amph-CpG 7909-TAMRA) were formulated into 1mL total injection volume in sterile saline and injected in one of three sites: 1) subcutaneously at the axillary node site (close to the node, not an intranodal injection), 2) intramuscularly at the quad, or 3) subcutaneously 5cm below the knee. Control animals received saline. Twenty-four hours later, lymph nodes were surgically resected for each of these three sites: 1) the axillary node, 2) the inguinal node, or 3) the popliteal node. Macaques were anesthetized with ketamine for shaving the site of injection and injections, and under isoflurane anesthesia for the lymph node biopsy surgery. One monkey received three total injections of either entirely amph-vaccine, entirely soluble vaccine, or saline, and axillary/popliteal injections were done on the same side and inguinal was performed on the opposite side. Lymph nodes were stored in 50mL conical tubes filled with RPMI (10% FBS, pen/strep), packed with cold packs, and transported for analysis approximately 8-12 hours after surgery. Lymph nodes were imaged using IVIS to quantify total lymph node fluorescence for each channel, then mechanically dissociated, digested with 0.8 mg/ml Dispase, 0.2 mg/ml Collagenase, and 0.1

mg/ml DNase I in RPMI at 37°C for 20 minutes with gentle agitation, and a single cell suspension was created. Cells were stained for flow cytometry and run on the LSR Fortessa. Trafficking studies were coordinated and performed with Alphagenesis, with veterinary staff performing the injections and surgeries.

## **Statistical analysis**

Statistical methods were not used to determine sample size, but sample numbers were chosen based on estimates from pilots and published results such that appropriate statistical tests may yield statistically significant results. Unless otherwise stated, analysis of tetramer and ICS results were analyzed by using one-way ANOVA with a Tukey *post hoc* test using GraphPad Prism software. Pmel-1 proliferation data was analyzed using student's t-test within a given lymph node to compare EGP peptide and amph-EGP. Where ANOVA was used, variance between groups was found to be similar by Bartlett's test. Statistics in Figure 5 to compare groups of interest were performed using a student's t-test. No samples were excluded from analysis.

# CHAPTER 3: Cell penetrating peptide antigen conjugates to enhance antigen presentation

## 3.1 Introduction

To prime CD8<sup>+</sup> T cell responses, peptides from the antigen of interest must be presented by antigen presenting cells on MHC class I. For exogenously provided antigen, as in the case of subunit vaccines, this presentation depends on cross-presentation. Cross-presentation of soluble protein and peptide antigens is a relatively inefficient process<sup>71</sup>, so it stands to reason that enhancing cross-presentation or allowing antigenic access to the cytosol independent of cross-presentation may improve the efficacy of peptide vaccines. The covalent linkage of cell penetrating peptides (CPPs) to antigens may allow for increased cytosolic access of the antigen cargo independent of cross-presentation; this increase in cytosolic access should translate to an increase in display of the T cell epitope of interest on MHC class I, which may improve T cell responses.

The first identified CPP was TAT from HIV, discovered independently by two groups in 1988<sup>198,199</sup>. Since then, many CPPs have discovered or synthetically generated, which may access the cytosol via a number of distinct mechanisms. One sequence notable among the naturally derived CPPs is penetratin, a 16-amino acid peptide derived from *Drosophila* first discovered in 1994<sup>200</sup>, and MPG is an example of an engineered sequence, first developed in 1998<sup>201</sup>. CPPs are generally classified as either cationic, amphipathic, or hydrophobic, and are under investigation for delivery of various cargos including DNA/RNA oligos, small molecules, proteins, and peptides<sup>202</sup>. One class of cytosolic-access mechanisms involves direct membrane transit (which is independent of active cellular processes like endocytosis), which can occur via direct transient pore formation in the plasma membrane or via an 'inverted micelle' model where the CPP induces invagination of the cellular membrane<sup>203</sup>. There are also characterized pathways that do involve active cellular processes where the CPPs can escape from endosomes to access the cytosol, though the mechanism of endosomal escape remains elusive, and likely depends on the specific CPP and cargo of interest<sup>203</sup>.

Although there have been a few examples of cell penetrating peptides fused to peptide antigens to augment T cell priming in the literature, in general there has been little systematic

evaluation of many different CPPs in the same study, vaccinations have primarily utilized highly immunogenic model antigens, and the T cell responses primed have not been potent. It would therefore be attractive to investigate a panel of CPPs linked to an antigen that is clinically relevant and poorly immunogenic on its own. We refer the reader to a recent review for a thorough overview of the use of CPPs in vaccination<sup>204</sup>, and provide a few examples as a point of reference for results in this chapter. CPP-SIINFEKL constructs have been shown to be presented in a TAP-independent manner, generate anti-SIINFEKL CD8<sup>+</sup> T cell responses, and these responses were capable of protecting against EG.7-OVA challenge<sup>205</sup>. Other initial studies utilized cell-based vaccine approaches where DCs were pulsed *ex vivo* with CPP-antigen constructs and then transferred into recipient mice<sup>206,207</sup> but such approaches are expensive and difficult to translate. Woo et al. demonstrated that TAT-CEA fusions could induce detectable T cell responses against CEA when adjuvanted with CpG<sup>208</sup>, although high doses were required, especially of the adjuvant: 50µg peptide and 2µmol CpG were used (5x and 1600x the doses used in Chapter 2 for peptide and CpG, respectively). Recently, Belnoue et al. immunized against gp100, the melanoma antigen utilized here and in Chapter 2, with constructs fused to both CPPs and to MHC class II epitopes to provide CD4<sup>+</sup> T cell help, but detection of T cell responses in their system necessitated *ex vivo* culture for 7 days in the presence of peptide to expand gp100-specific T cells prior to quantification<sup>209</sup>.

In this brief chapter, we summarize our efforts to augment CD8<sup>+</sup> T cell responses to peptide antigens using a number of cell penetrating peptides, ranging from synthetically generated sequences to naturally occurring viral sequences. We uncover a number of cell penetrating peptides that augment *in vivo* T cell responses when covalently linked to antigen, some more than 10-fold, and demonstrate Batf3-independent priming with at least one of these CPP-antigen constructs. We directly detect double-digit frequencies of antigen specific CD8<sup>+</sup> T cells from blood without *ex vivo* expansion. Our results indicate that CPPs can be used to enhance T cell responses to peptide antigens by an order of magnitude, and may be of interest for induction of responses to tumor antigens clinically.

## **3.2 Results**

### ***In vitro* survey of CPP-antigens**

There are hundreds of CPP sequences that have been described<sup>210</sup>. It is infeasible to try all CPP-peptide conjugates for *in vivo* immunizations, so it would be useful to perform an *in vitro*

screen to identify which CPPs may enhance presentation of the antigen of interest. To this end, twelve variants of the gp100 EGP long peptide were generated (**Table 1**) using a recently published novel rapid peptide synthesis that allows for coupling individual residues in 40 seconds per round<sup>196</sup>. Splenocytes were isolated from naïve mice and incubated *in vitro* with the peptides of interest, washed, and plated with CFSE-labeled TCR-transgenic pmel-1 T cells, which recognize the minimal epitope in gp100 (EGPRNQDWL).<sup>211</sup> To assay for antigen presentation, CD69 was analyzed at 24h after initiation of co-culture, and pmel-1 T cell proliferation was analyzed on day 3 via CFSE.

**Table 1: List of peptide and cell CPP-antigen constructs**

Name	Sequence	MW (Da)	Notes
EGP	AVGALEGPRNQDWLGVPRQL	2176.4	-
EGP-Arg8	AVGALEGPRNQDWLGVPRQL-[triazole]-RRRRRRRR	3660.1	-
EGP-Arg8 macrocycle	AVGALEGPRNQDWLGVPRQL-[triazole]-CRRRRRRRRC	4160.1	Cyclized between cysteines
EGP-B pep	AVGALEGPRNQDWLGVPRQL-[triazole]-RXRRBRRXRBR	4028.3	-
EGP-DPV6	AVGALEGPRNQDWLGVPRQL-[triazole]-GRPRESGKKRKRKRLKP	4469.6	-
EGP-MPG	AVGALEGPRNQDWLGVPRQL-[triazole]-(GLAFLGFLGAAGSTMGAWSQPKKRKV)	5255.8	inverted C-C linkage, attachment at MPG C-term
EGP-penetratin	AVGALEGPRNQDWLGVPRQL-[triazole]-RQIKIWFQNR(Nle)KWKK	4620.6	Nle = Norleucine
EGP-pVEC	AVGALEGPRNQDWLGVPRQL-[triazole]-LLIILRRRIRKQAHAAHSK	4601.7	-
EGP-pVEC-DPV6	AVGALEGPRNQDWLGVPRQL-[triazole]-LLIILRRRIRKQAHAAHSKGRPRESGKKRKRKRLKP	6660.0	-
EGP-TAT	AVGALEGPRNQDWLGVPRQL-[triazole]-RKKRRQRRR	3732.2	-
EGP-TP10	AVGALEGPRNQDWLGVPRQL-[triazole]-AGYLLGKINLKALAALAKKIL	4574.7	-
EGP optimal	EGPRNQDWL	1114.2	-

The conditions were optimized such that EGP long peptide induced a moderate level of CD69 upregulation on day 1 and clear but modest proliferation on day 3, whereas the optimal epitope showed nearly 100% upregulation of CD69 and high proliferation (Figure 13a). The 1h pulse was performed at either 37°C (Figure 13a-c) or at 4°C (Figure 14a) to suppress active

cellular processes, including endocytosis. At 37°C, the CPP-antigen constructs demonstrated varying ability to prime pmel-1 T cells *in vitro*, with all constructs showing at least modest enhancements over unmodified long peptide (Figure 13b-c). In particular, penetratin, MPG, B-pep and TAT all showed large improvements for inducing CD69 expression on pmel-1 CD8<sup>+</sup> T cells, whereas Arg8, Arg8 macrocycle, and pVEC-DPV6 performed more similarly to unmodified peptide.

At 4°C and 0.5µM peptide, none of the constructs tested showed very strong ability to

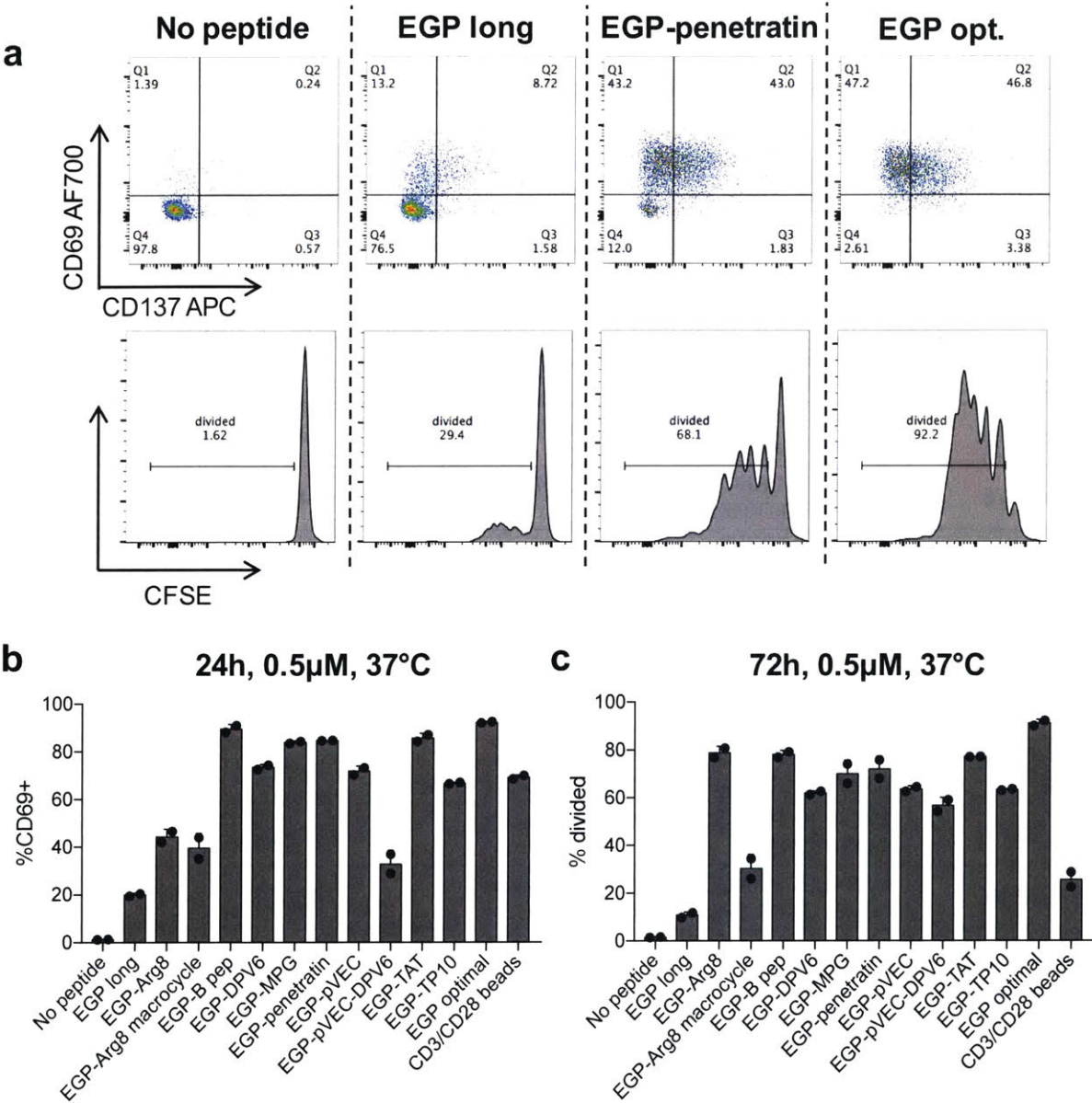


Figure 13 *In vitro* screening of cell penetrating peptides. **a-c**: Splenocytes were pulsed with 0.5µM peptide or peptide-CPP conjugate for 1h at either 37°C. Splenocytes were washed and plated with 50,000 CFSE-labeled pmel-1 T cells. Twenty-four hours after initiation of co-culture, half of the cell suspension was removed for analysis of CD69 on pmel-1 T cells. Three days after initiation of co-culture, the remaining cells were analyzed for proliferation of the CFSE-labeled pmel-1 T cells. Shown are representative flow plots, **a**, quantification of CD69 expression, **b**, and proliferation, **c**.

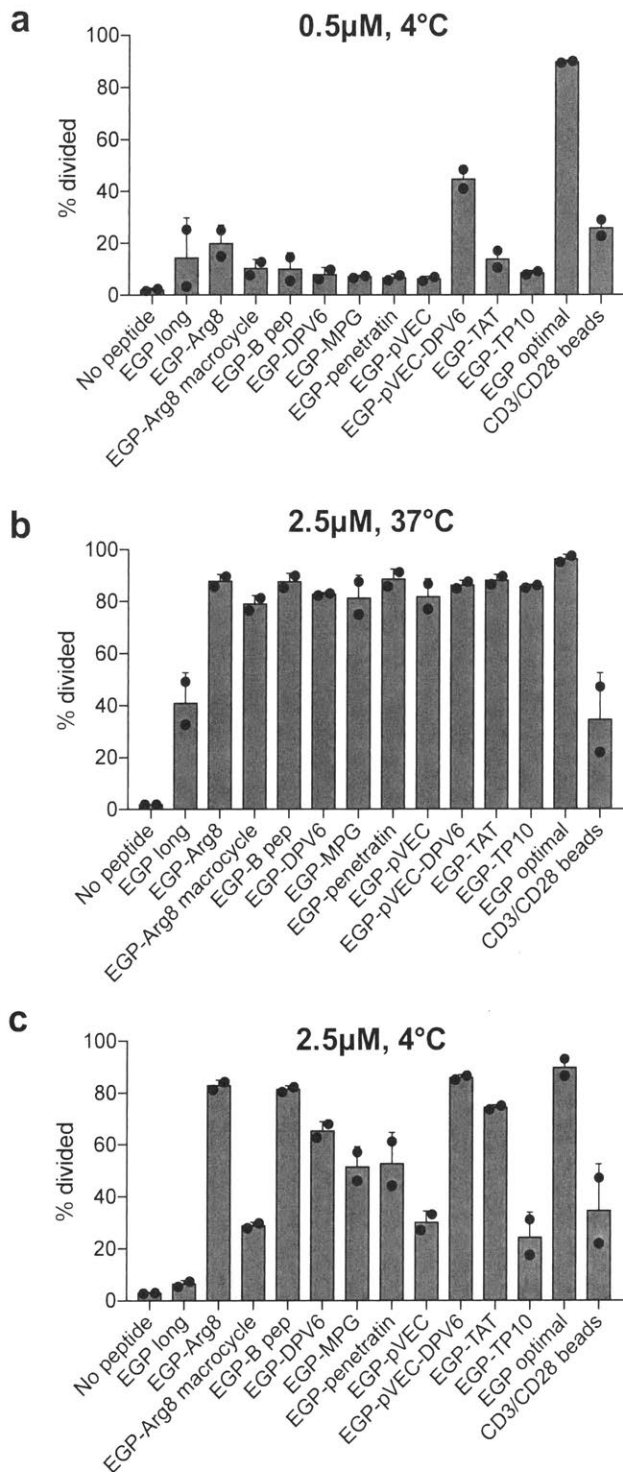


Figure 14 **Incubation at 4°C to inhibit active cellular processes.** **a**, The assay described in Figure 13 was performed with the incubation step at 4°C. **b-c**, the assay described in Figure 13 was performed with peptide pulse at 2.5μM either at 37°C, **b**, or 4°C, **c**. Shown is quantification of the % divided of pmel-1 CD8<sup>+</sup> T cells on day 3.

prime CD8<sup>+</sup> T cells (Figure 14a), with the possible exception of pVEC-DPV6. To increase the dynamic range of peptide constructs at 4°C, this experiment was performed at 2.5μM peptide. Although this concentration approached complete saturation for the 37°C incubation (Figure 14b), it did allow for differences to be observed for incubation at 4°C (Figure 14c). Under these conditions, active endocytosis is suppressed, making direct membrane transit the likely method of entry, and a number of constructs showed some ability to access the cytosol for presentation on MHC I: DPV6, MPG, and penetratin showed intermediate ability, and B pep, Arg8, pVEC-DPV6, and TAT showed high ability (Figure 14c).

### ***In vivo* priming of transferred pmel-1 T cells with EGP-penetratin**

*In vitro* priming may not translate to *in vivo* T cell priming due to the increased complexity of *in vivo* systems. As a step towards endogenous priming, an *in vivo* pmel-1 priming study was performed, with penetratin chosen as a model CPP. Mice were immunized with EGP peptide, EGP-penetratin, or no antigen, and 24h later, CFSE-labeled pmel-1 T cells were transferred intravenously. Lymph nodes were excised 48h after pmel-1 T cell transfer and proliferation was measured.



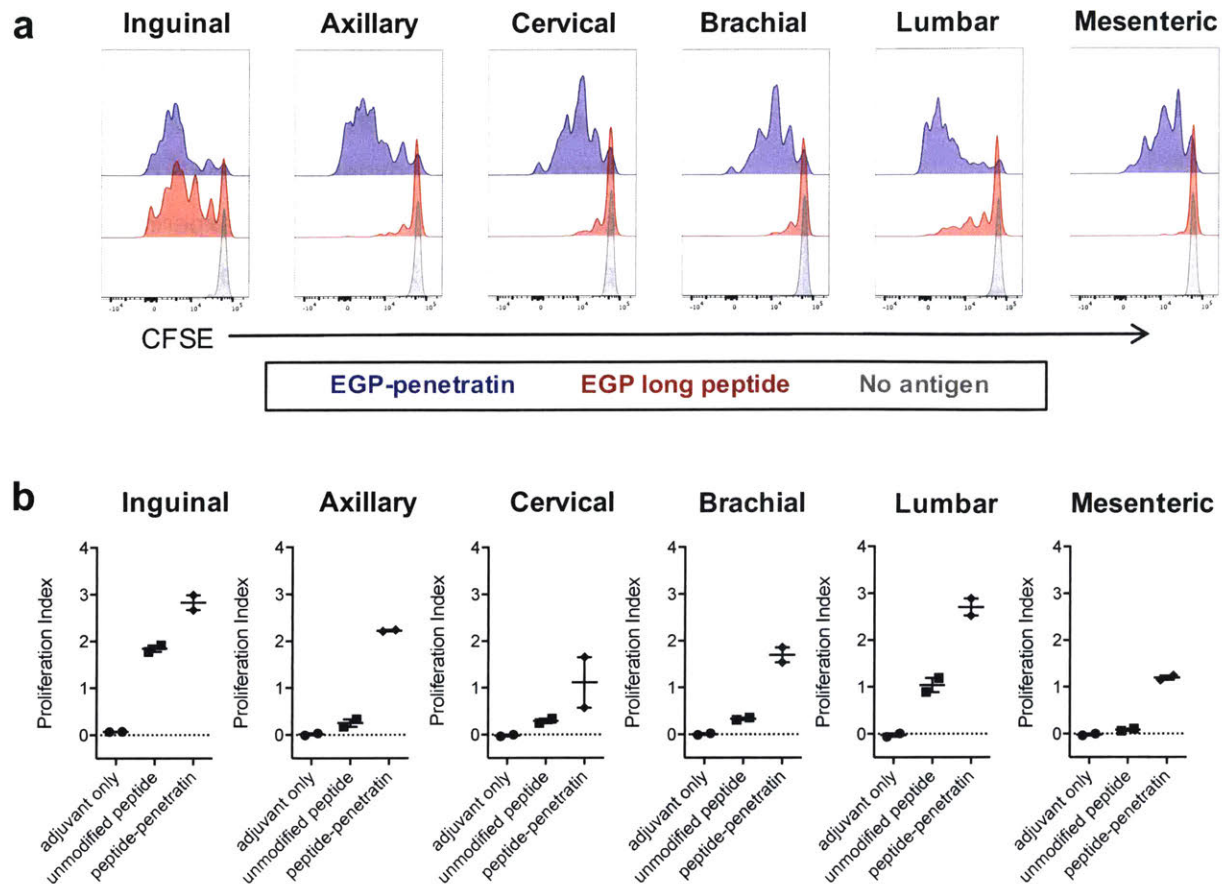


Figure 15 *In vivo* priming of adoptively transferred pmel-1 CD8<sup>+</sup> T cells. Mice were immunized with 25µg c-di-GMP and 5nmol of either EGP peptide or EGP-penetratin or received no antigen. Twenty-four hours later, 0.5 million CFSE-labeled purified pmel-1 T cells were transferred intravenously, and two days later, lymph nodes were isolated and proliferation among Thy1.1<sup>+</sup> CD8<sup>+</sup> pmel-1 T cells was measured. Shown are raw flow plots for each node, **a**, and quantification of proliferation index, **b**.

Encouragingly, the pmel-1 T cells showed much higher proliferation with the EGP-penetratin construct compared to unmodified EGP peptide in all lymph nodes analyzed (Figure 15a-b), setting the stage for endogenous priming studies.

### Endogenous priming with CPP-antigen constructs

Five antigen-CPP constructs were chosen to test for endogenous vaccination studies *in vivo* based on their performance *in vitro*. Mice were primed and boosted with indicated constructs and endogenous T cell responses were measured via ICS. All CPP-modified peptides showed improved activity over EGP, with enhancement ranging from modest (TAT) to >10-fold (MPG/penetratin) (Figure 16a-b). To assess if T cell priming can occur independently of cross-presenting DCs, Batf3<sup>-/-</sup> mice were immunized with indicated constructs (Figure 16c-d).



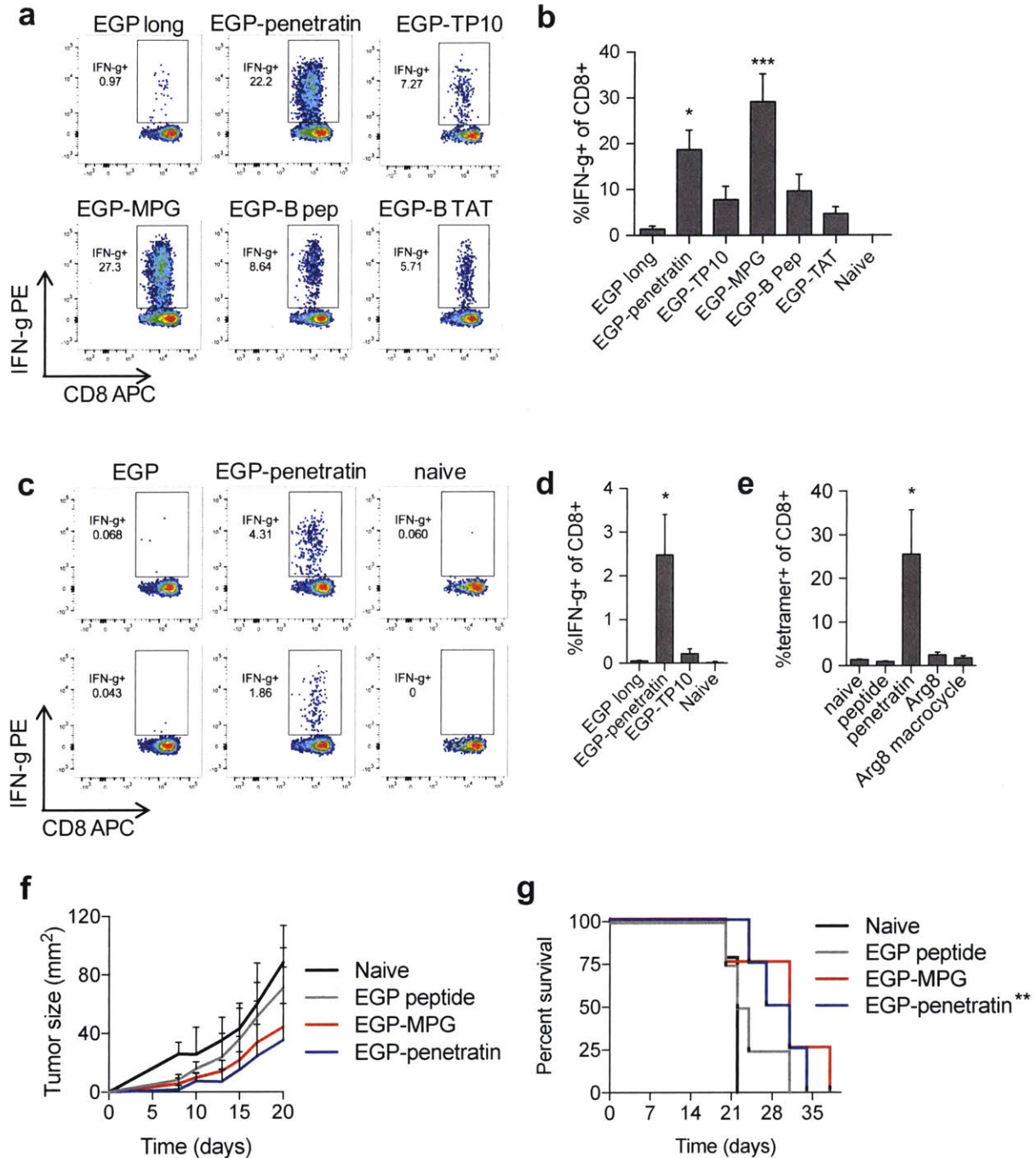


**Figure 16 Endogenous priming with CPP-antigen constructs and tumor protection.** **a-b**, female 8-week old C57BL6/J mice were primed and boosted 5nmol of the indicated construct (adjuvanted with 25 $\mu$ g c-di-GMP) and ICS was performed in blood on day 20. Shown are representative flow plots, **a**, and mean T cell responses quantified as % IFN- $\gamma$ <sup>+</sup> of CD8<sup>+</sup>, **b**. **c-d**, the immunization shown in **a-b** but in Batf3<sup>-/-</sup> mice. Shown are representative flow plots, **c**, and mean T cell responses, **d**. Note that **a-d** were performed in the same experiment. **e**, a separate experiment performed as described for **a-b**, shown are mean T cell responses post boost. **f-g**, mice were primed and boosted as previously described with the indicated constructs and challenged subcutaneously on the flank 40 days after boost with 10<sup>5</sup> B16F10 cells. Shown are mean tumor area over time, **f**, and survival, **g**. Mice were euthanized when tumor area exceeded 100mm<sup>2</sup>. \* $P$  < 0.05, \*\* $P$  < 0.01, \*\*\* $P$  < 0.001 by one-way ANOVA with Dunnett's post-test versus naïve for ICS and by Log-rank (Mantel-Cox) test for **g**.

EGP long peptide, which requires processing for presentation on class I because of its length, showed no ability to prime T cells in *Batf3*<sup>-/-</sup> mice, but EGP-penetratin showed clear ability, although the magnitude of response was significantly diminished compared to wild type (Figure 16c-d). In a separate experiment, in agreement with the *in vitro* priming study, low endogenous priming was seen to Arg8 and Arg8 macrocycle (Figure 16e). To see if the primed T cell responses are capable of offering protection in a challenge assay, mice primed and boosted with the indicated EGP constructs were challenged subcutaneously 40 days after boost with B16F10 tumor cells, which express gp100. Tumor size and survival were monitored over time (Figure 16f-g). Immunization with EGP peptide offered modest protection, and either MPG- or penetratin- antigen further suppressed tumor growth and increased survival, although only penetratin reached statistical significance in this experiment (Figure 16f-g). Thus, cell penetrating peptides linked to antigens enhance T cell priming, show activity independent of cross presenting DCs, and the T cells primed show functionality via delaying tumor outgrowth in a challenge setting.

### **Trafficking of CPP constructs**

Priming *in vivo* relies not only on ability of a given construct to access the cytosol of antigen presenting cells, but also the ability to reach antigen presenting cells in the first place. Thus, we performed trafficking studies to determine lymph node uptake of a number of CPP-antigen constructs. Fluorescently labeled versions of the indicated CPP constructs were synthesized and injected subcutaneously at the base of the tail of 8-week old C57BL6/J mice, and inguinal and axillary lymph nodes were resected 24h later and imaged using IVIS (Figure 17a-c). Uptake of all CPP constructs was higher than unmodified free peptide, ranging from modestly increased (Arg8, MPG, B Pep, and TAT) to greatly increased (penetratin and TP10) (Figure 17a-c).

### **Double modification of peptide to enhance both trafficking and cytosolic access**

EGP-penetratin shows effective T cell priming (Figure 16a,b,e) but its lymph node trafficking only led to 3x higher fluorescence compared to unmodified peptide (compared, for example, the approximately 8-fold increase in fluorescence seen with lipoCpG compared to CpG<sup>10</sup>). We hypothesized that by further increasing lymph node targeting via conjugation to DSPE-PEG<sub>2000</sub> (see Chapter 2) that T cell priming may be further enhanced. Therefore, a

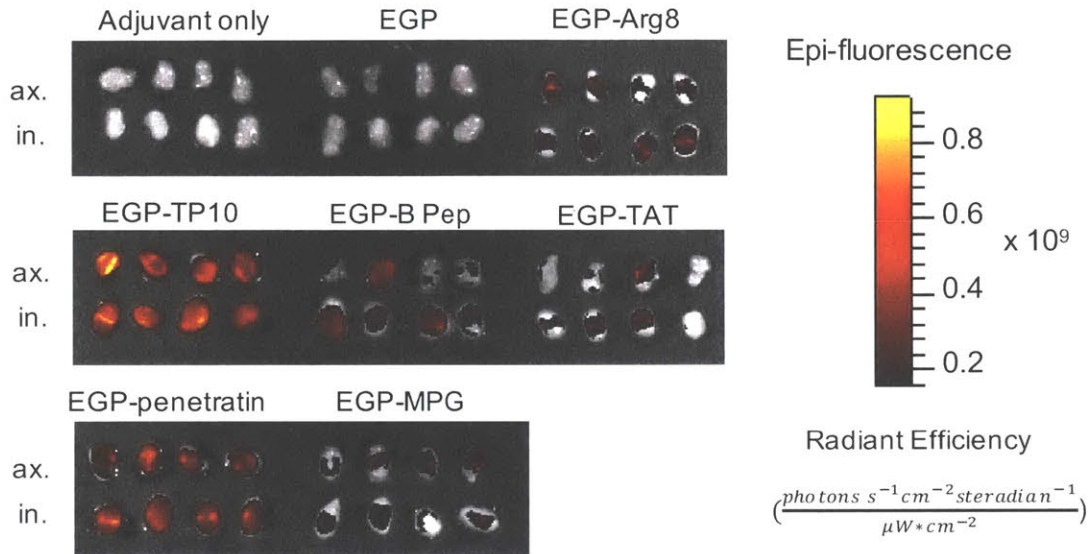
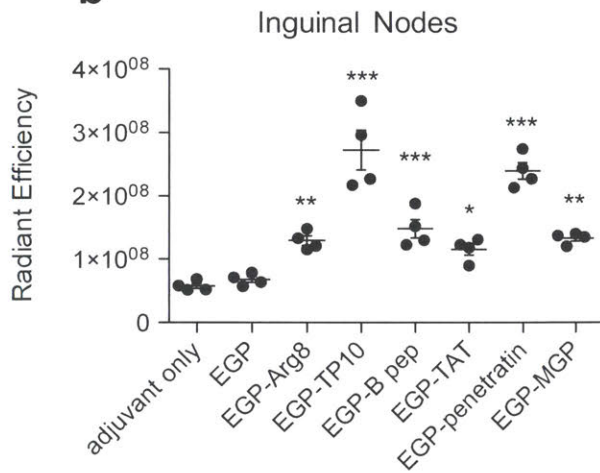
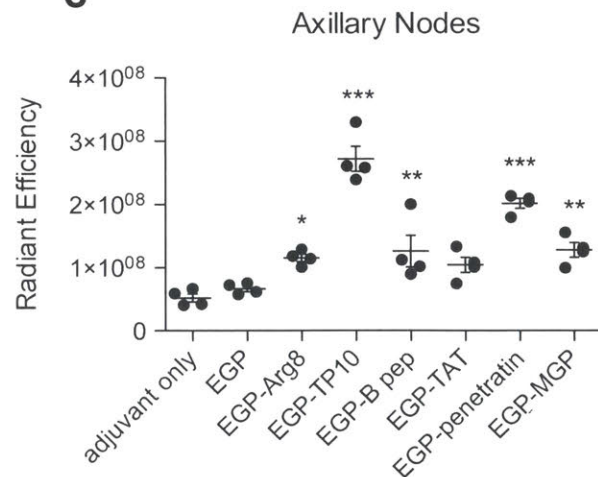
**a****b****c**

Figure 17 **Lymph node trafficking properties of CPP-antigen constructs.** a-c, female 8-week old C57BL6/J mice were injected subcutaneously at the base of the tail with 25 $\mu$ g c-di-GMP and 25nmol of the indicated sulfo-Cy5 labeled constructs. Inguinal and axillary lymph nodes were resected 24h later and fluorescently imaged via IVIS. Shown are images of lymph node fluorescence, **a**, and quantification of total radiant efficiency ((photons\*s<sup>-1</sup>\*cm<sup>-2</sup>\*steradian<sup>-1</sup>)/( $\mu$ W\*cm<sup>2</sup>)) per lymph node for inguinal nodes, **b**, and axillary nodes, **c**. \* $P < 0.05$ , \*\* $P < 0.01$ , \*\*\* $P < 0.001$  by one-way ANOVA with Dunnett's post-test versus adjuvant only.

construct was synthesized with N-terminal DSPE-PEG<sub>2000</sub> and C-terminal penetratin. When mice were immunized with this doubly-modified construct, however, the T cell responses were actually lower than either construct individually, diminished by approximately two-fold (Figure 18a). This may indicate that the addition of DSPE with a long PEG linker inhibits the ability of penetratin to mediate cytosolic access, as cytosol access of CPP-conjugates is known to be cargo dependent<sup>203</sup>, and/or that the presence of penetratin linked C-terminally hampers DSPE-PEG<sub>2000</sub>-mediated lymphatic re-targeting, or (non-exclusively), that this double-modification hampers proteasomal processing.

### **Are CPP-antigens presented by non-professional APCs *in vivo*?**

Because CPPs have the potential to access the cytosol of cells that would normally be incapable of presentation, we wondered if part of the mechanism of action of these CPP-constructs could be presentation and priming by additional cell types. For example, B cells may be of interest if they are capable of presenting antigens linked to CPPs because they are highly abundant and are capable of expressing co-stimulatory molecules needed for effective T cell priming. Indeed, B cells have been explored as potential antigen presenting cells in cell-based vaccines systems where they can be mechanically manipulated to allow cytosolic access of antigen<sup>212</sup>. To investigate this, mice were immunized with EGP or EGP-MPG or EGP-penetratin and 24h later inguinal lymph nodes were isolated, digested, and stained for flow sorting. DCs (CD11c<sup>+</sup>F4/80<sup>low</sup>), macrophages (F4/80<sup>high</sup>), and B cells (B220<sup>+</sup>) were individually sorted and incubated with purified, CFSE-labeled pmel-1 T cells. Twenty-four hours after initiation of co-culture, CD69 and CD137 upregulation was measured on pmel-1 T cells, and two days later, proliferation was measured by CFSE dilution (Figure 18b-e). Among CD11c<sup>+</sup> DCs, clear upregulation of CD69 and CD137 was seen with all constructs compared to naïve, however, there was little difference between the CPP constructs and unmodified peptide (Figure 18b). There was no upregulation of CD69 or CD137 seen in any condition among B cells, but if peptide was added *in vitro*, B cells showed clear ability to activate pmel-1 T cells, indicating that there is no general defect in ability of B cells to activate CD8<sup>+</sup> T cells (Figure 18c). Priming among macrophages showed a slight trend towards higher CD69 and CD137 expression with constructs including CPPs, but the difference was not dramatic (Figure 18d). Looking at CFSE dilution on day 3, only sorted DCs were capable of promoting clear proliferation above background, and there were not significant differences between peptide and peptide-CPP constructs (Figure 18e). Therefore, under the conditions tested here, we did not uncover



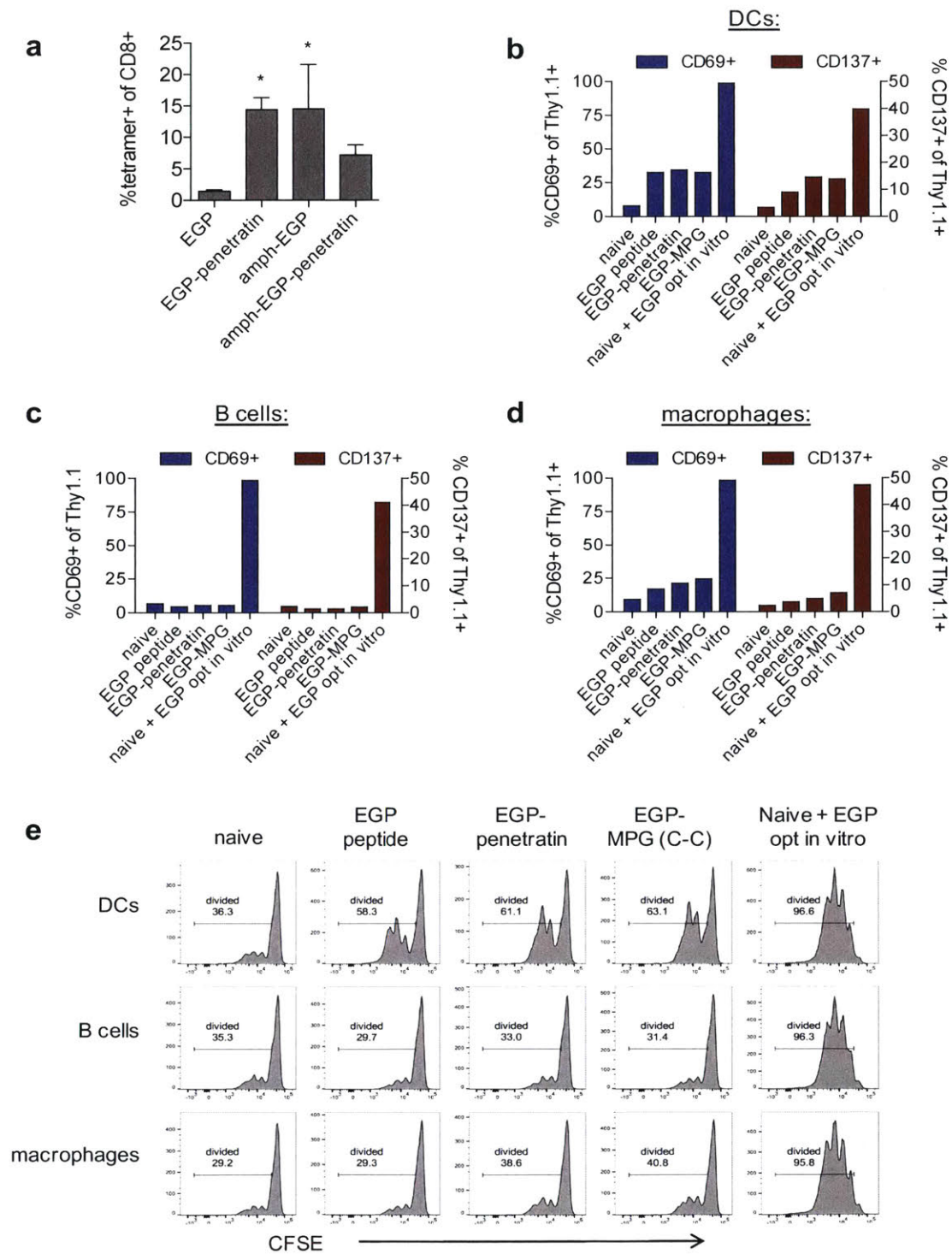


**Figure 18 Doubly-modified constructs; ex vivo analysis of LN resident APC antigen presentation.** **a**, mice were immunized and T cell responses were characterized as described in Figure 9; shown is mean T cell response quantified as % IFN- $\gamma^+$  of CD8 $^+$ . **b-e**, Eight-week old C57BL6/J mice were injected with 25 $\mu$ g c-di-GMP and 10nmol of indicated construct. Twenty-four hours later, inguinal lymph nodes were isolated, digested, stained with antibodies against CD11c, B220, F4/80, and DAPI. Cells were sorted; 10,000 live B cells, macrophages, or dendritic cells per condition. Fifty-thousand CFSE-labeled pmel-1 T cells were added to each well. On day 1, CD69 and CD137 expression among Thy1.1 $^+$  T cells was measured, and on day 3, CFSE dilution was measured. Shown is quantification of CD69 and CD137 expression on day 1 within each population, **b-d**, and analysis of proliferation via CFSE dilution, **e**. \* $P < 0.05$ , \*\* $P < 0.01$ , \*\*\* $P < 0.001$  by one-way ANOVA with Dunnett's post-test versus naive for **a**.

evidence that non-professional antigen present epitopes attached to CPPs *in vivo*, but a more thorough investigation will be necessary to draw firm conclusions.

### **3.3 Discussion and Future Work**

In vaccine development, the most important metric of a platform's success is the ability to prime endogenous, *de novo* responses. The *in vitro* assay was useful as a first pass to screen potential candidates, and *in vitro* responses correlated to some extent with *in vivo* endogenous priming where responses were measured. For example, Arg8 showed little activity over unmodified peptide both *in vitro* and *in vivo*, and EGP-MPG and EGP-penetratin showed clear benefit in both. However, the correlation was not perfect, for example, TAT performed as well as penetratin and MPG constructs *in vitro*, but showed significantly weaker responses for *in vivo* priming. This is likely reflective of the fact that cytosolic access is only one part of a number of complex mechanisms that must occur for effective vaccine-mediated T cell priming, one important part of which is access to lymphoid organs, where priming occurs. Trafficking alone was also not entirely predictive of *in vivo* priming—TP10 appeared to traffic best, but *in vivo* T cell priming was approximately half the magnitude of MPG and penetratin constructs. These results are not necessarily in conflict with the *in vivo* priming responses because it is likely the integration of trafficking and cytosolic access efficiency (as well as other factors, like proteasomal processing) that together determine T cell priming magnitude.

None of the constructs tested showed strong ability to prime cells when the incubation occurred at 0.5 $\mu$ M and 4°C, with the possible exception of pVEC-DPV6. However, when this assay was performed at 5x higher concentration, there was clear ability of a number of constructs to access the cytosol. The TAT-antigen construct was one of the best performers at 4°C, indicating that it can access the cytosol via direct membrane transit, in agreement with some previous reports<sup>213,214</sup>. (Note that TAT is capable of both direct membrane transit as well as endocytosis- and macropinocytosis- dependent transit to the cytosol<sup>215,216</sup>.)

The responses in Batf3<sup>-/-</sup> mice to EGP-penetratin were clear, however, the magnitude was diminished significantly. This may be reflective of the fact that these constructs are presented both via traditional cross-presentation and also by CPP-enhanced cytosolic access. It may also indicate that the missing CD8 $\alpha$ <sup>+</sup> and CD103<sup>+</sup> cross presenting dendritic cells in Batf3<sup>-/-</sup> mice are critical cell types for presentation of CPP-antigen constructs, and thus, enhancement of cytosolic access within these cell types cannot be assessed because they are missing in

Batf3<sup>-/-</sup> mice. Nonetheless, this result confirms that EGP-penetratin can be presented and prime T cell responses in mice that are incapable of cross-presentation.

All modifications seemed to enhance lymphatic trafficking to some extent, which is interesting because the small size increase alone would not be predicted to dramatically enhance lymphatic uptake based on experiments performed in sheep looking at the relationship between molecular weight and lymph node uptake<sup>72</sup>. The constructs tested all had a net positive charge, so it may be possible that they interact *in vivo* with negatively charged serum proteins, which would lead to enhanced lymphatic uptake as described in Chapter 2, but more work will be needed to determine if this is the case.

Although the tumor challenge suppression may not appear impressive, this inoculum is 4-fold higher than the 100% lethal dose of B16F10<sup>217</sup> and the challenge occurred 40 days post boost, when T cell responses would have contracted significantly. Future studies should be performed to assess protection when mice are challenged at the peak of T cell responses, approximately 7 days after boost, which may yield more impressive tumor protection data.

This work is ongoing, and there are a number of areas for follow-up study in addition to those listed above. First, it would be interesting to try MPG that is linked C-N instead of the flipped orientation used in this chapter (C-C), because it was the only construct synthesized in this orientation. Alternatively, it could be interesting to try C-C linkage for some of the other sequences—there may be benefits to the unusual orientation, like perhaps epitope protection from serum proteases. Further, it would be useful to perform some microscopy on fluorescently labeled CPP-antigen constructs to visualize cytosolic access and to better understand the kinetics of this process. The control of antigen admixed with CPP (not physically linked) would be important to show that the membrane transit relies on covalent attachment. Extending to other antigens to demonstrate that these findings are not just limited to EPG would also be beneficial, and it may also be useful to explore whether or not the constructs that demonstrate superior trafficking (especially EGP-TP10 and EGP-penetratin) demonstrate binding to serum proteins, which may explain this enhancement. TP10, which showed the best lymphatic drainage, is a relatively hydrophobic sequence, so it may be possible that it binds one of the lipid-binding pockets on serum albumin. Binding of constructs to serum albumin can be measured using bilayer interferometry. Finally, it could be beneficial to undertake similar studies as those performed here with adjuvant delivery for molecules that require cytosolic access for action. A chief example where this may be applied is STING agonists, like cyclic dinucleotides, which have cytosolic receptors and are capable of inducing potent type I IFN responses<sup>218</sup>.



There is evidence that CPPs linked to antigens of interest can preferentially target the MHC class I pathway, which may be advantageous in immunization where CD8<sup>+</sup> T cell responses are desired over CD4<sup>+</sup> T cell responses<sup>219</sup>. For example, in both recent phase I neoantigen vaccine clinical trials, although the bioinformatics pipelines used were meant to prioritize for CD8<sup>+</sup> T cell responses to neoantigens, both groups saw high CD4<sup>+</sup> T cell responses, whereas CD8<sup>+</sup> T cell responses were harder to detect and less frequent<sup>37,38</sup>; incorporating a CPP may increase these desired CD8<sup>+</sup> T cell responses (although it's worth noting that there is ample evidence that anti-tumor CD4<sup>+</sup> T cell responses can impart significant activity<sup>220-222</sup>). In summary, CPP-antigen constructs have the potential the immunogenicity of peptide antigens, and future work in this vein may yield to better understanding of how to increase antigen presentation and T cell priming.

### **3.4 Methods**

#### **Peptide synthesis**

EGP long antigen peptide and the indicated CPPs were synthesized via automated solid-phase peptide synthesis<sup>196</sup>. Briefly, equal volumes of a protected amino acid monomer (0.4 M in DMF, Chem Impex) and HATU (0.34 M in DMF) were combined with diisopropylethylamine (neat, final concentration 1 M; Sigma) at 90°C to form an active ester and coupled onto RINK-amide PEG (PCS Biomatrix) resin in flow at 90°C. After a DMF wash, the N-terminus of the coupled monomer was deprotected with piperidine (final concentration 1 M in DMF; Sigma), the peptidyl resin was washed with DMF, and the cycle was repeated. These iterative coupling reactions (<1 min each) were performed in by a custom-built automated synthesizer as described. 1 Azido-ornithine was included at the C-terminus of the EGP peptide and 4-pentynoic acid was included at the N-terminus of each CPP to provide chemical handles for Cu(I)-catalyzed click chemistry. The single exception was the CPP denoted 'MPG C-term,' in which propargylglycine was incorporated at the C-terminus as the alkyne click handle. The N-terminus of MPG C-term was acetylated to maintain the same charge between the MPG placement variants. All click chemistry monomers and the N-terminal acetic acid in MPG C-term were coupled in batch at room temperature for 30 min. Peptides were cleaved from resin overnight at RT (by volume, 82.5% trifluoroacetic acid, 5% water, 5% thioanisole, 5% phenol, and 2.5%

ethane dithiol; each from Sigma), triturated in cold diethyl ether, and purified via reversed-phase HPLC.

The EGP long antigen was then conjugated to each CPP via Cu(I)-catalyzed click chemistry. Approximately 1  $\mu\text{mol}$  of each reagent was combined in a septum vial with a catalytic amount of CuBr. The vial was flushed with  $\text{N}_2$  and 2.5 mL dry DMF was added using anhydrous technique. The reactions were incubated at room temperature for 2h, quenched in water with 0.1% TFA additive, purified via reversed-phase HPLC, and isolated in with >90% purity. Product identity and purity were verified via LC-MS.

### **Evaluation of immune responses and flow cytometry**

Methods used for tetramer staining and intracellular staining, including the gp100 sequences used, are the same as reported in Chapter 2. For the lymph node sort, anti-CD11c PE (clone N418, BioLegend), anti-B220 FITC (clone RA3-6B2, BioLegend), and anti-F4/80 APC (clone BM8, BioLegend) were used prior to flow sorting. For analysis of early activation markers in the co-culture systems, Thy1.1 AlexaFluor700 (clone OX-7, BioLegend), CD69 BUV395 (clone H1.2F3, BD Biosciences), and CD137 APC (4-1BB, clone 17B5, BioLegend) were used.

### ***In vitro* presentation assay**

An 8-week old C56BL6/J female mouse was sacrificed and a single cell suspension of splenocytes was obtained. These whole splenocytes were pulsed with 0.5 $\mu\text{M}$  or 2.5 $\mu\text{M}$  peptide or peptide-CPP conjugate for 1h at either 37°C or 4°C (to inhibit active endocytosis). These splenocytes were washed 3 times and plated (100,000 per condition) in 96-well V-bottom tissue culture plates with 50,000 CFSE-labeled pmel-1 T cells in 200 $\mu\text{L}$  total volume of complete RPMI + 10% FBS + p/s + IL-2. Twenty-four hours after initiation of the co-culture, half of the cell suspension was removed for analysis of CD69 and CD137 expression on pmel-1 T cells (identified via Thy1.1), and 100 $\mu\text{L}$  of fresh media with IL-2 was added. Three days after initiation of co-culture, the remaining cells were analyzed for proliferation of the CFSE-labeled pmel-1 T cells.

## **Adoptive transfer proliferation studies**

Methods used for adoptive transfer and detection of proliferated pmel-1 T cells are the same as reported in Chapter 2, with immunization on day 0, transfer of pmel-1 T cells 24h later, and analysis of expansion in LNs by flow cytometry 48h after transfer.

## **Lymph node antigen presenting cell sort and *in vitro* co-culture**

Eight-week old C57BL6/J mice were injected with 25µg c-di-GMP and 10nmol of either EGP peptide, EGP-penetratin, EGP-MPG, or no antigen in 100µL PBS. Twenty-four hours later, inguinal lymph nodes were isolated, digested with 0.8 mg/ml Dispase, 0.2 mg/ml Collagenase, and 0.1 mg/ml DNase I in RPMI at 37°C for 20 minutes with gentle agitation, and a single cell suspension was created. Cells were labeled with antibodies against CD11c, B220, F4/80, and DAPI for live/dead discrimination. Cells were sorted using the FACS Aria (BD Biosciences); 10,000 B cells, macrophages, or dendritic cells were sorted per condition. Pmel-1 T CD8<sup>+</sup> cells were isolated from pmel-1 splenocytes, CFSE labeled, and 50,000 pmel-1 CD8<sup>+</sup> T cells were added to the 10,000 sorted APCs per well. On day 1, half of the co-culture volume was analyzed for CD69 and CD137 (4-1BB) expression among Thy1.1<sup>+</sup> T cells, and on day 3, the remaining cells were analyzed for CFSE dilution among Thy1.1<sup>+</sup> T cells.

## **Cells and tumor challenge**

B16F10 were purchased from ATCC and was cultured in complete DMEM (DMEM supplemented with 10% FBS, 100 units/mL penicillin, 100 µg/mL streptomycin, and 4 mM L-alanyl-L-glutamine). Cells were tested regularly for mycoplasma contamination and for rodent pathogens and none used tested positive at any point.

Forty days after boost, an inoculum of 10<sup>6</sup> tumor cells was injected s.c. on the right flank of mice in 50 µL sterile PBS. Tumor size was measured as an area (longest dimension x perpendicular dimension) three times weekly, and mice were euthanized when tumor area exceeded 100 mm<sup>2</sup>.

## Lymph node uptake of fluorescent constructs

Twenty-five nmol of sulfo-Cy5 labeled peptide constructs and 25µg c-di-GMP were injected subcutaneously at the base of the tail in 100µL PBS (50µL on each side) of 8-week old C57BL6/J female mice. One day later, inguinal and axillary lymph nodes were isolated and imaged using IVIS. Uptake was measured with fluorescence: total radiant efficiency per lymph node ( $\text{photons}\cdot\text{s}^{-1}\cdot\text{cm}^{-2}\cdot\text{steradian}^{-1}$ )/( $\mu\text{W}\cdot\text{cm}^{-2}$ ), quantified using Living Image (PerkinElmer) software.

## Statistical analysis

Statistical methods were not used to determine sample size, but sample numbers were chosen based on estimates from pilots and published results such that appropriate statistical tests may yield statistically significant results. Unless otherwise stated, analysis of tetramer, ICS, and lymph node trafficking results were analyzed by using one-way ANOVA with a Dunnett's post-test versus naïve using GraphPad Prism software. Statistics were not performed on *in vitro* screen because the assay was performed with only two replicates per condition. Where ANOVA was used, variance between groups was found to be similar by Bartlett's test. No samples were excluded from analysis.

# CHAPTER 4: Combination immunotherapy engaging innate and adaptive immunity

Adapted from: Moynihan KD\*, Opel CF\*, et al. Eradication of large established tumors in mice by combination immunotherapy that engages innate and adaptive immune responses. *Nat Med.* 2016 Dec; 22(12): 1402–1410. DOI: 10.1038/nm.4200.

## 4.1 Introduction

Checkpoint blockade therapies prove that an endogenous immune response can regress human tumors, but significant responses remain restricted to a minority of patients<sup>6,223</sup>. Combination treatments may improve response rates<sup>224-226</sup>, and immunotherapies implementing three or more agents in tandem are already in clinical testing<sup>227-230</sup>. However, even in preclinical models, complete tumor rejection is usually only achieved by treating very small tumors and/or treating at very early times preceding the establishment of a fully developed tumor microenvironment, unless adoptive transfer of *ex vivo*-expanded T-cells is employed<sup>231,232</sup>. Autochthonous tumors induced in genetically-engineered animals, which may generate immunosuppressive networks more akin to human tumors, are also generally refractory to immunotherapy<sup>233,234</sup>. The general characteristics of an endogenous immune response capable of reliably eradicating large immunosuppressive tumor burdens remain unclear.

We recently reported that therapies combining anti-tumor antibodies and extended half-life IL-2 (IL-2 fused with mouse serum albumin (MSA-IL-2) or Fc) exhibited striking synergy in tumor therapy<sup>9</sup>. This combination was curative when augmented with adoptive T-cell transfer. We hypothesized such results might be achieved in the setting of a wholly endogenous immune response by replacing T-cell transfer with a powerful vaccine. To this end, we employed a potent lymph node-targeted vaccine composed of peptide antigens and CpG DNA conjugated to albumin-binding lipids. These amphiphile-vaccines reversibly bind to albumin present in interstitial fluid and efficiently traffic to lymph nodes, leading to robust T-cell responses<sup>10</sup>. We also included systemic anti-PD-1 administration due to its capacity to enhance vaccine responses and further modulate the tumor microenvironment<sup>7,223</sup>. In multiple transplanted tumor models as well as the BRAf/Pten genetically engineered mouse model of melanoma, this quaternary combination immunotherapy regressed a majority of established tumors and

established long-lived protective memory. Optimal responses required all 4 components and were accompanied by an intratumoral cytokine storm, recruitment of innate and adaptive leukocytes to the tumor microenvironment, and depended on cross-presenting dendritic cells, CD8<sup>+</sup> T-cells and innate effectors. These findings establish the capacity of the endogenous immune response to eradicate large established tumors and identify characteristics of highly protective multivariate anti-tumor immunity.

## 4.2 Results

### **Combining a potent vaccine with anti-tumor antibody, extended-PK IL-2, and checkpoint blockade eradicates large established tumors.**

Motivated by the synergy observed between extended-PK IL-2 and anti-tumor antibodies<sup>9</sup> and our discovery of a strategy to target vaccines to lymph nodes<sup>10</sup>, we explored combination treatments bringing these reagents together with checkpoint blockade. To simplify reference to this therapy, we designate combinations of these components by single initials: A (anti-tumor antibody), I (MSA-IL-2), P (anti-PD-1), and V (amph-vaccine). We evaluated this combination treatment in 3 tumor models: B16F10 melanoma, DD-Her2/neu (a Her2/neu-expressing breast cancer), and TC-1 tumors expressing the HPV oncoantigens E6/E7. For each tumor, appropriate A and V components were selected (Figure 19a): Antibodies against Trp1 (TA99) and Her2/neu (7.16.4) were used to treat B16F10 and DD-Her2/neu, respectively, while an antibody surrogate 2.5F-Fc (Fc fused with an engineered binding protein that recognizes tumor-expressed  $\alpha_v\beta_3$ ,  $\alpha_v\beta_5$ , and  $\alpha_5\beta_1$  integrins<sup>235</sup>) was used to target TC-1 tumors (Figure 20a-c). In parallel, highly immunogenic amphiphile-peptide vaccines were synthesized targeting Trp2, Her2/neu, and HPV E7 (Figure 20d-g, and ref <sup>10</sup>). Tumor cells ( $10^6$ ) were injected s.c. and allowed to establish for 8 days prior to initiation of therapy, providing initial tumor sizes of ~40-60 mm<sup>2</sup>, depending on the tumor model. The therapeutic components were injected once per week, with P and V administered 3 times and A and I given 5 times (Figure 19a). Treating B16F10 melanomas, AIPV therapy induced robust tumor regression and durable cures in 75% of mice (Figure 19b-c), while combinations of 3 or fewer of the components elicited weaker responses ranging from modestly reduced efficacy (AIP) to outcomes barely different from untreated tumors (APV) (Figure 19b-c, Figure 21a-d). Greater than 80% of AIPV-treated long term survivors rejected a rechallenge with  $10^5$  B16F10 cells two months after cessation of

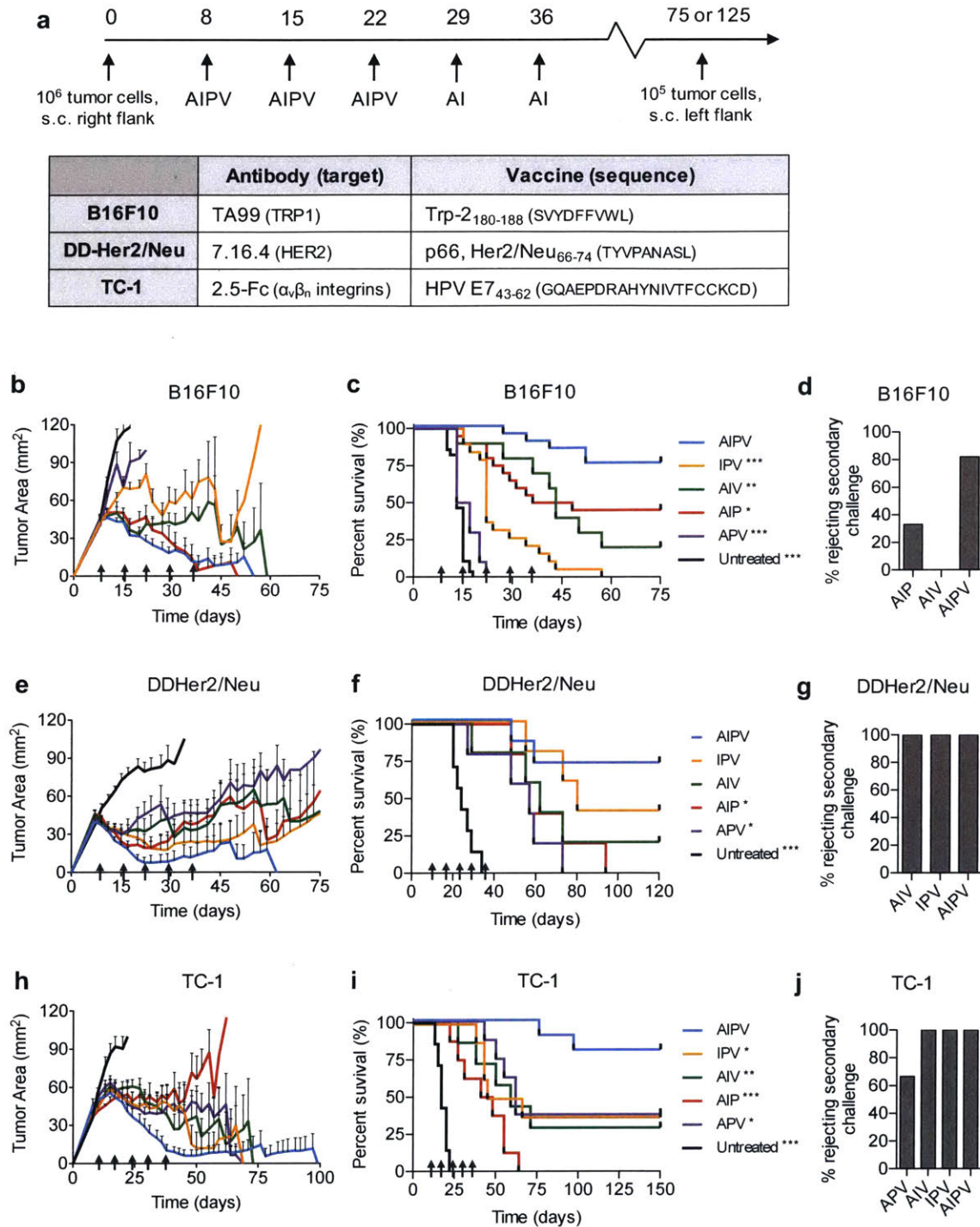


**Figure 19 AIPV immunotherapy cures large established tumors and establishes protective memory in multiple tumor models.** **a**, Components of AIPV therapy and timeline of treatment. **b-j**, Groups of mice were inoculated with  $10^6$  tumor cells s.c. in the flank: B16F10 (**b-d**,  $n = 10$ /group for APV, 20/group for all other groups) and TC-1 (**h-j**,  $n = 8$ /group) tumor cells were injected in C57Bl/6 mice while DD-Her2/neu tumor cells (**e-g**,  $n = 7$  for untreated and AIPV,  $n = 5$  for all other groups) were injected in balb/c mice. On day 8 post implantation, AIPV treatment was initiated following the timeline in **a**. Shown are tumor growth (**b, e, h**) and survival (**c, f, i**) over time and the fraction of long term survivors that rejected a rechallenge with  $10^5$  tumor cells on day 75 for B16F10 and day 125 for TC-1 and DD-Her2/Neu (**d, g, j**). Shown are mean tumor size  $\pm$  s.e.m. in **b, e, h**. Data compiled from 2-3 independent experiments. Gray arrows indicate treatment time points. \*  $p < 0.05$ , \*\*  $p < 0.01$ , \*\*\*  $p < 0.001$  versus AIPV by Log-rank (Mantel-Cox) test.



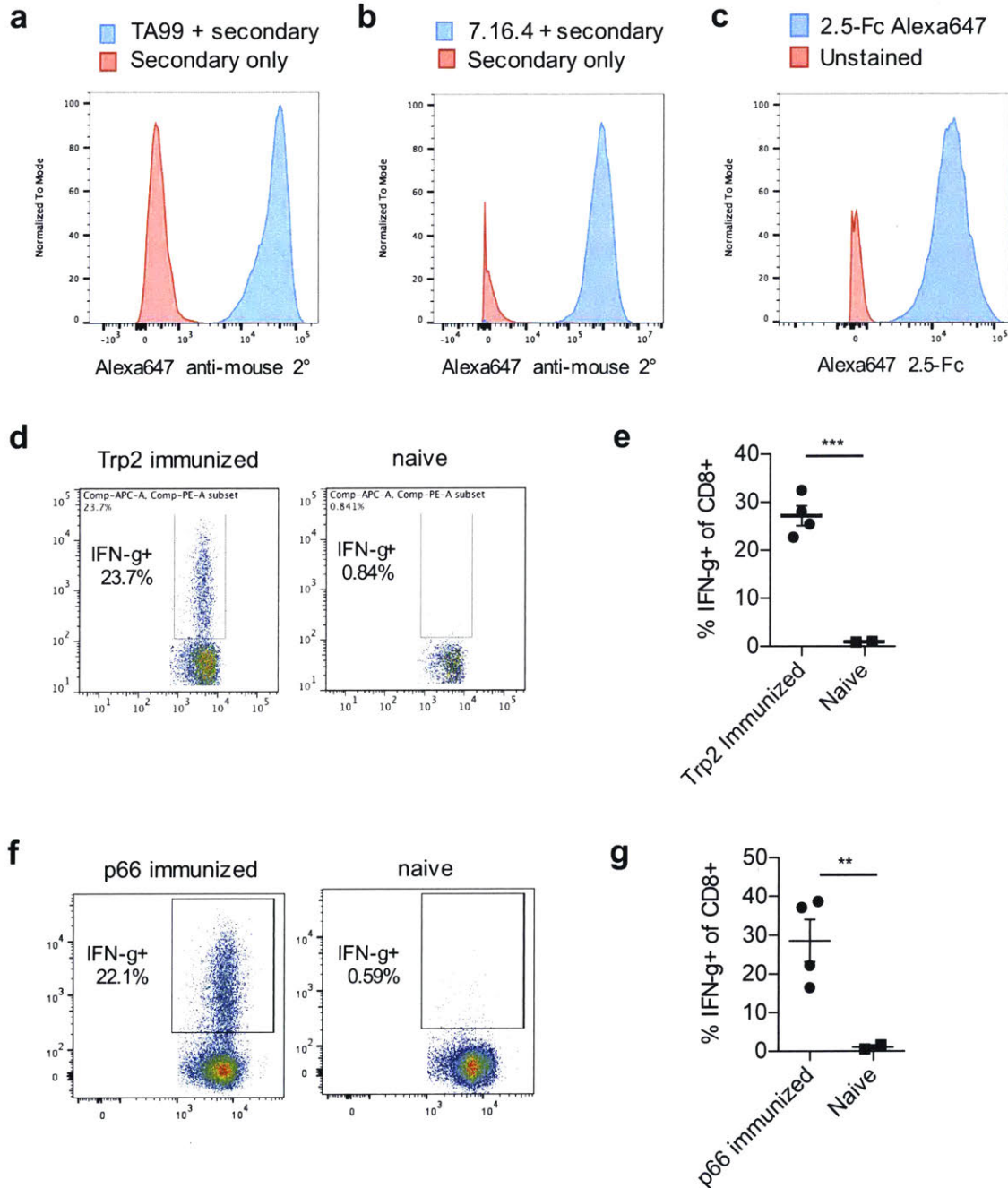


**Figure 20 Selection of A (monoclonal anti-tumor antibody) and V (amphiphile-vaccine) components for treatment of B16F10, DD-Her2/Neu, and TC-1 tumors.** **a**, B16F10 cells were incubated with 20 $\mu$ g/mL TA99 for 20 minutes at 4°C, washed, and stained with AlexaFluor647 labeled anti-mouse IgG followed by flow cytometry analysis. **b**, DD-Her2/neu cells were incubated with 20 $\mu$ g/mL 7.16.4 for 20 minutes at 4°C, washed, and stained with AlexaFluor647 labeled anti-mouse IgG followed by flow cytometry. **c**, TC-1 cells were incubated with 20 $\mu$ g/mL AlexaFluor647 labeled 2.5-Fc for 20 minutes at 4°C, washed, and analyzed by flow cytometry. **d-e**, C57Bl/6 mice ( $n = 4$  animals/group) were primed and boosted 14 days later with amph-vaccine (20  $\mu$ g amph-Trp2 and 1.24 nmol amph-CpG) against Trp-2. Six days following the boost, intracellular cytokine staining was performed on peripheral blood cells to quantify anti-Trp2 responses. Shown are representative plots (**d**) and mean $\pm$ s.e.m. %IFN- $\gamma$  among CD8<sup>+</sup> T-cells (**e**). **f-g**, Balb/c mice ( $n = 4$  animals/group) were primed and boosted 14 days later with amph-vaccine against p66 (20  $\mu$ g amph-p66 and 1.24 nmol amph-CpG). Six days following boost, ICS was performed to quantify anti-p66 responses. Shown are representative plots (**f**) and mean $\pm$ s.e.m. %IFN- $\gamma$  among CD8<sup>+</sup> T-cells (**g**).

therapy (Figure 19d). Similarly, in the DD-Her2/neu and TC-1 tumor models greater than 70% of mice achieved complete tumor rejection when treated with AIPV, and 100% of long term survivors rejected tumors on rechallenge (Figure 19e-j, Figure 21e-h). Triple combinations of AIPV components demonstrated significantly lower efficacy, though each of the 3 tumor models showed a different hierarchy of efficacy among the ternary combinations. A limited exploration of alternate 4-agent combinations revealed that could be replaced by anti-CTLA-4, but several other combinations failed to replicate AIPV in eliminating B16F10 tumors (Figure 22a-f). Importantly, despite high rates of response, AIPV therapy was associated with minimal systemic toxicity (Figure 23a-c).

### **AIPV therapy remodels the tumor microenvironment and promotes a combined innate and adaptive immune attack on tumors.**

To understand the underlying mechanisms, we further analyzed responses to AIPV therapy in the B16F10 model. AIPV treatment expanded Trp2-specific CD8<sup>+</sup> T-cells systemically (Figure 24a-b), correlating with striking vitiligo in treated animals (Figure 23d-f). However, comparable Trp2-specific T-cell responses were elicited by ineffective AIV and IPV treatments (Figure 24b). We thus looked for changes within tumors that distinguished treatments. Luminex quantification of intratumoral cytokines and chemokines during AIPV or subcombination treatments revealed a heavily modified microenvironment containing five clusters of co-regulated proteins, with many pro-inflammatory factors significantly increased in the most effective therapies (Figure 24c and Figure 25). We used partial least squares regression (PLSR) to construct models using cytokines from each cluster to predict log<sub>10</sub> tumor mass. Analysis of the variance in tumor mass explained by each model revealed that cluster 3 cytokines captured the most variance (Figure 24d), and therefore provided the most predictive model. Variable importance in projection (VIP) scores identified 4 predictive biomarkers from cluster 3– MIP-1 $\alpha$ , RANTES (CCL5), eotaxin, and IL-4– whose levels were inversely correlated with tumor size and predicted tumor mass across all 5 treatment combinations (Figure 24e-f, R<sup>2</sup>=0.69).

Motivated by this chemoattractant-rich protective signature, we analyzed cellular infiltrates in treated tumors. AIPV therapy induced tumor infiltration by effector CD4<sup>+</sup> and CD8<sup>+</sup> T-cells, CD11b<sup>+</sup>Ly6G<sup>+</sup>Ly6C<sup>low</sup> neutrophils<sup>236,237</sup>, NK cells, and other myeloid cells (Figure 26a-d, Figure 27a-d). PD-1<sup>+</sup>TIM-3<sup>+</sup>CD8<sup>+</sup> cells were infrequent in all treatment groups, but AIPV induced a large increase in the CD8<sup>+</sup> T-cell/T<sub>reg</sub> ratio (Figure 26c, Figure 27g-h), a significant outcome given the potential for IL-2 treatment to increase T<sub>reg</sub> numbers. Immunohistochemical analysis of

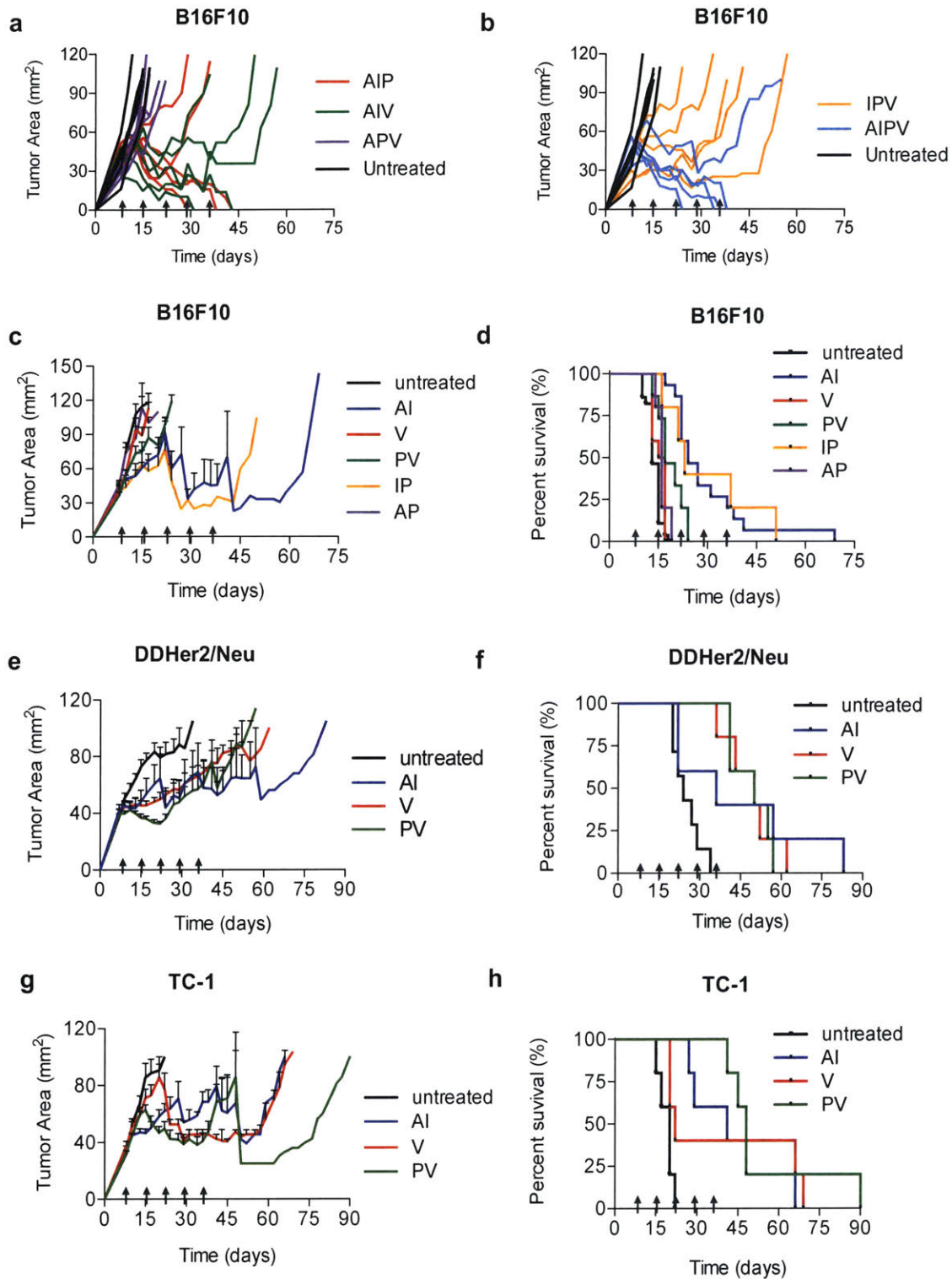


**Figure 21 Individual tumor growth kinetics and therapeutic efficacy of single and double agent therapies in B16F10, DD-Her2/Neu, and TC-1 tumor models.** a-h, Groups of mice were inoculated with  $10^6$  tumor cells s.c. in the flank: B16F10 (a-b,  $n = 5$  animals/group, representative of 4 independent experiments, c-d,  $n = 5$ /group for untreated and IP, 20 animals/group V, PV, and AI) and TC-1 (g-h,  $n = 5$  animals/group) tumor cells were injected in C57Bl/6 mice while DD-Her2/neu tumor cells (e-f,  $n = 5$  animals/group) were injected in balb/c mice. On day 8 post implantation, treatment was initiated following the timeline in Figure 19a using the indicated paired or individual components of AIPV. Shown are individual mice (a, b), or mean tumor area  $\pm$  s.e.m (c, e, g) and survival. Gray arrows indicate treatment time points.

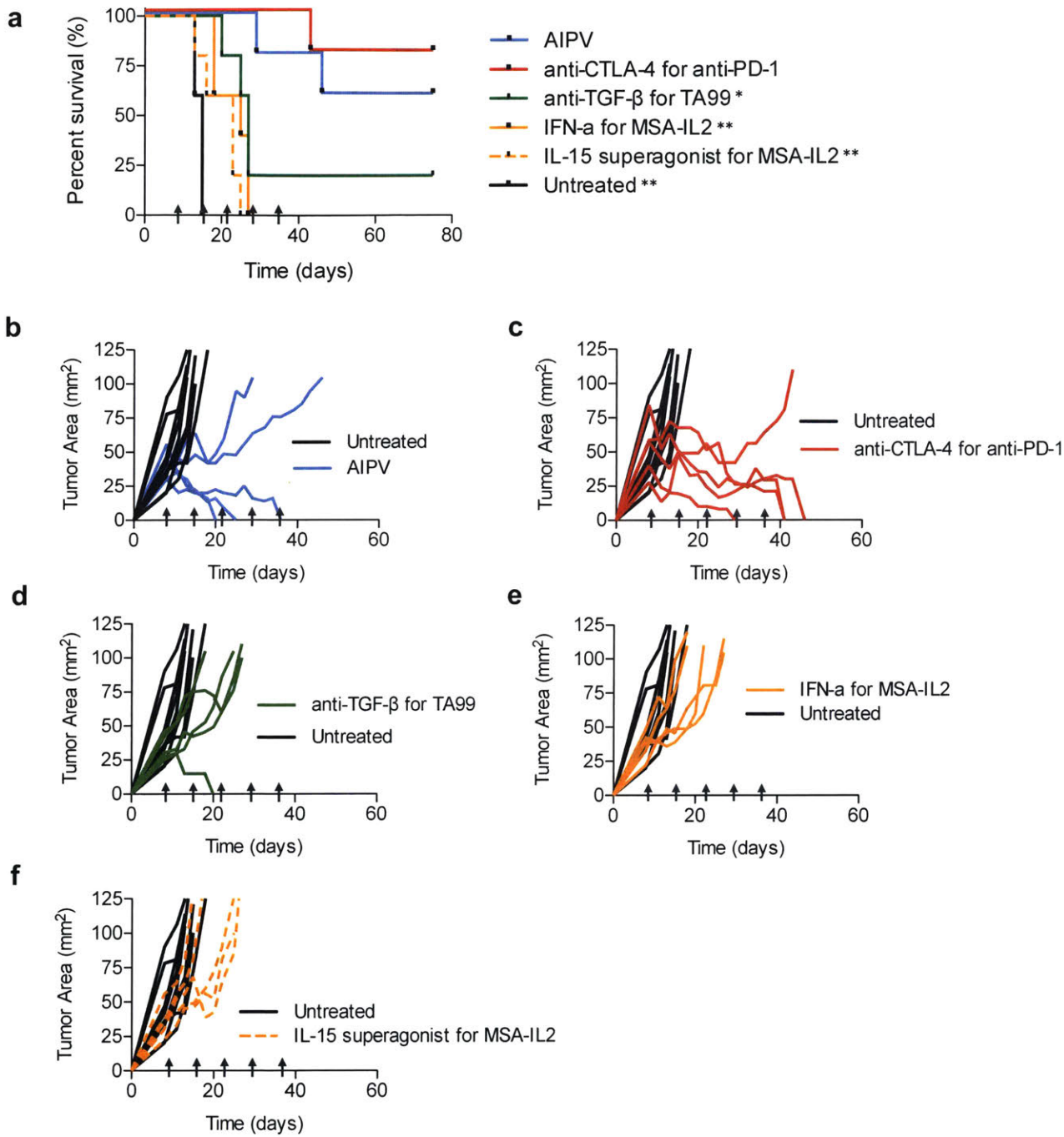
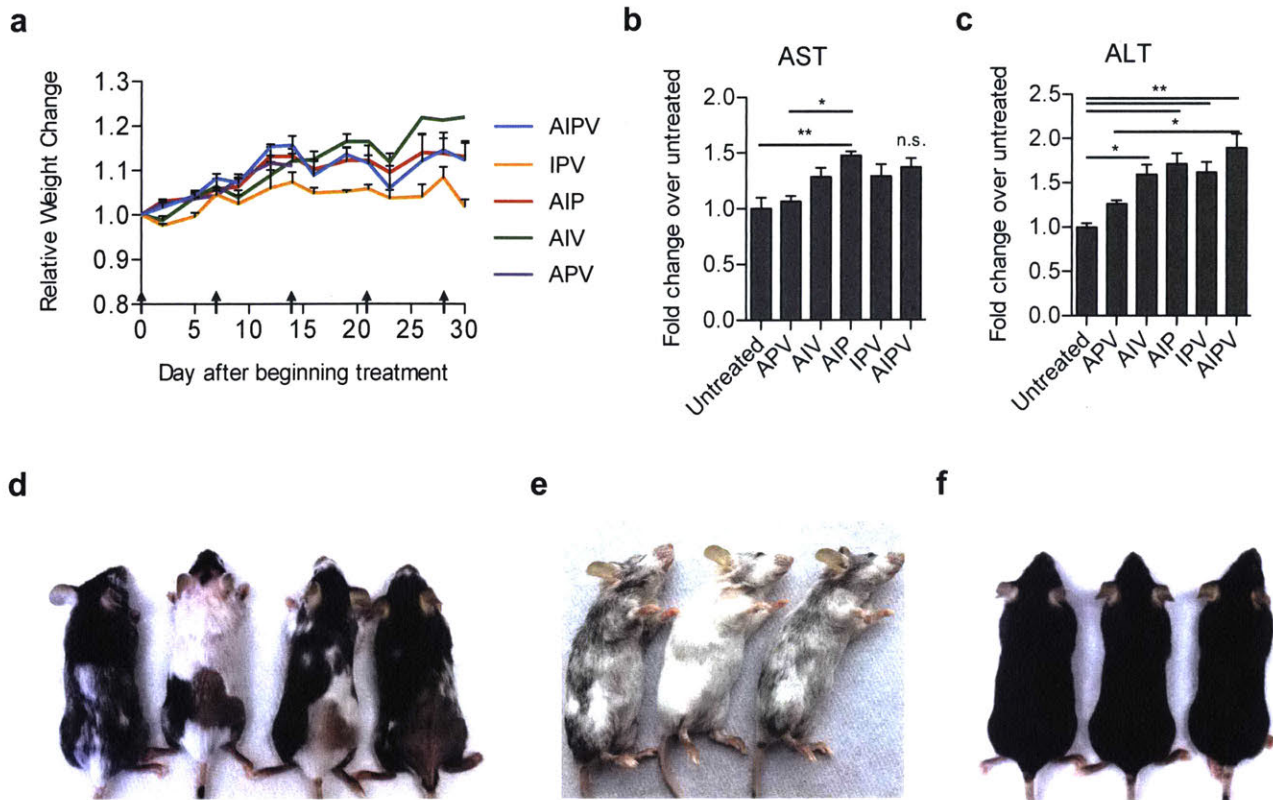


Figure 22 **Exploration of alternative quaternary combination therapies for treatment of B16F10 melanomas.** Groups of C57Bl/6 mice ( $n = 5$  animals/group) were inoculated with  $10^6$  B16F10 cells s.c. in the flank. On day 8 post implantation, treatment was initiated following the timeline in Figure 19a with either AIPV or with quaternary treatments substituting one of the components of AIPV with an alternative immunotherapy agent as indicated (see Methods). Shown are survival (**a**) and tumor growth in individual mice (**b-g**). Shown are survival (**a**), and mean tumor area  $\pm$  s.e.m (**b-f**). Gray arrows indicate treatment time points. \*  $P < 0.05$ , \*\*  $P < 0.01$ , \*\*\*  $P < 0.001$  versus AIPV by Log-rank (Mantel-Cox) test.





**Figure 23 AIPV therapy is well tolerated but accompanied by pronounced vitiligo.** a-c, C57Bl/6 mice ( $n = 5$  animals/group) were inoculated with  $10^6$  B16F10 cells s.c. in the flank and treatment was initiated following the timeline in Figure 19a. Shown are body weight measurements over time normalized to initial weights (a) and analysis of serum AST and ALT liver enzyme levels in serum of mice 36 hours after treatment initiation (b-c). d-e, representative images of AIPV treated mice 65 days (d) and 125 days (e) after tumor inoculation. f, non-tumor bearing mice were primed and boosted 14 days later with amph-Trp2 vaccine. Shown are representative images at 111 days after boost; no vitiligo was detected. Images in d-f are representative of 2-5 independent experiments. Gray arrows indicate treatment time points. \* $P < 0.05$ , \*\* $P < 0.01$ , \*\*\* $P < 0.001$  by one-way ANOVA with Bonferroni post-test, n.s. not significant for all comparisons.

treated tumors revealed  $CD8^+$  T-cells were present at high density throughout AIPV-treated tumors, with less effective triple-combination therapies eliciting progressively fewer  $CD8^+$  cells in the bulk tumor mass (Figure 26e, Figure 27e-f).

Antibody depletion of leukocyte subsets showed that  $CD8^+$  T-cells were critical to tumor rejection (Figure 26f, Figure 28a). Macrophage, NK cell, or neutrophil depletion also led to significant reductions in overall survival rates, while IL-5 or  $CD4^+$  T-cell depletion did not impact efficacy (Figure 26f, Figure 28a-b). Of note, mice that were depleted of  $CD4^+$  T cells during therapy rejected rechallenge with B16F10 at a similar rate as mice that were not depleted of  $CD4^+$  T cells during therapy (7/8 in  $CD4$ -depleted versus 9/11 in non-depleted, data not shown).

Thus, AIPV treatment elicited substantial remodeling of the tumor microenvironment with contributions from diverse effector cells.

**The antibody component of AIPV therapy delivers antigen to cross-presenting dendritic cells and promotes antigen spreading.**

We next assessed whether *de novo* adaptive immune responses unrelated to the vaccine were primed by AIPV treatment. Given the critical role of CD8<sup>+</sup> T-cells, we first analyzed the impact of AIPV on antigen acquisition/presentation in the tumor-draining lymph nodes (TDLNs). AIPV-treated Batf3<sup>-/-</sup> mice failed to reject tumors, indicating a requirement for cross-presenting DCs (Figure 29a). Anti-tumor antibodies promote cross-presentation of tumor antigens<sup>238</sup>, and thus we treated GFP-expressing B16F10 tumors with AIPV or subcombinations and analyzed the uptake of GFP and fluorescent TA99 in dendritic cells in TDLNs (Figure 29b-c). We examined two Batf3-dependent cross-presenting DC populations that may have distinct roles in tumors, CD8α<sup>+</sup> DCs and CD103<sup>+</sup> DCs<sup>239-241</sup>. Labeled TA99 accumulated in these DC populations, and treatment combinations including TA99 significantly increased GFP uptake by both CD8α<sup>+</sup> and CD103<sup>+</sup> DCs over untreated tumors (Figure 29d-g). Further, ovalbumin (OVA)-expressing B16F10 tumors treated with AIPV (vaccinating against Trp2) induced a clear anti-OVA T cell response substantially greater than that observed in untreated or IPV-treated tumors, indicating a role for the antibody in priming T-cell responses to new tumor antigens (Figure 29h-i). Following AIPV treatment of parental B16F10 tumors, splenic T-cells strongly recognized both B16F10 cells and a Trp2-deleted B16F10 cell line (Figure 30a-b) by ELISPOT, indicating antigen spreading to new B16F10 antigens (Figure 29j-k). In addition, 50% of AIPV-treated mice cured of primary tumors also rejected a rechallenge with Trp2-deleted B16F10 cells on day 125 (Figure 30c). These data suggest the antibody component of AIPV promoted antigen spreading, leading to functional *de novo* T-cell responses against new antigens not targeted by the therapy directly.

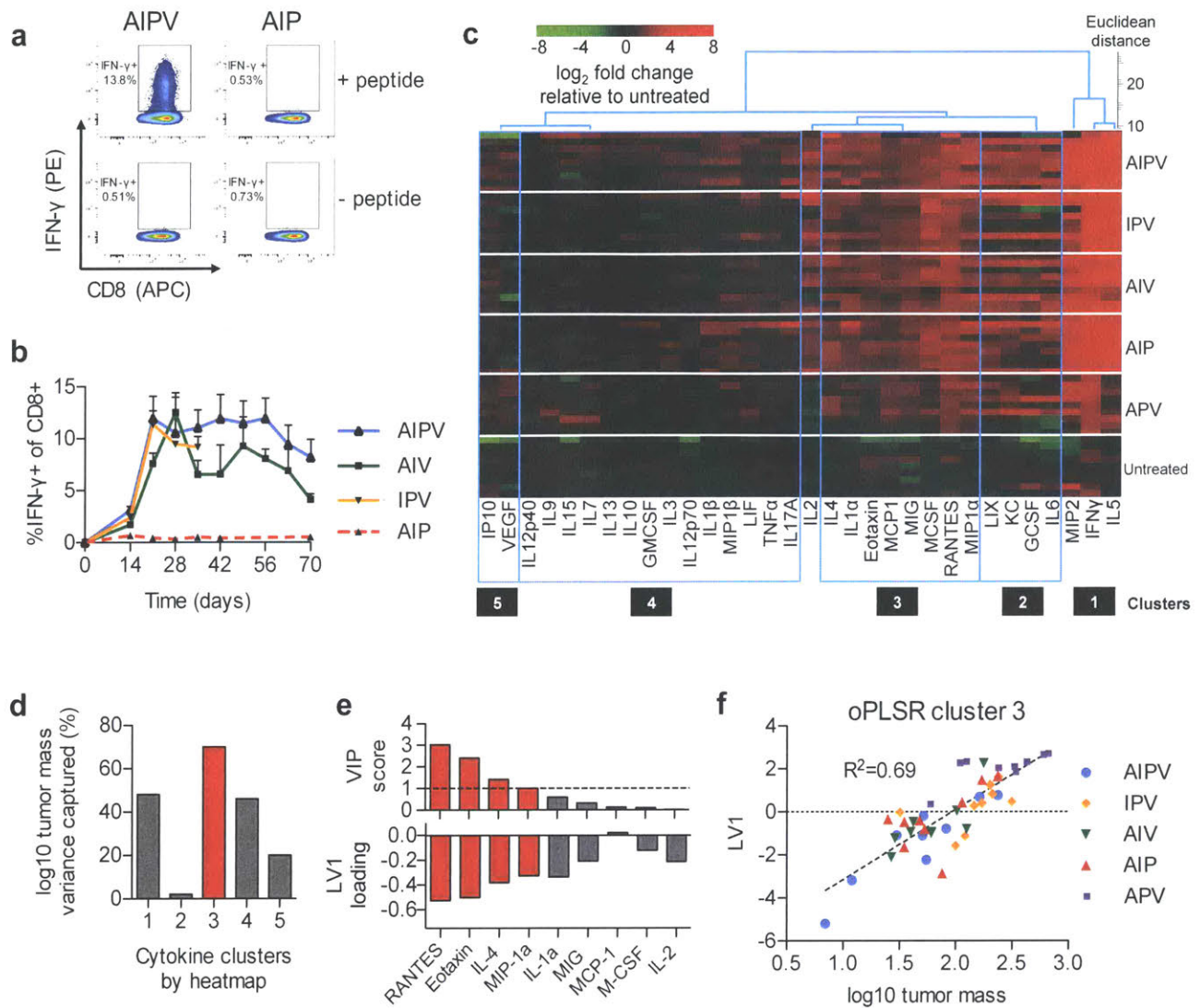


**Figure 24 AIPV therapy primes sustained vaccine-specific T-cell responses and remodels the microenvironment of established tumors.** B16F10 tumors in C57Bl/6 mice were treated with AIPV or ternary subcombinations of the therapy components as in Figure 19a. **a-b**, Representative intracellular cytokine staining to detect Trp2-specific CD8<sup>+</sup> T-cells in peripheral blood on day 21 (**a**) and mean responses over time from the same experiment ( $n = 5/\text{group}$ , **b**). **c-f**, Untreated or treated B16F10 tumors were isolated on day 17 and cytokine and chemokine levels in tumors were measured by Luminex ( $n = 9/\text{group}$ ). Luminex data were analyzed to determine relative protein levels in tumors (**c**), and 5 co-regulated protein clusters were identified (Figure 25). These clusters were independently tested for their ability to predict log-transformed tumor size in treated mice on day 17 using a single latent variable (LV) in an orthogonalized partial least squares regression (oPLSR) model (**d**: red bar), VIP scores were used to assess the contribution of individual proteins from the cluster to the oPLSR model; VIP scores >1 were considered significant (**e**: top, red bars) and the loading factors for LV1 of the oPLSR model are shown (**e**: bottom). A scatter plot shows the oPLSR model performance for individual mice from all treatment groups and the best fit linear regression (**f**).



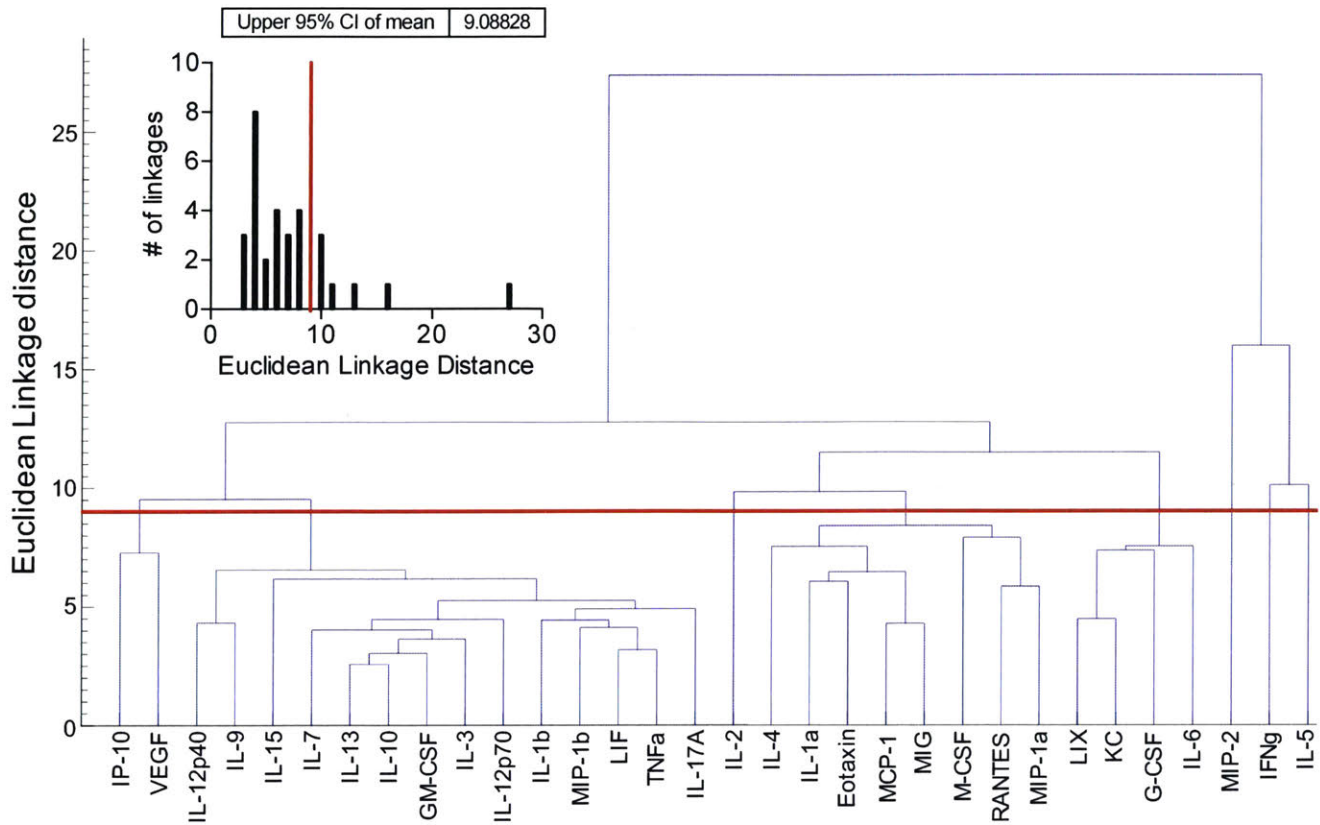


Figure 25 **Extended analysis of intratumoral cytokines/chemokine profiles.** C57Bl/6 mice were inoculated with  $10^6$  B16F10 cells s.c. in the flank and treatment with AIPV or subcombination therapies was initiated following the timeline in Figure 19a. Tumors were analyzed on day 17. A hierarchical binary cluster tree was created using Euclidean Linkage distance for log<sub>2</sub>-fold change of all cytokines and chemokines measured; each protein was designated a leaf. Tree pruning was performed by collapsing all leaves with a linkage distance less than the 95% confidence interval (red line).

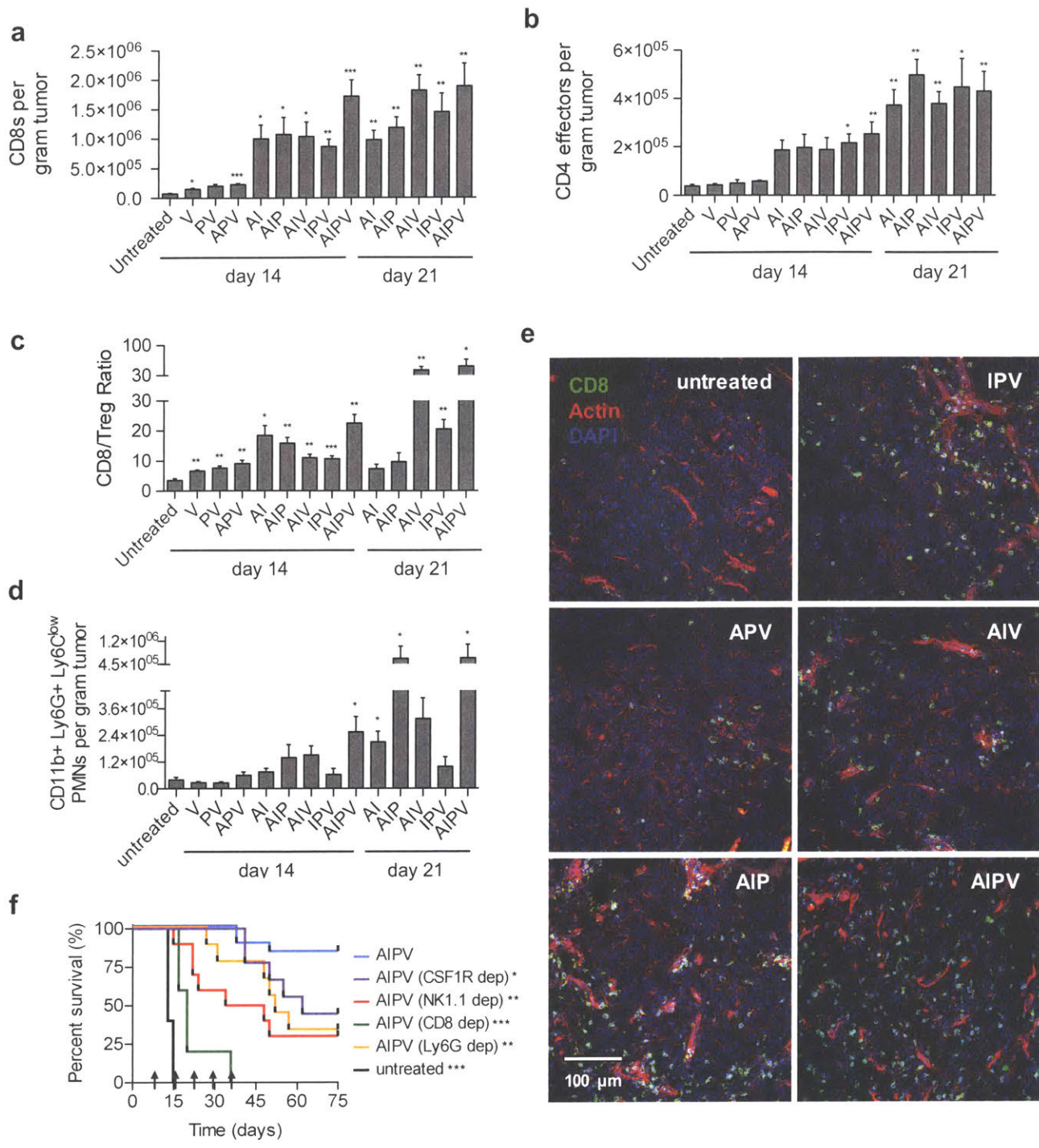
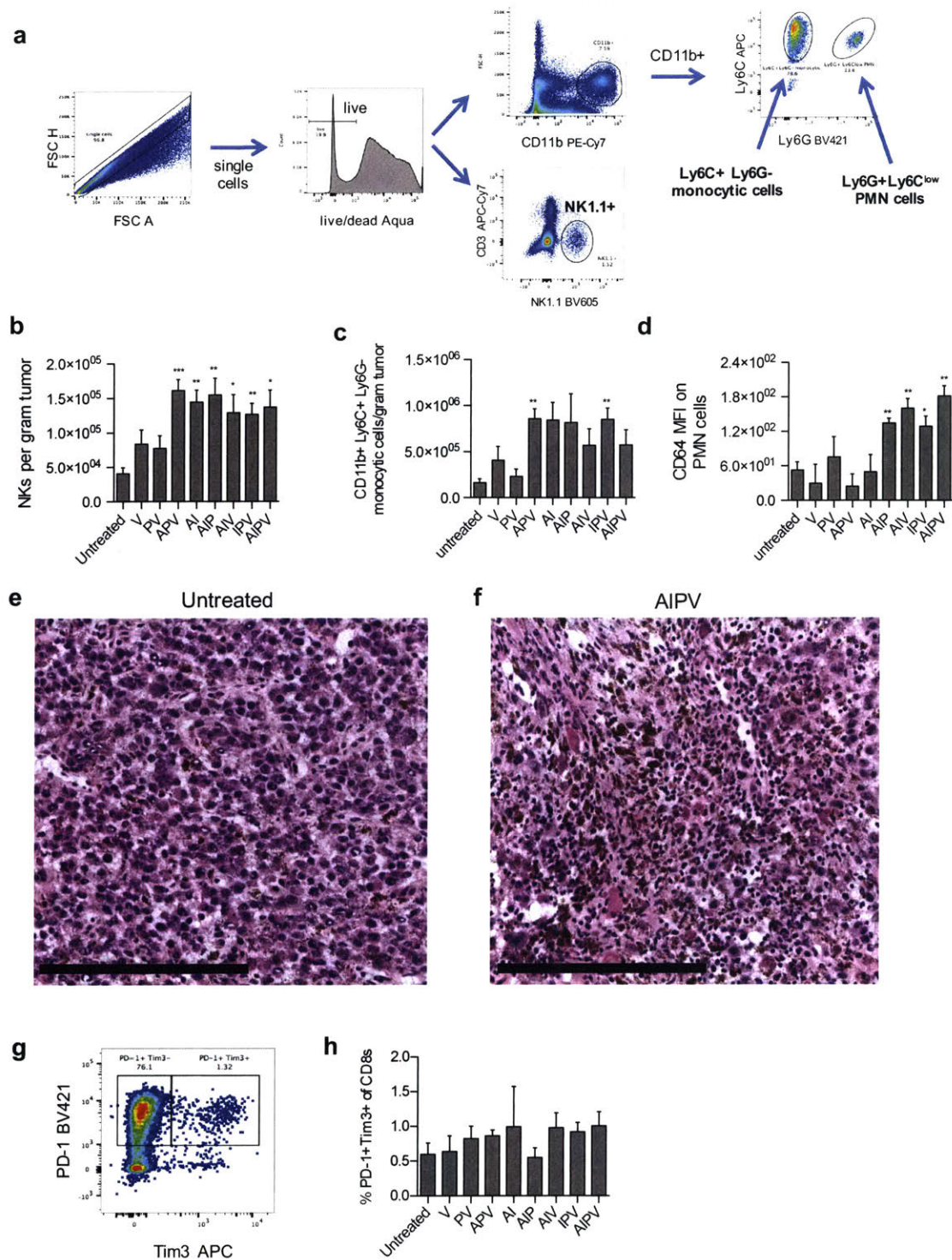
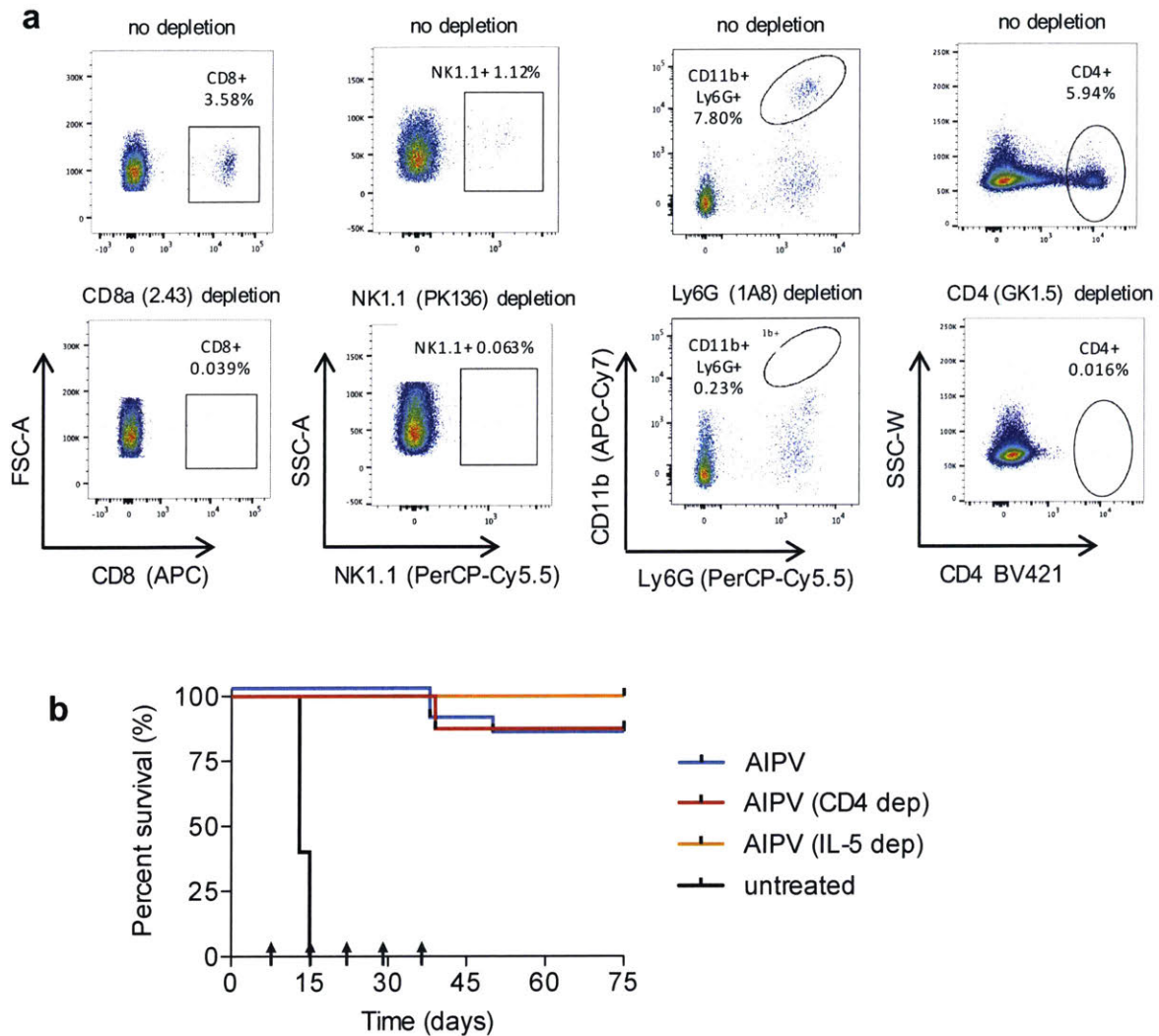


Figure 26 **AIPV therapy induces pronounced immune infiltration of tumors with efficacy dependent on innate and adaptive immune cells.** **a-d**, Untreated or treated B16F10 tumors were isolated on days 14 and 21 and analyzed by flow cytometry ( $n = 15$  animals/group for day 14, 9 animals/group for day 21, at least 2 independent experiments). Shown are mean values  $\pm$  s.e.m. for tumor-infiltrating CD8<sup>+</sup> T-cells (**a**), CD4<sup>+</sup>FoxP3<sup>-</sup> T-cells (**b**), the ratio of CD8<sup>+</sup> T-cells to CD4<sup>+</sup>CD25<sup>hi</sup>Foxp3<sup>+</sup> T<sub>reg</sub>s (**c**), CD11b<sup>+</sup>Ly6G<sup>+</sup>Ly6C<sup>low</sup> polymorphonuclear (PMN) cells (**d**), and representative immunofluorescence images from day 14 (**e**). **f**, Depleting antibodies against the indicated surface markers were administered i.p. beginning one day prior to initiation of AIPV therapy to deplete macrophages (CSF1R), NK cells (NK1.1), CD8<sup>+</sup> T-cells (CD8), or neutrophils (Ly6G). Gray arrows indicate treatment time points. Shown is survival over time ( $n = 5$  animals/group for CD8 depletion,  $n = 10$  animals/group for NK1.1, CSF1R, and Ly6G depletion, 2 independent experiments). \* $P < 0.05$ , \*\* $P < 0.01$ , \*\*\* $P < 0.001$  by Welch's t test versus untreated with Bonferroni correction for **a-d**. \* $P < 0.05$ , \*\* $P < 0.01$ , \*\*\* $P < 0.001$  versus AIPV by Log-rank (Mantel-Cox) test for **f**.





**Figure 27 Immune cell infiltration during AIPV therapy.** C57Bl/6 mice were inoculated with  $10^6$  B16F10 cells s.c. in the flank and treatment with AIPV or subcombination therapies was initiated following the timeline in Figure 19a. **a**, Tumors were isolated and digested for flow cytometry analysis on day 14. Shown is representative gating for NK cells, polymorphonuclear myeloid cells (PMNs), and monocytic infiltrating cells. **b**, mean numbers of intratumoral NK cells. **c**, mean numbers of intratumoral CD11b<sup>+</sup> Ly6C<sup>+</sup> Ly6G<sup>-</sup> monocytic cells. **d**, MFI of CD64 on CD11b<sup>+</sup> Ly6G<sup>+</sup> Ly6C<sup>low</sup> PMN, taken as a marker for activated anti-tumor neutrophil populations. (shown is mean  $\pm$  s.e.m.,  $n = 15$  animals/group, 2 independent experiments). **e-f**, representative haematoxylin and eosin stained sections from untreated, **e**, and AIPV treated, **f**, mice on day 18 after tumor inoculation. ( $n = 5$  animals/group, 3 independent experiments, scale bar = 200  $\mu$ m). **g-h**, Tumors were isolated and analyzed by flow cytometry on day 14 for expression of PD-1 and Tim3. Shown is a representative plot, gated on CD8 $\alpha^+$  T cells, **g**, and mean fraction of PD-1<sup>+</sup> Tim3<sup>+</sup> of total CD8 $\alpha^+$  T cells  $\pm$  s.e.m. **h**, ( $n = 15$  animals/group, 2 independent experiments). \* $P < 0.05$ , \*\* $P < 0.01$ , \*\*\* $P < 0.001$  by Welch's t test versus untreated with Bonferroni correction.



**Figure 28 Depletion of selected cellular subsets during AIPV therapy.** Groups of C57Bl/6 mice ( $n = 10$  animals/group for NK1.1, Ly6G, and CD4 depletion,  $n = 5$ /group for CD8 depletion) were inoculated with  $10^6$  B16F10 cells s.c. in the flank. Cellular subsets were depleted by administering 400  $\mu$ g of depleting antibody i.p. twice weekly beginning one day prior to initiation of AIPV therapy following the timeline of Figure 19a. Depletions included CD8<sup>+</sup> T-cells with anti-CD8 $\alpha$ ; CD4<sup>+</sup> T-cells with anti-CD4; NK cells with anti-NK1.1; neutrophils with anti-Ly-6G; and eosinophils via blockade of IL-5, which was depleted using 1 mg of anti-IL-5 weekly beginning one day prior to treatment. **a**, Confirmation of depletions for CD8<sup>+</sup> T-cells, NK cells, neutrophils, and CD4<sup>+</sup> T-cells from PBMCs on day 14. **b**, Survival of tumor-bearing animals treated with AIPV in the presence of CD4 depletion or IL-5 blockade to eliminate eosinophils. Gray arrows indicate treatment time points.



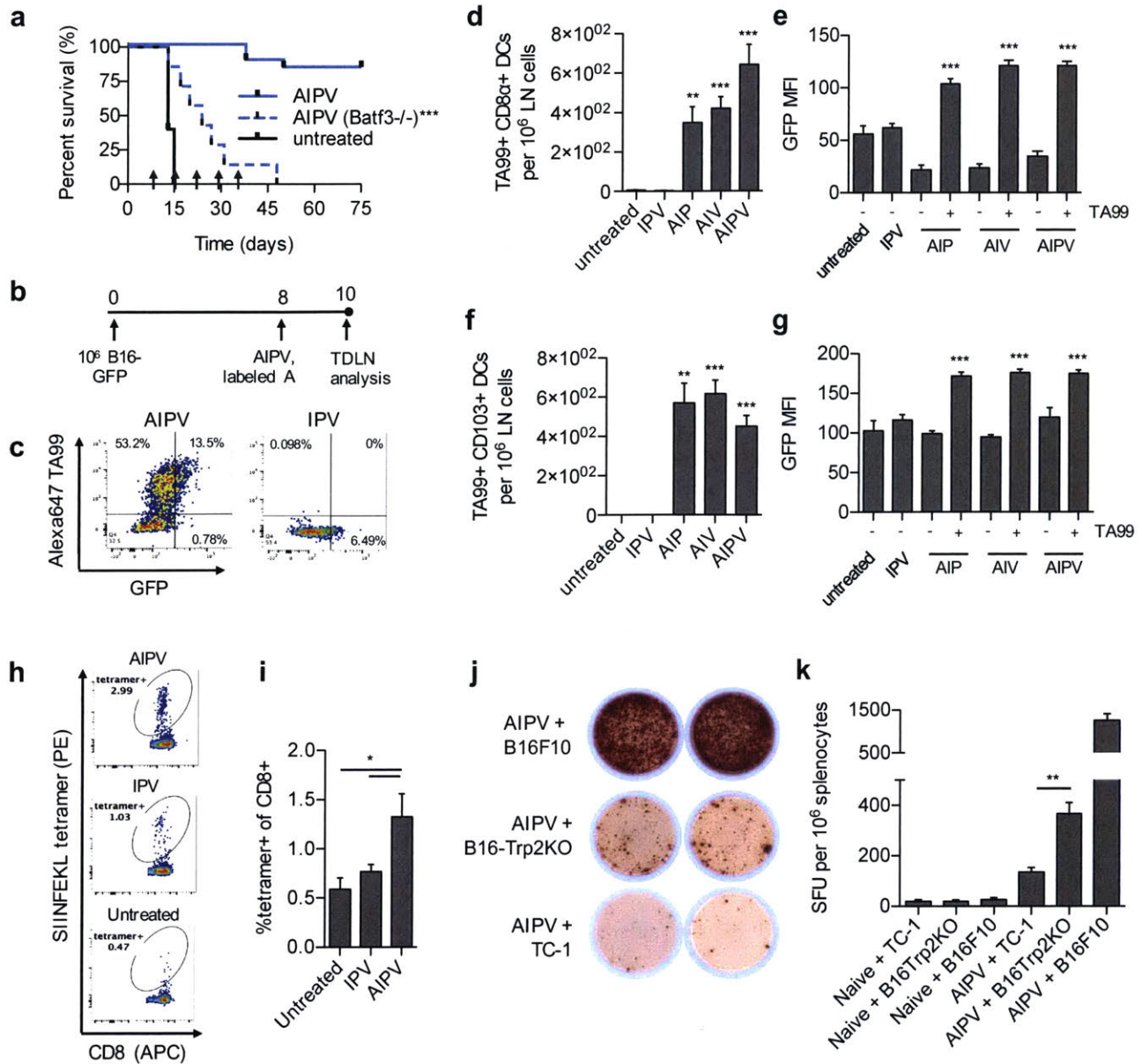


**Figure 29 Combination therapy elicits antibody-enhanced antigen spreading and *de novo* T-cell responses.** **a**, AIPV treatment was carried out in wild type or Batf3<sup>-/-</sup> mice ( $n = 7$  animals/group) bearing established B16F10 tumors; mice were euthanized when tumor area exceeded 100 mm<sup>2</sup>. Shown is survival over time; gray arrows indicate treatment time points. **b-g**, B16-GFP cells (10<sup>6</sup>) were injected s.c. ( $n = 10$  animals/group) and AIPV or subcombination treatment was applied with AlexaFluor647-labeled TA99 antibody, followed by tumor-draining LN isolation, digestion, and analysis by flow cytometry (**b**). Shown are representative scatter plots of CD11c<sup>+</sup> DCs (**c**), enumeration of TA99<sup>+</sup> CD11c<sup>+</sup>CD8α<sup>+</sup>CD11b<sup>-</sup> and CD11c<sup>+</sup>CD103<sup>+</sup> DCs (**d** and **f**, respectively) and MFI of GFP within CD11c<sup>+</sup>CD8α<sup>+</sup>CD11b<sup>-</sup> and CD11c<sup>+</sup>CD103<sup>+</sup> DCs (**e** and **g**, respectively) gated on either TA99<sup>+</sup> or TA99<sup>-</sup> cells. **h-i**, B16-OVA cells (10<sup>6</sup>) were injected s.c. and tumors were treated with AIPV as in Figure 19a (with vaccine against Trp2); staining with SIINFEKL/H-2K<sup>b</sup> tetramers on peripheral blood mononuclear cells was performed on day 15. Shown are representative flow plots (**h**) and mean±s.e.m. (**i**) from 1 of 2 independent experiments ( $n = 10$  animals/group). **j-k**, Splenocytes were isolated from AIPV-treated (day 81) or naïve mice and tested for reactivity against a Trp2-KO B16F10 line generated using CRISPR/Cas9, parental B16F10 cells, or control TC-1 cells via ELISPOT. Shown are representative wells, **j**, and mean spots±s.e.m, **k** ( $n = 6$  animals/group). \* $P < 0.05$ , \*\* $P < 0.01$ , \*\*\* $P < 0.001$  by Welch's t test versus untreated with Bonferroni correction for **d** and **f**, by Welch's t test versus the TA99<sup>-</sup> fraction within the same treatment group for **e** and **g**, by ANOVA with Bonferroni post-test for **i**, and by t test for **k**.

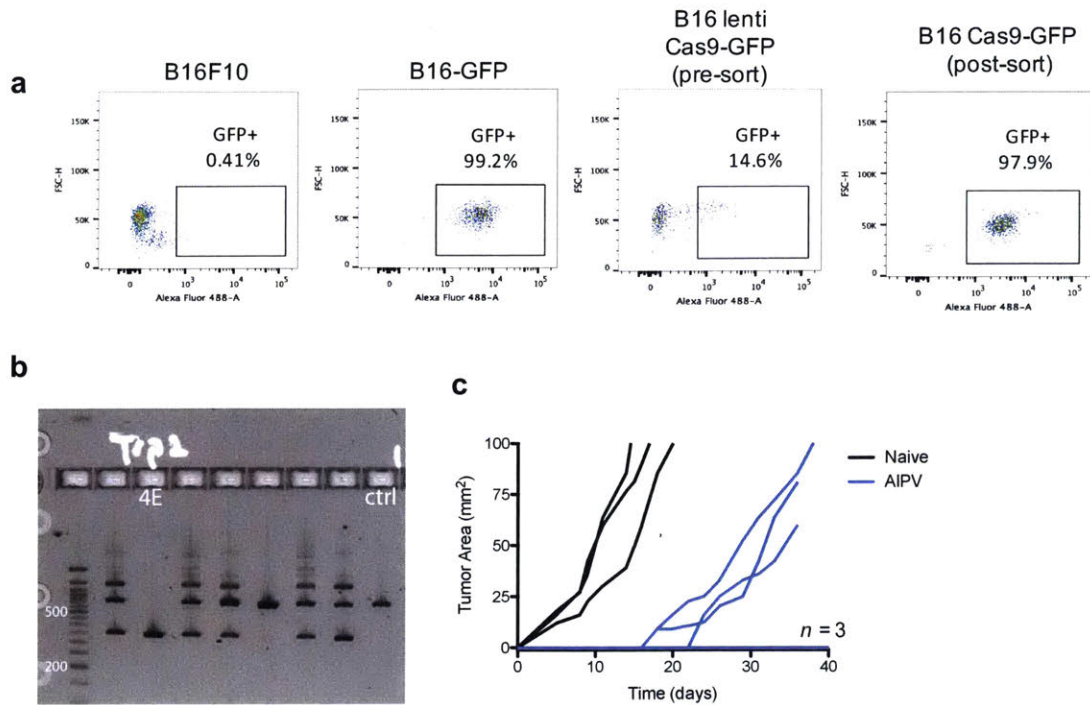


**Figure 30 Generation of a TRP2-KO cell line using Crispr/Cas9.** **a**, B16-GFP-Cas9 cells were generated by transduction of B16F10 cells with lentivirus expressing SpCas9-P2A-EGFP from an EFS promoter. Clones were isolated by single cell flow cytometry for GFP positive cells and evaluated for stable expression. **b**, RNA expression vectors were created by cloning a human U6 promoter and sgRNA sequences into a minimal vector with an ampicillin-selectable marker and a ColE1 replication origin with guide sequences indicated in **Table 2: Guide Sequences**. PCR amplification of an internal region of Trp2 using the sequences shown in **Table 3: Primer Sequences** was performed on clones that grew out of this single cell sort after selection in 2  $\mu$ g/mL puromycin. Clone 4E was designated B16-Trp-2KO. **c**, AIPV treated mice that successfully rejected rechallenge with  $10^5$  B16F10 on day 75 were challenged again with  $10^5$  B16-Trp2-KO on day 125. Shown is tumor area over time for individual animals ( $n = 6$  animals/group treated with AIPV and  $n = 3$  age-matched animals/group as naive controls).

### Combination therapy elicits a polyclonal antibody response targeting diverse tumor cell antigens, which can protect against tumor challenge.

In parallel we evaluated endogenous antibody responses in AIPV-treated animals. In all 3 transplanted tumor models, AIPV therapy elicited antibodies that bound to the tumor cells (Figure 31a). We developed an approach to deplete TA99 antibody from sera recovered from mice undergoing treatment, in order to analyze the endogenous IgG response over time (Figure 32a-f). Using this approach, we found that both AIPV and the less effective triple subcombinations elicited anti-tumor antibodies, which were detectable as early as 7 days following start of treatment and expanded over 30 days for combinations that promoted better survival (Figure 31b and Figure 32f). An immunoblot of sera from B16F10 tumor-bearing mice



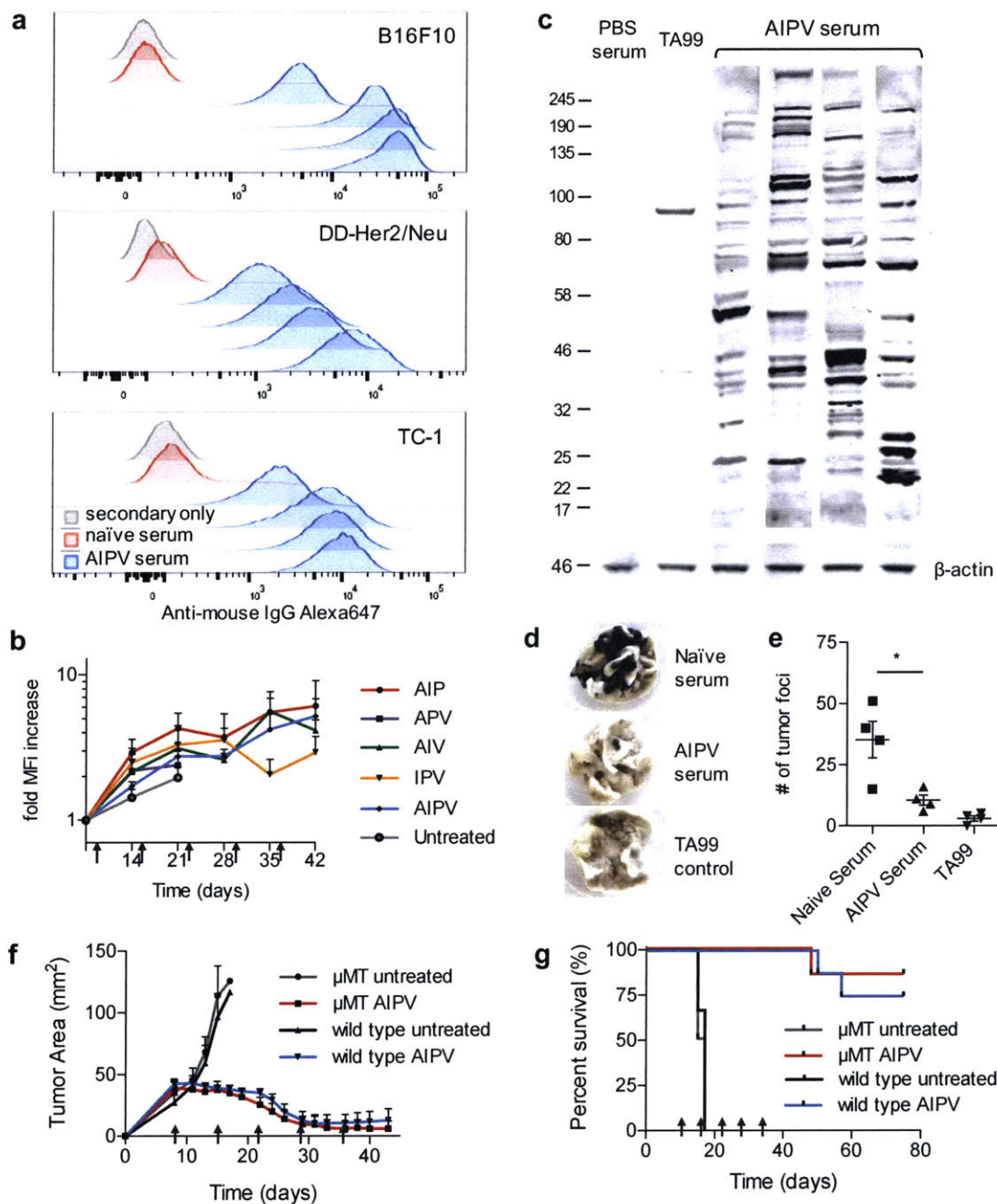


**Figure 31 AIPV therapy induces *de novo* endogenous anti-tumor antibody responses.** **a-c**, Indicated tumor cells were incubated with 5% serum collected on day 150 from AIPV-treated mice that had previously rejected B16F10 (top), DD-Her2/neu (middle), or TC-1 (bottom) tumors, or age-matched naïve mice. The cells were secondary stained with Alexa647 anti-mouse IgG, and analyzed by flow cytometry (shown are results for sera from individual treated animals, representative of 2 independent experiments of  $n =$  at least 4). **b**, C57Bl/6 mice bearing B16F10 tumors were treated with the indicated combination therapies as in Figure 19a using biotinylated TA99. Mice were bled weekly and serum was depleted of TA99-biotin using streptavidin resin (Figure 32), then binding of remaining endogenous IgG to B16F10 cells was measured by flow cytometry as in **a**. Plotted is the fold change in MFI of anti-mouse IgG over time  $\pm$  s.e.m. ( $n = 5$ /group) **c**, Western blot of B16F10 tumor cell lysate stained with serum from AIPV-treated mice, PBS-treated mice, or TA99 antibody followed by an anti-mouse-IgG-IRDye800 secondary imaged on an Odyssey fluorescence scanner. Shown is 1 representative of 2 independent experiments. **d-e**, 350  $\mu$ L serum from AIPV treated mice or age-matched naïve mice ( $n = 4$  animals/group) was incubated at 57°C for 1h to inactivate complement and transferred into naïve recipients, followed by challenge with  $2.5 \times 10^5$  B16F10 cells i.v. Lungs were isolated 17 days later and nodules were counted in a blinded fashion. Shown are representative lungs (**d**) and mean counts  $\pm$  s.e.m. (**e**). Data shown is 1 representative of 2 independent experiments. **f-g**, B cell-deficient  $\mu$ MT or wild type C57Bl/6 mice were inoculated with B16F10 tumors and left untreated or received AIPV therapy as in Figure 19a. Shown are mean  $\pm$  s.e.m tumor growth curves (**f**) and overall survival (**g**) ( $n = 8$ /group for AIPV treated groups,  $n = 4$ /group for untreated). Gray arrows indicate treatment time points. \* $P < 0.05$ , \*\* $P < 0.01$ , \*\*\* $P < 0.001$  by one-way ANOVA with Bonferroni post-test.



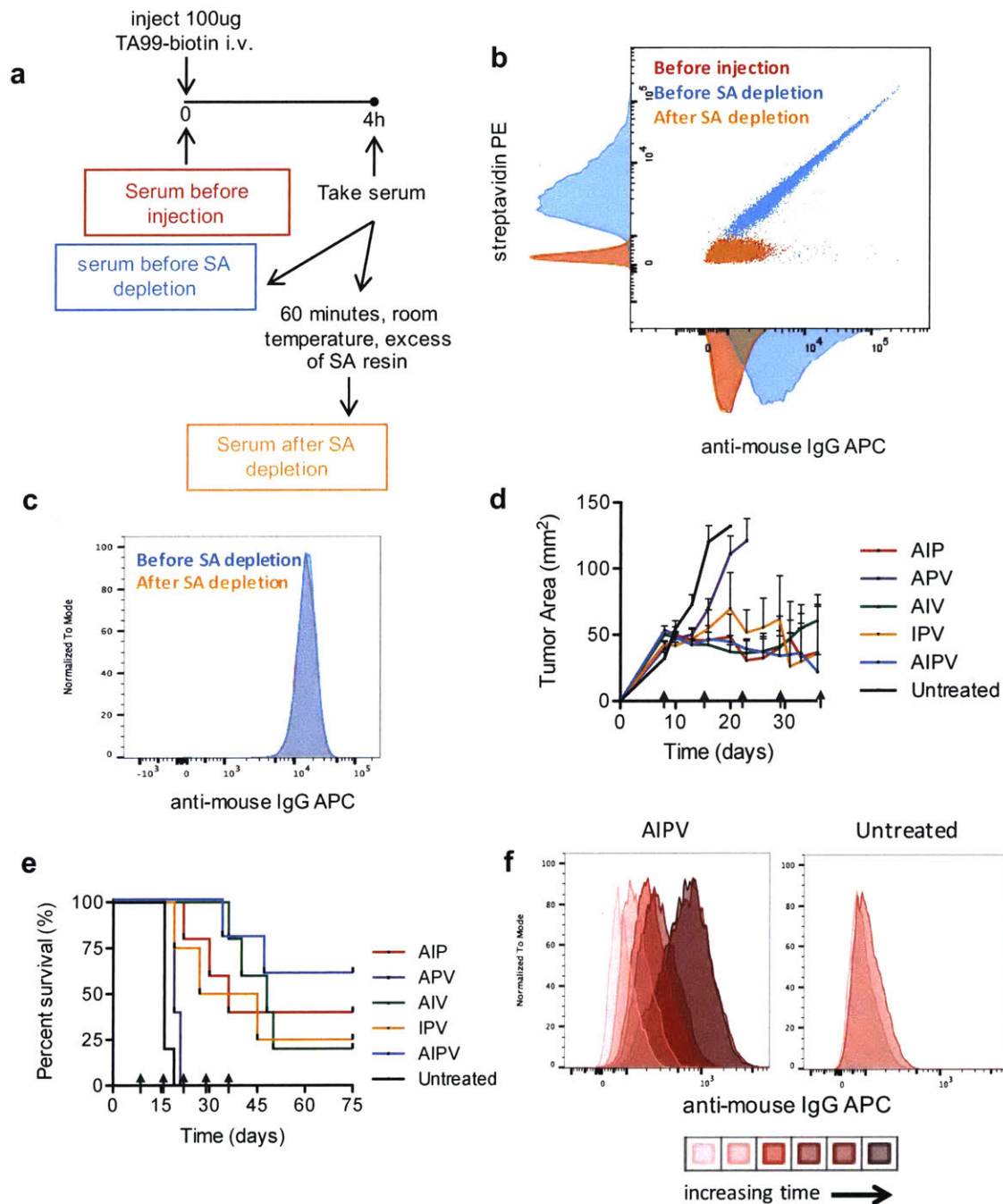


**Figure 32 Depletion of serum TA99 to detect endogenous anti-B16F10 antibody responses during therapy.** **a**, Experimental protocol: Serum was isolated from C57Bl/6 mice immediately prior to and 4 hours following i.v. administration of 100 $\mu$ g of biotinylated TA99. Serum was incubated with an excess of streptavidin agarose for 1h at 25 $^{\circ}$ C and binding to B16F10 was determined using flow cytometry as in Figure 31a-c. **b**, Shown is one representative of three replicates of dual staining to detect the presence of biotinylated TA99 binding to tumor cells (via streptavidin) and endogenous IgG binding (via anti-mouse IgG secondary), before and after streptavidin agarose depletion of biotin-TA99 from serum. **c**, Serum was isolated from AIPV-treated mice 150 days after rejection of B16F10 and incubated with streptavidin agarose and binding to B16F10 was assessed by flow cytometry. High endogenous IgG binding to B16F10 cells was detected that was not affected by streptavidin agarose depletion. Shown is one representative of three replicates. **d-e**, C57Bl/6 mice were treated with AIPV as indicated in Figure 19a using biotinylated TA99. Shown are tumor area  $\pm$ s.e.m and survival curves for mice treated with AIPV and subcombinations using biotinylated TA99, showing that use of biotin-TA99 did not interfere with efficacy of the therapy. **f**, C57Bl/6 mice were treated with AIPV as indicated in Figure 19a using biotinylated TA99. Mice were bled weekly and serum was depleted of TA99-biotin as described above and binding was measured as in Figure 31. Shown is a representative plot of MFI of anti-mouse IgG throughout therapy for an AIPV treated mouse over time ( $n = 5$ /group). Gray arrows indicate treatment time points.

treated with AIPV against B16F10 lysate revealed that these endogenous antibodies recognized numerous antigens (Figure 31c). These therapy-induced antibodies were functional, as serum transferred from AIPV-treated mice protected against intravenous B16F10 challenge (Figure 31d-e). However, administration of AIPV therapy to B-cell-deficient  $\mu$ MT bearing established B16F10 tumors led to a similar frequency of tumor regressions as observed in wild type mice, suggesting that the endogenous antibody response does not contribute incrementally beyond the administered antibody component of the AIPV regimen (Figure 31f-g). Together, these experiments indicate that AIPV broadly promoted both antibody and T-cell responses against novel antigens not directly targeted by the therapy components.

### **AIPV therapy regresses tumors in the inducible Braf/Pten melanoma model.**

Transplanted tumors do not mimic the histology of human cancers well, and often have a high mutational burden that constitutes potential neoantigens. To assess the efficacy of AIPV in a model more closely mimicking the pathophysiology of human disease and simultaneously determine the impact of a low frequency of neoantigens, we tested treatment of the Braf<sup>CA</sup> Pten<sup>loxP</sup> Tyr::CreER<sup>T2</sup> (Braf/Pten) inducible melanoma model<sup>242</sup>. We first enhanced the potency of AIPV by increasing the valency of the vaccine component<sup>243</sup>. AIPV therapy using a trivalent amphiphile-vaccine targeting gp100, Trp1, and Trp2 strikingly cured 100% of B16F10 tumor-bearing mice with mean initial tumor sizes of 50 mm<sup>2</sup> (Figure 33a-b). This enhanced AIPV was then tested in the Braf/Pten model: Tumors were induced on the ears of Braf/Pten mice and when visible lesions were present (~4 weeks), treatment was initiated. Melanomas grew progressively and by week 10 completely covered the ears of untreated mice (Figure 33c). By contrast, trivalent-vaccine AIPV induced regression of pigmented lesions, leading to complete clearance in the majority of animals and a significant improvement in overall survival compared to untreated mice (Figure 33c-d). This result was coincident with strong T-cell responses against all three vaccine antigens in the peripheral blood (Figure 33e) and a massive infiltration of CD8<sup>+</sup> T-cells throughout AIPV-treated Braf/Pten tumors (Figure 33f). To our knowledge this is the first immunotherapy to regress a majority of induced lesions in this autochthonous tumor model.

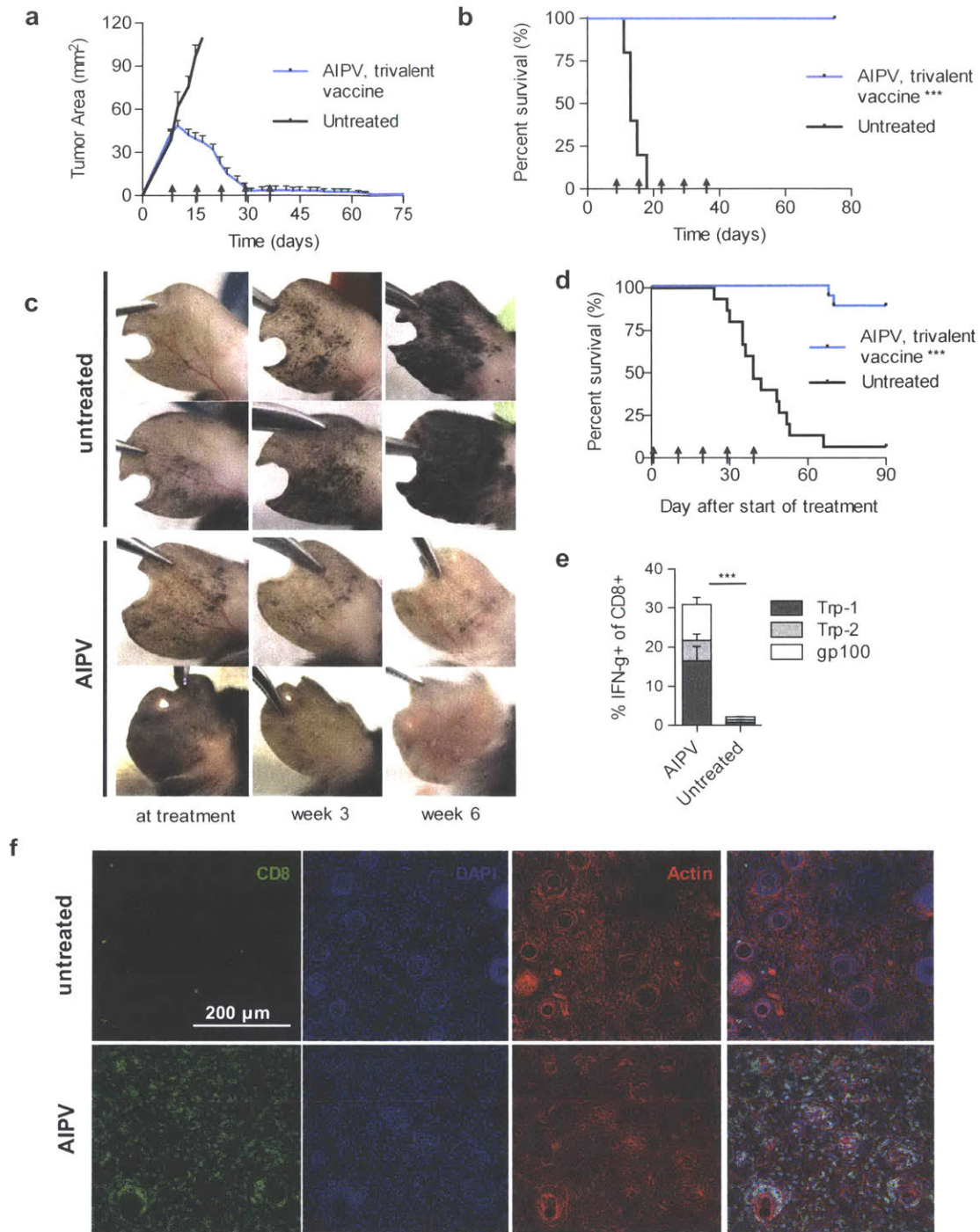


**Figure 33 AIPV with a trivalent vaccine is curative for established B16F10 tumors and induces regression in BRAF/Pten autochthonous melanoma.** **a-b**, Established B16F10 tumors were treated with AIPV as outlined in Figure 19a using a trivalent vaccine targeting Trp2, Trp1, and gp100. Shown are tumor area measurements (**a**, mean $\pm$ s.e.m.) and survival (**b**) ( $n = 10$  animals/group). **c-e**, BRAF<sup>CA</sup>Pten<sup>loxP</sup>Tyr::CreER<sup>T2</sup> mice were painted with 4-hydroxytamoxifen on one ear and treated with AIPV (including trivalent vaccine) beginning 28 days later when visible lesions were apparent. Shown are representative photographs of AIPV treated or untreated ears at treatment, week 7, and week 10, (**c**) and survival over time (**d**) ( $n = 16$  animals/group, compiled from 4 independent experiments). Mice were euthanized when tumor coverage exceeded 90% of the ear. **e**, intracellular cytokine staining was performed on peripheral blood on day 48 to assess CD8<sup>+</sup> T-cell responses against each vaccine antigen (mean $\pm$ s.e.m. as a fraction of total CD8<sup>+</sup> T-cells,  $n = 7$  animals/group). **f**, BRAF<sup>CA</sup>Pten<sup>loxP</sup>Tyr::CreER<sup>T2</sup> mice were painted with 4-hydroxytamoxifen on the left flank and treated with AIPV (including trivalent vaccine) beginning on day 36. Shown are images of representative immunofluorescence from tumors taken on day 70 ( $n = 8$  tumors per condition). Gray arrows indicate treatment time points. \*\*\* $P < 0.0001$  by Welch's t test for **d**, or by Log-rank (Mantel-Cox) test for **b** and **e**.

### **4.3 Discussion and Future Work**

While promising results in a minority of patients are now being obtained clinically with several immunotherapy drugs<sup>1,2</sup>, the diversity of mechanisms by which tumors evade immunity suggest that combination treatments acting on multiple facets of immunosuppression/immune activation will be required to achieve tumor eradication in a majority of patients<sup>3,5</sup>. Many combination treatments acting by complementary pathways to drive anti-tumor immunity are now being evaluated in animal models and early clinical trials<sup>224-230</sup>. To date, complete elimination of large, poorly immunogenic tumors in immunocompetent animal models has only been reliably achieved by combination therapies employing large numbers of adoptively transferred T-cells<sup>226,231,244</sup>. Thus, it has remained an outstanding question whether an endogenous immune response can be stimulated to overcome advanced tumors in a majority of animals. Here we demonstrate in several transplanted tumor models and a genetically-engineered model of melanoma the capacity of endogenous immunity to achieve a majority of complete responses in mice, using a four-component immunotherapy that was safe yet potently eradicated large tumors. As shown in Figure 19 and Figure 21, all four components incorporated in AIPV were required for treatment of several difficult tumor models, and other treatment combinations were often less effective or very toxic. Notably, the models selected for study here were in part motivated by their resistance to immunotherapy treatment; we found that a number of commonly used immunogenic tumors (e.g., EG7.OVA, CT26, and MC-38) could be cured by double- or triple-component subcombinations of AIPV (unpublished data).

Many immunotherapy studies focus on CD8<sup>+</sup> T-cell responses to tumors, but important roles for innate immune effector cells are also well described. Especially in the presence of tumor-opsonizing antibodies, NK cells, neutrophils and macrophages can all contribute to direct antibody-dependent phagocytosis, reactive oxygen-mediated cytotoxicity against tumors, and secretion of inflammatory cytokines and chemokines<sup>122,128,245</sup>. This innate attack creates intertwined positive feedback loops: opsonized tumor antigen is released that is efficiently cross presented by DCs<sup>225,246,247</sup>; inflammatory cytokines and immune complexes are released that activate DCs, stimulate their migration to draining lymph nodes, and promote adaptive effector functions<sup>9,248,249</sup>; and additional innate effectors and T-cells are recruited to the tumor<sup>9,127,248</sup>. Consistent with the importance of the innate immune response, maximal efficacy of AIPV therapy was dependent not only on CD8<sup>+</sup> T-cells but also neutrophils, macrophages, NK cells, and cross-presenting DCs. AIPV therapy completely failed in Batf3-deficient mice, and was in fact even less effective than AIP treatment, suggesting that the loss in efficacy in these



knockout animals reflected more than loss of responsiveness to the vaccine component (unpublished data). Although models of infectious disease and systemic immunization have implicated CD8 $\alpha$ <sup>+</sup> dendritic cells as key cross-presenting cells for T-cell immunity<sup>250,251</sup>, recent data has suggested that in growing tumors, a second Baff3-dependent DC lineage, CD103<sup>+</sup> DCs, plays a critical role in tumor antigen presentation<sup>239,240</sup>. Consistent with these reports, we found both CD8 $\alpha$ <sup>+</sup> and CD103<sup>+</sup> DCs acquired tumor antigen in a manner enhanced by the antibody component of AIPV.

Treatment of multiple tumor models with AIPV therapy revealed distinct hierarchies of importance for the four components. For example, the monoclonal antibody component was a critical contributor to efficacy in the B16F10 model, but the least important component in the DD-Her2/neu model. A key aspect of AIPV treatment is that this set of 4 agents collectively mounts an integrated response overcoming tumor resistance mechanisms in all of the models evaluated here— suggesting that the appropriate combination of immune effectors can overcome a range of tumor microenvironments and possible immunosuppressive pathways. Notably, therapy excluding the extended-PK IL-2 (APV treatment) showed greatly reduced efficacy in all 3 transplanted tumor models, correlating with greatly reduced inflammatory cytokines and chemokine expression in tumors and CD4<sup>+</sup> and CD8<sup>+</sup> T-cell infiltration. Which cell types IL-2 must act on for therapeutic efficacy remains to be defined, but besides supporting the proliferation and effector functions of T-cells, IL-2 is known to also drive expansion and enhance the sensitivity of NK cells<sup>252</sup>, promote neutrophilia and eosinophilia, and induce the production of myriad additional cytokines and chemokines that may support a combined innate/adaptive immune attack on tumors<sup>253</sup>. Despite the potential of IL-2 to expand T<sub>reg</sub>S, we found that intratumoral CD8:T<sub>reg</sub> ratios were greatly amplified relative to untreated tumors during AIPV therapy.

Although it remains an understudied area, prior work has demonstrated that the number of antigens targeted by cancer vaccines can be an important variable, with vaccines targeting more antigens leading to greater anti-tumor efficacy<sup>243</sup>. In agreement with these data, we found that the efficacy of AIPV therapy was sensitive to the valency of the vaccine; targeting a single epitope in the B16F10 model led to a 75% cure rate (Figure 19c), while a modest increase in vaccine valency to target 3 melanocyte antigens led to cures of 100% of treated mice (Figure 33a-b). There is currently much enthusiasm for targeting neoantigens formed by mutations in tumors, but our data demonstrate that combination immunotherapy targeting only tumor-associated self antigens can elicit pronounced tumor regressions, even in the setting of a genetically-induced mouse model bearing an intrinsically low burden of mutations. However,

AIPV also promoted responses to additional antigens not present in the vaccine, which could protect against challenge with tumor cells lacking the vaccine-targeted antigens. We attempted to evaluate whether AIPV could be protective in the absence of antigen spreading by treating pmel-1 transgenic mice<sup>231</sup> that lack T-cells capable of responding to peptides other than gp100, but when treated with AIPV incorporating a gp100 peptide as the vaccine component, these animals developed severe inflammatory toxicity. Antigen spreading promoted by immunotherapy has also been observed in recent clinical studies melanoma patients<sup>254</sup>, and may be important for dealing with tumor heterogeneity and preventing escape by tumor antigen loss variants<sup>255</sup>.

Endogenous antibody responses were also primed by AIPV as well as subcombinations of the four reagents, and AIPV treatment induced antibodies that were protective when transferred to naïve recipients. Despite these findings, B-cells were not required for AIPV treatment efficacy, and we speculate that because the therapy itself includes a potent monoclonal tumor-opsonizing antibody, the endogenous response may be redundant. An interesting question for future work will be whether the monoclonal antibody component could be removed from the treatment regimen once the endogenous antibody response develops, i.e. by the second or third treatment.

AIPV incorporates two tumor-specific reagents, the lymph node-targeted peptide vaccine and a monoclonal opsonizing antibody. While still a challenge in some diseases, identification of shared T-cell target antigens has been well delineated for many cancers over the past 20 years by the cancer vaccine field<sup>256</sup> and a number of pipelines for finding unique mutant antigens have been recently developed<sup>257,258</sup>. Identifying an effective opsonizing monoclonal antibody also presents a development hurdle to apply AIPV to an arbitrary given tumor. However, the demonstration that the integrin binding protein 2.5F-Fc, which contains an Fc domain for antibody effector functions and recognizes  $\alpha_v\beta_3$ ,  $\alpha_v\beta_5$ , and  $\alpha_5\beta_1$  integrins over-expressed in a broad range of cancers<sup>259</sup>, makes the 2.5F-Fc protein potentially applicable to many tumor types.

Studying AIPV as a representative effective immunotherapy may be useful for delineating what the immunological characteristics of a powerful anti-tumor immune response are, which may allow for rational design of future next-generation immunotherapies. In particular, studies listed here primarily focused on characterization of the immune response at days to weeks post treatment, but it would be interesting to investigate the very early events that occur following AIPV. Single cell RNAseq may be particularly suited for this because it would provide an unbiased snapshot of transcriptional changes that occur early after treatment; FcγR-

expressing cells may be of special interest here given that TA99 is likely to opsonize tumor cells quickly, leading to a wave of innate-cell-mediated tumor killing. Comparisons between AIPV and IPV at early time points using single cell RNA-seq would likely be most fruitful. Additional questions that remain include: what are the antigenic targets of the T cells that are primed via antigen spreading? Is antigen spreading required for therapeutic efficacy? Is efficacy maintained with a vaccine that primes CD4<sup>+</sup> T cell responses instead of CD8<sup>+</sup> T cell responses? Would efficacy be superior with neoantigen-targeted vaccines? To which proteins are the endogenously generated anti-tumor antibodies binding? Future investigation along these lines may yield insight into mechanistically how AIPV provides such potent anti-tumor immunity and how to harness this insight for more effective immunotherapies.

In summary, we have demonstrated that a rational combination of four complementary immunomodulatory agents, each of which have modest anti-tumor efficacy individually, can lead to robust complete responses in the setting of large, immunosuppressive tumors. As shown here, successful rejection of established tumors relied on an orchestrated response invoking diverse effector mechanisms of the immune system. Although a quaternary treatment regimen will be challenging for direct clinical translation, insights from this successful protocol provide a framework for devising simpler regimens and extensions to other treatment modalities.

## 4.4 Methods

### Mice

B6 mice (C57BL/6NTac) were purchased from Taconic. Balb/c mice (BALB/cJ), *Batf3*<sup>-/-</sup> mice (B6.129S(C)-*Batf3*<sup>tm1Kmm</sup>/J), Braf/Pten mice (B6.Cg-Braf<sup>tm1Mmcm</sup> Pten<sup>tm1Hwu</sup> Tg(Tyr-cre/ERT2)13Bos/BosJ), and mT/mG mice (B6.129(Cg)-Gt(ROSA)26Sor<sup>tm4(ACTB-tdTomato,-EGFP)Luo</sup>/J) were purchased from The Jackson Laboratory. Mice used in the inducible cancer model (Braf/Pten-TG) were crosses of Braf/Pten and mT/mG bred in-house and having the following genotype: Braf<sup>tm1Mmcm +/-</sup>, Pten<sup>tm1Hwu +/-</sup>, Tg(Tyr-cre/ERT2)13Bos<sup>+</sup>, Gt(ROSA)26Sor<sup>tm4(ACTB-tdTomato,-EGFP)Luo +/-</sup>, where "+" indicates presence of the mutant/transgenic allele. All Braf/Pten mice were genotyped via Transnetyx. Mice were used in studies when 6-8 weeks old. All animal work was conducted under the approval of the Massachusetts Institute of Technology (MIT) Division of Comparative Medicine in accordance with federal, state, and local guidelines.



## Cells

B16F10 were purchased from ATCC. TC-1 cells were kindly provided by Dr. T. C. Wu at John Hopkins University. B16-OVA and DD-Her2/neu cells were kindly provided by Dr. Glenn Dranoff at Dana-Farber. B16-GFP-Luc cells were generated as previously described<sup>260</sup>. DD-Her-2/neu breast tumor cells were derived from a spontaneous breast tumor in a Balb/c Her-2/neu (Balb-NeuT) transgenic mouse, in which MMTV promoter-driven breast epithelium-specific expression of the activated oncogenic form of rat Her-2/neu drives progressive development of breast tumors in transgenic Her-2/neu female mice<sup>261</sup>. The DD cell line was found to lose Her-2/neu expression *in vitro*, and thus cells were infected with pMFG-Her-2/neu virus to achieve stable expression of high levels of oncogenic rat Her-2/neu both *in vitro* and *in vivo*. HEK293 cells were purchased from Life Technologies.

Tumor cell lines were cultured in complete DMEM (DMEM supplemented with 10% FBS, 100 units/mL penicillin, 100 µg/mL streptomycin, and 4 mM L-alanyl-L-glutamine) with the exception of TC-1 cells, which were cultured in complete RPMI. T-cells and splenocytes were cultured in RPMI with 10% heat inactivated FBS, 20 mM HEPES, 1 mM sodium pyruvate, 0.05 mM beta-mercaptoethanol, 100 units/mL penicillin, 100 µg/mL streptomycin, 2 mM L-alanyl-L-glutamine, and 1X MEM non-essential amino acids. Hybridomas were cultured in CD Hybridoma AGT Medium (Life Technologies). HEK293 cells were cultured in Freestyle Media (Life Technologies). All cell lines and assay cultures were maintained at 37°C and 5% CO<sub>2</sub>. All cells were tested regularly for mycoplasma contamination and for rodent pathogens and none used tested positive at any point.

## Vaccine and protein production

Amphiphile-CpG (amph-CpG) was produced as previously described, by solid phase synthesis of a Class B CpG 1826 sequence with G<sub>2</sub> spacer (5' diacyl lipid - \*G\*G\*T\*C\*C\*A\*T\*G\*A\* C\*G\*T\*T\*C\*C\*T\*G\*A\*C\*G\*T\*T- 3') conjugated via the 5' end to an 18-carbon diacyl tail<sup>10</sup>. Amphiphile-peptides (amph-peptides) were produced as previously described<sup>10</sup>, via conjugation of cys residues of peptide antigens to 1,2-distearoyl-sn-glycero-3-phosphoethanolamine-N-[maleimide(polyethylene glycol)-2000] (Avanti Polar Lipids). Vaccine sequences are as follows: Trp<sub>2180-188</sub> (CSVYDFFVWL); Her2/Neu<sub>66-74</sub> (p66, CTYVPANASL),

HPV E7<sub>43-62</sub> (GQAEPDRAHYNIVTFCKCD), Tyrp1<sub>opt455-463</sub> (optimized A463M<sup>262</sup>, CTAPDNLGYM), gp100<sub>opt120-39</sub> (optimized S27P, EGP long<sup>211</sup>, CAVGALEEGPRNQDWLGVPRQL). TA99 and MSA-IL2 were produced in HEK293 cells as previously described<sup>9</sup>. 2.5-Fc was generated by fusing an integrin ( $\alpha_V\beta_3$ ,  $\alpha_V\beta_5$ , and  $\alpha_5\beta_1$ ) binding domain to a murine IgG2a Fc region to create an antibody-like tumor targeting molecule<sup>23</sup>. 2.5-Fc was produced by transient transfection of HEK293 cells and purified by Protein A. The 7.16.4 monoclonal antibody to rat Her2/neu was generated from hybridoma 7.16.4 purchased from ATCC, and was purified using Protein A. IFN- $\alpha$  was expressed as a SUMO fusion using the pE-SUMOpro vector (LifeSensors) in Rosetta-gami 2 (DE3) competent cells (Novagen). After IMAC purification using TALON metal affinity resin according to the manufacturer's instructions (Clontech Laboratories), the SUMO tag was removed by incubation with SUMO protease and reapplication on TALON resin as detailed previously<sup>263</sup>. Finally, the protein was passed through Detoxi-Gel endotoxin removal resin (Thermo Scientific) until endotoxin levels were below 0.1 total EU/dose as measured by the QCL-1000 chromogenic LAL assay (Lonza). The IL-15 superagonist<sup>42</sup> was produced by transiently transfecting HEK293 cells with a plasmid encoding His-tagged IL-15 superagonist and purified using Ni-NTA agarose (Qiagen) on a PD-10 column (Bio-Rad) followed by further purification using a His-Spin Protein Miniprep (Zymo Research). Anti-TGF- $\beta$ , a homodimeric fusion between murine IgG2a Fc and the extracellular domain of the type II TGF- $\beta$  receptor, was produced by transient transfection of HEK293 cells and purified by Protein A.

## Tumor inoculation and subcutaneous tumor therapy

An inoculum of  $10^6$  tumor cells was injected s.c. on the flank of mice in 50  $\mu$ L sterile PBS. Eight days following injection, treatment was initiated as indicated (Figure 19a). The tumor-targeting antibody (**A**) was administered at 100  $\mu$ g per dose i.p. for B16F10 and DD-Her2/Neu models. 2.5-Fc was administered at 500  $\mu$ g per dose (i.p.). MSA-IL2 (**I**) was administered i.p. at 30  $\mu$ g (6  $\mu$ g molar equivalent IL-2) per dose. Anti-PD-1 (**P**) (clone RMP1-14, BioXCell) was administered at 200  $\mu$ g i.p. The vaccine, composed of 1.24 nmol amph-CpG and 20  $\mu$ g of amph-peptide, was administered s.c. at base of the tail, half the dose given on each side. For experiments exploring other quaternary combos, the following doses were used as indicated in Figure 22: anti-CTLA-4 (clone 9D9, BioXCell) was administered at 200  $\mu$ g per dose i.p., IFN- $\alpha$  was administered at 50  $\mu$ g per dose i.p., IL-15 superagonist at 4  $\mu$ g per dose i.p., and anti-TGF- $\beta$  at 100  $\mu$ g per dose i.p. Mice were randomized into treatment groups on day 8 following tumor inoculation, immediately prior to treatment. Tumor size was measured as an

area (longest dimension x perpendicular dimension) three times weekly, and mice were euthanized when tumor area exceeded 100 mm<sup>2</sup>. Mice that rejected tumors were rechallenged as indicated with 10<sup>5</sup> tumor cells s.c. on the opposite flank.

## Flow cytometry

Antibodies to CD8 $\alpha$  (53-6.7), IFN- $\gamma$  (XMG1.2), TNF- $\alpha$  (MP6-XT22), CD3 $\epsilon$  (500A2), IgM (RMM-1), CD19 (6D5), NK1.1 (PK136), Ly-6G (1A8), F4/80 (BM8), CD11b (M1/70), CD25 (PC61), PD-1 (29F.1A12), Tim-3 (B8.2C12), Ly-6C (HK1.4), and CD64 (X54-5/7.1) were purchased from BioLegend. Antibodies to CD4 (RM4-5) and Foxp3 (FJK-16s) were purchased from eBioscience. Trp2 tetramer (iTag Tetramer/PE H-2K<sup>b</sup> TRP2) and OVA tetramer (iTag Tetramer/PE H-2K<sup>b</sup> OVA) were purchased from MBL. Tetramer staining was performed in buffer containing 50 nM dasatinib to enhance staining. Viability was assessed by LIVE/DEAD Fixable Aqua purchased from Life Technologies. TA99 was labeled with Alexa Fluor 647 NHS Ester (Life Technologies) to generate TA99-647. Foxp3 was stained using the Transcription Factor Buffer Set from BD.

Intracellular Cytokine Staining (ICS) was performed as described previously<sup>10</sup>. Peptides used for restimulation were 10  $\mu$ g/mL of the relevant antigen: Trp2<sub>180-188</sub> (SVYDFFVWL), Her2/Neu<sub>66-74</sub> (TYVPANASL), Tyrp-1<sub>455-463</sub> native (TAPDNLGYA), or gp100<sub>25-33</sub> native (EGSRNQDWL). Immune cell infiltrates of tumors were analyzed as previously described<sup>9</sup>, briefly: tumors were resected from mice on day 14 or 21, weighed, and mechanically disrupted to generate a single cell suspension. Cells were stained to identify infiltrating immune and quantified using flow cytometry. Shown are cell counts normalized by tumor mass. For antibody and GFP uptake experiments, lymph nodes were resected from tumor bearing mice on day 10, digested with 0.8 mg/ml Dispase, 0.2 mg/ml Collagenase, and 0.1 mg/ml DNase I in RPMI at 37°C for 20 minutes with gentle agitation, and a single cell suspension was created. Cells were stained to identify DC populations and run on the cytometer. Cells were analyzed using BD FACS LSR II, BD FACS LSR Fortessa, and BD FACSCanto flow cytometers, and data was analyzed using FlowJo.

## Depletions

Cellular subsets were depleted by administering 400  $\mu$ g of depleting antibody i.p. twice weekly beginning one day prior to therapy as indicated: CD8<sup>+</sup> T-cells with anti-CD8 $\alpha$  (clone

2.43, BioXCell), CD4 T-cells with anti-CD4 (clone GK1.5, BioXCell), NK cells with anti-NK1.1 (clone PK136, BioXCell), neutrophils with anti-Ly-6G (clone 1A8, BioXCell), with the exception of CSF1R and IL-5, which were depleted using 300 µg (clone AFS98, BioXCell) every other day and 1 mg (clone TRFK5, BioXCell) weekly respectively.<sup>9</sup> Cellular depletions of CD8<sup>+</sup> T cells, CD4<sup>+</sup> T cells, neutrophils, and NK cells were confirmed by flow cytometry of PBMC (Figure 28).

### **Autochthonous tumor model induction and therapy**

BRaf<sup>CA</sup> Pten<sup>loxP</sup> Tyr::CreER<sup>T2</sup> mice<sup>27</sup> on the C57BL/6 background<sup>264</sup> were crossed with mT/mG mice<sup>265</sup> to generate BRaf/Pten-TG mice. To induce tumors, 2 µL of 5 mg/mL tamoxifen was administered to the left ear on three consecutive days. Tumors were allowed to develop for 24-26 days, at which time visible pigmented tumors were present. Treatment schedule and doses were the same as B16F10 s.c. model, except that vaccine used was a combination of three amph-peptides (15 µg amph-gp100, 15 µg amph-Trp1, and 15 µg amph-Trp2) and 1.24 nmol amph-CpG. Mice were euthanized when pigmented lesions covered greater than 90% of the ear.

### **Liver enzyme measurements**

Serum was isolated from mice 36 hours after treatment and liver enzymes AST and ALT were quantified using a colorimetric Aspartate Aminotransferase Activity Assay Kit (Sigma Aldrich) and Alanine Aminotransferase Activity Assay Kit (Sigma Aldrich) respectively according to the manufacturer's protocol.

### **Endogenous antibody detection and serum transfer**

For endogenous antibody binding measurements following therapy, B16F10 cells, TC-1 cells, or DD-Her2/Neu cells were incubated with 5% serum from AIPV-treated mice (day 150) or age-matched naïve mice in PBS for 30 minutes at 4°C, washed twice with PBS, 1% BSA, 5mM EDTA, then incubated with AlexaFluor647 labeled anti-mouse IgG for 20 minutes at 4°C. Cells were washed in PBS, 1% BSA, 5mM EDTA with DAPI included to exclude dead cells and were subsequently run on the BD FACSCanto for analysis. To measure endogenous antibody responses during therapy in the B16F10 model, TA99 antibody used as part of the therapy needed to be depleted from serum samples. To this end, biotinylated TA99 was used for

therapy, which could be removed from recovered sera using streptavidin resin. TA99 was biotinylated using an N-hydroxy succinimide-activated biotin according to the manufacturer's protocol (Thermo Fisher Scientific) and excess biotin was removed using desalting columns (Zeba). Biotin labeling was quantified using the colorimetric Biotin Quantitation Kit (Pierce), and a degree of labeling of 5.1 biotins per TA99 molecule was achieved for the experiments shown. For serum antibody measurement during therapy, serum was isolated from mice weekly and incubated with an excess of streptavidin resin (GenScript) for 1h at 25°C. Serum was frozen and stored at -80°C and thawed on the day of the binding assay, which was performed as described above.

For serum transfer studies, serum was obtained from AIPV treated mice or age-matched naïve mice and complement was inactivated by incubating for 30 minutes at 57°C. Serum (350 µL) or TA99 (200 µg) was injected i.p. into naïve recipients six hours prior to injection of 250,000 B16F10 cells i.v. through the tail vein. Lungs were isolated 17 days later and lung nodules were counted in a blinded fashion.

## **Generation of Trp2 KO cell line**

B16-Trp2-KO cells were generated using CRISPR-Cas9. B16-GFP-Cas9 cells were generated by transduction of B16F10 cells with lentivirus expressing humanized SpCas9-P2A-EGFP from an EFS promoter (unpublished, kindly provided by Tim Wang in Dr. David Sabatini's Lab at the Whitehead Institute). Clones were isolated by single cell flow cytometry for GFP positive cells. A clone stably expressing Cas9 was designated B16-GFP-Cas9. Guide RNA expression vectors were created by cloning a human U6 promoter and sgRNA sequences into a minimal vector with an ampicillin-selectable marker and a ColE1 replication origin. The optimized sgRNA sequence described previously<sup>266</sup> were used. Sequences for the sgRNAs (**Table 2: Guide Sequences**) were designed using tools provided by the Zhang Lab at the Broad Institute (available at <http://crispr.mit.edu/>). B16-GFP-Cas9 cells were co-transfected with 2 sgRNAs expression vectors targeting Trp2 and a plasmid expressing EGFP and a puromycin selectable marker from a CAG promoter using Xfect (Clontech) according to manufacturer's instructions. Stable cells were selected for with 2 µg/mL puromycin followed by single cell FACS. Clones were grown for 3 weeks before being analyzed for knockout by PCR amplification of the Trp2 gene (Primers shown in **Table 3: Primer Sequences**). The final clone was then selected and designated B16-Trp2-KO. PCR amplification of genomic DNA showed a

smaller fragment (Figure 30) and sequencing confirmed deletion of the a 283 bp fragment containing the Trp2 peptide sequence (data not shown).

**Table 2: Guide Sequences**

Name	Sequence	Position of Targeted Sequence
Dct-sg 2	5'-CGACTGTAATCGGAAGAAGC GTTTAAGAGCTATGCTGGAAACAGCATAGCAAGTTTAAATAA GGCTAGTCCGTTATCAACTTGAAAAAGTGGCACCGAGTCGG TGC-3'	8991-9013
Dct-sg 4	5'-GAGGCTTGTGACCCGGGTGG GTTTAAGAGCTATGCTGGAAACAGCATAGCAAGTTTAAATAA GGCT GTCCGTTATCAACTTGAAAAAGTGGCACCGAGTCGGTGC-3'	9274-9296

**Table 3: Primer Sequences**

Name	Sequence	Location
Trp2 forward primer	5'-CACAGAGAACCCTCCGAGAA-3'	8745-8764
Trp2 reverse primer	5'-ACAGGCGGTGTTTGGTAATC-3'	9375-9394

## **ELISPOT assay**

Target B16F10, TC-1, or B16-Trp2-KO cells were treated with 500 U/mL mIFN- $\gamma$  (Peprotech) for 12 hr, then irradiated (120 Gy). Effector cells were splenocytes isolated from AIPV-treated mice that had rejected tumors 6 days after rechallenge with  $10^6$  B16F10 cells. A Mouse IFN- $\gamma$  ELISPOT Kit (BD) was used. Targets cells were seeded at 25,000 cells per well. Effector cells were seeded at  $10^6$  cells per well. Plates were wrapped in foil and cultured for 24 hours then developed according to manufacturer's protocol. Plates were scanned using a CTL-ImmunoSpot Plate Reader and data was analyzed using CTL ImmunoSpot Software.

## **Immunoblot**

B16F10 cell lysate was run on an SDS-PAGE gel, transferred to nitrocellulose membranes, blocked for 1 hr at 25°C, and then stained with serum from treated mice and rabbit anti-beta-actin overnight at 4°C. Membranes were then washed and stained with goat anti-mouse-IRDye800 and anti-rabbit-IRDye680 for 1 hr at 25°C. Imaging was performed on an Odyssey scanner (Licor). As a control, TA99 was used in place of mouse serum in the protocol above to show the presence of Trp1 in the B16F10 lysate.

## **Tumor cytokine Luminex assay**

Tumors were harvested at day 17 (2 days after 2<sup>nd</sup> treatment). All tumors from a treatment group were collected up to a maximum of ~250 mg for processing in a bead beater tube. Tissue samples were lysed in lysis buffer (5  $\mu$ L/mg tumor): 50 mM tris-HCl (pH 7.5), 10% glycerol, 150 mM NaCl, 1% NP-40, and freshly supplemented with Halt Protease & Phosphatase Inhibitor Cocktail (Life Technologies). Lysates were aliquoted and stored at -80°C until analysis. Samples diluted 1:1 with Assay Buffer and assayed using a Luminex bead-based ELISA (MILLIPLEX MAP Mouse Cytokine/Chemokine Magnetic Bead Panel, Millipore) following manufacturer's instructions with the following modifications: magnetic capture beads and detection antibodies were both used at 1/5x recommended amounts. Concentrations were normalized to total protein input. All samples and analytes were above the limit of detection.



## Histology

Tumor inoculation and treatment were performed following the timeline in Figure 19a. For hematoxylin and eosin staining, mice were sacrificed 3 days after the second treatment, and tumors were fixed in 10% formalin, embedded in paraffin, and stained with hematoxylin and eosin. For immunofluorescence, tumors were isolated on day 14 and processed as previously detailed<sup>267</sup>. Flank tumors were used to analyze infiltrate by immunofluorescence in the Braf<sup>CA</sup> Pten<sup>loxP</sup> Tyr::CreER<sup>T2</sup> model to allow for higher quality sectioning. For staining, anti-CD8 (CT-CD8a, Cedar Lane), DAPI, and phalloidin were used. The images were acquired using an Olympus Fluoview FV1200 microscope equipped with 10X (NA 0.40) and 30X (NA 1.05) objectives and optimum lasers and filter sets. The images were acquired under identical acquisition setting and subsequently processed using Fiji image analysis software.

## Multivariate Analysis of Cytokine Data

Cytokine levels for each tumor were normalized to the median of “Untreated” controls and log<sub>2</sub> transformed. Heatmaps and clustering trees were generated using the clustergram function in Matlab (Mathworks). Euclidean distance was used for hierarchical clustering of cytokines only. The resulting dendrogram was pruned by collapsing leaves with Euclidean distance <95% confidence interval for all 32 potential leaves.

Partial least squares regression was applied using raw cytokine concentrations (pg/μg total protein) regressed against a vector of total tumor mass using PLS\_Toolbox R7 (Eigenvector Research). Orthogonalization was used to maximize tumor mass variance captured in the first latent variable; model performance was assessed by random subsets cross-validation with maximum splits and iterations performed.

## Statistical Analysis

Statistical methods were not used to predetermine necessary sample size, but sample sizes were chosen based on estimates from pilot experiments and previously published results such that appropriate statistical tests could yield significant results. Experiments were not performed in a blinded fashion. Intratumoral infiltrates, serum transfer foci quantitation, tetramer stain, AST, and ALT, were analyzed using one-way ANOVA with Bonferroni post-test using GraphPad Prism software. Where ANOVA was used, variance between groups was found to be

similar by Bartlett's test. Survival curves were analyzed using the Log-rank (Mantel-Cox) test, and two-tailed student's t test was used for the antigen spreading ELISPOT. For the tumor infiltrate data and DC uptake data, Welch's t test (with Bonferroni correction) was used for each condition versus untreated due to unequal variance between groups. No samples were excluded from analysis.

# CHAPTER 5: Antigen heterogeneity in solid tumors

## 5.1 Introduction

Tumors are subject to Darwinian selection pressures, with tumor cell clones that possess fitness advantages surviving and expanding over time. This has been considered in the past in the context of selective pressure applied by chemotherapy, targeted therapy, and more recently, by the immune system in immunotherapy<sup>268</sup>. For example, selection pressure led to antigen-escaped clones in adoptive cell transfer settings with T cells recognizing MART-1 in melanomas<sup>269</sup>, and more recently, with CD19-targeted CAR-Ts in B-cell acute lymphoblastic leukemia<sup>270</sup>. The issue of antigenic heterogeneity in immunotherapy has been explored in the context of T cells in a few settings by Hans Schreiber<sup>271,272</sup> and others<sup>273</sup>, but there are a number of concerns with interpretation of the experimental results due to the models used. For example, in some studies<sup>271</sup>, either Rag2<sup>-/-</sup> or OT-I mice were used as recipients in adoptive cell transfer models, which means not only are recipient mice lacking normal polyclonal CD8<sup>+</sup> T cell repertoires, but they lack a CD4<sup>+</sup> T cell compartment entirely, because CD4<sup>+</sup> T cell development is prevented in OT-I mice due to allelic exclusion<sup>274</sup>; both polyclonal T cell populations would be present in patients receiving immunotherapy, and may play a role in combatting antigen-escaped clones via antigen spreading. Further, although the studies are motivated by the goal of addressing tumor cells that have lost expression of the target antigen, it is later revealed that the non-tamoxifen-induced control cells still express residual levels of the target antigen due to construct leakiness<sup>271</sup>, and this is problematic for interpretation because it has been shown that even as few as one peptide-MHC complex can activate T cells<sup>275</sup>. In other models exploring antigenic heterogeneity, the cell lines used as antigen-expressing and antigen-negative have had such different properties that conclusions are hard to draw. For example, in one study<sup>273</sup>, The melanoma line B78H1 was used as a Trp1-negative tumor line, and B16F10 was used as the Trp1-expressing tumor in the context of adoptive cell transfer with CD4<sup>+</sup> T cells targeting Trp1. However, B78H1 tumors do not express class I (even when treated with IFN- $\gamma$ <sup>276</sup>) or class II<sup>277</sup>, whereas B16F10 can express both *in vivo* (ref. for class II<sup>278</sup>). The growth of B78H1 tumors is so much slower *in vivo* than B16F10 that injection of 10-fold more B78H1 cells were required<sup>273</sup>, thus, mosaic tumors were actually composed of 91% Trp1-non-expressing cells and only 9% Trp1-expressing cells. There are more recent studies using immunocompetent mice

with tumors expressing model CD4 and CD8 antigens, however, the tumor line used was not capable of presenting the relevant CD4<sup>+</sup> T cell or CD8<sup>+</sup> T cell epitopes because it lacked the appropriate MHC, and further, the specific mechanisms by which tumor destruction occurred were not elucidated<sup>272</sup>. A cleaner setting to investigate the role of antigenic heterogeneity in immunotherapy would be to use immunocompetent mice with normal CD4<sup>+</sup> T cell and CD8<sup>+</sup> T cell repertoires with tumor mosaics composed of otherwise identical tumor cells (with similar *in vivo* growth rates) in which one expresses the antigen of interest and the other does not.

In this chapter, Trp1-KO tumor cells are used as antigen-deleted variants in tumor comprised of otherwise genetically identical parental cells. Although much emphasis recently has been placed on neoantigens as targets for immunotherapy, in the context of the recruitment of FcγR-expressing innate effectors via antibody based immunotherapy, the target of the antibody is likely to be a non-mutated tumor associated antigen. As described above, a number of studies have been conducted on T cell based immunotherapy targeting antigens that are expressed heterogeneously, but similar studies performed using immunotherapies incorporating anti-tumor antibodies could be beneficial, given mAbs many roles in promoting anti-tumor immunity (reviewed in Chapter 1). Here we show that minorities of antigen-deleted variants can be eliminated in therapy with an extended PK IL-2 and TA99, and we develop an effective models system to explore antigenic heterogeneity in immunotherapy in the future.

## **5.2 Results**

### **Generation and characterization of antigen knockout lines**

B16Trp1KO cells were generated as described in Chapter 4 for the Trp2KO line, except that the sgRNAs used targeted Trp1 instead of Trp2. The knockout was confirmed using PCR and genomic sequencing. A table of the tumor cell lines used in this chapter is shown in Table 4. To confirm complete deletion of the CD8<sup>+</sup> T cell epitopes within the targeted protein, mice were immunized against Trp1 or Trp2 and an ELISPOT was performed to look for reactivity against the antigen of interest. Trp1KO targets were indistinguishable from wells without any targets for Trp1-specific CD8<sup>+</sup> T cells, and the same was true for Trp2 specific CD8<sup>+</sup> T cells with Trp2KO target cells (Figure 34a-c). Interestingly, lower reactivity against Trp2 was seen with Trp2-specific CD8<sup>+</sup> T cells against the Trp1KO cells compared to other lines, indicating that the presence of Trp1 may be important for Trp2 protein levels in these cells. Trp1 has been shown

Table 4: Cell lines generated using CRISPR/Cas9 to investigate antigenic heterogeneity

Cell Line	Mycoplasma?	KO confirmed by PCR?	KO confirmed by genomic sequencing (TOPO cloned)	Cas9	EGFP
B16F10	clean 3/28/16	N/A	N/A	none	none
B16-Cas9	clean 3/28/16	N/A	N/A	Cas9 <sup>+</sup>	EGFP <sup>+</sup>
B16-Trp1KO	clean 3/28/16	Yes	Yes, 178-bp deletion	Cas9 <sup>+</sup>	EGFP <sup>+</sup>
B16-Trp2KO	clean 3/28/16	Yes	Yes, 283-bp deletion	Cas9 <sup>+</sup>	EGFP <sup>+</sup>
B16-gp100 KO	clean 3/28/16	unclean PCR	Yes, 328-bp deletion	Cas9 <sup>+</sup>	EGFP <sup>+</sup>

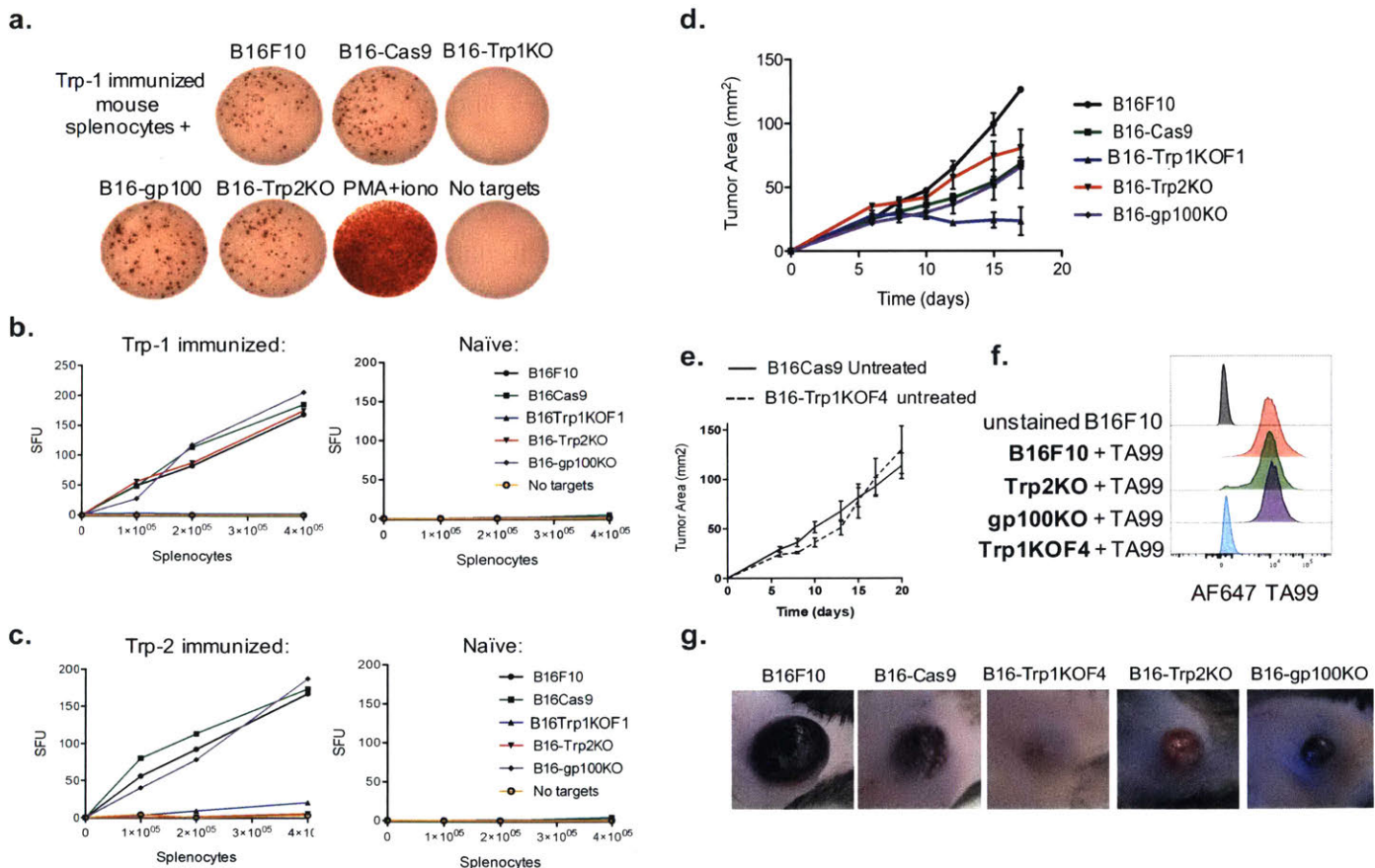


Figure 34 **Characterization of melanoma tumor-associated-antigen knockout lines.** **a-c**, Mice previously primed and boosted with 10 $\mu$ g of amph-Trp1 or amph-Trp2 and 25 $\mu$ g CDNs were sacrificed and splenocytes were isolated. These splenocytes were plated with 25,000 irradiated tumor cells of the type indicated and an ELISPOT was performed. Shown are representative wells, **a**, and quantitation of spot forming units (SFU) as a function of the number of splenocytes seeded from immunized mice, **b-c**. **d**, 8-week-old female C57BL6/J mice were injected with 1 million cells of the indicated tumor type; shown is tumor growth over time (n = 5/group). **e**, Trp1KOF1 was passaged *in vivo* 4 times to generate Trp1KOF4 and 1 million tumor cells were injected into 8-week-old female C57BL6/J mice; shown is tumor growth over time. **f**, Indicated tumor lines were stained with AF647-labeled TA99 and run on the cytometer. **g**, representative images of the indicated tumors showing a range of *in vivo* melanin production.

to stabilize levels of tyrosinase<sup>279</sup> in a multienzyme complex in which Trp2 is also present—it may be that Trp1 stabilizes Trp2 in this context as well, leading to lower levels of Trp2 protein in the Trp1KO cells in the absence of this stabilization.

The Trp1KO line expresses both Cas9 and EGFP, therefore the relevant control for *in vivo* tumors studies is B16Cas9-EGFP (hereafter referred to as B16Cas9). The *in vivo* growth rates of the knockout lines were measured and compared to the parental B16Cas9 line (Figure 34d), and while B16Trp2KO and B16gp100KO showed overlapping growth curves with B16Cas9, the B16Trp1KO line showed severely retarded growth *in vivo*. Therefore, in order to create a cell line with growth characteristics that more closely match the parental B16Cas9 line, the B16Trp1KO line was passaged *in vivo*. The original B16Trp1KO line (B16Trp1KOF1) only formed tumors in half of injected mice, but after four consecutive passages *in vivo*, the growth rate was identical to the parental B16Cas9 line (Figure 34e), with all injected mice forming tumors that grew progressively until the mice required euthanasia due to tumor burden. To re-confirm that Trp1 was still knocked out in this B16Trp1KOF4 line and to characterize surface expression levels in the other lines, all tumor cells were stained with fluorescently labeled TA99 (Figure 34f), and as expected, all lines except showed high expression of Trp1 except for the B16Trp1KOF4, which showed no expression. The *in vivo* melanin production of these lines varies due to the involvement of the knocked out proteins in melanogenesis (Figure 34g).

### **Antigenically heterogeneous tumors: mosaics with cells lacking Trp1 expression.**

To investigate how the Trp1KOF4 line responds to immunological pressure targeting the antigen of interest, tumors were either treated with AI (TA99 + MSA-IL2) or amph-vaccine targeting Trp1 (Figure 35a,e). As shown, AI therapy or vaccination against Trp1 had no significant impact on tumor growth (Figure 35c,g) or survival (Figure 35d,h) in B16Trp1KOF4 cells, while both AI and vaccination had significant impact on growth and survival in the parental, Trp1-expressing line, B6Cas9 (Figure 35b,d,f,h). Thus, the non-antigen specific components of these two therapies (namely, MSA-IL2 in AI and c-di-GMP in vaccine therapy) did not have substantial effect on the growth of B16Trp1KOF4 cells in this treatment context. In line with previous data with amph-vaccine in B16 tumor models<sup>10</sup> vaccine against Trp1 did not cure any of the B16Cas9 tumors, whereas AI resulted in approximately half of the treated tumors being completely eliminated. Given the quite divergent efficacy resulting from AI therapy with B16Cas9 compared to B16Trp1KOF4, this presented a useful working system to



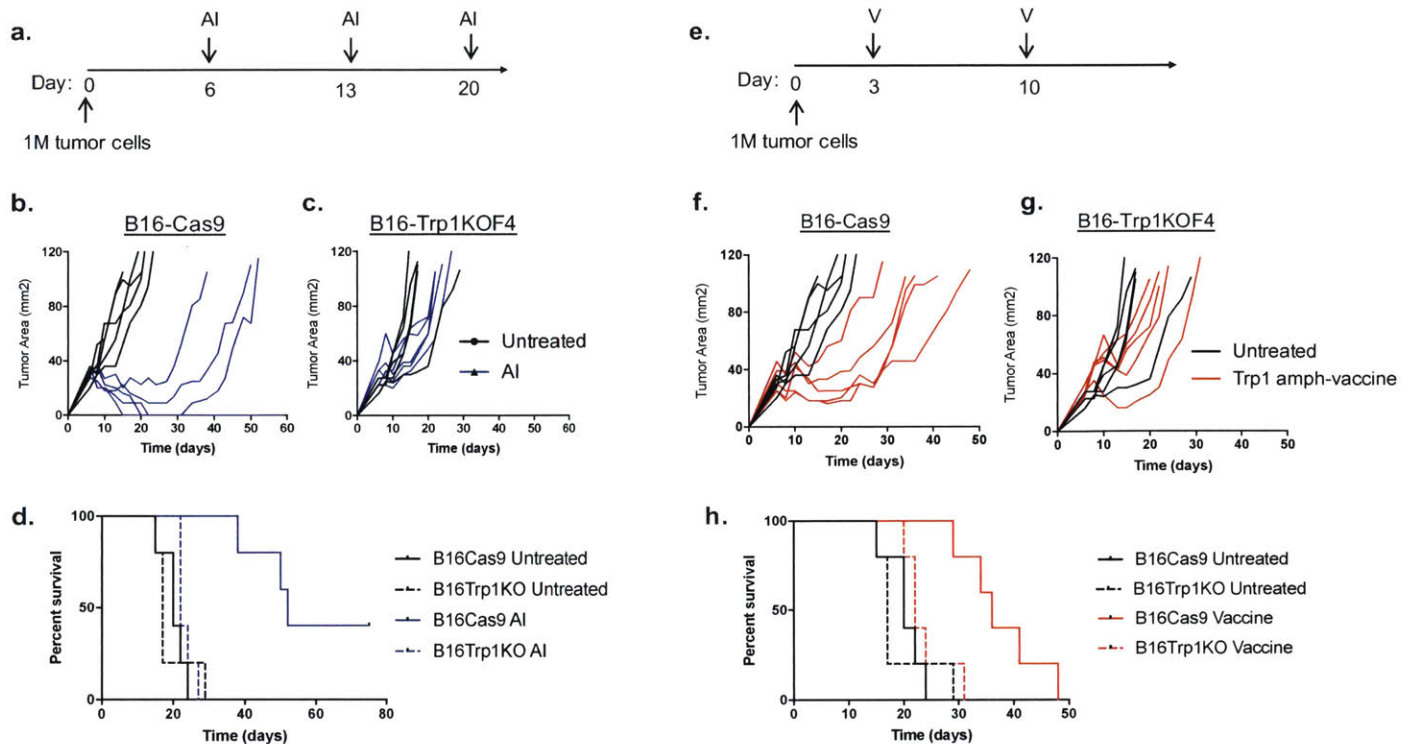


**Figure 35 Immunotherapies targeting Trp1 antigen do not significantly impact growth in Trp1KO tumors.** **a-d**, 8-week-old female C57BL6/J mice were treated with AI as shown in **a**; shown are tumor growth curves, **b-c** and survival plots, **d**, for the indicated tumor types. **e-h**, 8-week-old female C57BL6/J mice were treated with Trp1 amph-vaccine (adjuvanted with 25 $\mu$ g c-di-GMP) as shown in **e**; shown are tumor growth curves, **f-g**, and survival plots, **h**, for the indicated tumor type. Mice were euthanized when tumors exceeded 100mm<sup>2</sup> area.

investigate the effects of heterogeneous antigen expression of the target of the antibody in immunotherapy.

Mosaic tumors were formed with ranging percentages of cells deleted for Trp1 by injecting 0%, 10%, 25%, 50%, 75%, or 100% B16Trp1KOF4 cells. All mice received 1 million total cells, with the remainder composed of Trp1-expressing B16Cas9 cells. Mice were treated with AI (Figure 36a) and outcome was monitored. Compositions with 10% or 25% B16Trp1KOF4 cells showed clear therapeutic benefit, with approximately half of mice completely rejecting their tumors, whereas higher fractions of antigen-deleted cells resulted in significantly lower efficacy, with none of the mice showing a complete response (Figure 36b-c). Treatment of 10% B16Trp1KOF4 cells is particularly interesting to consider because therapeutic outcome was indistinguishable from treatment of the parental B16Cas9 line. However, the 10% Trp1KOF4 tumors only received 100,000 B16Trp1KOF4 cells (along with 900,000 B16Cas9 cells), while the 100% B16Trp1KOF4 tumors received 1,000,000 B16Trp1KOF4. To ensure that

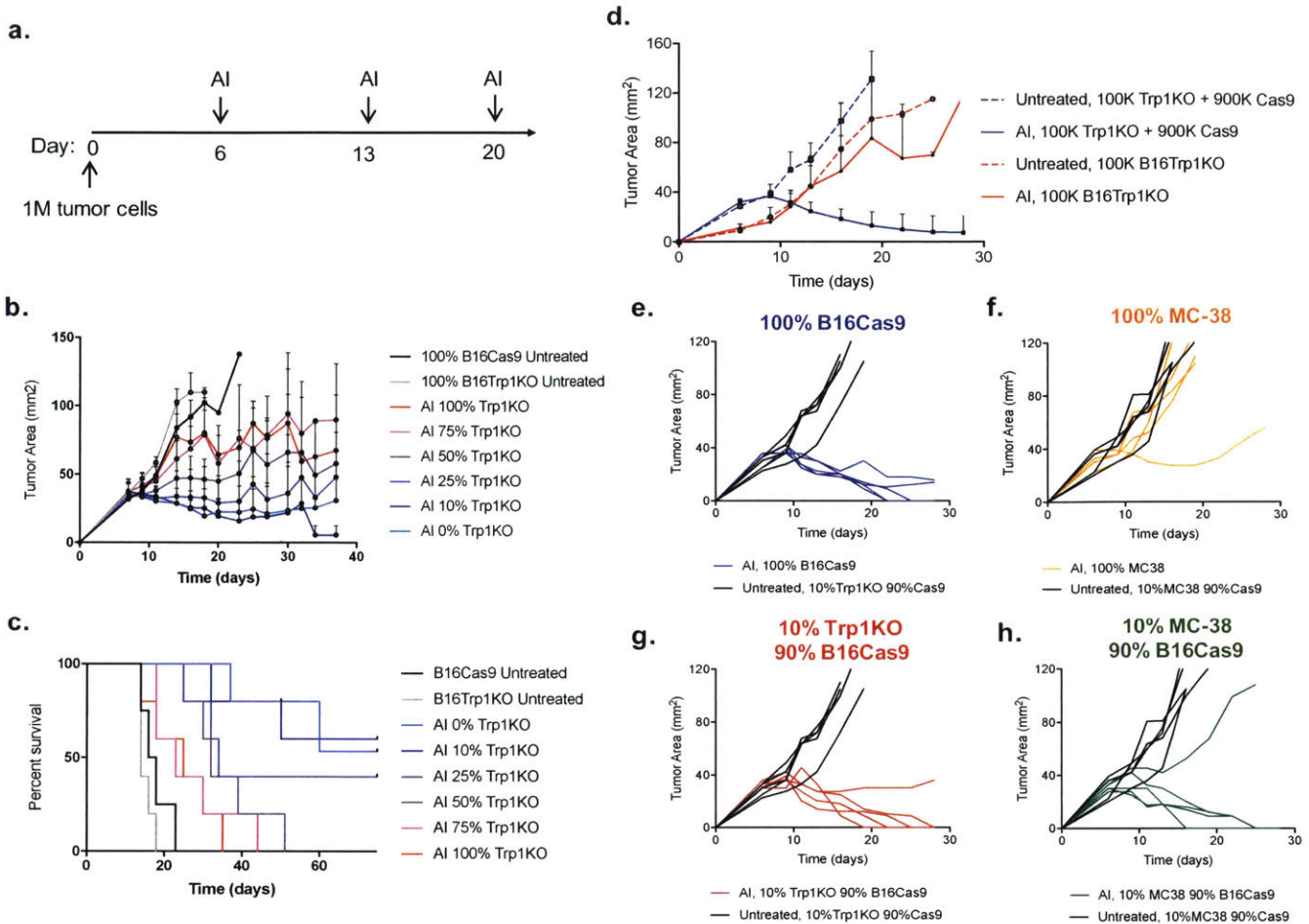


**Figure 36 AI in tumors that are antigenically heterogeneous for the antibody target: minority proportions of antigen deleted cells can be killed.** **a**, Treatment scheme for AI therapy in antigenically heterogeneous tumors. 8-week-old female C57BL6/J mice were injected with the indicated tumor compositions; shown are tumor growth curves, **b**, and survival plots, **c**, for the indicated tumors and treatments. **d**, 8-week-old female C57BL6/J mice were injected with the indicated tumor types with matching total number of Trp1KO cells, shown is tumor area over time. **e-h**, 8-week-old female C57BL6/J mice were injected with the indicated tumor types, shown is tumor area over time. Note that all Trp1KO tumor lines used in this figure are Trp1KOF4. Mice were euthanized when tumor sizes exceeded 100mm<sup>2</sup> area.

B16Trp1KOF4 cells were being eliminated due to immune-mediated tumor destruction of the nearby B16Cas9 cells, and not simply due to their low numbers, a study was performed in which the total *number* of B16Trp1KOF4 cells inoculated was the same. Mice treated with AI that received an initial inoculum of 100,000 B16Trp1KOF4 were still resistant to treatment with AI and progressively grew out, indicating that the initial number of B16Trp1KOF4 cells was not the primary decider of therapeutic outcome, and that elimination of these cells in the 10% B16Trp1KOF4 case relied on the presence of Trp1-expressing B16Cas9 cells (Figure 36d).



To explore whether the eliminated minority of cells in mosaic tumors that did not express Trp1 required shared antigens with the antigen-expressing population (B16Cas9), a study was performed in which the antigen-negative population was composed of a completely different cell type, the cell line MC-38, which should not express Trp1 as it is derived from the colon. Consistent with previous experiments, B16Cas9 cells were susceptible to AI, and as expected, the Trp1-negative MC-38 cells were resistant to AI therapy (Figure 36e-f). The 10% B16Trp1KOF4/90% B16Cas9 mosaic tumors were again susceptible to AI, and interestingly, the 10% MC-38/90% B16Cas9 mosaic tumors responded in an indistinguishable fashion compared to the 10% B16Trp1KOF4 mosaics (Figure 36g-h), indicating that shared antigens are not necessary for the elimination of antigen-negative cells with AI therapy.

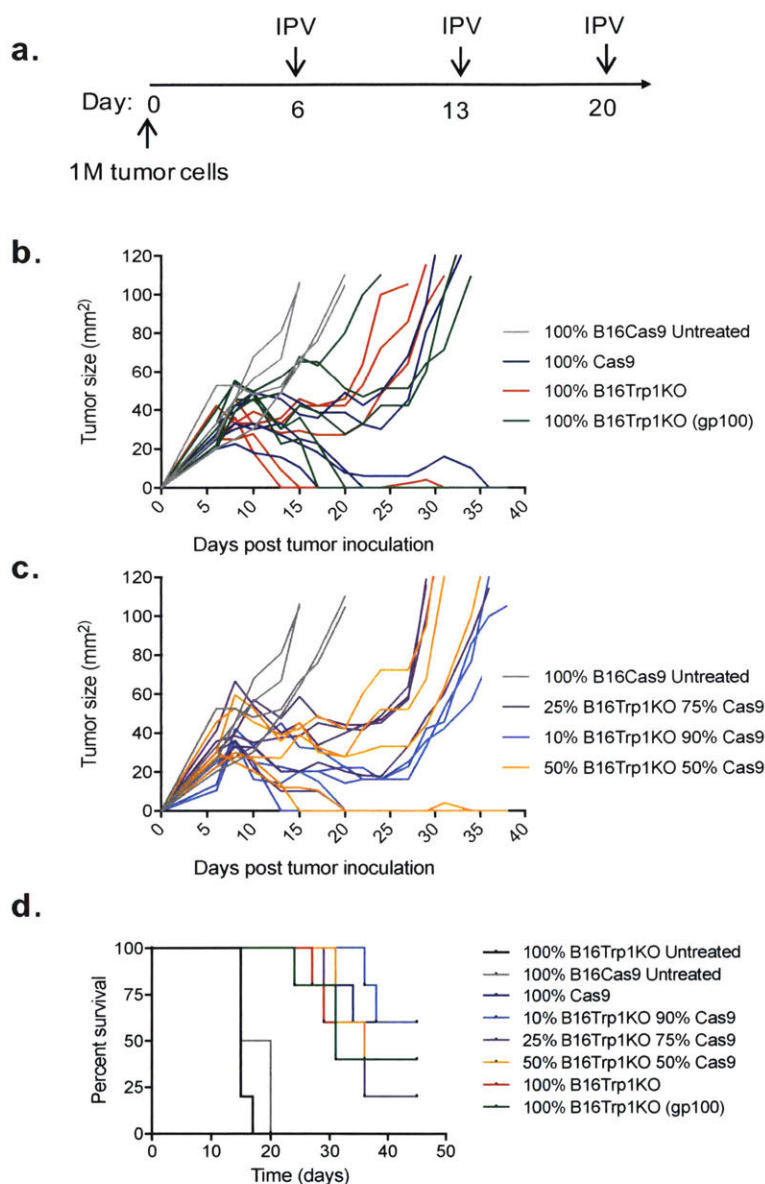


**Figure 37 MSA-IL2 and anti-PD-1 dominate therapeutic response in IPV-treated antigenically heterogeneous tumors.** a-d, 8-week-old female C57BL6/J mice were treated with IPV with vaccine against Trp1 (adjuvanted with 25 $\mu$ g c-di-GMP) as shown in a; shown are tumor growth curves, b-c, and survival plots, d, for the indicated tumor compositions. Note that all Trp1KO tumor lines used in this figure are B16 Trp1KOF4. Mice were sacrificed when tumor sizes exceeded 100mm<sup>2</sup>.

The majority of work dissecting antigenic heterogeneity with T cell epitopes has taken place in the context of adoptive transfer of large numbers of CD4<sup>+</sup> or CD8<sup>+</sup> T cells. It would be useful to have a therapeutic setting in which an endogenous T cell response against tumor antigens could be explored. Although vaccination against Trp1 alone was only moderately effective

against B16Cas9 tumors (Figure 35e-h), the anti-tumor effects may be amplified with the addition of other immunomodulators like checkpoint blockade or cytokine therapy. To that end, IPV therapy with vaccine against Trp1 (or gp100 as a control) was carried out in mosaic tumors composed of 0%, 10%, 25%, 50%, or 100% B16Trp1KOF4, with the remainder of the tumor composed of antigen-expressing B16Cas9 cells (Figure 37a-d). There was significant anti-tumor activity seen in all treated groups compared to untreated controls, but the efficacy was similar, regardless of what fraction of the tumor was composed of the B16Trp1KOF4 cells or whether the vaccine antigen targeted Trp1 or gp100 (Figure 37b-d). This indicates that the dominant factors in determining therapeutic efficacy in this treatment setting were antigen independent, namely, the MSA-IL2, anti-PD-1, and possibly the vaccine adjuvant (c-di-GMP).

### **5.3 Discussion and Future Work**

This chapter includes preliminary data relating to exploration of antigenically heterogeneous tumors in immunotherapy. It is my hope that future experiments along this line of inquiry will be conducted to dissect the mechanisms of elimination of antigen-negative cells in the context of antibody-based immunotherapy.

Minorities of cells knocked out for Trp1 could be eliminated with an immunotherapy regimen using an antibody targeting Trp1, and this elimination depended on the presence of antigen-expressing cells (Figure 36d). The kinetics of elimination of the mosaic tumors suggest that an antigen-specific CD8<sup>+</sup> T cell response primed by AI therapy may not be the primary driver of therapeutic efficacy in elimination. Tumors expressing Trp1 show regression beginning just 2-3 days after therapy with AI (Figure 35b), which is likely to be driven primarily by innate immune effectors. The kinetics of regression with AI in the 10% B16Trp1KOF4 mosaic tumors match the B16Cas9 line, indicating that the bystander killing observed of antigen-negative cells may not be CD8<sup>+</sup> T cell driven, though more definitive evidence is needed to draw firm conclusions. In line with this hypothesis, the 10% MC-38 tumor mosaics were eliminated in a fashion similar to the 10% Trp1KOF4, and MC-38 is not known to share immunogenic antigens with B16F10 (other than the endogenous retroviral product p15e). Therapy with AI has been previously shown to depend on FcγR-expressing innate effectors like neutrophils and NK cells.<sup>9</sup> It may be possible that elimination of the antigen-negative population was achieved by bystander killing mediated by these FcγR-expressing effectors.

Unfortunately, a clear setting in which the endogenous T cell response to a heterogeneously-expressed tumor antigen could be explored was not found. In the setting of early treatment with vaccine alone (Figure 35e-h) the Trp1 vaccine extended life over untreated mice by only a little over a week, which would complicate interpretation of mosaic tumors and necessitate extremely high  $n$  to draw conclusions about differences in therapeutic outcome. Additionally, when combined with MSA-IL2 and anti-PD-1, these two proteins dominated the therapeutic response, with 40-60% of mice achieving a complete response regardless of the antigen targeted by the vaccine. Future experiments can be conducted to find the correct experimental setting where larger differences in therapeutic efficacy can be seen between the antigen-expressing and antigen-deleted tumors when treated with a vaccine targeting that antigen (with or without other immunomodulators), after which time mosaic tumors can be explored.

A number of potentially fruitful avenues of investigation remain for investigating antigenic heterogeneity in the setting of AI therapy in which the antibody target is expressed heterogeneously. Namely, there is preliminary data to suggest that elimination of antigen-negative cells does not depend on antigen specific T cell responses, but previous studies have shown that AI therapy relies on CD8<sup>+</sup> T cells<sup>9</sup>, though it is not clear if antigen-specificity is required. Thus, it would be useful to conduct mosaic studies with 10% minority populations of antigen-negative cells in mice where antigen spreading is prevented (for example, in OT-I mice, or Batf3<sup>-/-</sup> mice), and to quantify the antigen-specific T cell responses in wild type mice in the different tumor settings, for example via ELISPOT. Additionally, treating a B16Trp1KOF4 line that expresses a distinct fluorophore from the B16Cas9 line would be useful for tracking how the populations of antigen-expressing and antigen-deleted cells change in proportion throughout therapy and for imaging studies.

In future studies, care should be taken to distinguish between effects a cell type has on AI therapy as a whole and its effect in elimination of the antigen-negative population. For example, depletion of NK cells would be expected to harm therapy to the parental B16Cas9 line, as NK cell depletion has been shown to harm AI therapy in B16F10<sup>9</sup>. In wild type mice, therapeutic efficacy is the same between 100% B16Cas9 tumors and mosaics composed of 10% B16Trp1KOF4; interesting cell types would be indicated by a change outcome between these two tumor compositions rather than the un-depleted control within the same tumor composition. Taking the NK cell example, the relevant comparison would be between NK-depleted therapy in 100% B16Cas9 tumors versus NK-depleted therapy in 10% B16Trp1KOF4 tumors/90% B16Cas9, rather than between NK-depleted and undepleted in mosaic tumors.

Mechanistically dissecting how antigen-deleted minority populations can be killed may inform the design of future immunotherapies that could better treat antigenically heterogeneous tumors.

## **5.4 Methods**

### **B16Trp1KOF4 generation**

The B16Trp1KO cells were generated as described in Chapter 4 using lenti-Cas9-GFP followed by transfection with guides targeting Trp1. *In vivo* passaging was performed by injecting 4-5 flank tumors and selecting the largest tumor after 2 weeks of growth, isolating it, and plating it as a single cell suspension. Media was changed every day for 1 week, followed by 3 passages to ensure that non-transformed cells did not survive. This process was repeated and the number of tumors that grew out and the speed of growth were measured until they matched the parental B16Cas9 tumor line.

### **Reagents and flow cytometry**

Reagents and flow cytometry methods are as described in Chapter 4.

### **ELISPOT**

Mice were primed and boosted with amph-vaccine as described in Chapter 2 (with 25 µg c-di-GMP as adjuvant) against Trp2 or Trp1. The tumor cells indicated were irradiated with 100Gy, harvested, counted, and plated at 25,000 cells per well into a 96-well plate: Mouse IFN-γ ELISPOT Kit (BD). No mIFN-γ pre-treatment was used in this experiment (though it is recommended by the author for future experiments). Splenocytes from immunized mice were isolated and subjected to ACK lysis and seeded at 10<sup>6</sup> cells per well on top of the tumor cells. Plates were wrapped in foil and cultured for 24 hours then developed according to manufacturer's protocol. Plates were scanned using a CTL-ImmunoSpot Plate Reader and data was analyzed using CTL ImmunoSpot Software.



## **Tumor studies**

Tumor studies were carried out in 8-week old female C57BL6/J mice from Jackson Laboratories. All other methods are as described in Chapter 4.

## CHAPTER 6: Conclusions and Outlook

Although each chapter of this thesis has conclusions related to the specific content covered, it is worth presenting a brief general conclusion at a higher level to address some remaining challenges in the field. In this thesis, we have contributed data on two main topics to the expanding repertoire of literature on tumor immunotherapy. The first is improving the magnitude of CD8<sup>+</sup> T cell responses to vaccination using relatively simple covalent modifications, either by improving trafficking and stability with attachment of albumin-binding domains, or presentation on MHC class I with inclusion of cell penetrating peptides. The second area is on combination immunotherapy, with the description of an extremely powerful, 4-component combination immunotherapy that recruits both innate and adaptive immunity. We hope that future studies will build upon these two areas of work to further uncover mechanisms of action that may allow for the design of even more effective immunotherapy approaches.

So, one might ask, where is immunotherapy headed? Here, we offer some brief speculation on what areas of research may be particularly fruitful for improving immunotherapy treatment. This section is not exhaustive—there are many other areas of research that will almost certainly bear fruit clinically, but that are outside the scope of this thesis. For example, further refinement of the bioinformatics pipelines to predict neoantigens<sup>280</sup>, modulation of immuno-metabolism<sup>281</sup>, manipulation of the microbiome<sup>282,283</sup>, and novel screens<sup>284-286</sup> to identify new targets on T cells, other immune cells, or malignant cells are all promising avenues of research that are beyond the scope of this thesis.

One important unmet need is addressing resistance to checkpoint blockade. Checkpoint blockade against PD-1 and CTLA-4 is yielding tremendous benefit clinically, but there are patients who are resistant to therapy (exhibiting primary resistance) and patients who initially respond and then relapse and progress (exhibiting acquired resistance)<sup>149</sup>. Uncovering primary resistance to checkpoint has been the goal of many studies where responders have been compared to non-responders, summarized well in a recent review<sup>287</sup>. Approaches to address primary resistance will likely depend on the specific mechanisms of resistance (and identification of these resistance mechanisms may need to be analyzed on a patient-by-patient basis), but approaches to increase immunogenicity of the tumor cells, recruit immune effectors to the tumor, or re-polarize the tumor microenvironment may help in promoting the transition of these so-called “cold” tumors to inflamed tumors, which are more likely to benefit from checkpoint blockade<sup>7</sup>.

Acquired mechanisms of resistance to checkpoint blockade may be addressed by using complementary combination immunotherapy approaches, which have frequently been cited as the future of immunotherapy<sup>7,17,29,287,288</sup>. Many current combination immunotherapy approaches are focused on further pushing forward T cell activity against tumors, for example, by combining anti-PD-1 and other T cell checkpoint inhibitors or cytokines. However, while combination therapies centered around T cells can yield additional benefit clinically over monotherapy (for example, ipilimumab plus pembrolizumab<sup>3</sup>), the mechanisms of acquired resistance to checkpoint blockade therapy suggest that priming more or better T cells may not be the ultimate solution. For example, in a recent study, a handful of patients who initially showed a response to PD-1 treatment followed by a relapse had their pre-treatment and post-relapse tumors analyzed for mutations<sup>289</sup>. Many of the mutations found were in pathways that make the tumor cells either invisible or non-responsive to T cell pressure, including frameshift mutations in beta-2-microglobulin and loss-of-function mutations in IFN- $\gamma$ R pathway genes (JAK1 and JAK2)<sup>289</sup>. In these patients, whose tumors have lost MHC class I expression or sensitivity to IFN- $\gamma$ , providing more numerous or more activated CD8<sup>+</sup> T cells is unlikely to help. Instead, perhaps inclusion of immunomodulators that are capable of recruiting innate effectors (for example, anti-tumor mAbs to recruit Fc $\gamma$ R-expressing innate effectors) would be more beneficial. Another avenue to consider is blocking of checkpoints against other cell types, for example, the non-canonical class I molecule HLA-G, which is expressed by many tumors to suppress NK cell function<sup>290</sup>. Indeed HLA-G blockade may be particularly well suited for combination with checkpoint blockade: cells that lose class I expression in order to evade T cell pressure must also evade NK cell mediated killing (which should normally occur via 'missing self' when MHC class I is lost<sup>291</sup>), however, tumors can express HLA-G to evade this mechanism of killing<sup>292</sup>. Thus, blockade of HLA-G would directly address one mechanism of resistance to checkpoint blockade by re-sensitizing tumor cells that have lost class I expression to NK-cell mediated killing. There are likely many other molecules that could work in a similarly complementary fashion to rationally address known resistance mechanisms to checkpoint blockade, and future studies identifying resistance mechanisms are likely to yield promising new therapeutic targets.

Another important unmet need is decoupling efficacy from toxicity. The first large-scale clinical trial combining ipilimumab and pembrolizumab yielded very impressive survival data in melanoma patients, but this combination treatment also induced a significantly higher frequency of grade 3 or 4 adverse events compared to either drug individually<sup>3</sup>. In CAR-T therapy, activation and expansion of the transferred T cells is desired for clinical efficacy, but this activation correlates with cytokine release syndrome, which can be life threatening for

patients<sup>293</sup>. Additionally, it has been shown that the patients who develop colitis in response to CTLA-4 blockade are significantly more likely to show tumor regression<sup>294</sup>. Are efficacy and toxicity inextricably linked? There is evidence that this is not necessarily the case. For example, in a small TIL trial from the Rosenberg lab, transfer of 100 billion neoantigen-specific T cells induced regression in a metastatic colorectal cancer patient in the absence of adverse effects<sup>295</sup>; studies like this have led Rosenberg and colleagues to hypothesize that targeting neoantigens may be the “Final common pathway” of human cancer immunotherapy (not only for safety reasons but also efficacy)<sup>296</sup>, and indeed targeting specifically neoantigens makes intuitive sense for avoiding systemic toxicity. Mitigation of toxicity may also be achievable by modulating the timing of administration of individual immunotherapies (Rothschilds et al., unpublished), sequestering immunomodulators at the tumor site<sup>106</sup>, engineering CAR-Ts using synthetic biology approaches<sup>297</sup>, or engineering synthetic cytokines (‘synthekines’) with more desirable signaling programs<sup>46</sup>, for example. Moving forward, uncovering what the drivers of toxicity are may yield mechanistic insights into how to decouple it from efficacy so that more patients may receive therapeutic benefit without inflammatory toxicities.

In summary, immuno-oncology is truly a renaissance, and therapeutic outcomes for patients will continue to improve as we as a field gain more knowledge and draw upon this information to design more effective and safer next-generation immunotherapies.

## REFERENCES

- 1 Hodi, F. S. *et al.* Improved Survival with Ipilimumab in Patients with Metastatic Melanoma. *New England Journal of Medicine* **363**, 711-723, doi:doi:10.1056/NEJMoa1003466 (2010).
- 2 Topalian, S. L. *et al.* Safety, Activity, and Immune Correlates of Anti-PD-1 Antibody in Cancer. *New England Journal of Medicine* **366**, 2443-2454, doi:doi:10.1056/NEJMoa1200690 (2012).
- 3 Larkin, J. *et al.* Combined Nivolumab and Ipilimumab or Monotherapy in Untreated Melanoma. *N Engl J Med* **373**, 23-34, doi:10.1056/NEJMoa1504030 (2015).
- 4 Mellman, I., Coukos, G. & Dranoff, G. Cancer immunotherapy comes of age. *Nature* **480**, 480-489, doi:10.1038/nature10673 (2011).
- 5 Drake, C. G. Combination immunotherapy approaches. *Annals of Oncology* **23**, viii41-viii46, doi:10.1093/annonc/mds262 (2012).
- 6 Gajewski, T. F. The Next Hurdle in Cancer Immunotherapy: Overcoming the Non-T-Cell-Inflamed Tumor Microenvironment. *Semin Oncol* **42**, 663-671, doi:10.1053/j.seminoncol.2015.05.011 (2015).
- 7 Sharma, P. & Allison, J. P. The future of immune checkpoint therapy. *Science* **348**, 56-61, doi:10.1126/science.aaa8172 (2015).
- 8 Smyth, M. J., Ngiow, S. F., Ribas, A. & Teng, M. W. L. Combination cancer immunotherapies tailored to the tumour microenvironment. *Nat Rev Clin Oncol* **advance online publication**, doi:10.1038/nrclinonc.2015.209 (2015).
- 9 Zhu, E. F. *et al.* Synergistic innate and adaptive immune response to combination immunotherapy with anti-tumor antigen antibodies and extended serum half-life IL-2. *Cancer Cell* **27**, 489-501, doi:10.1016/j.ccell.2015.03.004 (2015).
- 10 Liu, H. *et al.* Structure-based programming of lymph-node targeting in molecular vaccines. *Nature* **507**, 519-522, doi:10.1038/nature12978 (2014).
- 11 Park, A. What If Your Immune System Could Be Taught to Kill Cancer? *Time Magazine* (2016).
- 12 Grady, D. Harnessing the Immune System to Fight Cancer. *The New York Times*, Page A1 (2017).
- 13 Weintraub, A. Jimmy Carter, Melanoma And The Promise Of Immunotherapy In The Elderly. *Forbes*.
- 14 Coley, W. B. The treatment of malignant tumours by repeated inoculations of erysipelas: with a report of ten original cases. . *Am. J. Med. Sci.* **105**, 487-511 (1893).
- 15 Rosenberg, S. A. IL-2: The First Effective Immunotherapy for Human Cancer. *The Journal of Immunology* **192**, 5451 (2014).
- 16 Leach, D. R., Krummel, M. F. & Allison, J. P. Enhancement of Antitumor Immunity by CTLA-4 Blockade. *Science* **271**, 1734 (1996).
- 17 Hoos, A. Development of immuno-oncology drugs -- from CTLA4 to PD1 to the next generations. *Nat Rev Drug Discov* **15**, 235-247, doi:10.1038/nrd.2015.35 (2016).
- 18 Adam Feuerstein, D. G. Novartis CAR-T cancer therapy wins expert support for FDA approval. *STAT*
- 19 Ribas, A. *et al.* New Challenges in Endpoints for Drug Development in Advanced Melanoma. *Clinical Cancer Research* **18**, 336 (2012).
- 20 M, K. D. & Le Gros, G. The role of CTLA-4 in the regulation of T cell immune responses. *Immunol Cell Biol* **77**, 1-10 (1999).
- 21 Simpson, T. R. *et al.* Fc-dependent depletion of tumor-infiltrating regulatory T cells co-defines the efficacy of anti-CTLA-4 therapy against melanoma. *The Journal of Experimental Medicine* **210**, 1695 (2013).
- 22 Selby, M. J. *et al.* Anti-CTLA-4 Antibodies of IgG2a Isotype Enhance Antitumor Activity through Reduction of Intratumoral Regulatory T Cells. *Cancer Immunology Research* **1**, 32 (2013).
- 23 Bulliard, Y. *et al.* Activating Fc  $\gamma$  receptors contribute to the antitumor activities of immunoregulatory receptor-targeting antibodies. *The Journal of Experimental Medicine* **210**, 1685 (2013).
- 24 Schadendorf, D. *et al.* Pooled Analysis of Long-Term Survival Data From Phase II and Phase III Trials of Ipilimumab in Unresectable or Metastatic Melanoma. *Journal of Clinical Oncology* **33**, 1889-1894, doi:10.1200/JCO.2014.56.2736 (2015).

- 25 Grosso, J. *et al.* Association of tumor PD-L1 expression and immune biomarkers with clinical activity in patients (pts) with advanced solid tumors treated with nivolumab (anti-PD-1; BMS-936558; ONO-4538). *Journal of Clinical Oncology* **31**, 3016-3016, doi:10.1200/jco.2013.31.15\_suppl.3016 (2013).
- 26 Anderson, Ana C., Joller, N. & Kuchroo, Vijay K. Lag-3, Tim-3, and TIGIT: Co-inhibitory Receptors with Specialized Functions in Immune Regulation. *Immunity* **44**, 989-1004, doi:http://dx.doi.org/10.1016/j.immuni.2016.05.001 (2016).
- 27 Chen, L. & Flies, D. B. Molecular mechanisms of T cell co-stimulation and co-inhibition. *Nature reviews. Immunology* **13**, 227-242, doi:10.1038/nri3405 (2013).
- 28 Suntharalingam, G. *et al.* Cytokine Storm in a Phase 1 Trial of the Anti-CD28 Monoclonal Antibody TGN1412. *New England Journal of Medicine* **355**, 1018-1028, doi:10.1056/NEJMoa063842 (2006).
- 29 Khalil, D. N., Smith, E. L., Brentjens, R. J. & Wolchok, J. D. The future of cancer treatment: immunomodulation, CARs and combination immunotherapy. *Nat Rev Clin Oncol* **13**, 273-290, doi:10.1038/nrclinonc.2016.25 (2016).
- 30 Sznol, M. *et al.* Phase I study of BMS-663513, a fully human anti-CD137 agonist monoclonal antibody, in patients (pts) with advanced cancer (CA). *Journal of Clinical Oncology* **26**, 3007-3007, doi:10.1200/jco.2008.26.15\_suppl.3007 (2008).
- 31 Garber, K. Beyond Ipilimumab: New Approaches Target the Immunological Synapse. *JNCI: Journal of the National Cancer Institute* **103**, 1079-1082, doi:10.1093/jnci/djr281 (2011).
- 32 Baruch, E. N., Berg, A. L., Besser, M. J., Schachter, J. & Markel, G. Adoptive T cell therapy: An overview of obstacles and opportunities. *Cancer* **123**, 2154-2162, doi:10.1002/cncr.30491 (2017).
- 33 Yang, Y., Jacoby, E. & Fry, T. J. Challenges and Opportunities of Allogeneic Donor-Derived CAR T cells. *Current opinion in hematology* **22**, 509-515, doi:10.1097/MOH.000000000000181 (2015).
- 34 Kingwell, K. CAR T therapies drive into new terrain. *Nat Rev Drug Discov* **16**, 301-304, doi:10.1038/nrd.2017.84 (2017).
- 35 Rosenberg, S. A., Yang, J. C. & Restifo, N. P. Cancer immunotherapy: moving beyond current vaccines. *Nat Med* **10**, 909-915, doi:10.1038/nm1100 (2004).
- 36 Melero, I. *et al.* Therapeutic vaccines for cancer: an overview of clinical trials. *Nat Rev Clin Oncol* **11**, 509-524, doi:10.1038/nrclinonc.2014.111 (2014).
- 37 Sahin, U. *et al.* Personalized RNA mutanome vaccines mobilize poly-specific therapeutic immunity against cancer. *Nature advance online publication*, doi:10.1038/nature23003 <http://www.nature.com/nature/journal/vaop/ncurrent/abs/nature23003.html#supplementary-information> (2017).
- 38 Ott, P. A. *et al.* An immunogenic personal neoantigen vaccine for patients with melanoma. *Nature advance online publication*, doi:10.1038/nature22991 <http://www.nature.com/nature/journal/vaop/ncurrent/abs/nature22991.html#supplementary-information> (2017).
- 39 Dranoff, G. Cytokines in cancer pathogenesis and cancer therapy. *Nat Rev Cancer* **4**, 11-22 (2004).
- 40 Ilson, D. H. *et al.* A phase II trial of interleukin-2 and interferon alfa-2a in patients with advanced renal cell carcinoma. *Journal of Clinical Oncology* **10**, 1124-1130, doi:10.1200/JCO.1992.10.7.1124 (1992).
- 41 Leukemia, T. I. C. S. G. o. C. M. Interferon Alfa-2a as Compared with Conventional Chemotherapy for the Treatment of Chronic Myeloid Leukemia. *New England Journal of Medicine* **330**, 820-825, doi:10.1056/NEJM199403243301204 (1994).
- 42 Rubinstein, M. P. *et al.* Converting IL-15 to a superagonist by binding to soluble IL-15R $\alpha$ . *Proceedings of the National Academy of Sciences* **103**, 9166-9171, doi:10.1073/pnas.0600240103 (2006).
- 43 Guo, Y. *et al.* IL-15 Superagonist-Mediated Immunotoxicity: Role of NK Cells and IFN- $\gamma$ . *The Journal of Immunology* **195**, 2353 (2015).
- 44 Charych, D. H. *et al.* NKTR-214, an Engineered Cytokine with Biased IL2 Receptor Binding, Increased Tumor Exposure, and Marked Efficacy in Mouse Tumor Models. *Clinical Cancer Research* **22**, 680 (2016).



- 45 Levin, A. M. *et al.* Exploiting a natural conformational switch to engineer an interleukin-2  
/ 'superkine/'. *Nature* **484**, 529-533,  
doi:http://www.nature.com/nature/journal/v484/n7395/abs/nature10975.html#supplementary-  
information (2012).
- 46 Moraga, I. *et al.* Synthekines are surrogate cytokine and growth factor agonists that compel  
signaling through non-natural receptor dimers. *eLife* **6**, e22882, doi:10.7554/eLife.22882 (2017).
- 47 Weiner, L. M., Surana, R. & Wang, S. Monoclonal antibodies: versatile platforms for cancer  
immunotherapy. *Nat Rev Immunol* **10**, 317-327, doi:10.1038/nri2744 (2010).
- 48 Radford, K. J., Tullett, K. M. & Lahoud, M. H. Dendritic cells and cancer immunotherapy. *Current  
Opinion in Immunology* **27**, 26-32, doi:http://doi.org/10.1016/j.coi.2014.01.005 (2014).
- 49 Palucka, K. & Banchereau, J. Cancer immunotherapy via dendritic cells. *Nat Rev Cancer* **12**, 265-  
277 (2012).
- 50 Singh, M. & Overwijk, W. W. Intratumoral immunotherapy for melanoma. *Cancer Immunology,  
Immunotherapy* **64**, 911-921, doi:10.1007/s00262-015-1727-z (2015).
- 51 Aznar, M. A. *et al.* Intratumoral Delivery of Immunotherapy—Act Locally, Think Globally. *The  
Journal of Immunology* **198**, 31 (2016).
- 52 Ghiringhelli, F. *et al.* Metronomic cyclophosphamide regimen selectively depletes CD4+CD25+  
regulatory T cells and restores T and NK effector functions in end stage cancer patients. *Cancer  
Immunol Immunother* **56**, 641-648, doi:10.1007/s00262-006-0225-8 (2007).
- 53 Vacchelli, E. *et al.* Trial watch: IDO inhibitors in cancer therapy. *Oncoimmunology* **3**, doi:ARTN  
e957994  
DOI 10.4161/21624011.2014.957994 (2014).
- 54 Vanneman, M. & Dranoff, G. Combining immunotherapy and targeted therapies in cancer  
treatment. *Nat Rev Cancer* **12**, 237-251, doi:10.1038/nrc3237 (2012).
- 55 Fritsch, E. F., Hacohen, N. & Wu, C. J. Personal neoantigen cancer vaccines: The momentum  
builds. *Oncoimmunology* **3**, e29311, doi:10.4161/onci.29311 (2014).
- 56 Gubin, M. M. *et al.* Checkpoint blockade cancer immunotherapy targets tumour-specific mutant  
antigens. *Nature* **515**, 577-581, doi:10.1038/nature13988 (2014).
- 57 Yadav, M. *et al.* Predicting immunogenic tumour mutations by combining mass spectrometry and  
exome sequencing. *Nature* **515**, 572-576, doi:10.1038/nature14001 (2014).
- 58 Barnes, E. *et al.* Novel adenovirus-based vaccines induce broad and sustained T cell responses  
to HCV in man. *Sci Transl Med* **4**, 115ra111, doi:10.1126/scitranslmed.3003155 (2012).
- 59 Miller, J. D. *et al.* Human effector and memory CD8+ T cell responses to smallpox and yellow  
fever vaccines. *Immunity* **28**, 710-722, doi:10.1016/j.immuni.2008.02.020 (2008).
- 60 Speiser, D. E. *et al.* Rapid and strong human CD8+ T cell responses to vaccination with peptide,  
IFA, and CpG oligodeoxynucleotide 7909. *J Clin Invest* **115**, 739-746, doi:10.1172/JCI23373  
(2005).
- 61 Rosenberg, S. A. *et al.* Tumor progression can occur despite the induction of very high levels of  
self/tumor antigen-specific CD8+ T cells in patients with melanoma. *J Immunol* **175**, 6169-6176  
(2005).
- 62 Walter, S. *et al.* Multi-peptide immune response to cancer vaccine IMA901 after single-dose  
cyclophosphamide associates with longer patient survival. *Nature Medicine*, doi:10.1038/nm.2883  
(2012).
- 63 Odunsi, K. *et al.* Efficacy of vaccination with recombinant vaccinia and fowlpox vectors  
expressing NY-ESO-1 antigen in ovarian cancer and melanoma patients. *Proceedings of the  
National Academy of Sciences*, doi:10.1073/pnas.1117208109 (2012).
- 64 Schwartzenuber, D. J. *et al.* gp100 peptide vaccine and interleukin-2 in patients with advanced  
melanoma. *The New England journal of medicine* **364**, 2119-2127, doi:10.1056/NEJMoa1012863  
(2011).
- 65 Melief, C. J. M. & van der Burg, S. H. Immunotherapy of established (pre)malignant disease by  
synthetic long peptide vaccines. *Nature reviews Cancer* **8**, 351-360, doi:10.1038/nrc2373 (2008).
- 66 Sandoval, F. *et al.* Mucosal imprinting of vaccine-induced CD8(+) T cells is crucial to inhibit the  
growth of mucosal tumors. *Sci Transl Med* **5**, 172ra120, doi:10.1126/scitranslmed.3004888  
(2013).

- 67 Itano, A. A. *et al.* Distinct Dendritic Cell Populations Sequentially Present Antigen to CD4 T Cells and Stimulate Different Aspects of Cell-Mediated Immunity. *Immunity* **19**, 47-57, doi:10.1016/s1074-7613(03)00175-4 (2003).
- 68 Anandasabapathy, N. *et al.* Classical Flt3L-dependent dendritic cells control immunity to protein vaccine. *Journal of Experimental Medicine* **211**, 1875-1891, doi:10.1084/jem.20131397 (2014).
- 69 Johansen, P. *et al.* Direct intralymphatic injection of peptide vaccines enhances immunogenicity. *Eur J Immunol* **35**, 568-574, doi:10.1002/eji.200425599 (2005).
- 70 Maloy, K. J. *et al.* Intralymphatic immunization enhances DNA vaccination. *Proc Natl Acad Sci U S A* **98**, 3299-3303, doi:10.1073/pnas.051630798 (2001).
- 71 Bachmann, M. F. & Jennings, G. T. Vaccine delivery: a matter of size, geometry, kinetics and molecular patterns. *Nature Reviews Immunology* **10**, 787-796, doi:10.1038/nri2868 (2010).
- 72 Supersaxo, A., Hein, W. R. & Steffen, H. Effect of Molecular Weight on the Lymphatic Absorption of Water-Soluble Compounds Following Subcutaneous Administration. *Pharm Res* **7**, 167-169, doi:10.1023/A:1015880819328 (1990).
- 73 McLennan, D. N., Porter, C. J. H. & Charman, S. A. Subcutaneous drug delivery and the role of the lymphatics. *Drug Discovery Today: Technologies* **2**, 89-96, doi:10.1016/j.ddtec.2005.05.006 (2005).
- 74 Smirnov, D., Schmidt, J. J., Capecchi, J. T. & Wightman, P. D. Vaccine adjuvant activity of 3M-052: an imidazoquinoline designed for local activity without systemic cytokine induction. *Vaccine* **29**, 5434-5442, doi:10.1016/j.vaccine.2011.05.061 (2011).
- 75 Hanson, M. C. *et al.* Nanoparticulate STING agonists are potent lymph node-targeted vaccine adjuvants. *J. Clin. Invest.* (in press).
- 76 Hailemichael, Y. *et al.* Persistent antigen at vaccination sites induces tumor-specific CD8(+) T cell sequestration, dysfunction and deletion. *Nat Med* **19**, 465-472, doi:10.1038/nm.3105 (2013).
- 77 Reddy, S. T., Rehor, A., Schmoekel, H. G., Hubbell, J. A. & Swartz, M. A. In vivo targeting of dendritic cells in lymph nodes with poly(propylene sulfide) nanoparticles. *Journal of Controlled Release* **112**, 26-34, doi:10.1016/j.jconrel.2006.01.006 (2006).
- 78 Manolova, V. *et al.* Nanoparticles target distinct dendritic cell populations according to their size. *European Journal of Immunology* **38**, 1404-1413, doi:10.1002/eji.200737984 (2008).
- 79 Fifis, T. *et al.* Size-dependent immunogenicity: therapeutic and protective properties of nano-vaccines against tumors. *J Immunol* **173**, 3148-3154 (2004).
- 80 Moon, J. J. *et al.* Interbilayer-crosslinked multilamellar vesicles as synthetic vaccines for potent humoral and cellular immune responses. *Nat Mater* **10**, 243-251, doi:10.1038/nmat2960 (2011).
- 81 Kasturi, S. P. *et al.* Programming the magnitude and persistence of antibody responses with innate immunity. *Nature* **470**, 543-547, doi:10.1038/nature09737 (2011).
- 82 St John, A. L., Chan, C. Y., Staats, H. F., Leong, K. W. & Abraham, S. N. Synthetic mast-cell granules as adjuvants to promote and polarize immunity in lymph nodes. *Nature Materials*, doi:10.1038/nmat3222 (2012).
- 83 de Titta, A. *et al.* Nanoparticle conjugation of CpG enhances adjuvancy for cellular immunity and memory recall at low dose. *Proc Natl Acad Sci U S A* **110**, 19902-19907, doi:10.1073/pnas.1313152110 (2013).
- 84 Reddy, S. T. *et al.* Exploiting lymphatic transport and complement activation in nanoparticle vaccines. *Nature biotechnology* **25**, 1159-1164, doi:10.1038/nbt1332 (2007).
- 85 Thomas, S. N., Vokali, E., Lund, A. W., Hubbell, J. A. & Swartz, M. A. Targeting the tumor-draining lymph node with adjuvanted nanoparticles reshapes the anti-tumor immune response. *Biomaterials* **35**, 814-824, doi:10.1016/j.biomaterials.2013.10.003 (2014).
- 86 Fraser, C. C. *et al.* Generation of a universal CD4 memory T cell recall peptide effective in humans, mice and non-human primates. *Vaccine* **32**, 2896-2903, doi:10.1016/j.vaccine.2014.02.024 (2014).
- 87 Kourtis, I. C. *et al.* Peripherally administered nanoparticles target monocytic myeloid cells, secondary lymphoid organs and tumors in mice. *PloS one* **8**, e61646, doi:10.1371/journal.pone.0061646 (2013).
- 88 Shen, H. *et al.* Enhanced and prolonged cross-presentation following endosomal escape of exogenous antigens encapsulated in biodegradable nanoparticles. *Immunology* **117**, 78-88 (2006).

- 89 Krishnamachari, Y., Geary, S. M., Lemke, C. D. & Salem, A. K. Nanoparticle delivery systems in cancer vaccines. *Pharm Res* **28**, 215-236, doi:10.1007/s11095-010-0241-4 (2011).
- 90 Fang, R. H. *et al.* Cancer cell membrane-coated nanoparticles for anticancer vaccination and drug delivery. *Nano Lett* **14**, 2181-2188, doi:10.1021/nl500618u (2014).
- 91 von Andrian, U. H. & Mackay, C. R. T-Cell Function and Migration: Two Sides of the Same Coin. *The New England Journal of Medicine* **343**, 15 (2000).
- 92 Sandoval, F. *et al.* Mucosal imprinting of vaccine-induced CD8+ T cells is crucial to inhibit the growth of mucosal tumors. *Science translational medicine* **5**, 172ra120-172ra120 (2013).
- 93 Nochi, T. *et al.* Nanogel antigenic protein-delivery system for adjuvant-free intranasal vaccines. *Nat Mater* **9**, 572-578, doi:nmat2784 [pii] 10.1038/nmat2784 (2010).
- 94 Li, A. V. *et al.* Generation of effector memory T cell-based mucosal and systemic immunity with pulmonary nanoparticle vaccination. *Sci Transl Med* **5**, 204ra130, doi:10.1126/scitranslmed.3006516 (2013).
- 95 Li, A. V. *et al.* Generation of Effector Memory T Cell–Based Mucosal and Systemic Immunity with Pulmonary Nanoparticle Vaccination. *Science translational medicine* **5**, 204ra130-204ra130 (2013).
- 96 Matsuo, K. *et al.* Intranasal immunization with poly( $\gamma$ -glutamic acid) nanoparticles entrapping antigenic proteins can induce potent tumor immunity. *Journal of Controlled Release* **152**, 310-316, doi:10.1016/j.jconrel.2011.03.009 (2011).
- 97 Stano, A., Nembrini, C., Swartz, M. A., Hubbell, J. A. & Simeoni, E. Nanoparticle size influences the magnitude and quality of mucosal immune responses after intranasal immunization. *Vaccine*, doi:S0264-410X(12)01496-X [pii] 10.1016/j.vaccine.2012.10.050 (2012).
- 98 Nembrini, C. *et al.* Nanoparticle conjugation of antigen enhances cytotoxic T-cell responses in pulmonary vaccination. *Proceedings of the National Academy of Sciences* **108**, E989-E997, doi:10.1073/pnas.1104264108 (2011).
- 99 Zhu, Q. *et al.* Large intestine-targeted, nanoparticle-releasing oral vaccine to control genitoretal viral infection. *Nat Med* **18**, 1291-1296, doi:10.1038/nm.2866 (2012).
- 100 Morton, D. L. *et al.* BCG Immunotherapy of Malignant Melanoma: Summary of a Seven-year Experience. *Annals of Surgery* **180**, 635-641 (1974).
- 101 Marabelle, A. *et al.* Depleting tumor-specific Tregs at a single site eradicates disseminated tumors. *Journal of Clinical Investigation* **123**, 2447-2463, doi:10.1172/JCI64859 (2013).
- 102 Schulze, H. J. *et al.* Imiquimod 5% cream for the treatment of superficial basal cell carcinoma: results from a randomized vehicle-controlled phase III study in Europe. *British Journal of Dermatology* **152**, 939-947, doi:10.1111/j.1365-2133.2005.06486.x (2005).
- 103 Zamarin, D. *et al.* Localized Oncolytic Virotherapy Overcomes Systemic Tumor Resistance to Immune Checkpoint Blockade Immunotherapy. *Science Translational Medicine* **6**, 12 (2014).
- 104 Seung, S. K. *et al.* Phase 1 Study of Stereotactic Body Radiotherapy and Interleukin-2: Tumor and Immunological Responses. *Science Translational Medicine* **4**, 7 (2012).
- 105 Kwong, B., Gai, S. A., Elkhader, J., Wittrup, K. D. & Irvine, D. J. Localized immunotherapy via liposome-anchored Anti-CD137 + IL-2 prevents lethal toxicity and elicits local and systemic antitumor immunity. *Cancer Res* **73**, 1547-1558, doi:10.1158/0008-5472.CAN-12-3343 (2013).
- 106 Kwong, B., Liu, H. & Irvine, D. J. Induction of potent anti-tumor responses while eliminating systemic side effects via liposome-anchored combinatorial immunotherapy. *Biomaterials* **32**, 5134-5147, doi:10.1016/j.biomaterials.2011.03.067 (2011).
- 107 Egilmez, N. K. *et al.* In situ tumor vaccination with interleukin-12-encapsulated biodegradable microspheres: induction of tumor regression and potent antitumor immunity. *Cancer Res* **60**, 3832-3837 (2000).
- 108 Herpen, v., Huijbens, R., Looman, M. & de Vries, J. Pharmacokinetics and Immunological Aspects of a Phase Ib Study with Intratumoral Administration of Recombinant Human Interleukin-12 in Patients with .... *Clinical Cancer ...* (2003).
- 109 Hori, Y., Stern, P. J., Hynes, R. O. & Irvine, D. J. Engulfing tumors with synthetic extracellular matrices for cancer immunotherapy. *Biomaterials* **30**, 6757-6767, doi:10.1016/j.biomaterials.2009.08.037 (2009).

- 110 Pasquié, J.-I. *et al.* Sipuleucel-T Immunotherapy for Castration-Resistant Prostate Cancer. *New England Journal of Medicine*, 2373-2383, doi:10.1056/NEJMoa1407764 (2010).
- 111 Mitchell, D. A. *et al.* Tetanus toxoid and CCL3 improve dendritic cell vaccines in mice and glioblastoma patients. *Nature* **519**, 366-369, doi:10.1038/nature14320 (2015).
- 112 Palucka, K. & Banchereau, J. Dendritic-Cell-Based Therapeutic Cancer Vaccines. *Immunity* **39**, 38-48, doi:10.1016/j.immuni.2013.07.004 (2013).
- 113 Langer, R. & Vacanti, J. P. Tissue engineering. *Science* **260**, 920-926 (1993).
- 114 Kumamoto, T. *et al.* Induction of tumor-specific protective immunity by in situ Langerhans cell vaccine. *Nature biotechnology* **20**, 64-69, doi:10.1038/nbt0102-64 (2002).
- 115 Ali, O. a., Huebsch, N., Cao, L., Dranoff, G. & Mooney, D. J. Infection-mimicking materials to program dendritic cells in situ. *Nature materials* **8**, 151-158, doi:10.1038/nmat2357 (2009).
- 116 Ali, O. a., Emerich, D., Dranoff, G. & Mooney, D. J. In situ regulation of DC subsets and T cells mediates tumor regression in mice. *Science translational medicine* **1**, 8ra19-18ra19, doi:10.1126/scitranslmed.3000359 (2009).
- 117 Ali, O. A. *et al.* The efficacy of intracranial PLG-based vaccines is dependent on direct implantation into brain tissue. *Journal of Controlled Release* **154**, 249-257, doi:10.1016/j.jconrel.2011.06.021 (2011).
- 118 F. Stephen Hodi, M., Dana-Farber Cancer Institute. NCT01753089 (clinicaltrials.gov, 2014).
- 119 Chua, B. Y. *et al.* A single dose biodegradable vaccine depot that induces persistently high levels of antibody over a year. *Biomaterials* **53**, 50-57, doi:10.1016/j.biomaterials.2015.02.066 (2015).
- 120 Kim, J. *et al.* Injectable, spontaneously assembling, inorganic scaffolds modulate immune cells in vivo and increase vaccine efficacy. *Nature Biotechnology*, doi:10.1038/nbt.3071 (2014).
- 121 Chen, D. S. & Mellman, I. Oncology meets immunology: the cancer-immunity cycle. *Immunity* **39**, 1-10, doi:10.1016/j.immuni.2013.07.012 (2013).
- 122 Woo, S. R., Corrales, L. & Gajewski, T. F. Innate immune recognition of cancer. *Annu Rev Immunol* **33**, 445-474, doi:10.1146/annurev-immunol-032414-112043 (2015).
- 123 Engblom, C., Pfirschke, C. & Pittet, M. J. The role of myeloid cells in cancer therapies. *Nat Rev Cancer* **16**, 447-462, doi:10.1038/nrc.2016.54 (2016).
- 124 Singh, M. *et al.* Effective Innate and Adaptive Antimelanoma Immunity through Localized TLR7/8 Activation. *The Journal of Immunology* **193**, 4722-4731, doi:10.4049/jimmunol.1401160 (2014).
- 125 Reichman, H., Karo-Atar, D. & Munitz, A. Emerging Roles for Eosinophils in the Tumor Microenvironment. *Trends in Cancer* **2**, 664-675 (2016).
- 126 Siders, W. M. *et al.* Involvement of neutrophils and natural killer cells in the anti-tumor activity of alemtuzumab in xenograft tumor models. *Leukemia & Lymphoma* **51**, 1293-1304, doi:10.3109/10428191003777963 (2010).
- 127 Albanesi, M. *et al.* Neutrophils mediate antibody-induced antitumor effects in mice. *Blood* **122**, 3160-3164, doi:10.1182/blood-2013-04-497446 (2013).
- 128 Weiskopf, K. & Weissman, I. L. Macrophages are critical effectors of antibody therapies for cancer. *MAbs* **7**, 303-310, doi:10.1080/19420862.2015.1011450 (2015).
- 129 Golay, J. *et al.* Biologic response of B lymphoma cells to anti-CD20 monoclonal antibody rituximab in vitro: CD55 and CD59 regulate complement-mediated cell lysis. *Blood* **95**, 3900-3908 (2000).
- 130 Eruslanov, E. B. *et al.* Tumor-associated neutrophils stimulate T cell responses in early-stage human lung cancer. *J Clin Invest* **124**, 5466-5480, doi:10.1172/JCI77053 (2014).
- 131 Carretero, R. *et al.* Eosinophils orchestrate cancer rejection by normalizing tumor vessels and enhancing infiltration of CD8(+) T cells. *Nat Immunol* **16**, 609-617, doi:10.1038/ni.3159 (2015).
- 132 Srivastava, R. M. *et al.* Cetuximab-Activated Natural Killer and Dendritic Cells Collaborate to Trigger Tumor Antigen-Specific T-cell Immunity in Head and Neck Cancer Patients. *Clinical Cancer Research* **19**, 1858-1872, doi:10.1158/1078-0432.ccr-12-2426 (2013).
- 133 Bulliard, Y. *et al.* OX40 engagement depletes intratumoral Tregs via activating Fc[gamma]Rs, leading to antitumor efficacy. *Immunol Cell Biol* **92**, 475-480, doi:10.1038/icb.2014.26 (2014).
- 134 Klug, F. *et al.* Low-Dose Irradiation Programs Macrophage Differentiation to an iNOS<sup>+</sup>/M1 Phenotype that Orchestrates Effective T Cell Immunotherapy. *Cancer Cell* **24**, 589-602, doi:10.1016/j.ccr.2013.09.014 (2013).
- 135 Weiskopf, K. *et al.* Engineered SIRPalpha variants as immunotherapeutic adjuvants to anticancer antibodies. *Science* **341**, 88-91, doi:10.1126/science.1238856 (2013).

- 136 Carmi, Y. *et al.* Allogeneic IgG combined with dendritic cell stimuli induce antitumour T-cell immunity. *Nature*, 1-6, doi:10.1038/nature14424 (2015).
- 137 Müller, P. *et al.* Trastuzumab emtansine (T-DM1) renders HER2<sup>+</sup> breast cancer highly susceptible to CTLA-4/PD-1 blockade. *Science Translational Medicine* **7**, 315ra188 (2015).
- 138 Moore, E. C. *et al.* Established T-cell inflamed tumors rejected after adaptive resistance was reversed by combination STING activation and PD-1-pathway blockade. *Cancer Immunology Research* (2016).
- 139 Foote, J. B. *et al.* A STING Agonist Given with OX40 Receptor and PD-L1 Modulators Primes Immunity and Reduces Tumor Growth in Tolerized Mice. *Cancer Immunology Research* (2017).
- 140 Surace, L. *et al.* Complement is a central mediator of radiotherapy-induced tumor-specific immunity and clinical response. *Immunity* **42**, 767-777, doi:10.1016/j.immuni.2015.03.009 (2015).
- 141 Zhu, Y. *et al.* CSF1/CSF1R Blockade Reprograms Tumor-Infiltrating Macrophages and Improves Response to T-cell Checkpoint Immunotherapy in Pancreatic Cancer Models. *Cancer Research* **74**, 5057 (2014).
- 142 Young, A. *et al.* Co-inhibition of CD73 and A2AR Adenosine Signaling Improves Anti-tumor Immune Responses. *Cancer Cell* **30**, 391-403, doi:10.1016/j.ccell.2016.06.025 (2016).
- 143 Kohrt, H. E. *et al.* Stimulation of natural killer cells with a CD137-specific antibody enhances trastuzumab efficacy in xenotransplant models of breast cancer. *J Clin Invest* **122**, 1066-1075, doi:10.1172/JCI61226 (2012).
- 144 Kohrt, H. E. *et al.* Targeting CD137 enhances the efficacy of cetuximab. *The Journal of Clinical Investigation* **124**, 2668-2682, doi:10.1172/JCI73014 (2014).
- 145 Boyman, O. & Sprent, J. The role of interleukin-2 during homeostasis and activation of the immune system. *Nat Rev Immunol* **12**, 180-190, doi:10.1038/nri3156 (2012).
- 146 Moynihan, K. D. *et al.* Eradication of large established tumors in mice by combination immunotherapy that engages innate and adaptive immune responses. *Nat Med* **22**, 1402-1410, doi:10.1038/nm.4200 (2016).
- 147 Jackson, H. J., Rafiq, S. & Brentjens, R. J. Driving CAR T-cells forward. *Nat Rev Clin Oncol* **13**, 370-383, doi:10.1038/nrclinonc.2016.36 (2016).
- 148 Vivier, E., Ugolini, S., Blaise, D., Chabannon, C. & Brossay, L. Targeting natural killer cells and natural killer T cells in cancer. *Nat Rev Immunol* **12**, 239-252 (2012).
- 149 Sharma, P., Hu-Lieskovan, S., Wargo, J. A. & Ribas, A. Primary, Adaptive, and Acquired Resistance to Cancer Immunotherapy. *Cell* **168**, 707-723, doi:10.1016/j.cell.2017.01.017 (2017).
- 150 Parkhurst, M. R., Riley, J. P., Dudley, M. E. & Rosenberg, S. A. Adoptive Transfer of Autologous Natural Killer Cells Leads to High Levels of Circulating Natural Killer Cells but Does Not Mediate Tumor Regression. *Clinical Cancer Research* (2011).
- 151 Bachanova, V. *et al.* ALLOGENEIC NATURAL KILLER CELLS FOR REFRACTORY LYMPHOMA. *Cancer immunology, immunotherapy : CII* **59**, 1739-1744, doi:10.1007/s00262-010-0896-z (2010).
- 152 Kohrt, H. E. *et al.* Anti-KIR antibody enhancement of anti-lymphoma activity of natural killer cells as monotherapy and in combination with anti-CD20 antibodies. *Blood* **123**, 678 (2014).
- 153 Boissel, L. *et al.* Retargeting NK-92 cells by means of CD19- and CD20-specific chimeric antigen receptors compares favorably with antibody-dependent cellular cytotoxicity. *OncolImmunology* **2**, e26527, doi:10.4161/onci.26527 (2013).
- 154 Carlsten, M. *et al.* Efficient mRNA-Based Genetic Engineering of Human NK Cells with High-Affinity CD16 and CCR7 Augments Rituximab-Induced ADCC against Lymphoma and Targets NK Cell Migration toward the Lymph Node-Associated Chemokine CCL19. *Frontiers in Immunology* **7**, 105 (2016).
- 155 Deniger, D., Moyes, J. & Cooper, L. Clinical applications of gamma delta T cells with multivalent immunity. *Frontiers in Immunology* **5**, doi:10.3389/fimmu.2014.00636 (2014).
- 156 Tzeng, A. *et al.* Temporally Programmed CD8 $\alpha$ <sup>+</sup> DC Activation Enhances Combination Cancer Immunotherapy. *Cell Rep* **17**, 2503-2511, doi:10.1016/j.celrep.2016.11.020 (2016).
- 157 Golden, E. B. *et al.* Local radiotherapy and granulocyte-macrophage colony-stimulating factor to generate abscopal responses in patients with metastatic solid tumours: a proof-of-principle trial. *The Lancet Oncology* **16**, 795-803, doi:http://dx.doi.org/10.1016/S1470-2045(15)00054-6 (2015).

- 158 Westin, J. R. *et al.* Safety and activity of PD1 blockade by pidilizumab in combination with rituximab in patients with relapsed follicular lymphoma: a single group, open-label, phase 2 trial. *The Lancet Oncology* **15**, 69-77, doi:http://dx.doi.org/10.1016/S1470-2045(13)70551-5 (2014).
- 159 Chen, G. *et al.* A Feasibility Study of Cyclophosphamide, Trastuzumab, and an Allogeneic GM-CSF–Secreting Breast Tumor Vaccine for HER2<sup>+</sup> Metastatic Breast Cancer. *Cancer Immunology Research* **2**, 949 (2014).
- 160 Tarhini, A. A. *et al.* Safety and Efficacy of Combination Immunotherapy With Interferon Alfa-2b and Tremelimumab in Patients With Stage IV Melanoma. *Journal of Clinical Oncology* **30**, 322-328, doi:10.1200/JCO.2011.37.5394 (2012).
- 161 Khalil, D. N. *et al.* An Open-Label, Dose–Escalation Phase I Study of Anti-TYRP1 Monoclonal Antibody IMC-20D7S for Patients with Relapsed or Refractory Melanoma. *Clinical Cancer Research* **22**, 5204 (2016).
- 162 Rosenberg, S. A. Decade in review[mdash]cancer immunotherapy: Entering the mainstream of cancer treatment. *Nat Rev Clin Oncol* **11**, 630-632, doi:10.1038/nrclinonc.2014.174 (2014).
- 163 Melief, C. J. M., van Hall, T., Arens, R., Ossendorp, F. & van der Burg, S. H. Therapeutic cancer vaccines. *The Journal of Clinical Investigation* **125**, 3401-3412, doi:10.1172/JCI80009 (2015).
- 164 Sahin, U. *et al.* Personalized RNA mutanome vaccines mobilize poly-specific therapeutic immunity against cancer. *Nature* **547**, 222-226, doi:10.1038/nature23003  
<http://www.nature.com/nature/journal/v547/n7662/abs/nature23003.html#supplementary-information> (2017).
- 165 Ott, P. A. *et al.* An immunogenic personal neoantigen vaccine for patients with melanoma. *Nature* **547**, 217-221, doi:10.1038/nature22991  
<http://www.nature.com/nature/journal/v547/n7662/abs/nature22991.html#supplementary-information> (2017).
- 166 Mathur, D. *et al.* PEPlife: A Repository of the Half-life of Peptides. *Scientific Reports* **6**, 36617, doi:10.1038/srep36617  
<https://www.nature.com/articles/srep36617#supplementary-information> (2016).
- 167 Fan, Q. *et al.* Preclinical evaluation of Hematide, a novel erythropoiesis stimulating agent, for the treatment of anemia. *Experimental Hematology* **34**, 1303-1311, doi:https://doi.org/10.1016/j.exphem.2006.05.012 (2006).
- 168 Nguyen, L. T. *et al.* Serum Stabilities of Short Tryptophan- and Arginine-Rich Antimicrobial Peptide Analogs. *PLOS ONE* **5**, e12684, doi:10.1371/journal.pone.0012684 (2010).
- 169 Lindner, V. & Heinle, H. Binding properties of circulating evans blue in rabbits as determined by disc electrophoresis. *Atherosclerosis* **43**, 417-422, doi:http://dx.doi.org/10.1016/0021-9150(82)90040-5 (1982).
- 170 Tsopelas, C. & Sutton, R. Why Certain Dyes Are Useful for Localizing the Sentinel Lymph Node. *Journal of Nuclear Medicine* **43**, 1377-1382 (2002).
- 171 Qiao, S.-W. *et al.* Dependence of antibody-mediated presentation of antigen on FcRn. *Proceedings of the National Academy of Sciences* **105**, 9337-9342, doi:10.1073/pnas.0801717105 (2008).
- 172 Baker, K. *et al.* Neonatal Fc receptor for IgG (FcRn) regulates cross-presentation of IgG immune complexes by CD8–CD11b+ dendritic cells. *Proceedings of the National Academy of Sciences* **108**, 9927-9932, doi:10.1073/pnas.1019037108 (2011).
- 173 Bijker, M. S. *et al.* Superior induction of anti-tumor CTL immunity by extended peptide vaccines involves prolonged, DC-focused antigen presentation. *European Journal of Immunology* **38**, 1033-1042, doi:10.1002/eji.200737995 (2008).
- 174 Aichele, P., Brduscha-Riem, K., Zinkernagel, R. M., Hengartner, H. & Pircher, H. T cell priming versus T cell tolerance induced by synthetic peptides. *The Journal of Experimental Medicine* **182**, 261 (1995).
- 175 Toes, R. E., Offringa, R., Blom, R. J., Melief, C. J. & Kast, W. M. Peptide vaccination can lead to enhanced tumor growth through specific T-cell tolerance induction. *Proceedings of the National Academy of Sciences* **93**, 7855-7860 (1996).
- 176 Hildner, K. *et al.* Batf3 Deficiency Reveals a Critical Role for CD8 $\alpha$ + Dendritic Cells in Cytotoxic T Cell Immunity. *Science* **322**, 1097 (2008).
- 177 Danial, M., van Dulmen, T. H. H., Aleksandrowicz, J., Pötgens, A. J. G. & Klok, H.-A. Site-Specific PEGylation of HR2 Peptides: Effects of PEG Conjugation Position and Chain Length on HIV-1



- Membrane Fusion Inhibition and Proteolytic Degradation. *Bioconjugate Chemistry* **23**, 1648-1660, doi:10.1021/bc3002248 (2012).
- 178 Aucouturier J, e. a. Montanide ISA 720 and 51: a new generation of water in oil emulsions as adjuvants for human vaccines. *Expert Review of Vaccines* **1**, 111-118, doi:10.1586/14760584.1.1.111 (2002).
- 179 Dutertre, C.-A. *et al.* TLR3-Responsive, XCR1+ CD141(BDCA-3)+ Equivalent Dendritic Cells Uncovered in Healthy and Simian Immunodeficiency Virus-Infected Rhesus Macaques. *The Journal of Immunology* **192**, 4697 (2014).
- 180 Fanali, G., Fasano, M., Ascenzi, P., Zingg, J.-M. & Azzi, A.  $\alpha$ -Tocopherol binding to human serum albumin. *BioFactors* **39**, 294-303, doi:10.1002/biof.1070 (2013).
- 181 Rehli, M. Of mice and men: species variations of Toll-like receptor expression. *Trends in Immunology* **23**, 375-378, doi:http://dx.doi.org/10.1016/S1471-4906(02)02259-7 (2002).
- 182 de Fougères, A., Vornlocher, H.-P., Maraganore, J. & Lieberman, J. Interfering with disease: a progress report on siRNA-based therapeutics. *Nat Rev Drug Discov* **6**, 443-453 (2007).
- 183 Rajagopal, D. *et al.* Plasmacytoid dendritic cell-derived type I interferon is crucial for the adjuvant activity of Toll-like receptor 7 agonists. *Blood* **115**, 1949 (2010).
- 184 Gleave, M. E. & Monia, B. P. Antisense therapy for cancer. *Nat Rev Cancer* **5**, 468-479 (2005).
- 185 Hanson, M. C. *et al.* Nanoparticulate STING agonists are potent lymph node-targeted vaccine adjuvants. *The Journal of Clinical Investigation* **125**, 2532-2546, doi:10.1172/JCI79915 (2015).
- 186 Herzner, A.-M. *et al.* Sequence-specific activation of the DNA sensor cGAS by Y-form DNA structures as found in primary HIV-1 cDNA. *Nat Immunol* **16**, 1025-1033, doi:10.1038/ni.3267 <http://www.nature.com/ni/journal/v16/n10/abs/ni.3267.html#supplementary-information> (2015).
- 187 Hornung, V., Hartmann, R., Ablasser, A. & Hopfner, K.-P. OAS proteins and cGAS: unifying concepts in sensing and responding to cytosolic nucleic acids. *Nat Rev Immunol* **14**, 521-528, doi:10.1038/nri3719 (2014).
- 188 Liu, Z. & Chen, X. Simple bioconjugate chemistry serves great clinical advances: albumin as a versatile platform for diagnosis and precision therapy. *Chemical Society Reviews* **45**, 1432-1456, doi:10.1039/C5CS00158G (2016).
- 189 Dennis, M. S. *et al.* Albumin Binding as a General Strategy for Improving the Pharmacokinetics of Proteins. *Journal of Biological Chemistry* **277**, 35035-35043, doi:10.1074/jbc.M205854200 (2002).
- 190 Li, L. *et al.* Cross-dressed CD8 $\alpha$ + /CD103+ dendritic cells prime CD8+ T cells following vaccination. *Proceedings of the National Academy of Sciences* **109**, 12716-12721 (2012).
- 191 Merlot, A. M., Kalinowski, D. S. & Richardson, D. R. Unraveling the mysteries of serum albumin—more than just a serum protein. *Frontiers in Physiology* **5**, 299, doi:10.3389/fphys.2014.00299 (2014).
- 192 Johansen, P. *et al.* Antigen kinetics determines immune reactivity. *Proceedings of the National Academy of Sciences* **105**, 5189-5194 (2008).
- 193 Bachmann, M. F. *et al.* Long-lived memory CD8+ T cells are programmed by prolonged antigen exposure and low levels of cellular activation. *European Journal of Immunology* **36**, 842-854, doi:10.1002/eji.200535730 (2006).
- 194 Bonifaz, L. C. *et al.* In Vivo Targeting of Antigens to Maturing Dendritic Cells via the DEC-205 Receptor Improves T Cell Vaccination. *The Journal of Experimental Medicine* **199**, 815 (2004).
- 195 Hailemichael, Y. *et al.* Persistent antigen at vaccination sites induces tumor-specific CD8+ T cell sequestration, dysfunction and deletion. *Nat Med* **19**, 465-472, doi:http://www.nature.com/nm/journal/v19/n4/abs/nm.3105.html#supplementary-information (2013).
- 196 Mijalis, A. J. *et al.* A fully automated flow-based approach for accelerated peptide synthesis. *Nat Chem Biol* **13**, 464-466, doi:10.1038/nchembio.2318 <http://www.nature.com/nchembio/journal/v13/n5/abs/nchembio.2318.html#supplementary-information> (2017).
- 197 van Stipdonk, M. J. B. *et al.* Design of Agonistic Altered Peptides for the Robust Induction of CTL Directed towards H-2D<sup>b</sup>; in Complex with the Melanoma-Associated Epitope gp100. *Cancer Research* **69**, 7784 (2009).

- 198 Green, M. & Loewenstein, P. M. Autonomous functional domains of chemically synthesized human immunodeficiency virus tat trans-activator protein. *Cell* **55**, 1179-1188, doi:http://dx.doi.org/10.1016/0092-8674(88)90262-0 (1988).
- 199 Frankel, A. D. & Pabo, C. O. Cellular uptake of the tat protein from human immunodeficiency virus. *Cell* **55**, 1189-1193, doi:http://dx.doi.org/10.1016/0092-8674(88)90263-2 (1988).
- 200 Derossi, D., Joliot, A. H., Chassaing, G. & Prochiantz, A. The third helix of the Antennapedia homeodomain translocates through biological membranes. *Journal of Biological Chemistry* **269**, 10444-10450 (1994).
- 201 Morris, M. C., Vidal, P., Chaloin, L., Heitz, F. & Divita, G. A new peptide vector for efficient delivery of oligonucleotides into mammalian cells. *Nucleic Acids Research* **25**, 2730-2736 (1997).
- 202 Milletti, F. Cell-penetrating peptides: classes, origin, and current landscape. *Drug Discovery Today* **17**, 850-860, doi:http://dx.doi.org/10.1016/j.drudis.2012.03.002 (2012).
- 203 Guidotti, G., Brambilla, L. & Rossi, D. Cell-Penetrating Peptides: From Basic Research to Clinics. *Trends in Pharmacological Sciences* **38**, 406-424, doi:http://dx.doi.org/10.1016/j.tips.2017.01.003 (2017).
- 204 Brooks, N. A., Pouniotis, D. S., Tang, C.-K., Apostolopoulos, V. & Pietersz, G. A. Cell-penetrating peptides: Application in vaccine delivery. *Biochimica et Biophysica Acta (BBA) - Reviews on Cancer* **1805**, 25-34, doi:http://dx.doi.org/10.1016/j.bbcan.2009.09.004 (2010).
- 205 Pouniotis, D. S., Apostolopoulos, V. & Pietersz, G. A. Penetratin tandemly linked to a CTL peptide induces anti-tumour T-cell responses via a cross-presentation pathway. *Immunology* **117**, 329-339, doi:10.1111/j.1365-2567.2005.02304.x (2006).
- 206 Shibagaki, N. & Udey, M. C. Dendritic Cells Transduced with Protein Antigens Induce Cytotoxic Lymphocytes and Elicit Antitumor Immunity. *The Journal of Immunology* **168**, 2393 (2002).
- 207 Shibagaki, N. & Udey, M. C. Dendritic cells transduced with TAT protein transduction domain-containing tyrosinase-related protein 2 vaccinate against murine melanoma. *European Journal of Immunology* **33**, 850-860, doi:10.1002/eji.200323709 (2003).
- 208 Woo, S.-J. *et al.* Co-administration of carcinoembryonic antigen and HIV TAT fusion protein with CpG-oligodeoxynucleotide induces potent antitumor immunity. *Cancer Science* **99**, 1034-1039, doi:10.1111/j.1349-7006.2008.00760.x (2008).
- 209 Belnoue, E. *et al.* Enhancing Antitumor Immune Responses by Optimized Combinations of Cell-penetrating Peptide-based Vaccines and Adjuvants. *Molecular Therapy* **24**, 1675-1685, doi:http://dx.doi.org/10.1038/mt.2016.134 (2016).
- 210 Gautam, A. *et al.* CPPsite: a curated database of cell penetrating peptides. *Database: The Journal of Biological Databases and Curation* **2012**, bas015, doi:10.1093/database/bas015 (2012).
- 211 van Stipdonk, M. J. B. *et al.* Design of Agonistic Altered Peptides for the Robust Induction of CTL Directed towards H-2Db in Complex with the Melanoma-Associated Epitope gp100. *Cancer Research* **69**, 7784-7792, doi:10.1158/0008-5472.can-09-1724 (2009).
- 212 Szeto, G. L. *et al.* Microfluidic squeezing for intracellular antigen loading in polyclonal B-cells as cellular vaccines. **5**, 10276, doi:10.1038/srep10276  
https://www.nature.com/articles/srep10276#supplementary-information (2015).
- 213 Hu, Y. & Patel, S. Thermodynamics of cell-penetrating HIV1 TAT peptide insertion into PC/PS/CHOL model bilayers through transmembrane pores: the roles of cholesterol and anionic lipids. *Soft Matter* **12**, 6716-6727, doi:10.1039/C5SM01696G (2016).
- 214 Vivès, E., Brodin, P. & Lebleu, B. A Truncated HIV-1 Tat Protein Basic Domain Rapidly Translocates through the Plasma Membrane and Accumulates in the Cell Nucleus. *Journal of Biological Chemistry* **272**, 16010-16017 (1997).
- 215 Kaplan, I. M., Wadia, J. S. & Dowdy, S. F. Cationic TAT peptide transduction domain enters cells by macropinocytosis. *Journal of Controlled Release* **102**, 247-253, doi:http://dx.doi.org/10.1016/j.jconrel.2004.10.018 (2005).
- 216 Duchardt, F., Fotin-Mleczek, M., Schwarz, H., Fischer, R. & Brock, R. A Comprehensive Model for the Cellular Uptake of Cationic Cell-penetrating Peptides. *Traffic* **8**, 848-866, doi:10.1111/j.1600-0854.2007.00572.x (2007).
- 217 Ly, L. V., Sluijter, M., van der Burg, S. H., Jager, M. J. & van Hall, T. Effective cooperation of monoclonal antibody and peptide vaccine for the treatment of mouse melanoma. *Journal of immunology (Baltimore, Md. : 1950)* **190**, 489-496, doi:10.4049/jimmunol.1200135 (2013).

- 218 Danilchanka, O. & Mekalanos, John J. Cyclic Dinucleotides and the Innate Immune Response. *Cell* **154**, 962-970, doi:10.1016/j.cell.2013.08.014.
- 219 Pietersz, G. A., Li, W. & Apostolopoulos, V. A 16-mer peptide (RQIKIWFQNRRMKWKK) from antennapedia preferentially targets the Class I pathway. *Vaccine* **19**, 1397-1405, doi:http://dx.doi.org/10.1016/S0264-410X(00)00373-X (2001).
- 220 Schumacher, T. *et al.* A vaccine targeting mutant IDH1 induces antitumour immunity. *Nature* **512**, 324-327, doi:10.1038/nature13387  
<http://www.nature.com/nature/journal/v512/n7514/abs/nature13387.html#supplementary-information> (2014).
- 221 Kreiter, S. *et al.* Mutant MHC class II epitopes drive therapeutic immune responses to cancer. *Nature* **520**, 692-696, doi:10.1038/nature14426 (2015).
- 222 Tran, E. *et al.* Cancer Immunotherapy Based on Mutation-Specific CD4+ T Cells in a Patient with Epithelial Cancer. *Science* **344**, 641 (2014).
- 223 Zou, W., Wolchok, J. D. & Chen, L. PD-L1 (B7-H1) and PD-1 pathway blockade for cancer therapy: Mechanisms, response biomarkers, and combinations. *Sci Transl Med* **8**, 328rv324, doi:10.1126/scitranslmed.aad7118 (2016).
- 224 Curran, M. A., Kim, M., Montalvo, W., Al-Shamkhani, A. & Allison, J. P. Combination CTLA-4 blockade and 4-1BB activation enhances tumor rejection by increasing T-cell infiltration, proliferation, and cytokine production. *PLoS One* **6**, e19499, doi:10.1371/journal.pone.0019499 (2011).
- 225 Carmi, Y. *et al.* Allogeneic IgG combined with dendritic cell stimuli induce antitumour T-cell immunity. *Nature* **521**, 99-104, doi:10.1038/nature14424 (2015).
- 226 Hu-Lieskovan, S. *et al.* Improved antitumor activity of immunotherapy with BRAF and MEK inhibitors in BRAFV600E melanoma. *Science Translational Medicine* **7**, 279ra241-279ra241, doi:10.1126/scitranslmed.aaa4691 (2015).
- 227 Rapoport, A. P. *et al.* Combination immunotherapy after ASCT for multiple myeloma using MAGE-A3/Poly-ICLC immunizations followed by adoptive transfer of vaccine-primed and costimulated autologous T cells. *Clin Cancer Res* **20**, 1355-1365, doi:10.1158/1078-0432.CCR-13-2817 (2014).
- 228 Lum, L. G. *et al.* Targeted T-cell Therapy in Stage IV Breast Cancer: A Phase I Clinical Trial. *Clin Cancer Res* **21**, 2305-2314, doi:10.1158/1078-0432.CCR-14-2280 (2015).
- 229 Ribas, A., *et al.* Phase I study combining anti-PD-L1 (MEDI4736) with BRAF (dabrafenib) and/or MEK (trametinib) inhibitors in advanced melanoma. *J Clin Oncol* **33**, suppl, abstr 3003 (2015).
- 230 Chen, G. *et al.* A Feasibility Study of Cyclophosphamide, Trastuzumab, and an Allogeneic GM-CSF–Secreting Breast Tumor Vaccine for HER2+ Metastatic Breast Cancer. *Cancer Immunology Research*, doi:10.1158/2326-6066.cir-14-0058 (2014).
- 231 Overwijk, W. W. *et al.* Tumor regression and autoimmunity after reversal of a functionally tolerant state of self-reactive CD8+ T cells. *J Exp Med* **198**, 569-580, doi:10.1084/jem.20030590 (2003).
- 232 Klebanoff, C. A. *et al.* Determinants of successful CD8+ T-cell adoptive immunotherapy for large established tumors in mice. *Clin Cancer Res* **17**, 5343-5352, doi:10.1158/1078-0432.CCR-11-0503 (2011).
- 233 DuPage, M. *et al.* Endogenous T cell responses to antigens expressed in lung adenocarcinomas delay malignant tumor progression. *Cancer Cell* **19**, 72-85, doi:10.1016/j.ccr.2010.11.011 (2011).
- 234 Stromnes, I. M. *et al.* T Cells Engineered against a Native Antigen Can Surmount Immunologic and Physical Barriers to Treat Pancreatic Ductal Adenocarcinoma. *Cancer Cell* **28**, 638-652, doi:10.1016/j.ccell.2015.09.022 (2015).
- 235 Moore, S. J. *et al.* Engineered knottin peptide enables noninvasive optical imaging of intracranial medulloblastoma. *Proceedings of the National Academy of Sciences* **110**, 14598-14603, doi:10.1073/pnas.1311333110 (2013).
- 236 Rose, S., Misharin, A. & Perlman, H. A novel Ly6C/Ly6G-based strategy to analyze the mouse splenic myeloid compartment. *Cytometry A* **81**, 343-350, doi:10.1002/cyto.a.22012 (2012).
- 237 Ostrand-Rosenberg, S. & Sinha, P. Myeloid-derived suppressor cells: linking inflammation and cancer. *J Immunol* **182**, 4499-4506, doi:10.4049/jimmunol.0802740 (2009).

- 238 Rafiq, K., Bergtold, A. & Clynes, R. Immune complex – mediated antigen presentation induces tumor immunity. *The Journal of clinical investigation* **110**, 71-79, doi:10.1172/JCI200215640. Introduction (2002).
- 239 Broz, M. L. *et al.* Dissecting the tumor myeloid compartment reveals rare activating antigen-presenting cells critical for T cell immunity. *Cancer Cell* **26**, 638-652, doi:10.1016/j.ccell.2014.09.007 (2014).
- 240 Roberts, E. W. *et al.* Critical Role for CD103+/CD141+ Dendritic Cells Bearing CCR7 for Tumor Antigen Trafficking and Priming of T Cell Immunity in Melanoma. *Cancer Cell*, doi:10.1016/j.ccell.2016.06.003 (2016).
- 241 Salmon, H. *et al.* Expansion and Activation of CD103(+) Dendritic Cell Progenitors at the Tumor Site Enhances Tumor Responses to Therapeutic PD-L1 and BRAF Inhibition. *Immunity* **44**, 924-938, doi:10.1016/j.immuni.2016.03.012 (2016).
- 242 Dankort, D. *et al.* Braf(V600E) cooperates with Pten loss to induce metastatic melanoma. *Nat Genet* **41**, 544-552, doi:10.1038/ng.356 (2009).
- 243 Mendiratta, S. K., Thai, G., Eslahi, N. K. & Thull, N. M. Therapeutic tumor immunity induced by polyimmunization with melanoma antigens gp100 and TRP-2. *Cancer research*, 859-863 (2001).
- 244 Nelson, M. H. *et al.* Toll-like receptor agonist therapy can profoundly augment the antitumor activity of adoptively transferred CD8(+) T cells without host preconditioning. *J Immunother Cancer* **4**, 6, doi:10.1186/s40425-016-0110-8 (2016).
- 245 van Egmond, M. & Bakema, J. E. Neutrophils as effector cells for antibody-based immunotherapy of cancer. *Semin Cancer Biol* **23**, 190-199, doi:10.1016/j.semcancer.2012.12.002 (2013).
- 246 DiLillo, D. J. & Ravetch, J. V. Differential Fc-Receptor Engagement Drives an Anti-tumor Vaccinal Effect. *Cell* **161**, 1035-1045, doi:10.1016/j.cell.2015.04.016 (2015).
- 247 van Montfoort, N. *et al.* Antigen storage compartments in mature dendritic cells facilitate prolonged cytotoxic T lymphocyte cross-priming capacity. *Proc Natl Acad Sci U S A* **106**, 6730-6735, doi:10.1073/pnas.0900969106 (2009).
- 248 Guilliams, M., Bruhns, P., Saeys, Y., Hammad, H. & Lambrecht, B. N. The function of Fcγ receptors in dendritic cells and macrophages. *Nat Rev Immunol* **14**, 94-108, doi:10.1038/nri3582 (2014).
- 249 Clatworthy, M. R. *et al.* Immune complexes stimulate CCR7-dependent dendritic cell migration to lymph nodes. *Nat Med* **20**, 1458-1463, doi:10.1038/nm.3709 (2014).
- 250 Allan, R. S. *et al.* Migratory dendritic cells transfer antigen to a lymph node-resident dendritic cell population for efficient CTL priming. *Immunity* **25**, 153-162, doi:10.1016/j.immuni.2006.04.017 (2006).
- 251 den Haan, J. M., Lehar, S. M. & Bevan, M. J. CD8(+) but not CD8(-) dendritic cells cross-prime cytotoxic T cells in vivo. *J Exp Med* **192**, 1685-1696 (2000).
- 252 Gasteiger, G. *et al.* IL-2-dependent tuning of NK cell sensitivity for target cells is controlled by regulatory T cells. *J Exp Med* **210**, 1167-1178, doi:10.1084/jem.20122462 (2013).
- 253 List, J. *et al.* Cytokine responses to intraventricular injection of interleukin 2 into patients with leptomeningeal carcinomatosis: rapid induction of tumor necrosis factor alpha, interleukin 1 beta, interleukin 6, gamma-interferon, and soluble interleukin 2 receptor (Mr 55,000 protein). *Cancer Res* **52**, 1123-1128 (1992).
- 254 Carreno, B. M. *et al.* Cancer immunotherapy. A dendritic cell vaccine increases the breadth and diversity of melanoma neoantigen-specific T cells. *Science* **348**, 803-808, doi:10.1126/science.aaa3828 (2015).
- 255 DuPage, M., Mazumdar, C., Schmidt, L. M., Cheung, A. F. & Jacks, T. Expression of tumour-specific antigens underlies cancer immunoediting. *Nature* **482**, 405-409, doi:10.1038/nature10803 (2012).
- 256 Vigneron, N., Stroobant, V., Van den Eynde, B. J. & van der Bruggen, P. Database of T cell-defined human tumor antigens: the 2013 update. *Cancer Immunity Archive* **13** (2013).
- 257 Yadav, M. *et al.* Predicting immunogenic tumour mutations by combining mass spectrometry and exome sequencing. *Nature* **515**, 572-576, doi:10.1038/nature14001  
<http://www.nature.com/nature/journal/v515/n7528/abs/nature14001.html#supplementary-information> (2014).
- 258 Gubin, M. M. *et al.* Checkpoint blockade cancer immunotherapy targets tumour-specific mutant antigens. *Nature* **515**, 577-581, doi:10.1038/nature13988

- <http://www.nature.com/nature/journal/v515/n7528/abs/nature13988.html#supplementary-information> (2014).
- 259 Desgrosellier, J. S. & Cheresh, D. A. Integrins in cancer: biological implications and therapeutic opportunities. *Nature Reviews Cancer* **10**, 9-22 (2010).
- 260 Tzeng, A., Kwan, B. H., Opel, C. F., Navaratna, T. & Wittrup, K. D. Antigen specificity can be irrelevant to immunocytokine efficacy and biodistribution. *Proc Natl Acad Sci U S A* **112**, 3320-3325, doi:10.1073/pnas.1416159112 (2015).
- 261 Boggio, K. *et al.* Interleukin 12-mediated Prevention of Spontaneous Mammary Adenocarcinomas in Two Lines of Her-2/neu Transgenic Mice. *The Journal of Experimental Medicine* **188**, 589-596, doi:10.1084/jem.188.3.589 (1998).
- 262 Guevara, P. *et al.* Optimization of a self antigen for presentation of multiple epitopes in cancer immunity. *The Journal of Clinical Investigation* **116**, 1382-1390, doi:10.1172/JCI25591.
- 263 Malakhov, M. P. *et al.* SUMO fusions and SUMO-specific protease for efficient expression and purification of proteins. *Journal of Structural and Functional Genomics* **5**, 75-86, doi:10.1023/b:jsfg.0000029237.70316.52.
- 264 Hooijkaas, A. I., Gadiot, J., van der Valk, M., Mooi, W. J. & Blank, C. U. Targeting BRAFV600E in an inducible murine model of melanoma. *Am J Pathol* **181**, 785-794, doi:10.1016/j.ajpath.2012.06.002 (2012).
- 265 Muzumdar, M. D., Tasic, B., Miyamichi, K., Li, L. & Luo, L. A global double-fluorescent Cre reporter mouse. *Genesis* **45**, 593-605, doi:10.1002/dvg.20335 (2007).
- 266 Chen, B. *et al.* Dynamic imaging of genomic loci in living human cells by an optimized CRISPR/Cas system. *Cell* **155**, 1479-1491, doi:10.1016/j.cell.2013.12.001 (2013).
- 267 Joshi, Nikhil S. *et al.* Regulatory T Cells in Tumor-Associated Tertiary Lymphoid Structures Suppress Anti-tumor T Cell Responses. *Immunity* **43**, 579-590, doi:10.1016/j.immuni.2015.08.006.
- 268 Rosenthal, R., McGranahan, N., Herrero, J. & Swanton, C. Deciphering Genetic Intratumor Heterogeneity and Its Impact on Cancer Evolution. (2017).
- 269 Yee, C. *et al.* Adoptive T cell therapy using antigen-specific CD8+ T cell clones for the treatment of patients with metastatic melanoma: In vivo persistence, migration, and antitumor effect of transferred T cells. *Proceedings of the National Academy of Sciences* **99**, 16168-16173 (2002).
- 270 Ruella, M. *et al.* Treatment of leukemia antigen-loss relapses occurring after CD19-targeted immunotherapies by combination of anti-CD123 and anti-CD19 chimeric antigen receptor T cells. *Journal for ImmunoTherapy of Cancer* **3**, O5, doi:10.1186/2051-1426-3-S2-O5 (2015).
- 271 Spiotto, M. T., Rowley, D. A. & Schreiber, H. Bystander elimination of antigen loss variants in established tumors. *Nat Med* **10**, 294-298, doi:http://www.nature.com/nm/journal/v10/n3/suppinfo/nm999\_S1.html (2004).
- 272 Schietinger, A., Philip, M., Liu, R. B., Schreiber, K. & Schreiber, H. Bystander killing of cancer requires the cooperation of CD4(+) and CD8(+) T cells during the effector phase. *The Journal of Experimental Medicine* **207**, 2469-2477, doi:10.1084/jem.20092450 (2010).
- 273 Hirschhorn-Cymerman, D. *et al.* Induction of tumoricidal function in CD4(+) T cells is associated with concomitant memory and terminally differentiated phenotype. *The Journal of Experimental Medicine* **209**, 2113-2126, doi:10.1084/jem.20120532 (2012).
- 274 Clarke, S. R. *et al.* Characterization of the ovalbumin-specific TCR transgenic line OT-I: MHC elements for positive and negative selection. *Immunol Cell Biol* **78**, 110-117 (2000).
- 275 Irvine, D. J., Purbhoo, M. A., Krogsgaard, M. & Davis, M. M. Direct observation of ligand recognition by T cells. *Nature* **419**, 845-849, doi:http://www.nature.com/nature/journal/v419/n6909/suppinfo/nature01076\_S1.html (2002).
- 276 Chiang, E. Y., Henson, M. & Stroynowski, I. Correction of Defects Responsible for Impaired Qa-2 Class Ib MHC Expression on Melanoma Cells Protects Mice from Tumor Growth. *The Journal of Immunology* **170**, 4515 (2003).
- 277 Chen, C. *et al.* A bystander cell-based GM-CSF secreting vaccine synergized with a low dose of cyclophosphamide presents therapeutic immune responses against murine hepatocellular carcinoma. *Cellular and Molecular Immunology* **10**, 349-359, doi:10.1038/cmi.2013.20 (2013).
- 278 Quezada, S. A. *et al.* Tumor-reactive CD4(+) T cells develop cytotoxic activity and eradicate large established melanoma after transfer into lymphopenic hosts. *The Journal of Experimental Medicine* **207**, 637-650, doi:10.1084/jem.20091918 (2010).

- 279 Kobayashi, T., Imokawa, G., Bennett, D. C. & Hearing, V. J. Tyrosinase Stabilization by Tyrp1  
(the brown Locus Protein). *Journal of Biological Chemistry* **273**, 31801-31805 (1998).
- 280 Abelin, J. G. *et al.* Mass Spectrometry Profiling of HLA-Associated Peptidomes in Mono-allelic  
Cells Enables More Accurate Epitope Prediction. *Immunity* **46**, 315-326,  
doi:10.1016/j.immuni.2017.02.007.
- 281 Chang, C.-H. & Pearce, E. L. Emerging concepts of T cell metabolism as a target of  
immunotherapy. *Nat Immunol* **17**, 364-368, doi:10.1038/ni.3415 (2016).
- 282 Vétizou, M. *et al.* Anticancer immunotherapy by CTLA-4 blockade relies on the gut microbiota.  
*Science* **350**, 1079 (2015).
- 283 Sivan, A. *et al.* Commensal Bifidobacterium promotes antitumor immunity and facilitates anti-PD-  
L1 efficacy. *Science* **350**, 1084 (2015).
- 284 Wang, T., Wei, J. J., Sabatini, D. M. & Lander, E. S. Genetic Screens in Human Cells Using the  
CRISPR-Cas9 System. *Science* **343**, 80 (2014).
- 285 Shalem, O. *et al.* Genome-Scale CRISPR-Cas9 Knockout Screening in Human Cells. *Science*  
**343**, 84 (2014).
- 286 Manguso, R. T. *et al.* In vivo CRISPR screening identifies Ptpn2 as a cancer immunotherapy  
target. *Nature advance online publication*, doi:10.1038/nature23270  
<http://www.nature.com/nature/journal/vaop/ncurrent/abs/nature23270.html#supplementary-information>  
(2017).
- 287 Pitt, Jonathan M. *et al.* Resistance Mechanisms to Immune-Checkpoint Blockade in Cancer:  
Tumor-Intrinsic and -Extrinsic Factors. *Immunity* **44**, 1255-1269,  
doi:10.1016/j.immuni.2016.06.001 (2016).
- 288 Melero, I. *et al.* Evolving synergistic combinations of targeted immunotherapies to combat cancer.  
*Nat Rev Cancer* **15**, 457-472, doi:10.1038/nrc3973  
<http://www.nature.com/nrc/journal/v15/n8/abs/nrc3973.html#supplementary-information> (2015).
- 289 Zaretsky, J. M. *et al.* Mutations Associated with Acquired Resistance to PD-1 Blockade in  
Melanoma. *New England Journal of Medicine* **375**, 819-829, doi:10.1056/NEJMoa1604958  
(2016).
- 290 Carosella, E. D., Moreau, P., LeMaout, J. & Rouas-Freiss, N. HLA-G: from biology to clinical  
benefits. *Trends in Immunology* **29**, 125-132, doi:http://dx.doi.org/10.1016/j.it.2007.11.005 (2008).
- 291 Shifrin, N., Raulet, D. H. & Ardolino, M. NK cell self tolerance, responsiveness and missing self  
recognition. *Seminars in immunology* **26**, 138-144, doi:10.1016/j.smim.2014.02.007 (2014).
- 292 Carosella, E. D., Rouas-Freiss, N., Roux, D. T.-L., Moreau, P. & LeMaout, J. HLA-G: An Immune  
Checkpoint Molecule. *Advances in Immunology* **127**, 33-144,  
doi:http://dx.doi.org/10.1016/bs.ai.2015.04.001 (2015).
- 293 Maude, S. L. *et al.* Chimeric antigen receptor T cells for sustained remissions in leukemia. *N Engl  
J Med* **371**, doi:10.1056/NEJMoa1407222 (2014).
- 294 Beck, K. E. *et al.* Enterocolitis in Patients With Cancer After Antibody Blockade of Cytotoxic T-  
Lymphocyte-Associated Antigen 4. *Journal of Clinical Oncology* **24**, 2283-2289,  
doi:10.1200/JCO.2005.04.5716 (2006).
- 295 Tran, E. *et al.* T-Cell Transfer Therapy Targeting Mutant KRAS in Cancer. *New England Journal  
of Medicine* **375**, 2255-2262, doi:10.1056/NEJMoa1609279 (2016).
- 296 Tran, E., Robbins, P. F. & Rosenberg, S. A. 'Final common pathway' of human cancer  
immunotherapy: targeting random somatic mutations. *Nat Immunol* **18**, 255-262,  
doi:10.1038/ni.3682 (2017).
- 297 Wu, C.-Y., Rupp, L. J., Roybal, K. T. & Lim, W. A. Synthetic Biology Approaches to Engineer T  
cells. *Current opinion in immunology* **35**, 123-130, doi:10.1016/j.coi.2015.06.015 (2015).



## FUNDING

I am extremely grateful to have been personally supported during my doctorate by the John and Fanny Hertz Foundation Fellowship (specifically the Wilson Talley Hertz Fellowship), the NSF Graduate Research Fellowship Program, and the Siebel Scholarship.

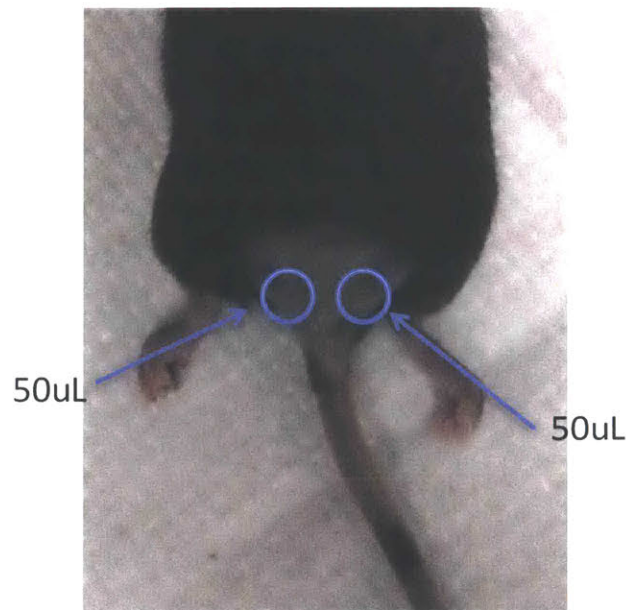
This thesis work was supported in part by the Koch Institute Support (core) grant P30-CA14051 from the National Cancer Institute, the US National Institutes of Health (NIH) grant CA174795, the Bridge Project partnership between the Koch Institute for Integrative Cancer Research and the Dana Farber–Harvard Cancer Center (DF–HCC), the V Foundation, the Ragon Institute, and the Howard Hughes Medical Institute.

# APPENDICES

## *1. Subcutaneous injections at the tail base*

Vaccination with amph-peptides and/or lipoCpG relies on efficient lymphatic drainage for optimal priming. Although subcutaneous injection anywhere on the mouse would be expected to give some access of the molecules to the lymphatics, experimental evidence suggests that injection at the tail base seems superior for priming (compared to subcutaneously at the cheek, flank, or neck). Here, a brief guide is included for subcutaneous injection at the base of the tail as performed in this thesis and in previous lab publications<sup>10</sup>.

For injection, 31G needles are recommended over other commonly used larger needles, like 29G. It is recommended to shave the mice at the base of the tail to ensure proper administration and for visual confirmation of the subcutaneous 'bubble' following injection. Easiest administration is performed on mice that have been anesthetized using isofluorane, and a nosecone can be used to assist. The mouse can be anchored by holding the tail during insertion of the needle. Insertion should be done with the bevel of the needle pointed away from the mouse, approximately 2mm up from where the skin transitions from fleshy to scaly at the base of the tail. The recommended injection volume is 50 $\mu$ L on either side of the base of the tail. Following injection, the needle should be withdrawn slowly, to prevent backflow. A clear bubble should be visible upon injection. A figure demonstrating the positioning is included below.



## ***II. Tetramer stain protocol***

### **Materials needed:**

K2/EDTA Tubes for blood collection

Greiner Bio-One GmbH MiniCollect tubes, 0.5mL K2E K2EDTA, Reference # 450480

Capillary tubes for retro-orbital bleeding

VWR® Microhematocrit Capillary Tubes, heparin coated, 15401-560

ACK Lysis buffer (various brands)

FACS Buffer: PBS, 1% BSA, 5mM EDTA

Tetramer stain buffer: PBS, 1% BSA, 5mM EDTA, 50nM Dasatinib

Tetramer (highly recommend using PE channel)

Anti-CD8 antibody

Fc block (anti CD16/32)

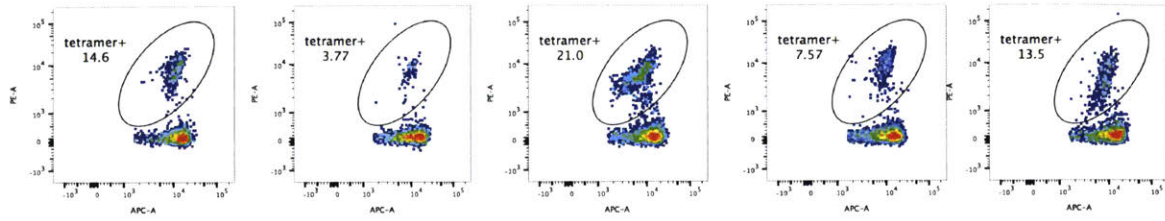
DAPI (used for live/dead—needs pacific blue or UV channel on flow cytometer)

### **Protocol:**

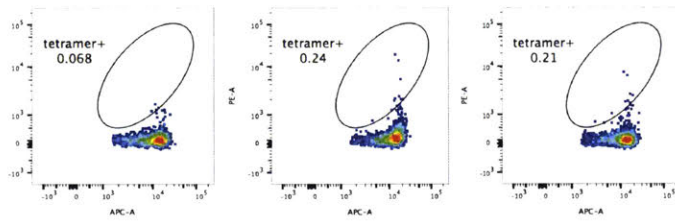
- Isolate 75-100uL of blood retro-orbitally into the K2/EDTA tubes using the heparin coated capillary tubes. Cap each tube and invert 3 times immediately after isolation. (The tubes have a coating on the inside to prevent clotting but it needs to be mixed with the blood.)

- After collection, spin tubes down for 3-5 seconds to get the blood off of the cap. Remove caps.
- Label a V-bottom plate.
- Transfer 70uL of blood per well to the plate.
- Add 130uL of ACK lysis buffer
- Incubate at room temperature for 4 minutes.
- Spin down and aspirate. At this point, there will be remaining un-lysed RBCs, don't worry if the pellets are not white.
- Resuspend in 200uL ACK lysis buffer and incubate at room temperature for 4 minutes.
- Spin down and aspirate. If pellets still appear pink you may complete one more round of lysis.
- Wash 1x with 200uL FACS Buffer.
- Resuspend in Tetramer Stain Buffer with tetramer and Fc block. I recommend staining in 50uL with a dilution of 1:50 to 1:100 for the tetramer (depending on the tetramer) and 1:100 Fc block.
- Incubate in the dark at room temperature for 30-40 minutes. For tetramer staining, room temperature is superior to 4 degrees.
- In the meantime, prepare a CD8 antibody solution: 1/100 anti-CD8 in Tetramer Stain Buffer, 50uL per well.
- After incubation, add CD8 antibody solution on top of the cells and mix. Note that the final staining concentration of anti-CD8 antibody is 1/200.
- Incubate at 4 degrees for 10 minutes. The short incubation time is because CD8 co-receptor is next to the TCR and the antibody-CD8 binding can compete to some degree with the lower affinity tetramer-TCR interaction, depending on the clone.
- In the meantime, prepare DAPI wash buffer for live/dead distinction: 100nM DAPI in FACS buffer.
- Wash 2x with DAPI wash buffer, at least 150uL/wash. This brief exposure is plenty to stain dead cells.
- For the final resuspension, put cells in Tetramer Stain Buffer and run on the cytometer.

Examples from mice with various responses, gated on live, single CD8<sup>+</sup> T cells:



Naïve mice:



### ***III. ICS protocol***

#### **Materials needed:**

K2/EDTA Tubes for blood collection

Greiner Bio-One GmbH MiniCollect tubes, 0.5mL K2E K2EDTA, Reference # 450480

Capillary tubes for retro-orbital bleeding

VWR® Microhematocrit Capillary Tubes, heparin coated, 15401-560

ACK Lysis buffer (various brands)

FACS Buffer: PBS, 1% BSA, 5mM EDTA

Media: RPMI (inc. glutamine and HEPES) with 10% FBS + pen/strep

Brefeldin A, 1000x, eBioscience

Amine reactive viability dye (ex. Live/Dead Aqua, Life Technologies)

anti-IFN- $\gamma$ , anti-TNF- $\alpha$ , anti-CD8 antibody, and any other markers of interest

BD Cytotfix/Cytoperm Fixation and permeabilization kit

Fc block (anti CD16/32)

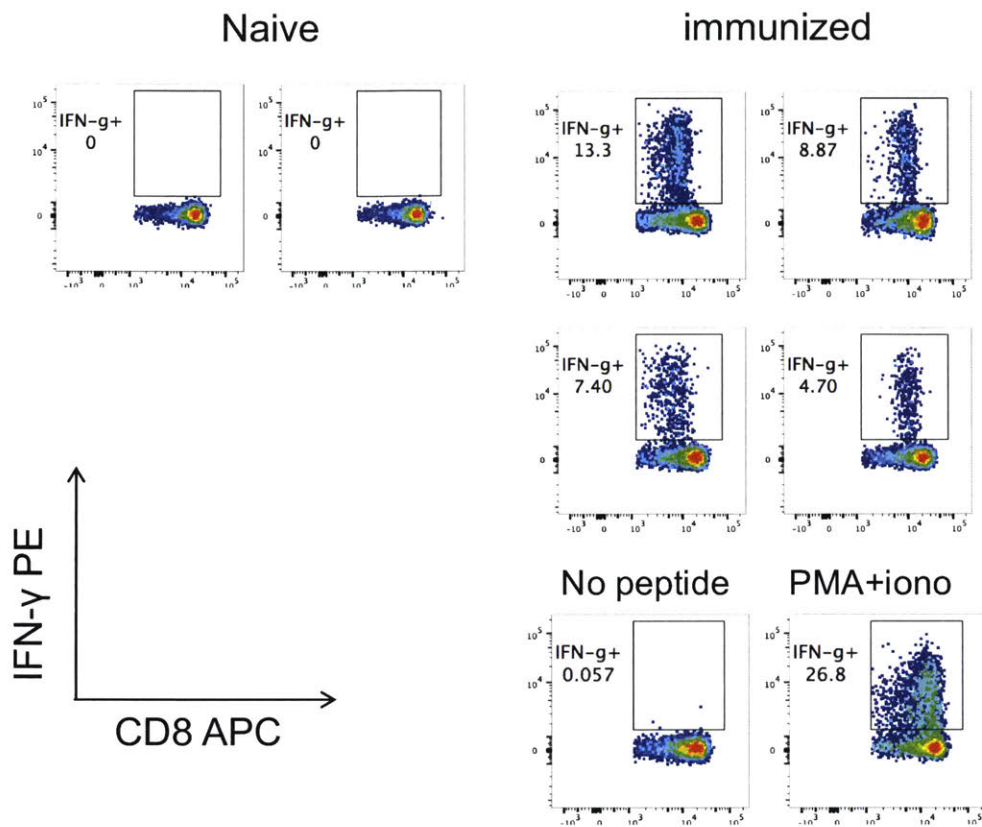
DAPI (used for live/dead—needs pacific blue or UV channel on flow cytometer)



## Protocol:

- Isolate and process blood as outlined in Appendix II.
- Plate in 100uL of complete RPMI media containing 10ug/mL peptide.
  - Remember PMA/ionomycin positive controls and no peptide negative controls. I usually pool leftover blood from each group to do this (so one positive and one negative per group).
  - Add brefeldin A immediately (1:1000, eBioscience) to PMA/ionomycin positive control wells.
- Leave for 2 hours in incubator at 37 degrees C.
- Add brefeldin A at recommended dilution to remaining wells.
- Incubate for 4 more hours, for a total of 6 hours with peptide.
- Wash cells with PBS
- Stain with fixable live/dead stain (Live/Dead Aqua by Life Technologies), 75uL/well with PBS as buffer (must be protein free), 4 degrees for 15 minutes.
- Quench with FACS buffer (I use PBS 1% BSA 5mM EDTA) and spin down.
- Stain extracellularly for CD4, CD8, etc., in FACS buffer (I do 4 degrees, 15 minutes)
- Wash once with FACS buffer.
- Fix using BD Cytofix for 15 minutes at 4 degrees.
- Wash 1x with BD Perm Wash (comes in BD Cytofix/Cytoperm kit, must be diluted 10x in water)
- Stain intracellularly for cytokines of interest (IFN- $\gamma$ , TNF- $\alpha$ , IL-2, etc.) in BD Perm Wash for 30 minutes at 4 degrees. I use these antibodies at 1:75.
- Wash 2x with perm buffer.
- Resuspend in 200uL FACS buffer and run on cytometer.
  - Note that the fixed/stained cells will remain excellent for running on the cytometer for at least 3 days at 4 degrees C.

Representative flow plots are shown below:



#### IV. List of selected murine CD8<sup>+</sup> T cell epitopes for amph-vaccination

Name	Strain	Source of antigen	Self, APL*, foreign?	MHC	Sequence (optimal epitope underlined)	Approx. avg % priming***
Trp2	black 6	B16F10	self	H-2Kb	<u>CSVYDFFVWL</u>	15%
Trp1	black 6	B16F10	self APL	H-2Db	<u>CTAPDNLGYM</u>	30%
gp100 EGP short	black 6	B16F10	self APL	H-2Db	<u>CEGPRNQDWL</u>	20%
gp100 EGP long	black 6	B16F10	self APL	H-2Db	AVGALE <u>EGPRNQDWL</u> GVPRQL	25%
gp100 KVP	black 6	B16F10	self APL (human)	H-2Db	<u>CKVPRNQDWL</u>	25%
p15e	black 6	many tumors, ex. B16F10, MC-38	endogenous retrovirus	H-2Kb	<u>CKSPWFTTL</u>	4%
Adpgk	black 6	MC-38	neoantigen	H-2Db	<u>CASMTNMELM</u>	5%
E7	black 6	HPV, TC-1	viral	H-2Db	GQAEPDRAHYNIVTF <u>CCKCD</u>	20%
gag 2	black 6	HIV	viral	H-2Db	LQPSLQTGSEELR <u>SLYNTVATLYCVHQRIE</u>	15%
p66	balb/c	Her2/neu	xenogantigen (rat)	H-2Kd	CQVVQGNLELTYVPANAS <u>LSFLQD</u>	25%
ALK9	balb/c	ALK	xenoantigen (human)	H-2Dd	<u>CPGPGRVAKI</u>	5%
gp70	balb/c	CT26, 4T1	APL of endogenous retrovirus	H-2Ld	CPRVTYH <u>SPSYAYHQFERRAK</u>	10% post prime

\*APL = altered peptide ligand. Note that the native, non-altered sequence was used for restimulation and/or tetramer staining.

\*\*If a cysteine was used to link the sequence to DSPE-PEG-maleimide, the cysteine is included in this table. Note that this cysteine is likely an unnatural cysteine not present in the original protein sequence.

\*\*\*post-boost responses, quantified as % antigen specific of total CD8<sup>+</sup>, either quantified using tetramer stain or ICS for best case vaccination (adjuvant = lipoCpG or c-di-GMP). If not measured post boost, post prime responses are included where indicated.

## V. DNA synthesis checklist

Provided here is a brief guide to using the DNA synthesizer ABI 394 (approx. 1989) with emphasis on how to prepare lipoCpG using a somewhat outdated synthesizer. Detailed methods including relevant chemistries are published<sup>10</sup>.

These notes are for standard synthesis with phosphorothioate backbone and the below listed bases:

1. deoxy Adenosine (n-bz) CED phosphoramidite
  2. Thymidine CED phosphoramidite
  3. deoxy Cytidine (n-acetyl) CED phosphoramidite
  4. deoxy Guanosine (n-ibu) CED phosphoramidite
- Turn nitrogen gas on, pressure should be at approximately 50 PSI.
  - Check levels of reagents:
    - Slots 1-4: DNA bases. These are only good for 2 weeks at room temperature—replace bases if they are more than 2 weeks old. Additionally, you need them to be at least 50% full for 4-column standard scale synthesis (for normal sequences like 1826. You will need to adjust if you're making something like polyT)
      - When replacing, use a syringe to inject anhydrous acetonitrile for base resuspension to avoid exposure to moisture where possible. (DNA reaction efficiency goes down with moisture.)
    - Slot 7 (or alternative) if adding a lipid: fill vial with DCM for warm-up sequence.
    - Slot 11: Cap A: at least 20% full
    - Slot 12: Cap B: at least 20% full
    - Slot 14: 3% DCA in DCM (DMT removal reagent)—must be **completely** full for a 4-column standard scale synthesis.
    - Slot 15: sulfurizing reagent, which is DDTT. If you do phosphodiester this reagent will change.
    - Slot 18: **anhydrous** acetonitrile. This can be either purchased as anhydrous or dried from standard acetonitrile using drying traps. At least 25% full.
    - Slot 19: dichloromethane, at least 25% full.

- Check that the hazardous waste collection jug is in a secondary container and that it is less than halfway full. The tag should read 80% acetonitrile, 20% dichloromethane, trace dichloroacetic acid.
- Run a 'warm up sequence' to cycle through each base and generally flush the instrument. Under sequences on the computer, this is #19 (should read A7TCGT if you are adding lipid from slot 7). Note that the last base (3' end) is not added by the synthesizer—the software assumes that it is conjugated to the bead. This will take approximately 40 minutes. The cycle should be #22—this is 90 second coupling time per base.
- Weigh out the beads into 4 synthesis columns. Use 20mg beads per column. Make sure that you twist well to tighten the columns.
- Before initiating synthesis, double-check the sequence and cycle.
  - Note that if you are synthesizing a dye-labeled oligo, the beads (ex. 3' TAMRA CPG) do not have a base on them, and you will need to add an additional base (any base) on the 3' end in the sequence on the computer. This is to account for the fact that the software does not add the 3' most base.
  - Cycle should be 22: 1um Sulfur | HP for 90 second coupling time/base.
- Begin synthesis (say 'yes' to ABI begin). Synthesis of CpG 1826 takes approximately 4-4.5 hours.
- Remove the columns if you're synthesizing non-lipidated DNA. (If no lipid is added, you should purify based on hydrophobicity of the DMT group present on the last base, then remove the DMT and perform an ethanol precipitation.)
- For lipid coupling, resuspend lipid in 1.2mL of DCM, add to the slot (ex. slot 7) and angle the vial so that all volume can be taken up by the tubing.
  - Choose cycle 24 for the lipid addition (this is 999 second coupling time), choose 7T = lipid addition (sequence #15) as the sequence, and start the synthesizer. This will take approximately 25-30 minutes.
- Remove the beads from the synthesizer and store at 4°C until deprotection and purification. The oligos on resin can be stored at 4°C for at least 6 months.



**Deprotection:**

Standard oligos: Use AMA (1:1 solution of 30% ammonium hydroxide and 40% aqueous methylamine) for 10 minutes at 65°C. (This is for both lipidated and non-lipidated DNA.)

Fluorophore labeled oligos: use 1:3 tertbutylamine in water (or TAMRA cocktail from Glen Research) for 6 hours at 65°C. (This is for both lipidated and non-lipidated DNA.)

Following deprotection, dilute in water, remove from beads, wash beads with water, and collect. Spin down collected oligo solution to remove any remaining beads prior to HPLC purification.

**Purification:**

Refer to Liu et al for details<sup>10</sup>. As of this writing in summer 2017, a suitable method can be found under methods in Kelly's folder, use 0.1M TEAA in water and methanol, and the lipoCpG will elute latest (approx. 14 min). To purify DNA without lipid, use hydrophobicity of DMT group (leave DMT on) and purify using a slightly less steep gradient. You will need to remove DMT after purification using 80% acetic acid for 2 hours at room temperature followed by an ethanol precipitation.